Estimating the upper ocean vertical temperature structure from surface temperature as applied to the southern Benguela

Carl K Wainman

Institute for Maritime Technology. A Division of Armscor Defence Institutes (PTY) Ltd.

Thesis presented for the degree of Doctor of Philosophy in the Department of Oceanography
University of Cape Town

November 2012

ABSTRACT

Underwater Sound Velocity Profiles (SVP) are used throughout the world by their respective navies for submarine and surface vessel strategic operations and exercises. Together with the sonar equations, the sound velocity profiles are of paramount importance to solve underwater sound detectability problems as they provide insight into the highly variable sound transmission loss. Oceanographic records of sea temperature-depth profiles are ordinarily incorporated into a sonar propagation model to determine the sound level at any point (range and depth). The ability to predict these environmental conditions with a defined level of confidence and accuracy significantly increases the situational awareness to in-theatre naval operators and fleet planners.

The hypothesis in this thesis is that thermal characteristics of the water column in the southern Benguela can be numerically modeled and deduced from a single Sea Surface Temperature (SST) value, if provided with sufficient historic temperature-depth profiles for that region. For operational use, the SST would ideally be provided from near real time remotely sensed satellite derived data.

The methodology used suitably pre-processed historic temperature-depth measurements in an artificial neural network Self Organising Map analysis, as a basis for selecting a representative temperature profile. The method combined static (climatological) temperature profiles and dynamic (near real time) surface temperatures to form a 'quasi-dynamic' solution.

As an effectiveness test of the results, a small number of qualifying source profiles were flagged for hind casting purposes and were then excluded from the dataset. The results were initially tested on a modest pilot study (45) and then an extended sample (634) of hind cast profiles. Statistically significant results were achieved in both cases, and when compared with the 'winning' or synthetic SOM profile, the first case, had a mean RMS of 0.883 °C and a mean correlation coefficient of 0.930; the second larger dataset had a mean RMS of 0.914 °C, with a mean correlation coefficient of 0.945.

Although no identical comparative study could be found in the literature, the results compared favourably with available published methods, and were shown to be within the same level of predictive confidence. The novelty of the present approach is to establish 15 "nodes" of synthetic profiles by combining two existing methods of parametric curve fitting and probabilistic SOM profiles. These represent the physical world for a selected month. Obtaining a unique profile in this way from SST observation is usually very difficult, and the thesis provides a relatively easy and robust method.

The naval operational concept of this research is to use available SST information from a remotely sensed infra-red band, earth-orbiting satellite sensor to match with vertical temperature values of a suitably representative (in time and space) 'synthetic' profile. This temperature profile is then converted into a sound velocity profile for use within an existing sound propagation and transmission loss model. Naval benefit of this enhanced technique can be derived in most instances where underwater acoustics are used in passive or active modes.

It is anticipated that the method has the potential to greatly improve the operations, safety and planning (ship routing, strategy and tactics) as a so called force multiplier. As a consequence, this technique may contibutue to maritime security and protection of sovereign rights in a state's Exclusive Economic Zone. Examples are the protection of offshore maritime assets, resources and shipping lanes.

Table of Contents

LIST OF FIGURES

LIST OF TABLES

1. INTRODUCTION

a. Overview

Oceanographic and meteorological information are important to all users of the ocean. This is especially true for naval users, where tactics and strategy based on an advanced understanding of the surrounding natural environment provides significant advantage. The ability to predict these parameters with some level of confidence and accuracy may create increased situational awareness to naval operators' and fleet planners, with significant advantage as a so-called "force-multiplier".

The usage of SONAR (SOund Navigation And Ranging) propagation modeling techniques by surface and sub-surface combat ships can result in the likelihood of a vessel being detected or not. SONAR usage is especially important for submarine operations, both as sound actively transmitted into the water, or passively in a listening mode. Whilst active sonars determine the range and bearing of a distant sound source (as return signals from reflected sound pulses), passive sonar on the other hand listens for sounds generated by some sound source (a vessel in this case). Modeling the propagation of sound through the water column is however critically dependent on information about the thermo-saline-pressure structure of the medium (the ocean). Note: The meanings to all acronyms are provided in Appendix G and a selection of definitions in Appendix H.

Vertical structures of temperature are used to generate a Sound Velocity Profile (SVP), as input to a sound propagation model. These synthesise in-situ propagation behaviour. Results may define a number of sound transmission conditions, for example within the SOFAR (SOnar Frequency And Ranging) channel (see ***Figure 1-1***), with a surface duct and shadow zone, bottom bounce and convergence. These transmission conditions are mostly dependent on the Sound Velocity Profile provided, but may also affected by bottom reflection properties and the bottom depth. Quantifying sound propagation is a challenge, especially in littoral waters, as it depends on properties of the SVP, the sea surface interface and the sea bottom interface. The calculation of sound transmission loss is used to quantify the transmission loss term in sonar equations. Such results are presented as average conditions, since geometry, arrival times and other temporal variables are averaged in the process.

Although thermal conditions are often recorded while in-situ, this is not always practical and is measured in isolation, since it only provides a 1-dimensional picture (at a single point in space and

time). Vertical thermal (quasi-real time) structure forecasting however can assist in providing the essential, more representative information required for the sound velocity profile.

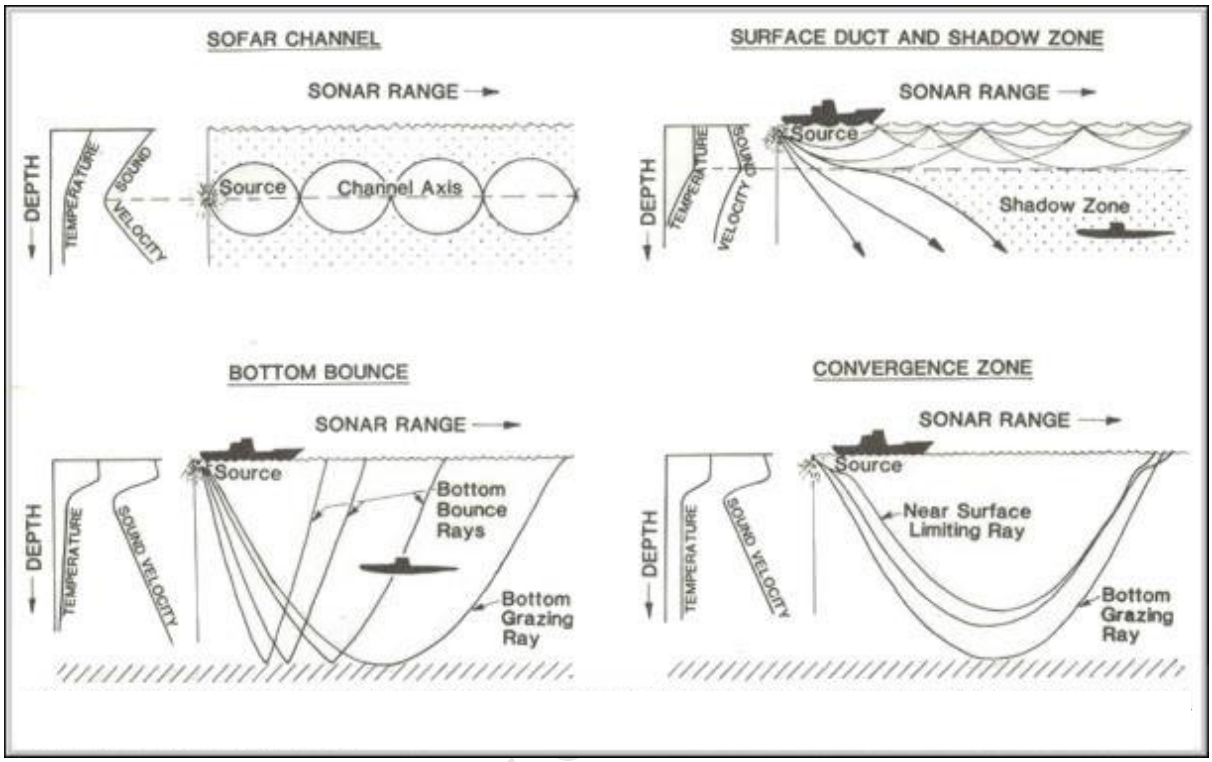

Figure 1-1: *Schematic of 4 temperature and sound velocity profile types, with their respective sound propagation paths originating from a single point sound source. After Bishop (1984).*

Formerly, ocean vertical thermal structure forecasting used empirically derived graphs and equations for air-sea interaction relationships, with data provided from on-scene data collections (Bishop (1984)). The processes in the ocean, such as diurnal heating and cooling, heat transfer, insolation, solar radiation, return radiation, evaporation, precipitation, heat flux, convection, advection, water masses at continental shelves, fronts, eddies, wind driven mixing, turbulence and internal waves all contribute to a complex natural environment that is challenging to forecast.

Estimating vertical temperature structures is made more difficult by the highly variable (dynamic) properties of the above parameters. These parameters vary in both time and space, especially prevalent in the South African Navy's primary operational area. In these Southern African oceans, features such as the Agulhas, Benguela, Angolan, Mozambique and Circumpolar currents play important roles in defining properties of oceanic water. In such circumstances, using climatological information to forecast or now-cast vertical temperature structures can result in large errors.

Bishop (1984) described a forecasting method that used the following processing steps: 1. Establish existing conditions, 2. Compute advection, 3. Compute heat budget, 4. Compute mixing and 5. Present results. The methodology used an understanding of the natural physical processes and the development of mathematical models to describe and hence predict processes and resultant water column structure. This prediction method is however used for future ocean states, largely different from this study that identifies underwater thermal structure from SST.

This study uses a different approach that largely ignores the processes and focuses instead on defining the statistical or mathematical properties of the water column in a region demarcated largely by its surface temperature ranges. A large number of previously measured temperature-depth profiles (also called static information) are then 'normalised' in terms of their depth values (standard depths) by using curve-fitting and line-smoothing techniques. They are then clustered into a representative synthetic continuum of profiles available for predictive purposes. Based only on the profile's surface temperature and its similarity to a sea surface temperature provided 'externally', a winning synthetic profile is proposed by the software. An association between profiles and their single surface temperature value is necessarily implicit in this process.

The naval operational concept of this research is to use available Sea Surface Temperature (SST) information from any remote sensed infra-red, earth-orbiting satellite sensor to match the vertical temperature values of a suitably representative (in time and space) 'synthetic' profile. This temperature profile is then converted into a sound velocity profile for use within an existing 2-dimensional sound propagation model. The significant naval benefit of the method proposed in this study is as follows: (A) Underwater surveillance through having a remote capability 'detached' from any current location at sea, which provides important information about its underwater acoustic signal and detection range. (B) Underwater acoustic own vulnerability to being detected, from another vessel, submarine or underwater mounted sensor such as a sea mine. This depiction of thermal vertical structure from an SST observation has the potential to greatly improve maritime safety and planning (ship routing, strategy and tactics) as so called force multiplier. As a consequence, this technique may contibutue to maritime security and protection of sovereign rights in a state's Exclusive Economic Zone (see Appendix H). These include amongst others, protection of offshore maritime assets, resources and shipping lanes.

In general terms, this parameterisation method combines static (climatological) profiles and dynamic (near real time) surface temperatures to form a 'quasi-dynamic' solution.

b. Hypothesis [Step A in Figure 3-1]

In order to explore the feasibility of such a concept the following hypothesis is posed:

Can thermal characteristics of the water column be modeled from a single sea surface temperature value, if provided with historic temperature-depth profiles for that region?

Details of the steps followed to answer the hypothesis are shown in ***Figure 1-2*** and ***Figure 3-1*** and referred to throughout the thesis.

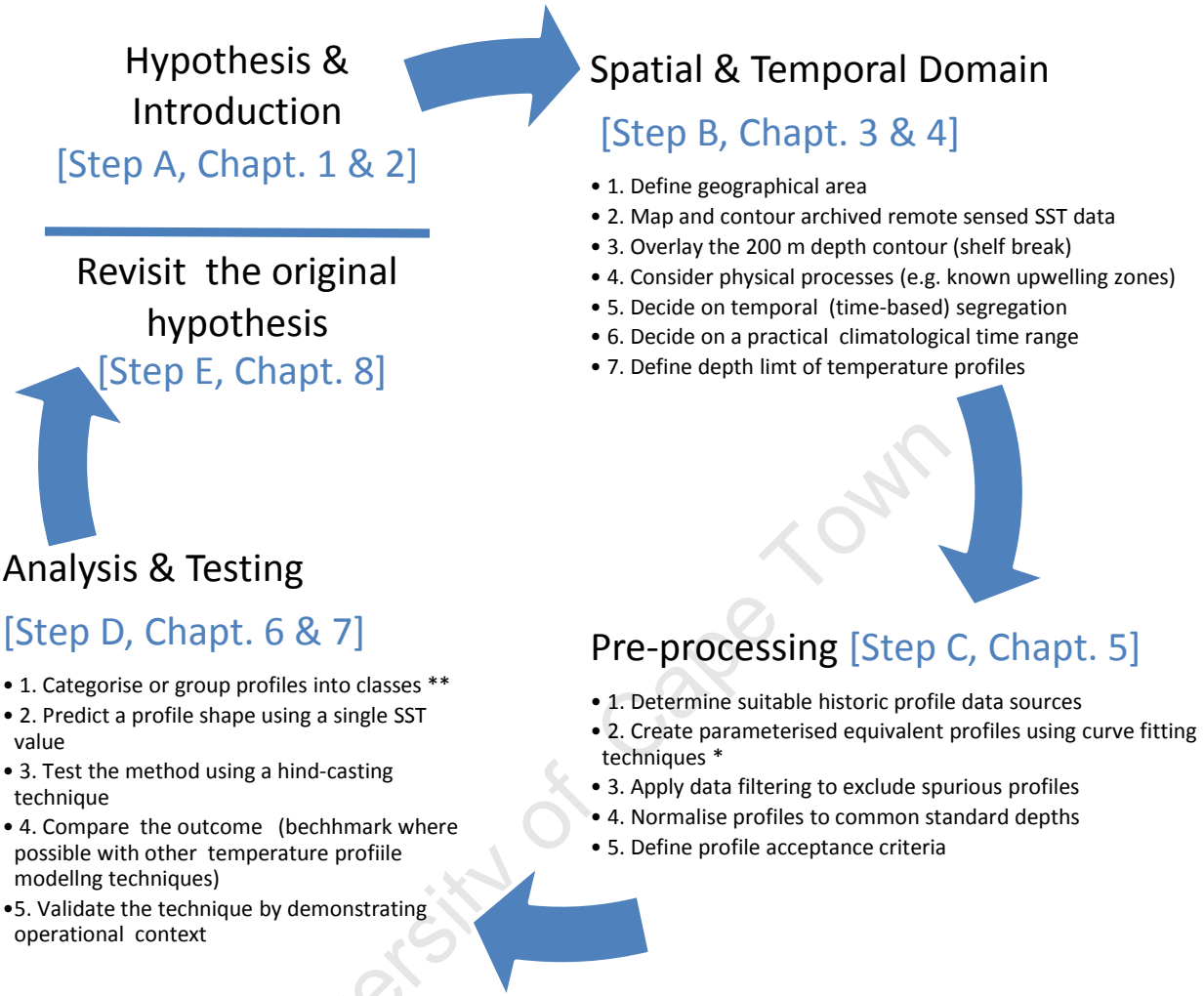

Figure 1-2: *Research process flow as addressed in the chapters that follow. The single asterisk * in Step C refers to a parametric approach whereas double asterisk ** in Step D refers to a probabilistic approach.*

The sequential 5-step structure starts with defining the hypothesis. Thereafter the spatial and temporal domains are specified, including the unique characteristics of the geographical setting. In the pre-processing step historic profiles are sourced, filtered, parameterised, normalised and reconstructed in preparation for the next step. During the analysis and testing stage, profiles undergo a mathematical classification process resulting in a number of synthetic profile classes. The upper-most surface temperature value is then used to associate or allocate (predict) the synthetic profile as a result of the SST value provided. Through a hind casting process, profiles reserved in the original dataset are then used to test the accuracy of the outcome. These profiles do not play any

role in the classification process that follows. The effectiveness of the method is then compared (benchmarked) with similar water column prediction methods. Predicted synthetic profiles are converted to sound velocity profiles and provided as input to a sound propagation model to demonstrate naval operational context. Finally, the original hypothesis is revisited.

c. Thesis guide

This thesis first introduces the research topic in the form of a literature review, starting from early theoretical studies and principles in fluid dynamics. Thereafter, various climatological predictive models and techniques are reviewed. Relevant published research papers were chosen to showcase similar initiatives and to provide a benchmark or yardstick for the effectiveness of their techniques. It is shown in the review that although this research contains components of other initiatives that are useful for 'calibration' purposes, it is novel in approach and content.

Chapter 1 introduces the topic and hypothesis, describes the structure and provides an overview of the thesis. Here the operational naval significance is also explained. Chapter 2 is a historic perspective and summary of former relevant research initiatives, ending with an overview of observational methodologies. Chapter 3 is a description of the methodology used in this thesis. The study area is described in oceanographic terms in Chapter 4, with special reference to relevant published literature. Data pre-processing, spatial-temporal climatology, varying sensor types, formats, standardisation of profiles and curve fitting techniques are covered in the Chapter 5. Chapter 6 defines, tests, implements and applies a neural network technique in the form of Self Organising Maps (SOM) to the dataset profiles prepared earlier. In the results (Chapter 7), a detailed account of the source profiles is presented, together with output results from the neural network analysis. Here an important component of this study is covered, where the effectiveness of the analysis is tested by statistically comparing observations with winning synthetic profiles using a hind casting technique. The predictive temperature profile is then converted into a sound velocity profile for input to an existing 2-dimensional sound propagation model (SMOD). The output from SMOD is briefly discussed and the predictive results validated. In Chapter 8, the details and comparisons with prior published literature and merits and shortcomings of the technique in relation to the oceanographic study of the region are discussed. Chapter 9 outlines the contribution to knowledge and understanding and the novelty and advance provided by the technique.

Specific steps are followed in the research process, from defining the hypothesis, providing a background, pre-processing of data, analysis and comparison, validation, reporting and finally re-

visiting the hypothesis. This sequence is shown in ***Figure 1-2*** and ***Figure 3-1*** as detailed steps and referenced throughout in the text.

A list of acronyms is provided in Appendix G and definitions of some terms used in this study in Appendix H.

2. BACKGROUND AND LITERATURE REVIEW

Before synthesising thermal properties of the water column (or 'profiles'), it is useful to have an understanding of the natural dynamics that created these conditions and the research that has led us to our present-day understanding of the processes.

The first half of this chapter (section a) is a review of pertinent scientific progress from first principles in fluid dynamics to the development of equations to describe eddy viscosity, diffusivity, heat flux and wind stress vertical mixing. The information, terms and equations provided here are intended only as informative background material in terms of appreciation for the complexity of the topic.

The second half of the chapter (section b) is also a review in sequential time of scientific progress. This section examines progress made to characterise or model vertical temperature profile patterns that describe the natural environment. This part of the literature review has some techniques that are somewhat similar to parts of those used in this study. These are later referred to in terms of the statistics they used to quantify their predictive success.

Sections c and d are provided mostly for background purposes, to understand the origin of the profile measurements and how these are eventually applied to sound propagation techniques and practical naval applications.

a. Physical processes

Molecular diffusion is a very slow process of heat transfer through the ocean originating from incoming short wave solar radiation in the atmosphere (solar heating) that propagates through its upper layers. The process is considerably sped up by surface winds and strongly modulated by turbulence of ocean currents. The effects of precipitation and evaporation are closely associated with salinity (see Appendix H) and density and are relatively small in this case.

Historically, research in upper-ocean thermal mixing was generally reported under the heading of fluid dynamics and the topic is reviewed here to assist in understanding the physical underlying processes contributing to thermal water column structures.

One of the earliest references of heat diffusion research can be traced back to Adolf Fick's work on liquid diffusion in 1855 Narasimhan (2004). Seen as a pioneer in this field, he dealt mainly with salt

flux that became known as Fick's Law, where molecular salt diffusion in liquids was viewed as a binary process with salt moving in one direction and water moving in the other, analogous to heat diffusion. Similar pioneers were Rossby and Montgomery (1935) after Munk and Anderson (1948) wherein the concept of turbulent eddy viscosity was first introduced.

Referred to as a landmark paper by some authors, Munk and Anderson (1948) proposed the concept of an upper mixed layer and presented "over-simplified" equations of turbulent flux under stable conditions, the determination of certain constants and the distribution of velocity with temperature and hence density. They proposed that the diffusion rate in the thermocline (see Appendix H) varied with the Richardson number. Richardson Number is defined as the ratio of buoyant production to stress production of turbulent kinetic energy, after Tennekes and Lumley (1983).

Munk and Anderson (1948) then compared their computed results with observed values in the mid-Pacific and concluded that the depth of the thermocline depended on wind speed, latitude, heat flux and the T-S correlation (see Appendix H).

Shonting (1964) of the US Naval Oceanographic Office reported short term diurnal heating and cooling in relation to vertical diffusion and its relation to meteorological parameters from a 7-day study in Bahamas. Thermal eddy diffusion coefficients were derived and compared with other methods. Of note was the observation that air exhibited three to four times the diurnal temperature amplitude of the surface water. It was also found that the air tended to absorb the incoming radiation rather uniformly within its volume, but the surface water absorbed it exponentially with depth, although also dependent on the transparency and scattering properties of water. Diurnal temperature variation was not detectable deeper than 25 - 30 m. Values of k (eddy diffusivity) varied from 10 cm^2/s at a depth of 12 m to 111 cm^2/s at 4 m. It was estimated that the Richardson number increased by a factor of 103 over a 5 hour interval due to diurnal temperature variations.

A one-dimensional model of the seasonal thermocline that accounted for wind mixing (stirring) and entrainment across the lower boundary of the mixed layer was proposed by Kraus and Turner (1967). Their model was proposed to be suitable for investigations of both diurnal and seasonal effects. It was later reported in Pacanowski and Philander (1981) that they were the first to parameterise mixing processes in the upper ocean, commonly termed the Kraus-Turner formulation.

Kraus and Turner (1967) suggested improvements to non-constant values for v (viscosity) and k (eddy diffusivity) that were described as Richardson number dependent. Thus, it was important to consider heat flux conditions at the ocean surface, due to its effect on stability and hence vertical

mixing. Heat budget calculations were performed whereby all the input and output energies were accounted for.

The absorption of radiation heat was observed to become approximately isotropic and exponential to a depth of 10 - 20 m in the open sub-tropical ocean (Kraus and Turner (1967)) as a result of diffusivity or vertical eddy diffusion (*k*). They proposed in general terms that isothermal layers become shallower if the penetrative convection does not reach down to its full potential depth. They concluded that the depth of these layers is at a minimum during the summer solstice, with a surface temperature maximum occurring later in the season. Thereafter the layers will become thicker by entrainment of water, if the downward heat flux is greater than zero (Kraus and Turner (1967)). Below this region, mixing becomes weak, with small temperature gradients and large shear, unless acted upon by an ocean undercurrent.

Haney (1971) in studies primarily for ocean circulation modeling formulated downward heat flux (Q) when provided with the surface and first 'level' sea temperatures.

$$\frac{Q}{\rho o \mathrm{C}} = \frac{k dT}{dz} = \frac{k}{\Delta z} (T_s - T_1)$$

Where ρo is the density of seawater, C the specific heat of seawater at constant pressure, Δz the depth of the first layer, k the vertical eddy diffusion coefficient, T_S the prescribed ocean surface temperature and T_1 the temperature at the first level below the surface. The primary weakness of formulating the heat flux using this method was an insufficient knowledge of the appropriate value of k for the surface layer. Given this shortcoming and by making the assumption that the surface layer was always mixed, T_A replaced T_S and heat flux (Q) across the air-sea interface was instead described as :-

$$Q = Q_2 (T_A^* - T_1)$$

Where T_A^* is the apparent zonally averaged annual mean surface air temperature and Q_2 is the zonally varying rate of heat take-up in the ocean, including the effect of wind as a coupled solution.

Mellor and Durbin (1975) indicated that a Richardson number in the range 0.21-0.25 was emerging as a remarkable general criterion for the existence of turbulence.

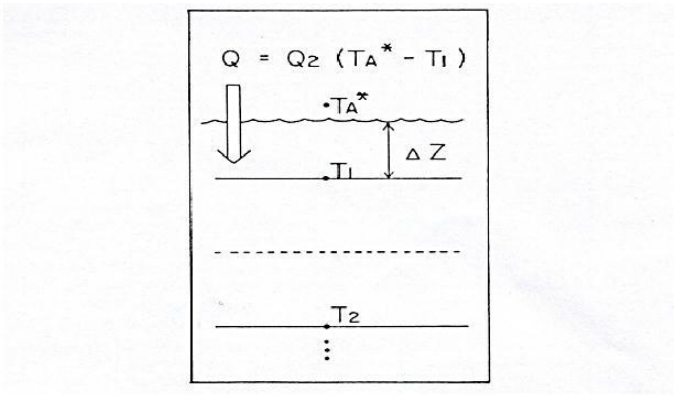

Figure 2-1*: Schematic showing the formulation of downward heat flux at the ocean surface according to the above formula, after Haney (1971).*

In a varying approach, Mellor and Durbin (1975) described most former mixed layer theories as 'integral' theories whereby distributed quantities were combined into integral values, involving complicated assumptions concerning the vertical profiles of velocity, temperature, heat flux and stress. They argued that such integral theories did not predict the existence of mixed layers and thermoclines as a consequence of oceanic boundary conditions.

Although they acknowledged the computational requirement of integral representations of mixed layer dynamics for general oceanic circulation models, they proposed a one dimensional unsteady model through solving a number of boundary layer conditions over space and time. In their viscosity-independent work, they examined the response of impulsive wind stress on their model and determined that molecular viscosity values of v from 0.134 to 10 cm^2/s (a factor of ten greater), all yielded the same results, with higher values tending to smooth the result (see ***Figure 2-2***).

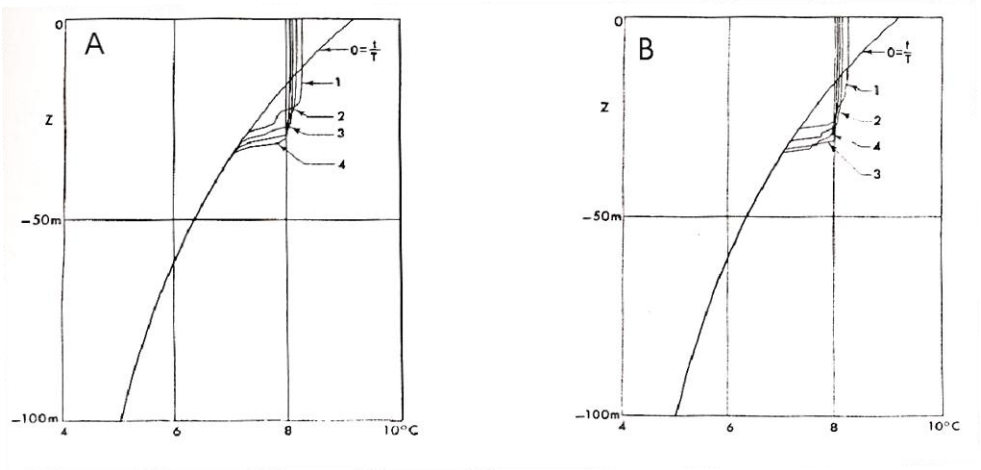

Figure 2-2: *(A) Time stepped variations in temperature due to an impulsive wind (wind stress = 2* N/m^2 *when t > 0) using a boundary conditions model as proposed by Mellor and Durbin (1975), (B) same as for A, except that the values of molecular viscosity were used.*

The contribution of wind- induced vertical mixing on heating and cooling of surface water can be seen in ***Figure 2-3***. This is evident when thermoclines are forced deeper by increased wind stress from *1* to 2 N/m^2 *as* seen in ***Figure 2-3*** (B). This vertical mixing variability, a consequence of wind stress changes, likely contribute to the variability of the wind mixed layer and can also be seen in this study. This is further evidenced in the seasonal wind stress curl seen in ***Figure 4-10*** and the variability in the measured vertically mixed surface water seen as hind casts in ***Figure 7-3***.

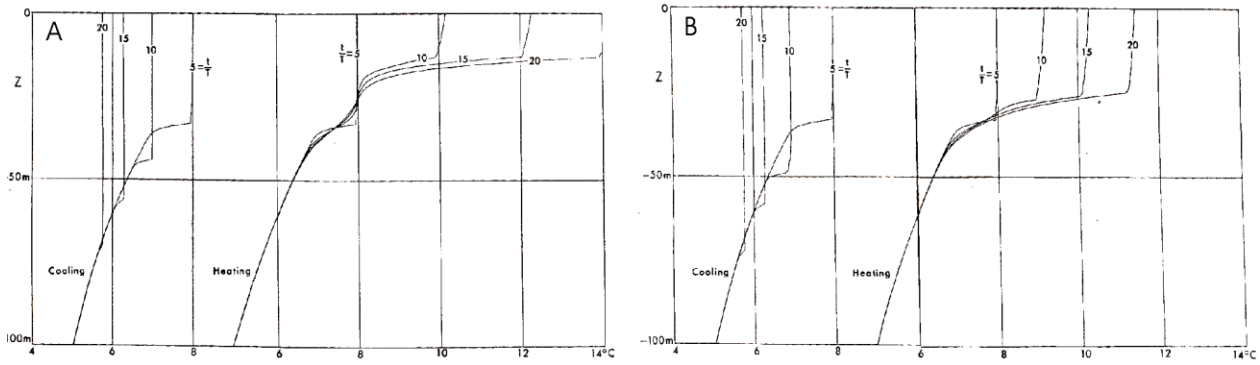

Figure 2-3: *(A) The effect of sudden heating or cooling with wind stress = 1* N/m^2 *(B) The effect of sudden heating or cooling with wind stress =* 2 N/m^2*, Mellor and Durbin (1975).*

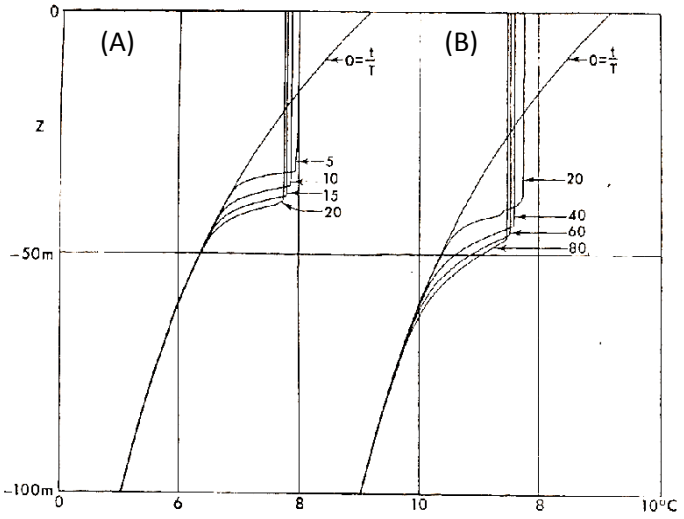

Figure 2-4: *Time stepped variations in temperature due to an impulsive wind (wind stress = 2* N/m^2 *when t > 0) using a boundary conditions model as proposed by Mellor and Durbin (1975). Plot (A) is t/T = 0.25 and (B) is t/T= 1, as explained in the text.*

As a test of their model's response to impulsive wind, they examined 2 scenarios, one using $t/T = 0.25$ and another using $t/T = 1$ where t=time and $T = 2\pi f^{-1}$ is the inertial period with $f = 10^{-4}\, s^{-1}$. Their results are shown in ***Figure 2-4*** depicting progressive deepening of the wind mixed layer due to increasing impulsive wind times.

By conducting in-situ measurements they were able to compare their computational methods with an "after-the-wind-stopped" scenario, in which it was found that no further deepening of the mixing layer took place. Another application was tested, where they maintained a constant wind stress of 2 N/m^2 over a number of time steps, with sudden input of surface heating and cooling heat flux. The results were shown as a comparison of computed versus observed isotherms on a time-depth plot at an observed station over a period of more than a month, which showed remarkable agreement (see ***Figure 2-5***).

Posmentier (1980) used a numerical model to investigate the warming of the mixed layer during early summer. It was proposed that …"the structure consists of two layers separated by a thermocline, across which there is both downward diffusion of heat and upward entrainment of the lower layer by the warmer upper layer". Through numerical experiments, a 'limiting Richardson number' = 0.6 was referred to. This corresponded with temperature gradients where heat flux was at a maximum and proportional to the vertical velocity squared.

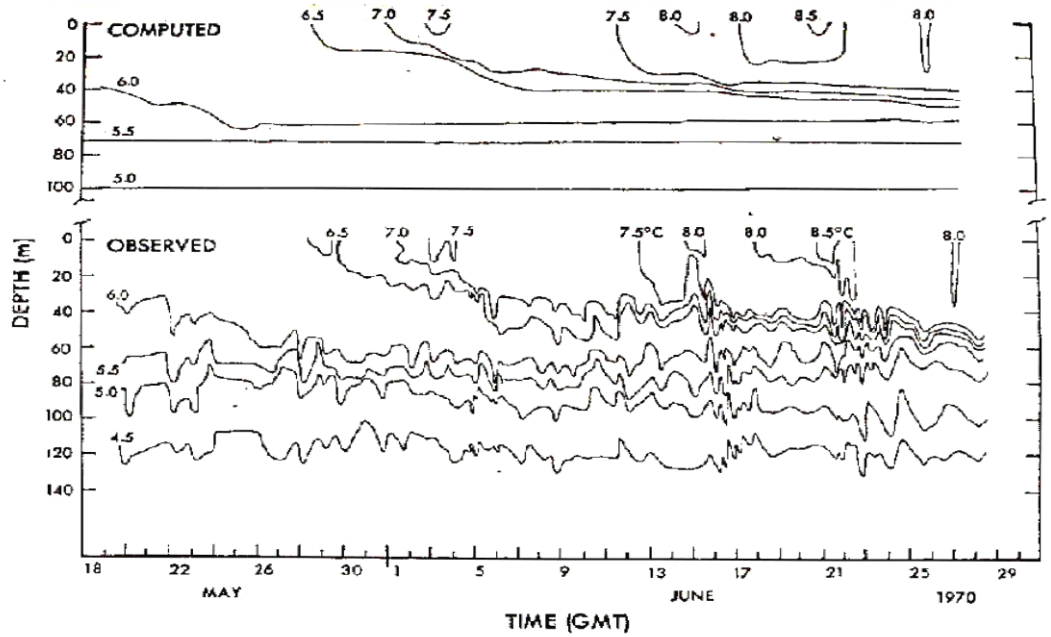

Figure 2-5: *Comparison of computed and observed time-depth contours at a monitoring site in the Sea of Okhotsk NNE of Japan, after Mellor and Durbin (1975).*

The model showed that low surface heat fluxes throughout early summer resulted in weak vertical warming. In contrast, high surface heat flux resulted in stronger vertical warming, confined to the surface layer. As a result, the significance of a 6-day period of strong surface heating at spring and early summer and its warming persistence throughout summer is noted. It was concluded that surface heat flux variations can have significant impact on the biological and chemical equilibrium in and below the mixed layer.

Pacanowski and Philander (1981), noted the rather crude nature of the constant values for the coefficients of vertical eddy viscosity (v) and eddy diffusivity (k) as first proposed by Kraus and Turner (1967). In addition, they found the value of v to vary from 30 - 100 cm^2/s in the mixed layer of the Atlantic North Equatorial Counter current and suggested that v ranges from 2 - 11 cm^2/s in a region of very small vertical density gradients. Similar values for v were suggested (about 1 cm^2/s above and 8 - 100 cm^2/s within the core of the undercurrent) by other authors in Pacanowski and Philander (1981).

Galperin et al (1987) refined the so called Mellor-Yamada hierarchy of the turbulent 2.5 level closure model and proposed a more robust quasi equilibrium model that made use of turbulent energy formulations.

Rosati and Miyakoda (1988) used equations originally developed by Bryan (1969) and Mellor-Yamada level 2.5 turbulence closure scheme, as well as horizontal non- linear viscosity to develop a general ocean circulation model. They used 12 vertical levels that thickened with depth. Instead of using a prescribed SST and determining downward heat flux using some eddy diffusion coefficient, they were interested in simulating the SST value. This meant that they were required to estimate the surface heat budget from available atmospheric and oceanic data. In their words, "Many researchers have tried to derive empirical equations relating the elements of standard marine meteorological observations to the heat budget of the ocean surface. All the equations suffer from a lack of accurate measurements of the budget components". Their strategy was therefore to only use formulae that were derived and verified with observations.

Derber and Rosati (1989) proposed a data assimilation system for producing seasonal forecasts, primarily to initialise coupled ocean atmosphere models such as those as developed by Rosati and Miyakoda (1988). Although in its infancy at the time, it showed good potential even though the system was restricted by poor data coverage for SST, altimeter and current measurements. The authors noted that ocean dynamics are very different in regions near the coast or in areas of strongly sloping bottom topography.

Rahmstorf (1992) applied a vertical mixing model to a location off the west coast of South Island, New Zealand, with the aim of simulating the seasonal cycle of temperature and mixed layer depth (see Appendix H for mixed layer depth) in the region. Using weather observation data to drive the model and observations from research ships, satellites and moored temperature sensors, Rahmstorf was able to show that seasonal variations in the depth of the mixed layer and temperature could be explained by solar forcing and local air-sea heat exchange, extending to a depth of approximately 20 m. Whereas the mixing depth of 140 - 200 m depends more on convection than wind in winter. Variability caused by advection from local effects of continental shelf waves and transient currents was superimposed on the signal.

The above introduction to fluid dynamics provided some insight into the natural physical processes responsible for vertical thermal profile structures, as well as a descriptive account of the creation, development and decay of these profiles. An ideal case is described, starting with a typical cool well-mixed water column, such as exists at mid-latitudes in winter (see profile (A) in **Figure 2-6**), created by ambient cooling and wind mixing affects. In the months that follow, the winter storms have mostly abated, reducing wind and wave mixing, while surface waters are heated slightly by the more

perpendicular angle of the sun. This results in the start of a weak surface thermocline as seen in profile (B) of **Figure 2-6**.

However wind events are not restricted to winter months and once a thermocline has formed due to surface heating in spring, the wind acts to mix and break down the thermocline as it appears to cool the surface waters by mixing it with cooler water below. Seasonal heating and vertical wind mixing processes therefore tend to oppose one another and create distinctive signatures in the vertical temperature profile structure that remain as remnant sinking (negatively buoyant) features long after the wind event has passed. This is schematically shown as profile (C) of **Figure 2-6**. A peak in mid-summer heating results in sea surface water temperatures also reaching a maximum value, with similar maximum thermocline development as seen by profile (D) of **Figure 2-6**.

On occasions where day/night temperature differences are large, evening surface water cooling and midday heating may occur, resulting in micro-structures or 'steps' in the profile shape that are also propagated downwards in the water column along the thermocline. During this time of the year, wind (and wave) episodic events may continue to 'disrupt' the tending parabolic shape of the upper profile, forcing warmer water downward in the water column and mixing it with cooler sub-surface layers, creating a more 'noisy' structure. These remnant mixing events may appear as 'step-like' functions in the profile shape. Whatever shape the remnants take on in the profile plot, their affect is reduced in time and depth, so that they are barely detectable towards the lower part of the thermocline and become completely mixed (disappear) at the maximum thermocline depth. This is seen in profile (E) of **Figure 2-6**.

During Autumn, the profile shape is tending back towards its winter well mixed (and cool) shape as surface cooling takes place in response to the reduced incident angle of the sun's rays. Weak thermoclines are observed, similar to those seen during spring. This is the third phase that represents the demise of the thermocline structure as winter approaches and the cycle is repeated. See profile (F) in **Figure 2-6**.

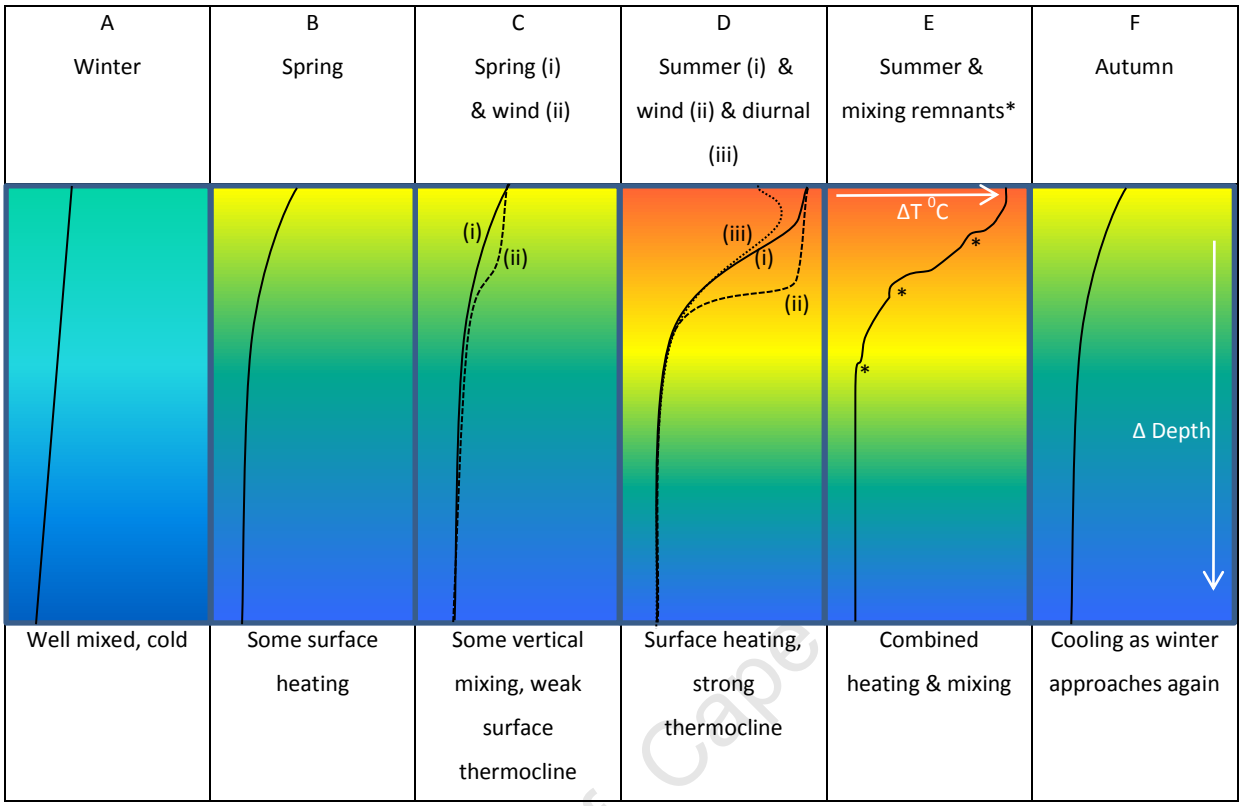

Figure 2-6: *Schematic showing generalized seasonal heating and cooling in the water column, with associated temperature-depth plots and contributing factors to changing profile shapes*.

In reality, observed profiles are indicators of physical changes that have preceded the measurement and are changed by many factors such as those mentioned above, but also influenced by advection of other water masses, depth of water, localised topography and others.

In conclusion, this introduction to the prediction of thermal profiles showed some of the preceding scientific progress in the fields of fluid dynamics and the application of equations to describe diffusion, eddy viscosity and diffusivity, heat flux and wind stress vertical mixing in the water column. As follow-on in the next section, these first principles as largely accepted and focus is shifted to techniques developed and progress made to define and describe numerical and statistical parameters that represent the real world. Here a review of prior research that describes the shape, variability and absolute values as derived temperature profiles, is examined.

b. Derived upper ocean temperatures and related techniques

In the previous section emphasis was placed on understanding the natural physical processes and the development of mathematical methods and models to describe and hence predict these processes and the resultant water column structure. In this section we examine derived profile methodologies in chronological order that largely ignore the process and concentrate instead on defining the statistical or mathematical features of the water column. Seasonal or monthly climatologically measured information (also termed static information) is used to establish a 'baseline' of statistical parameters that describes vertical temperature structures as input to a derived profile. This is defined as a derived parameterisation method.

Certain references shown in this section are not directly comparable with the methods used in this study. They are however also included here for completeness of depicting the range of parametric methods used to derive water column profiles and their respective assimilation success using Root Mean Square (RMS) as a common statistical tool. See Appendix H for a description of RMS.

It appears that the first published initiative to derive temperature profiles from sea surface parameters was by Khedouri and Szczechowki (1983). They used expendable bathythermograph datasets from repeated Gulf Stream crossings, originally collected as ground truth for the GEOSS-3 satellite to infer subsurface thermal structure by using dynamic height (see Appendix H) as a function of thermocline depth. The correlation of their results improved with depth, from an r^2 (or RMS) value of 0.84 °C for SST to 0.94 °C for temperature at 700 m. Temperatures between 100 m and 450 m were computed from mean dynamic heights, with a standard error of 0.51 °C. By using historic data, temperatures between 100 m and 450 m depths were computed using temporal dynamic height variability, with a standard error of 0.47 °C.

Feidler (1988) analysed bottle temperature data from the California Current for surface manifestations of vertical and subsurface mesoscale structure. It was concluded that surface temperature gave little useful information about the mixed layer depth. However some aspects of the subsurface structure portrayed surface manifestations potentially detectable by satellite sensors.

Later Carnes and Mitchell (1990) noted that the purely statistical methods of Khedouri and Szczechowki (1983) had shown only marginal success and in their paper compared derived synthetic temperature profiles from Geosat altimeter data with air-dropped expendable bathythermograph

profiles and proposed that sea surface height (see Appendix H) was an accurate indicator of subsurface temperature structure. They based their outcome on earlier published research where the statistical relationship between dynamic height (see Appendix H) at the surface and temperature at standard depths was constructed. They assembled profiles into monthly subsets and interpolated the data into 17 standard depths from the surface to 1000 m. Two Empirical Orthogonal Functions (EOF)-(see Appendix H) of vertical temperature profiles were computed across the Gulf Stream. The EOF amplitudes as a nearly linear function of dynamic height were used to generate synthetic temperature at any standard depth. Results were compared with observed profile values which showed a typical intra-seasonal pattern, with the smallest differences clustered at each side of the Gulf Stream front. Highest differences were found in the data-sparse region within the front and the lowest amplitude heights in the transition region between the slope and shelf water types. Root Mean Square (RMS) was used as a generally accepted statistical technique for comparing derived and observed temperatures.

Carnes and Mitchell (1990) achieved a RMS temperature error versus depth between the true and synthetic profile of between about 1 °C and 2.5 °C that decreased generally to about 0.8 °C below 200 m. The higher value of 2.5 °C is not however depicted in ***Figure 2-7*** where only 4 of the 12 months are shown. Seasonal differences were minor, except near the surface where errors were largest in January and April (see ***Figure 2-7*** (A) for the 4 months displayed). The complete monthly dataset as a mean RMS per month is shown in ***Figure 2-7*** (B) indicated as a maximum of 1.8 °C for the month of March.

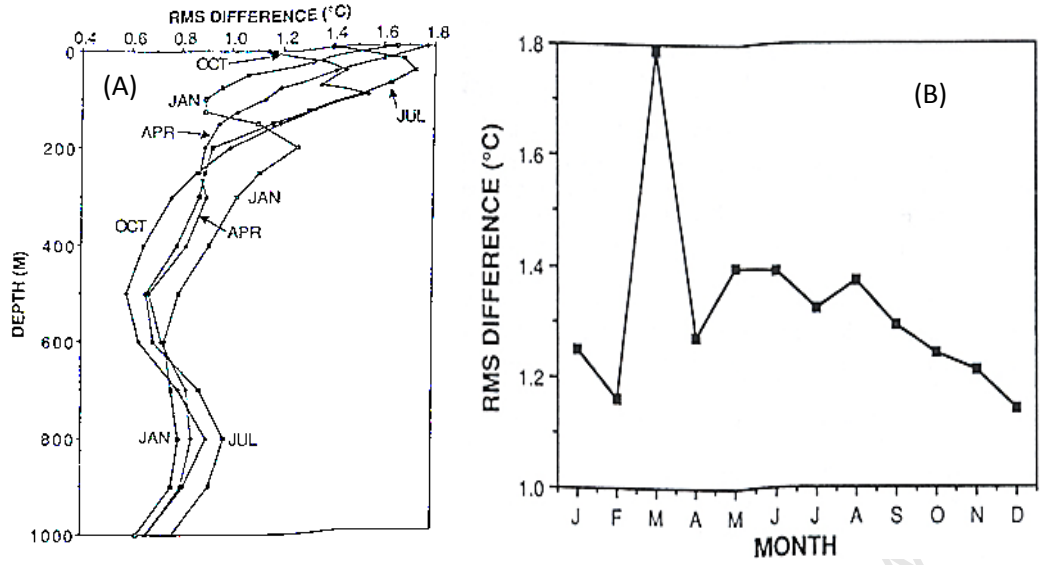

Figure 2-7: *The left hand plot (A) shows mean RMS temperature differences for 4 months, for all profiles and depths, between synthetic and actual measured profiles across the Gulf Stream. The right hand side plot (B), shows RMS values between synthetic and observed temperature for all months, after Carnes and Mitchell (1990).*

Chu et al (2000) of The Department of Oceanography, Naval Postgraduate School, Monterey California, undertook a study which resembles the concept and hypothesis of this research (see ***Figure 2-8***). In their research, they used a parametric model for determining sub-surface thermal structures from satellite sea surface temperature observations. Using curve fitting functions to represent features of the profile as developed by Teague et al (1990), profile data sets were compressed into a set of coefficients. These were based on a mixed layer structure, thermocline and deep water layer, and defined as seven specific parameters per profile, such as SST, mixed layer depth (MLD), thermocline bottom depth (TBD), thermocline temperature gradient (TTG), lower layer stratification, and deep layer temperature.

Thermal parametric model expressed as:

Ts – Gth (h2 – h1) = Tb

Where:

Ts = Temperature at the surface

Gth = Thermocline gradient

h2 = Upper depth or start of the thermocline,

also referred to as the mixed layer depth

h1 = Lower depth or maximum or bottom of the thermocline

Tb = Temperature at the bottom or in the deep layer

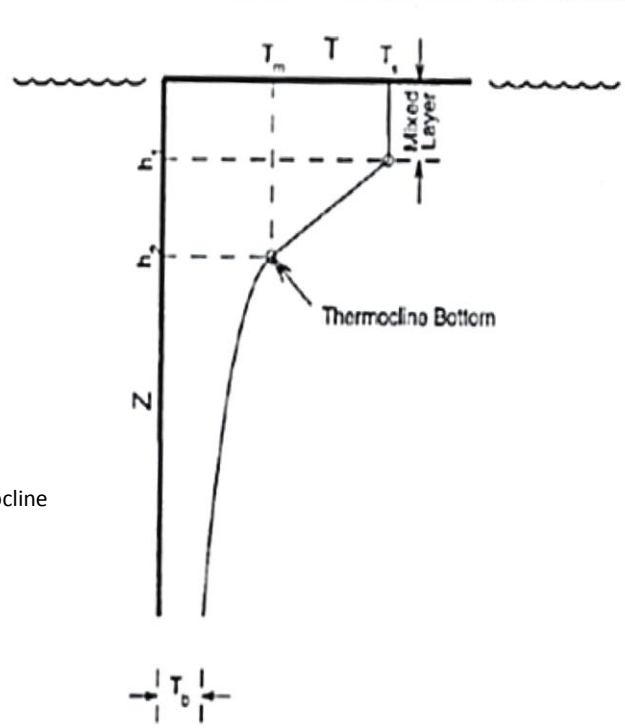

Figure 2-8: *Thermal parametric model as defined by Chu et al (2000).*

The US Navy's MOODS (Master Oceanographic Observation Data Set) dataset for the month of May in the South China Sea was used to validate their model. The dataset was conveniently separated into 1° x 1° grids and used to compute a mean and climatological standard deviation (SDV) profile using a regression method. Standard deviation of climatological profiles was used as a criterion for model validity. This so-called multi timescale inverse method (thermal parametric model) used Ts (or SST) from a satellite observation, and hence determining h1 and therefore the vertical profile from the parametric model formulae.

Using 40 inverted profiles they found that the observed profiles agreed quite well (RMS of 0.72 °C) compared to the regression method (RMS of 1.06 °C) and the climatological SDV result (RMS of 1.51 °C). They concluded that this result, including the high positive correlation (0.79) made the multi timescale inverse method valid for practical use. Results of their research are shown in ***Figure 2-9***. It is also of lesser comparative value for this study since it is based on the use of climatological profile data for a single month as its source, representing a spatial coverage of only 120 NM^2 for each block. In contrast, this study uses a more extensive area (36 000 NM^2) for all months, based on a grouping or categorisation of 15 profile types. For that reason, ***Figure 2-9*** is used here as background

information only and will not play any further comparative role in this study (see section 7. d, ***Table 9*** and ***Table 10***)

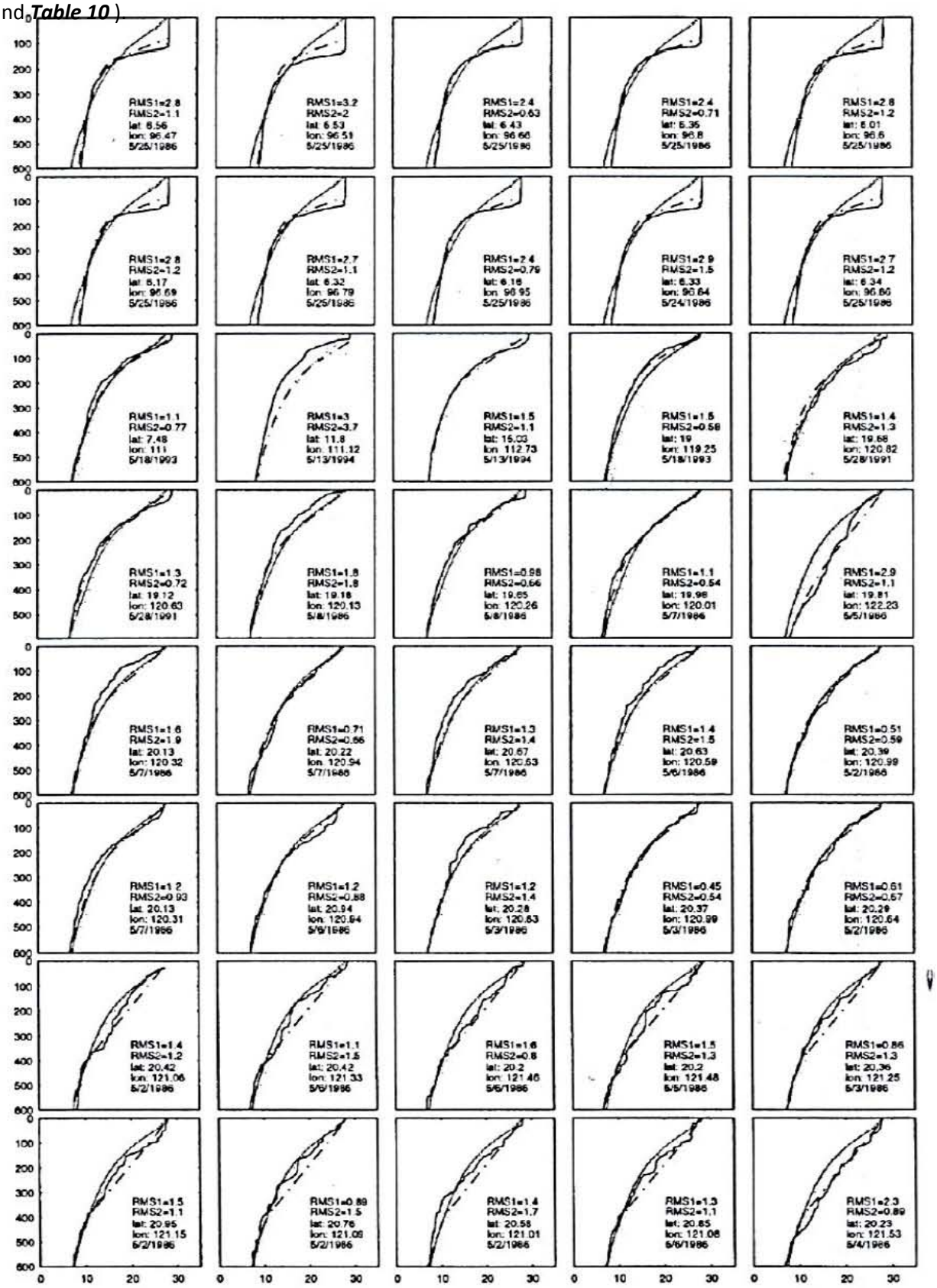

Figure 2-9: *Comparison between 40 regressed (dotted), inverted (dash-dotted) and observed (solid) profiles. After Chu et al (2000).*

In a similar approach using data collected in South African waters, Silulwane et al (2001) also used a parameterising method to describe subsurface chlorophyll concentrations (see Appendix H) in the water column by fitting a Gaussian curve to profile shapes. In this case four parameters were identified. These were: (1) The shape of the curve, (2) the background chlorophyll concentration, (3) the height parameter of the peak and (4) the depth of the chlorophyll peak. As a novel proof of concept, they then used an artificial neural network and Self Organising Maps (SOM) to characterize in-situ vertical profiles in the ocean, based on the curves identified. The technique was described as being more impartial than subjectively grouping profiles into classes. Output was easy to interpret compared to conventional multivariate techniques such as principle components, multi-dimensional scaling and cluster analysis. They reported that the SOM method made it possible to visualise large datasets consisting of potentially thousands of profiles.

In their discussion of 60 profile characteristics within the Benguela system, they found that a single profile was insufficient to capture the variability in chlorophyll patterns. Furthermore, they concluded that the shape of the vertical chlorophyll profiles was related to SST, surface chlorophyll, mixed layer depth and euphotic layer depth. Hence frequency maps from a SOM output were used semi-quantitatively to predict the probability of varying profile shapes at a particular level of an environmental variable. The profiles used by Silulwane et al (2001) were mostly measured on the continental shelf, shallower than those used in this study and covering more than double the latitude range (from Cape Columbine to the Kunene River).

Even though SOMs were used, they represent a completely different variable (chlorophyll a), the spatial coverage is vastly different, their data is limited to 'on-shelf' and small input dataset all contribute to lack of comparability with this study. The outputs from their SOM were also in units not easily comparable to this study. Graphics from their study were intentionally not provided here for the same reasons. The reference was used here as background information only.

Rhodes et al (2002) used 4900 XBT (Expendable Bathy Thermograph) and CTD (Conductivity Temperature Depth) measurements collected worldwide in January and February 2001 to independently evaluate their synthetic profiles. These were calculated using the Modular Ocean Data Assimilation System (MODAS) and Naval Research Laboratory Layered Ocean Model (NLOM) Sea Surface Height (SSH). Their results are shown in ***Figure 2-10***, especially with 'cut-outs' interpreted in (A) and (B) as referenced in the comparative testing section 7. d and ***Table 10***.

In a similar approach to Silulwane et al (2001), Richardson et al (2002) used an artificial neural network technique to identify classes of vertical chlorophyll *a* profiles in the coastal Benguela current domain and then classified profiles accordingly (see ***Figure 2-11***). Although the method is similar to that used in this study, the characteristic Gaussian curve shape and characteristics of chlorophyll *a* profiles differs significantly from that of temperature profiles. They were also more sparsely sampled and not comparable with temperature profile units. For their analysis of 155 profiles, they used a learning rate of 0.2, radius of 2 and 100 000 training steps or cycles to produce a suitable continuum of profile patterns. Although their results cannot be compared with temperature profile classifications, the unique application of their technique to oceanic data is similar to this study in some respects. Their method also differed from this study since they used a parametric method of fitting of a Gaussian curve to their vertical profile data.

In their discussion, they deal extensively with the challenges and limitations of using SOMS for this purpose. These are also addressed later in the data processing section of this thesis. They proposed that their approach could be used in a semi-quantitative manner to predict the subsurface Chlorophyll a field from known (water column depth) or easily measured variables from satellite such as sea temperature or chlorophyll.

The techniques used by Silulwane et al (2001) and Richardson et al (2002), as with the previous technique mentioned, are considered of minimal comparative benefit to the outcome of this study.

The technique however also used SOM to deduce vertical profiles, albeit chlorophyll a and not temperature. The lessons learnt from their method were of value in the devlopment of the the approach used in this study. Their results are provided here as background information only and will not play any further comparative role in this study. For this reason, they are therefore not depicted in section 7. d, ***Table 9*** and ***Table 10***).

No other cited chlorophyll predictive techniques were added due to these extensive differences noted.

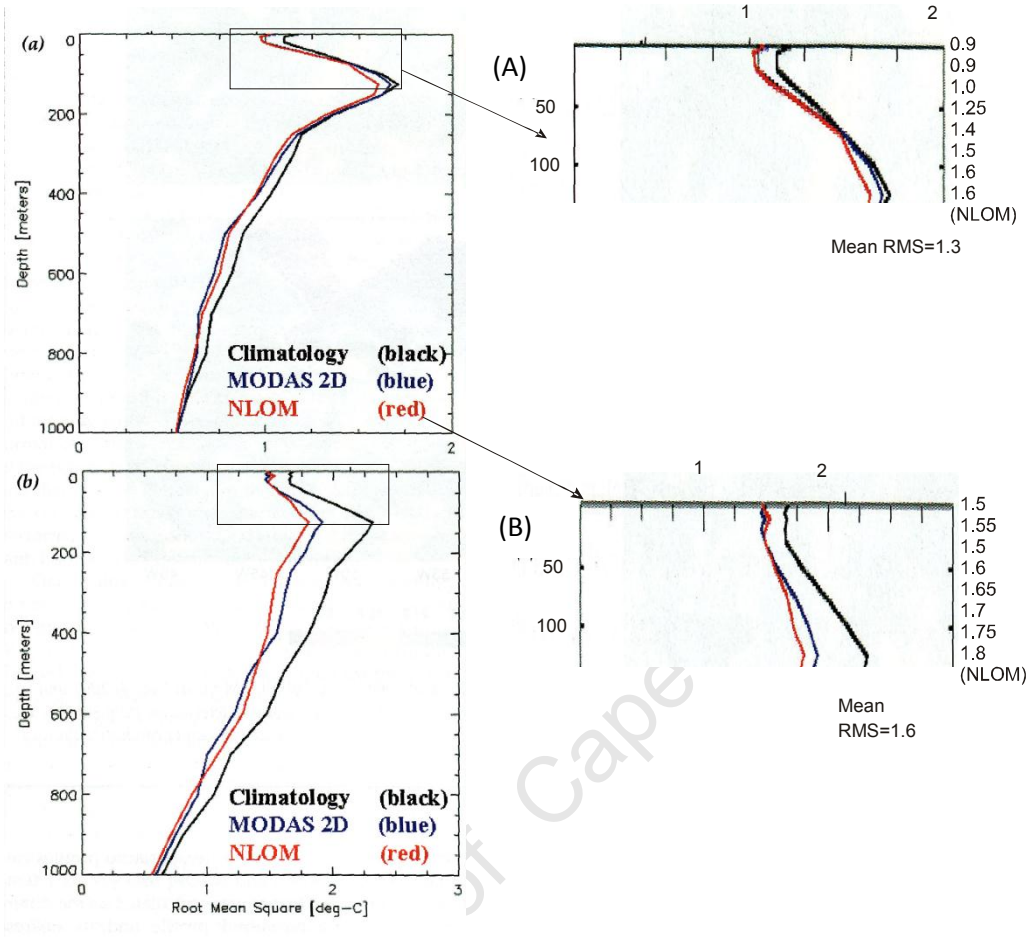

Figure 2-10: *After Rhodes et al (2002), showing RMS temperature error (^{0}C) vs. depth (meters) for MODAS climatology (black) and MODAS synthetic profiles calculated using MODAS 2-D SSH (blue) and NLOM SSH (red) compared with a) 4900 unassimilated global XBTs from January and February, 2001 and b) a subset of the global XBTs (~800 m) where MODAS and NLOM SSH at XBT location were both > 7 cm away from the climatological SSH. Inserts (A) and (B) were not part of the original figure. They are 'cut-outs' of the original graphic, with manually interpreted NLOM (shown in red) RMS values extracted and expanded here for comparative purposes and used as part of the validation discussion in* ***Table 10*** .

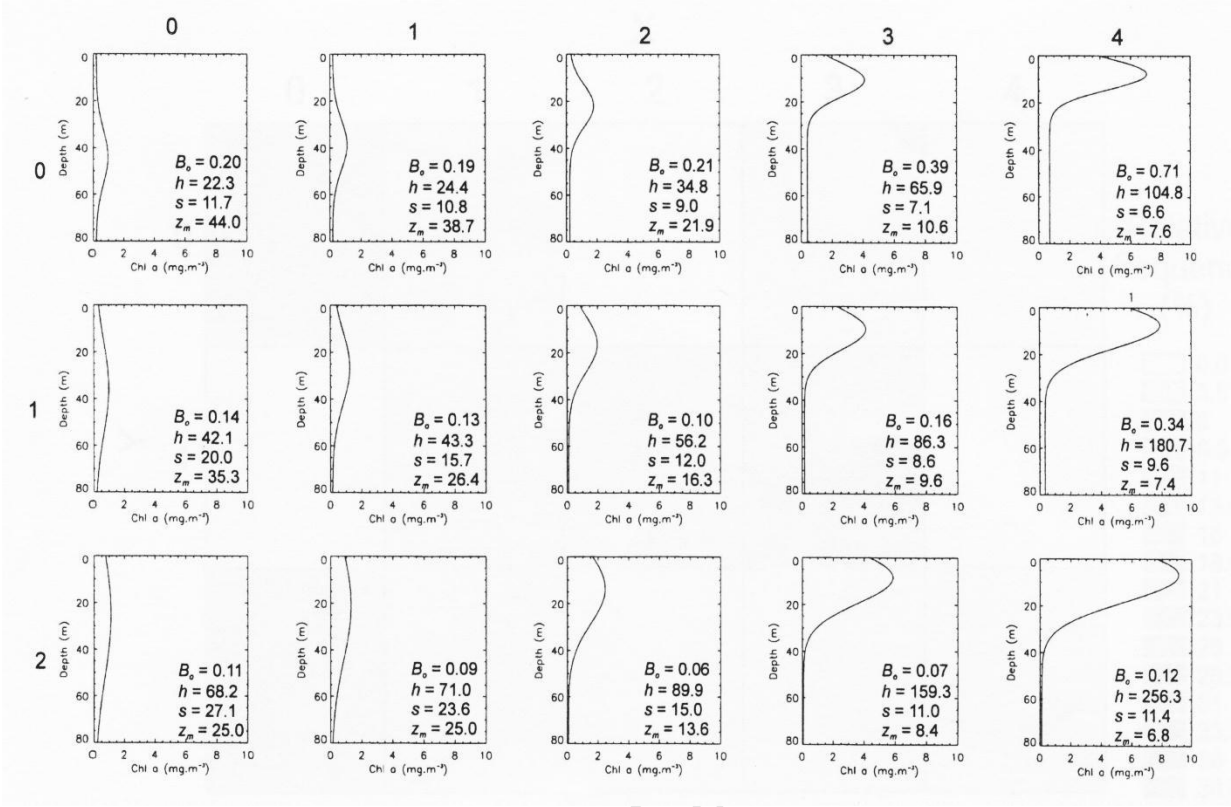

Figure 2-11: *The output map of a 5 x 3 SOM using 155 Chlorophyll a profiles described by 4 parameters (B_0 – background Chlorophyll concentration, h – total Chlorophyll concentration within the peak ,s-the standard deviation round the peak and z_m is the depth of the chlorophyll peak) of the shifted Gaussian curve as input. After Richardson et al (2002).*

Levitus was the first global climatological set of profiles published. The datsets were sourced from the National Oceanographic Data Center (NODC). A number of updates were incorporated between 1982 (inception) and 1998. The data was analysed on monthly, seasonal and annual time scales, gridded in 1° latitude-longitude cells from the surface to 5500 m water depth, after Fox et al (2002).

The Generalised Digital Environmental Model (GDEM) was developed at the Naval Oceangraphic Office and also provides global profile coverage of temperature and salinity. Grid sizes range from 1/2° to 1/6° latitude-longitude.

Fox et al (2002) of the Naval Research Laboratory described MODAS (Modular Ocean Data Assimilation System) as used by the U.S Navy for depiction of 3-dimensional fields of temperature and salinity over the global ocean. They noted that static climatologies cannot usually provide an accurate picture of present day conditions, however when updated with SST and SSH measurements

from satellite, their Dynamic MODAS (Dy. MODAS) model was able to portray an improved day-to-day estimate of ocean thermal conditions (see **Figure 2-12**).

The MODAS_Syn is a synthetic temperature profile generated from the sum of the climatological profile and the SSH and SST deviations from the climatological mean for a specific location.

The methodology for the construction of MODAS was described and compared with Levitus and Generalised Digital Environmental Model (GDEM – see Appendix H) climatologies, as well as observations of temperature and salinity from SeaSoar (direct measurements) in the Japan/East Sea (JES) to illustrate MODAS capabilities.

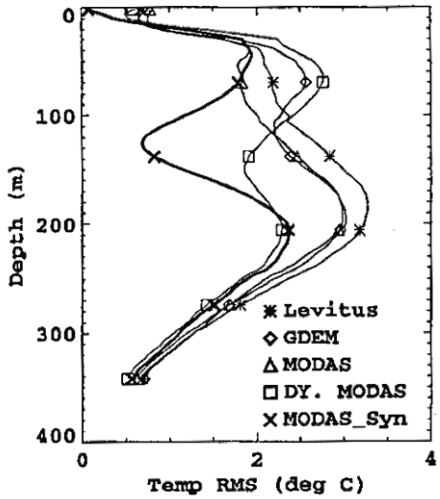

Figure 2-12: *RMS error values from various data assimilation methods of temperature profiles across the Japan/East Sea during May-June 1999, compared with observations from SeaSoar, after Fox et al (2002).Manually interpreted values from the plot (not provided in the original graphic) are presented in* ***Table 1****. The plot labels are described in the text above.*

In their evaluation of the MODAS performance, Fox et al (2002) used observations acquired from a 400 km-long section in the region of the subpolar front of the Japan/East Sea during May-June 1999 using a towed, undulating profiler (SeaSoar). Measurements were processed to yield vertical profiles with approximatly 3 km horizontal and 4 m vertical resolution. Processing was restricted to 400 m water depth since the Japan/East Sea waters are known to be nearly homogeneous below that depth. This method is also not directly comparable with the methods used in this study, but included here for completeness of depicting yet another parametric method. These results after Fox et al (2002) for temperature profiles are shown as RMS error values in **Figure 2-12**. ***Table 1*** is the

manual interpretation of the values from the plot (not provided in the original graphic) and referenced extensively later in the comparative testing section, 7. d and ***Table 10*** .

Depth (m)	Levitus	GDEM	MODAS	Dy. MODAS	MODAS_Syn
0	-	-	0.8	-	0.1
10	0.6	-	0.7	-	0.4
20	0.8	0.8	0.8	0.8	1.25
30	1.4	1.8	1.8	2	1.8
40	2	2.25	1.9	2.5	1.9
50	2.1	2.4	1.8	2.7	1.8
60	2.2	2.6	1.75	2.75	1.8
70	2.2	2.6	1.8	2.75	1.75
80	2.25	2.4	1.85	2.6	1.6
90	2.3	2.35	1.9	2.5	1.3
100	2.4	2.25	2.1	2.4	1.2
110	2.45	2.25	2.2	2.25	0.9
120	2.6	2.25	2.25	2.1	0.8
Mean RMS	1.94	2.18	1.67	2.31	1.32

Table 1*: Showing RMS values for modeled profiles across the Japan/East Sea, manually <u>interpreted</u> from the plot in* ***Figure 2-12*** *for comparative purposes later. Note: These values were not provided in the original publication.*

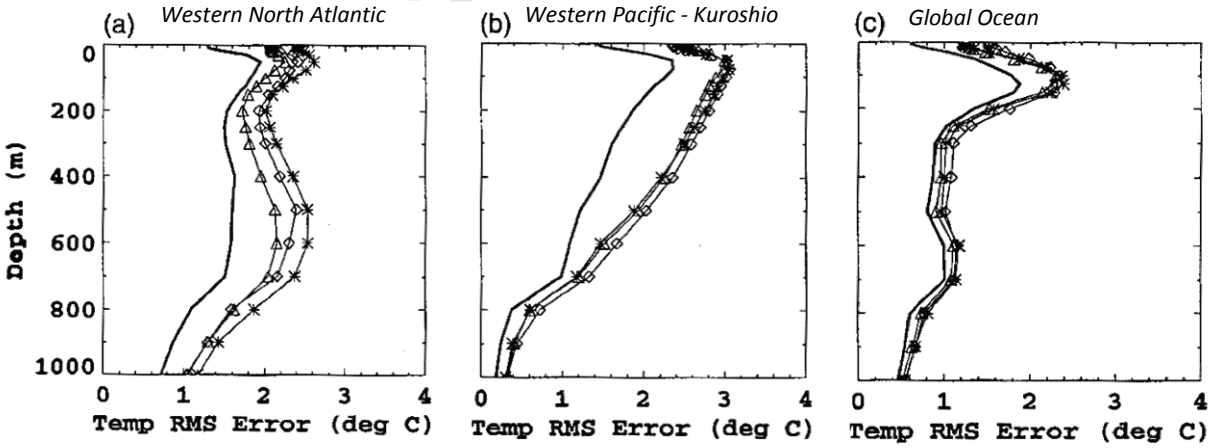

Figure 2-13: *RMS temperature differences between Levitus (asterisk), GDEM (diamond), MODAS (triangle), and Dynamic MODAS (thick line). These differences are shown plotted for (a) Western North Atlantic, (b) Western Pacific- Kuroshio and (c) the Global Ocean, after Fox et al (2002).*

Fox et al (2002) were able to show that dynamic MODAS which used remote sensed data as input, provided a better representation of in situ thermal structure of the "true ocean" than conventional static climatology. This method was considered somewhat comparable to this study and used extensively later in the comparative testing of section 7. d and ***Table 10***.

Depth (m)	Dynamic MODAS in ***Figure 2-13***		
	W N Atlantic	Kuroshio	Global
0	1.3	1.4	0.6
50	2.0	2.2	1.8
100	1.8	1.9	1.2
mean	1.7	1.8	1.2

Table 2: *Showing RMS values for modeled profiles in the Western North Atlantic, Western pacific – Kuroshio and Global Oceans, manually interpreted for 0 m, 50 m and 100 m depths from the plot in* ***Figure 2-13*** *for comparative purposes later. Note: These values were not provided in the original publication.*

Ali et al (2004) used a neural network approach to estimate the temperature-depth structure from sea surface temperature, sea surface height (see Appendix H), wind stress, net radiation and net heat flux. Data was sourced from an Arabian Sea mooring for the period October 1994 to October 1995. Results obtained showed that 50 % of the estimations were within an error of $\pm$ 0.5 ^{0}C and 90 % within $\pm$ 1.0 ^{0}C, with an average RMS error of 0.584 ^{0}C and a depth-wise correlation of 0.92. This appears to be the lowest published RMS value to date using comparable techniques and application. It is postulated that this may be due to the 'enclosed' shape of the Arabian Sea. This area is completely bounded in the north, where the physical dynamics are constrained in the spatial domain, rather than the open ocean where higher temporal-spatial variability exists. Their results are shown in the adapted ***Figure 2-14***.

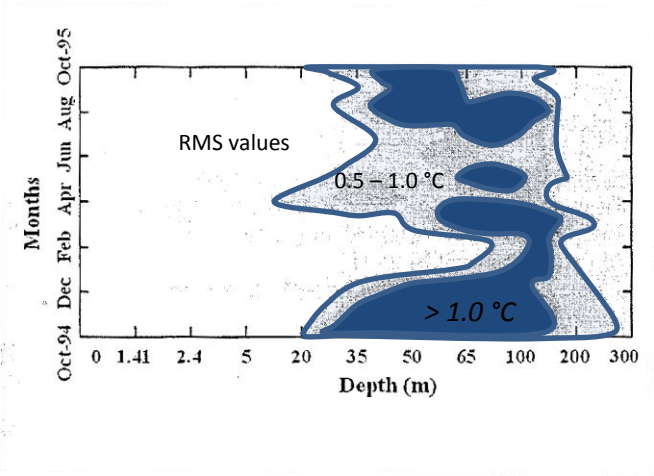

Figure 2-14: *Monthly root mean square errors at various depths below the surface, interpreted from the original graphic by Ali et al (2004). The light blue shaded contoured areas show RMS values of 0.5 °C to 1.0 °C and dark blue contoured areas show all RMS values greater than 1°C.*

The Abs. Error referred to by Ali et al (2004) is assumed here to represent the absolute difference between the measured and assimilated profile which closely approximates their RMS values. These are shown ***Figure 2-15***, together with the standard deviations for the original data, error and ratio. Reduced errors in the upper 25 m and lower 175 – 300 m are clearly evident (see ***Figure 2-16***). Higher standard deviation values occurred in the depth range of 50 – 100 m. Lower RMS values occurred below 200 m water depth and is likely a significant contributor to the overall lower RMS value attained in those results. Another significant contributor to the lower RMS values achieved by Ali et al (2004) is that the data used was sourced from a single point mooring, without indication of the spatial representation of the surrounding conditions. This is also a likely contributor to the reduced RMS values attained in the upper 25 m. Six of the predicted profiles for the months of November, January, March, May July and September are shown in ***Figure 2-16***.

This study specifically excludes such deeper temperature values since where sufficient low standard-deviation historic data exists, these and can instead be 'appended' to the assimilated profile. In addition, this method is constrained in the operational sense by any in-situ, real time data sources such as point source moorings. This method is also not directly comparable with the methods used in this study, but included here for completeness of depicting another parametric method.

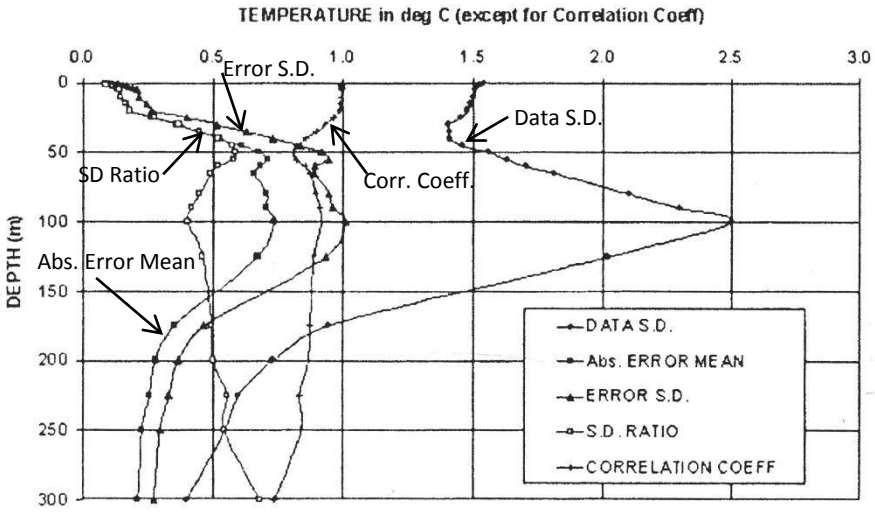

Figure 2-15: *Neural network model summary statistics. After Ali et al (2004).*

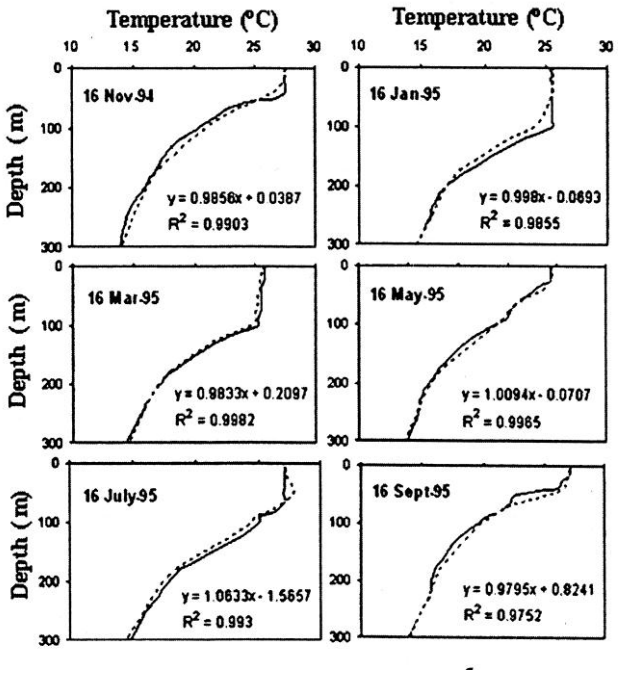

Figure 2-16: *Comparison of observed and predicted temperature profiles at different depths. Solid lines represent the in situ temperatures and dashed lines represent the estimated temperatures. After Ali et al (2004).*

As an early proof-of-concept (pre-study) to this research, Gildenhuÿs and Wainman (2007) showed that by knowing the SST value (potentially from remote sensed satellite sources) and viewing historic temperature-depth profiles as a backdrop for the calendar month of the prediction, it was possible

to coarsely infer vertical profiles using a visual subjective method to construct likely or probable vertical profile polylines (See ***Figure 2-17*** and ***Figure 2-18***).

As hind casts, they used CTD data routinely collected from two inshore-offshore monitoring lines: St Helena Bay Monitoring Line and Cape Point Monitoring Line (CPML), within the South Eastern Atlantic Ocean, within South Africa's Exclusive Economic Zone. Note only plots for the CPML are shown in ***Figure 2-18***. These datasets were collected by The Department of Environmental Affairs, Marine and Coastal Management.

Using that method, mean absolute temperature error values (not RMS error) of 1.0 ^{0}C and 1.5 ^{0}C were achieved. Although the approach was non-quantitative, encouraging results from these explorative conceptual attempts were achieved that provided the basis to pursue the hypothesis presented here and the quantitative methods to follow.

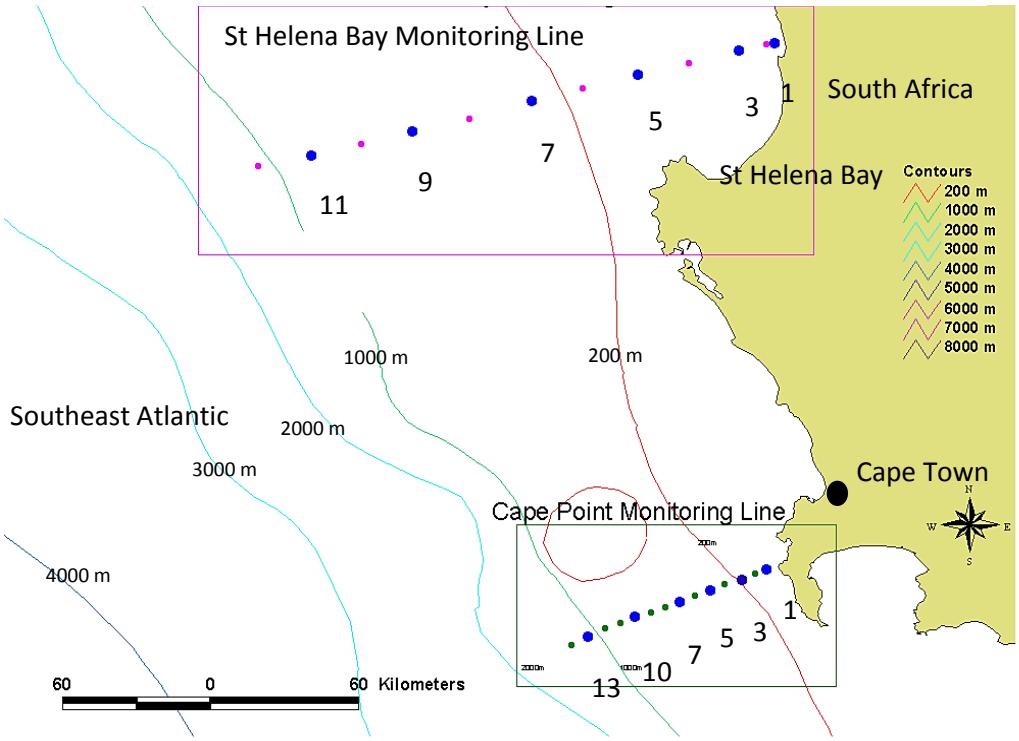

Figure 2-17: *Map showing locations of two monthly CTD monitoring lines (St Helena Bay ML and Cape Point ML in the south east Atlantic) collected by Oceans & Coast (formally Marine & Coastal Management). The stations or profile locations, seen here are marked in blue as used by Gildenhuÿs and Wainman (2007) to predict temperature-depth conditions as proof-of-concept for the numerical methods used in this study. Depth contour values are shown as coloured solid lines, with the edge of the continental shelf (200 m isobath) shown as a solid red line.*

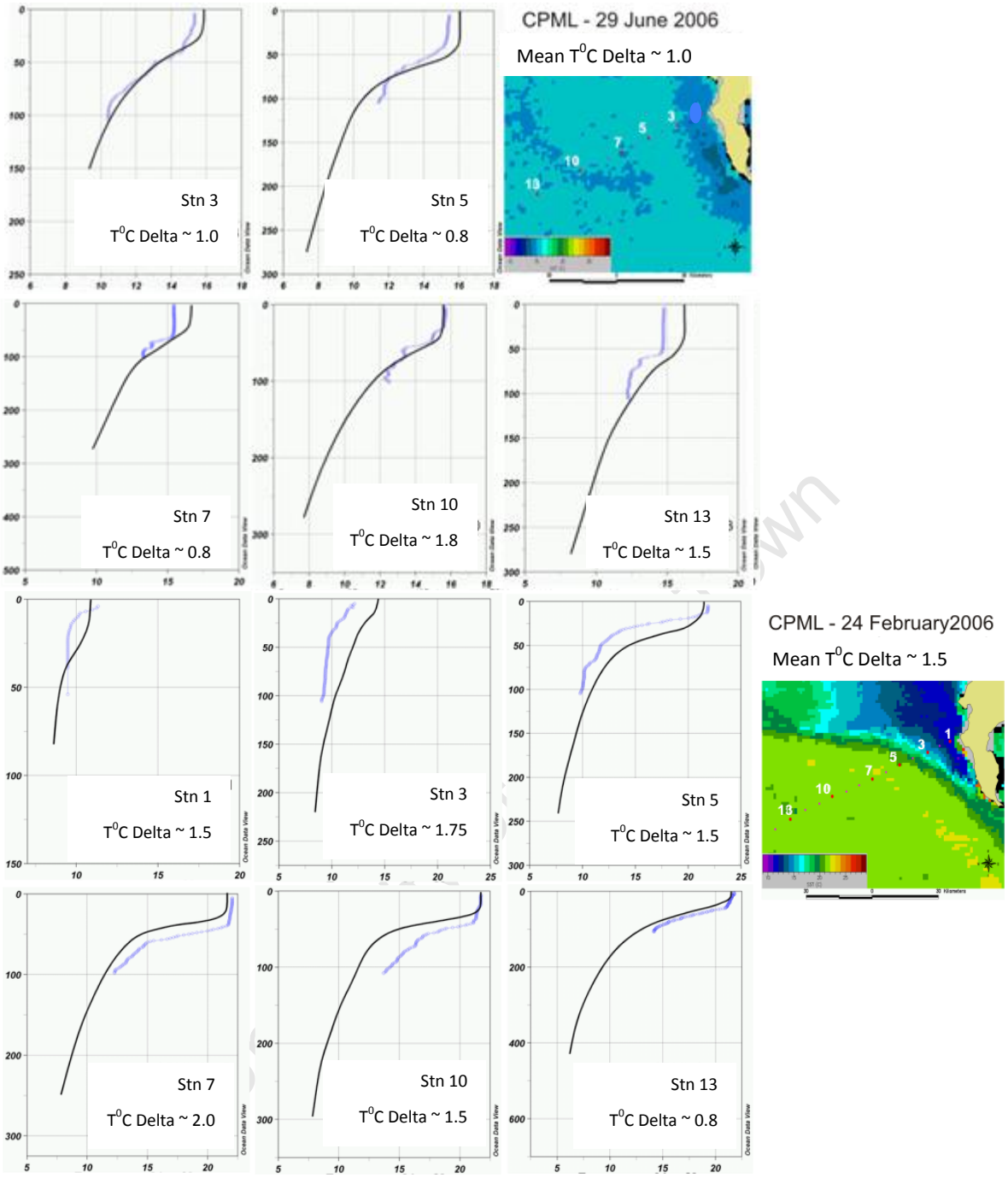

Figure 2-18: *Non-quantitative hind cast predictions as proof-of-concept tested by Gildenhuÿs and Wainman (2007) for CPML on29 June 2006 and 24 February 2006. Blue lines show the measured CTD profiles for temperature vs. depth (indicated as stn. 1[24 Feb. 2006 only], 3, 5, 7, 10 and 13). Black lines are the predicted profiles. Station numbers are indicated as depicted in the map alongside. Note that error values are provided in units of* ^{0}C as temperature differences or deltas – not RMS errors*, with mean delta errors for all profiles on that line for the day displayed in the header. The colour image is a remote sensed SST map for that day, overlaid with the station locations (CPML refers to Cape Point Monitoring Line). Note: No data was unfortunately available for Stn. 1 on 29 June 2006.*

In another approach, Doan et al (2008) used a genetic programming (GP) technique to project sea temperature profiles from sea surface temperature. In their first prediction, they made use of the Levitus98 averaged monthly temperatures for the month of May in the South China Sea, across 17 specific depths from 0 – 1500 m and achieved RMS differences of 0.0262 °C and 0.0287 °C. This appears to be the first time that RMS values have been used to report on average conditions (see ***Table 3*** (A)), and is therefore not comparable with this or similar former studies. In their second prediction, they used the AsiaEx dataset for a 5 and 2 day time period in May 2001, also in the South China Sea, with trained GP profiles from the Levitus98 dataset, to produce mean RMS differences of 0.49 °C and 0.60 °C respectively (see ***Table 3*** (B) and ***Figure 2-19*** (A, B)) .

(A) Prediction accuracy of GP for Levitus98 data

	Nash index (R^2)	RMSE
Training	0.9911	0.0286
Validation: Point 1	0.9923	0.0262
Validation: Point 2	0.9920	0.0287

(B) Performance accuracy of GP: AsiaEx data

Time period	Period	R^2	RMSE
1	3/05/01–8/05/01	0.98986	0.49075
2	14/05/01–16/05/01	0.98586	0.60059

Table 3: *Prediction accuracies for (A) the monthly averaged Levitas98 and (B) AsiaEx datasets. After Doan et al (2008)*

Carnes (2009) described and evaluated the GDEM-V 3.0 climatological model, whereby GDEM2 (an earlier version of GDEM-V 3.0) was defined as fitting a non-linear function of 6 coefficients to profiles in the upper 400 m and then gridding the coefficients of those profiles. Although the technique had some drawbacks, it was described as 'nearly unique' in its attempt to provide a vertically coherent gridding algorithm and was able to "adequately define the sharp changes in sound velocity in the near-surface sound channel". GDEM3 was developed to correct and smooth the vertical gradient (see ***Figure 2-20***) and able to improve the profile fit to a level suitable for their application, although RMS error or correlation coefficient values were unfortunately not provided.

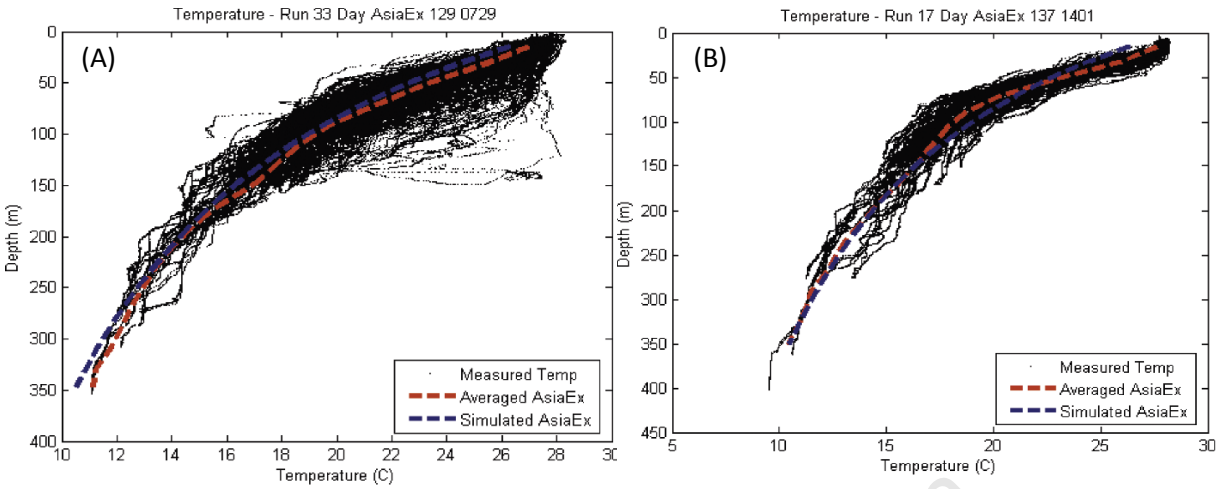

Figure 2-19: *Two predicted temperature profiles using the AsiaEx dataset from a 5 (A) and 2 day time period (B) in May 2001 in the South China Sea using trained GP profiles from the Levitus98 dataset, as shown in* ***Table 3*** *. After Doan et al (2008).*

Carnes (2010), described how GDEM4 was developed as an upgrade from GDEM3, by combining profiles from the Navy's MOODS, World Ocean Database (WOD 2005) and delayed mode Apex profiles (Argo floats), resulting in approximately 8 million profiles from 73 differing instrument types (see ***Table 4***).

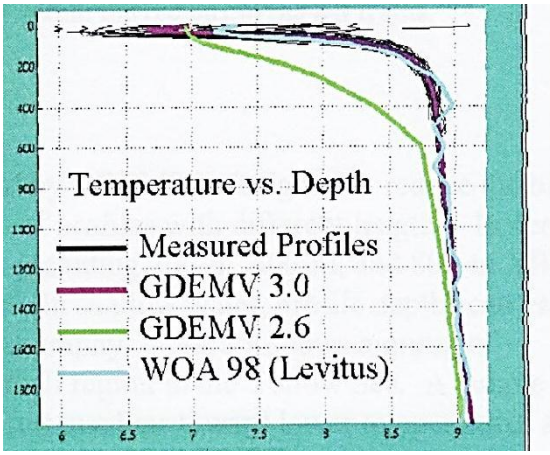

Figure 2-20: *Showing temperature profiles for January, February and March in a sub-region of the Black Sea (shown as black lines) taken from the GDEM-V 3.0 database, with coloured line overlays of various climatology profiles (GDEMV 3.0, GDEMV 2.6 and WOA 98 [Levitus]). After* Carnes (2009).

Instrument Type Number	Description of Instrument Type
1	Message data (regardless of instrument)
2	Mechanical Bathythermograph (MBT)
4	SEABIRD CTD Time Series
5	Air-deployed CTD (AXCTD)
9	Ship deployed AXBT
10	Some unknown electronic temperature depth instrument
11	Expendable bathythermograph
12	Air deployed expendable bathythermograph
13	Submarine deployed expendable bathythermograph (SXBT)
15	Expendable sound velocity profiler (XSV)
18	Time Series XBT (TSXBT)
19	Submarine deployed CTD
25	Hydrocast: bottles and reversing thermometers
30	Unknown electronic salinity, temp., depth instruments
31	Salinity, temperature and depth probe (STD)
32	Low-resolution STD from NODC
33	Conductivity, temperature, depth probe (CTD)
35	CTD time series (YO-YO)
36	Sound velocity, salinity, temp, and depth (SVSTD)
37	Sippican XCTD
38	Seabird CTD SBE-19 (Seacat profiler)
41	Seabird CTD SBE-911 (deep ocean)
42	Seabird CTD SBE-25
43	Falmouth CTD
51	Argo/Palace floats
62	tesac RTDHS message data
64	Palace/Apex floats RTDHS message data
65	Glider RTDHS message data
68	Autonomous Pinniped Buoy (APB)
69	Moored buoy (MRB)
70	Drifting buoy (DRB)
71	Undulating ocean recorder (UOR)
73	Unknown instrument

Table 4: *Description of measurement instrument types as used in the GDEM4 climatology database. After Carnes (2010).*

In ***Figure 2-21*** after Carnes (2010), it can be seen that the world distribution of profiles is strongly biased towards the northern hemisphere, in the eastern and western boundaries of the North Atlantic and Pacific Oceans, as well as the Mediterranean. In contrast only 3 of the squares, with greater than 400 profiles per block appear in the southern hemisphere. These are South Eastern Australia, near Papua New Guinea and South Eastern Atlantic off South Africa. This is especially significant since the profiles shown in the South African block are probably many of the profiles used in this study (not confirmed).

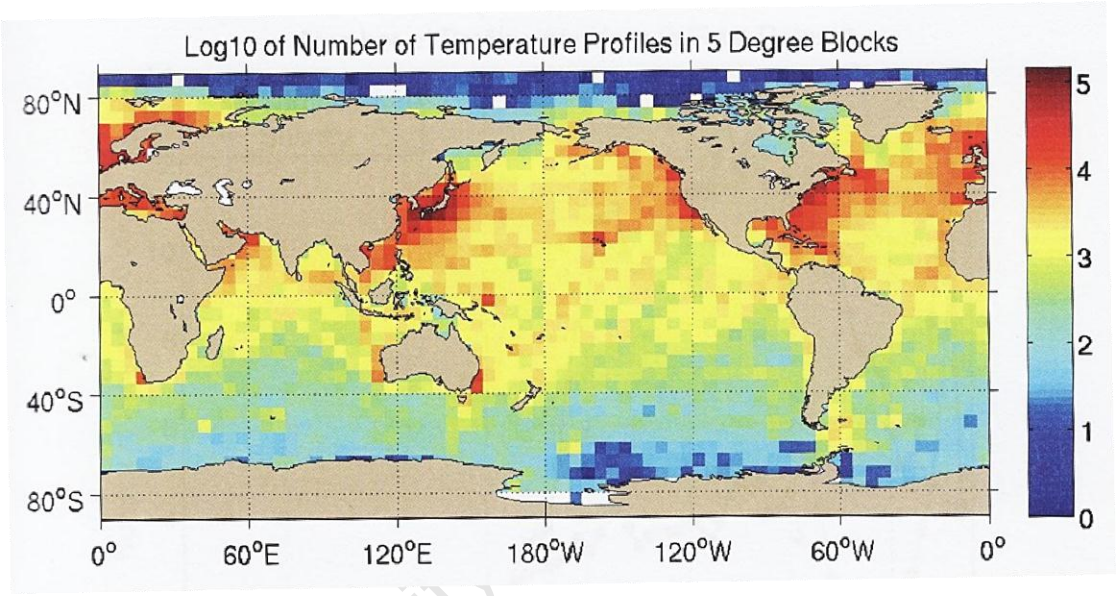

Figure 2-21: *Showing total number of temperature profiles (x log10) per 5 degree block as contained in GDEM4. Of note are the larger totals in the SE extreme of the South Atlantic (South African EEZ). After Carnes (2010).*

The number of profiles per year used in the GDEM4 global dataset showed a peak in observations between 1970 and 1995, with a distinct decline in numbers between 1985 and 2000, after which profile numbers increased again, as shown in ***Figure 2-22***.

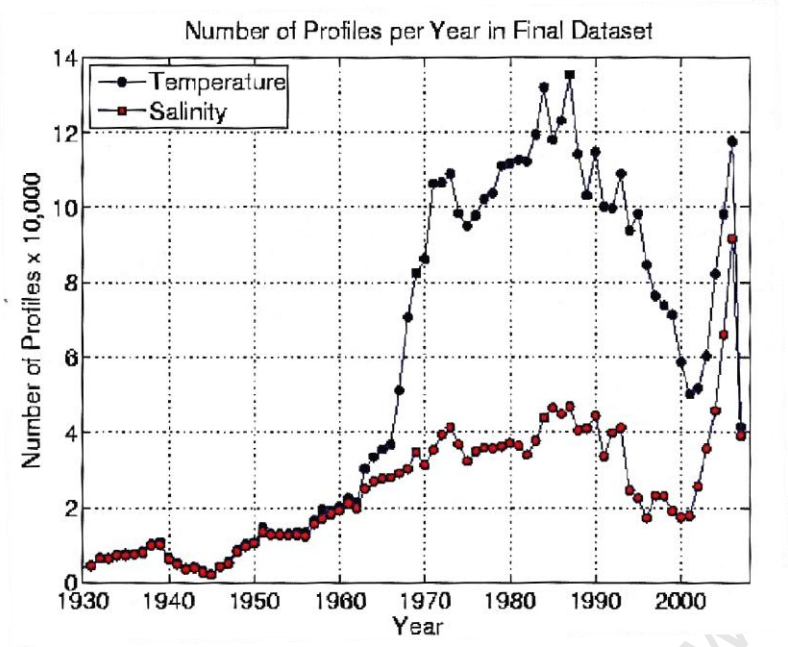

Figure 2-22: *Showing the number of temperature profiles (blue filled circles) and salinity profiles (red filled circles) used in the construction of GDEM4. After Carnes (2010).*

As with a number of previously reviewed techniques in this section, this technique is also of minimal benefit to the outcome of this study since it is a validation of a climatological model. For that reason, they were discussed and presented here in ***Figure 2-20***, ***Figure 2-21*** , ***Figure 2-22*** and ***Table 4*** as background information only and will not play any further comparative role in this study (see section 7. d, ***Table 9*** and ***Table 10***).

c. Observational methods and techniques

Obtaining observations of oceanic conditions is an expensive and time consuming exercise, which depends extensively on specific instrumentation and a suitable understanding of the changing natural environment. Coupled with this is the requirement for a capability to operate equipment, record information and make meaningful decisions often in challenging conditions at sea. It is for these reasons, as well as for many other research benefits, that temperature-depth profiles are highly valued by oceanographers.

Profiles were first measured using a mechanical bathythermograph (MBTs or BTs). These recorded temperature with depth using a needle scratching (controlled by a temperature conducting fluid filled tube) on a gold plated or smoked glass slide. Profiles then appeared as an analogue output directly as a plot of temperature versus depth. Specific calibrated templates were provided to extract the absolute temperature-depth conditions as a scribed line on a paper graph. Their accuracy

was estimated to be either 0.5 °C or 0.5 °F, since there appears to be some uncertainty about the units reported (Boyer et al (2006)).

These were superseded by reversing thermometers attached to reversing sample bottles that accounted for pressure changes with depth and were specifically designed to 'store' in-situ temperature values at depth by mechanically separating the mercury columns of 3 thermometers the instant they were reversed (inverted). Extensive calibration tables were provided to correct for the effects of pressure. Data was recorded manually in written form as data tables or deck chits. Reversing thermometers were reported to typically have an accuracy of 0.02 °C, after Boyer (2006).

These too were superseded by the advent of electronics, whereby an expendable bathythermograph or XBT was allowed to descend through the water column while the ship steamed ahead or drifted. The expendable part contained a temperature sensor that transmitted its data via a thin copper wire back to the ship. Depth was deduced from its rate of decent. Data was recorded on board the vessel.

Reported accuracies from the 2 manufacturers of these instruments were: ± 0.15 °C to ±0.1 °C (with a depth accuracy of ± 2%) and ±0.1 °C (with a depth accuracy of ± 2% or 5 m, whichever is larger). Boyer et al (2006) reported that the equation used to infer drop rate of various models are known to contain systematic errors as large as 25 – 30 m at 750 m.

Fundamental physical relationships between temperature (salinity, etc.) and the electromagnetic properties of sea water were used to develop CTD (Conductivity Temperature Depth) sensors (Boyer et al (2006). The response times of sensors is an important factor that allows the CTD to collect 'continuous' measurements. Lowering the CTD at a rate of 1 m/s can provide vertical profiling resolutions of 0.05 m to 0.3 m. In the past electronic storage limitations resulted in only selected levels being stored (Boyer et al (2006)). The temperature accuracy of a CTD typically varies from 0.005 °C to 0.001 °C. Since 1961 CTD probes were lowered over the side of a ship, sometimes together with a water sampling rosette of remotely triggered bottles. Their data was transmitted in real time mode to the ship above or stored in a self-contained, on-board data recorder (Boyer et al (2006)). CTDs are presently one of the prime instruments used by the scientific community.

In the past 10 years, free floating autonomous buoyancy controlled profiling buoys have been widely used throughout many of the oceans. These 'Argo' floats when first deployed remain at the surface for 10 hours; thereafter they descend to a depth of approximately 1000 m, where they remain, freely drifting for 8 - 10 days. They then descend from their 1000 m depth level to approximately 2000 m water depth whereupon they slowly ascend to the surface over a period of 10 hours,

recording temperature, depth and salinity as a profile. On returning to the surface, they download their recorded data via a communications link to an earth orbiting satellite (Argo satellite). About 3000 of these floats drift throughout the world's oceans, any one time, restricted to deeper water beyond continental shelf depths (> 200 m). See http://www.argo.net/ (August, 2012).Temperature sensor accuracy of the floats may be from 0.01 °C to 0.002 °C, depending on the sensor supplier (Boyer et al (2006)).

Sensor quality, recording devices, calibration facilities and improved techniques have resulted in an improvement in data quality, quantity and cost effectiveness. Where responsible data collection procedures are observed, these datasets generally tend to be stored in large databases specifically setup for this purpose, such as the National Oceanographic Data Center (NODC) Ocean climate Laboratory (OCL), World Data Centre (WDC) and the Southern African Data Centre for Oceanography (SADCO) amongst others. Data collaboration agreements may exist, whereby data is exchanged between these data repositories on a regular basis. The profile data used in this study was sourced from SADCO.

d. Sound Propagation and Transmission Loss Modeling

Although sound propagation modeling is not explored as part of this study, it is an important last component in the usage and application of the predicted temperature profiles. Sonar theory is therefore briefly mentioned here since it applied to the outcome of this study in an application sense. Temperature, salinity and water depth are used to calculate sound velocity (c), represented in units of m/s by the following formula (after Etter (1991), after la Grange (1993)):

$$c(T, S, z) = a_1 - a2T + a3T^2 + a4T^3 + a5(S - 35) + a6z + a7z^2 + a8T(S - 35) + a9Tz^3$$

With constants: a1 = 1448.96, a2 = 4.591, a3 = -5.304×10^{-2}, a4 = 2.374×10^{-4}, a5 = 1.340, a6 = 1.630×10^{-2}, a7 = 1.675×10^{-7}, a8 = -1.025×10^{-2} and a9 = -7.139×10^{-13}.

T, S and z represent the measured temperature, salinity and depth.

Sound velocity in the upper ocean is approximately 1450 m/s, for a temperature of 0 ^{0}C and a salinity of 35 PSU. This velocity increases by 1.3 m/s for every 1 PSU increase in salinity, by approximately 4.5 m/s for every 1 ^{0}C increase in temperature, and by approximately 1.7 m/s for every 100 m increase in depth (Bishop 1984). Although salinity and pressure contribute to the propagation of

underwater sound, their effects are approximately 1/10th that of temperature. Although this figure may at first appear too low, the reason is due to the higher range of temperature values that occur in the oceans, compared to the other parameters.

The typical shapes of temperature profiles are: a surface layer, seasonal thermocline and main thermocline as seen in ***Figure 2-6***. When applying sound velocity calculations to a temperature profile, an equivalent sound velocity profile is created (see section 1.a). An example of such a typical deep water sound velocity profile is shown in ***Figure 2-23***.

The 0 - 125 m temperature profiles used in this study are part of the surface layer, with some influence from the deeper seasonal thermocline.

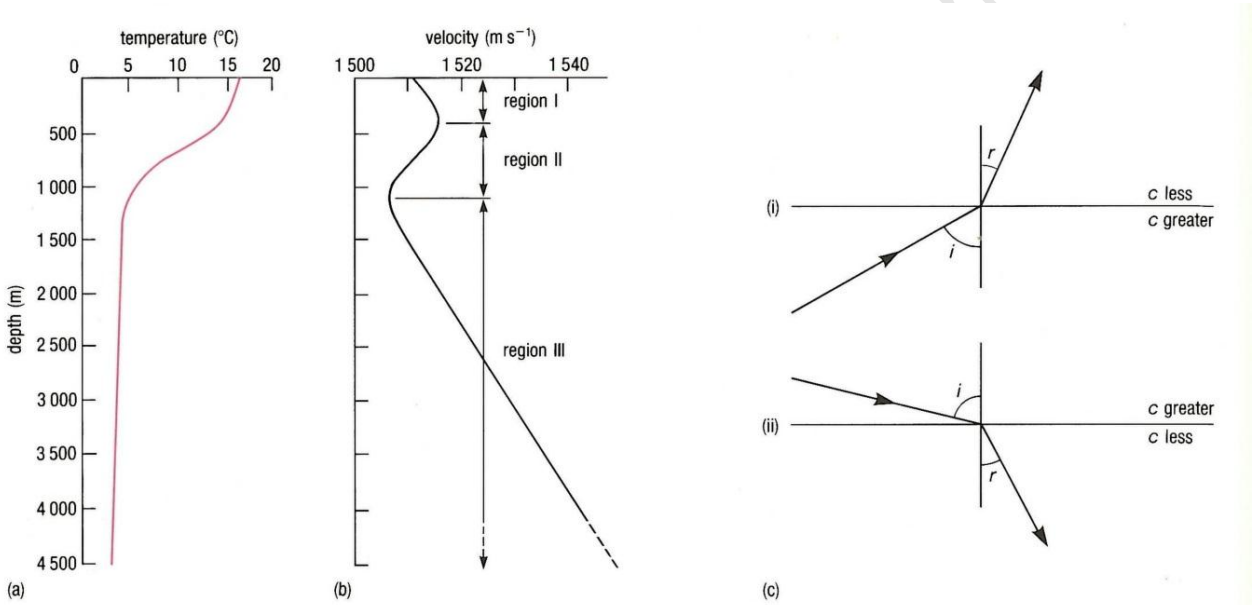

Figure 2-23: *(a) A typical temperature-depth profile in the ocean (b) A typical sound velocity profile in the ocean (c) idealized sketches illustrating refraction at the interfaces where the speed of sound changes (i) upward refraction (regions I and III); and (ii) downward refraction (region II). From Snell's Law:* $\frac{c\ greater}{c\ less} = \frac{\sin i}{\sin r}$ *after Brown et al (1989). 'c' Refers to sound velocity.*

The propagation of underwater sound is described mathematically by solution of the wave equation using the appropriate boundary and medium conditions for a particular problem (Urik 1967). The tracing of sound rays in linear gradients such as sea water is commonly employed. Arcs of sound rays are produced, propagating from its sound source at different angles. This may result in either upward, downward or no refraction of a sound wave front (See ***Figure 2-23***). Sound propagation modeling uses sound velocity profiles for determining transmission loss due to media interfaces,

reflections, spreading loss and absorption (Hodges (2010)). Transmission loss is a function of distance between individual ray-trace line plots in units of decibels (dB). Note: The RT acronym (for Ray-Trace) and (PoD for Probability of Detection) is used extensively in the Results section. Where ray trace lines diverge, shadow zones result, which may result in regions of reduced detection probability of an underwater 'target'. An example of a shallow water ray trace, propagation loss and probably of detection plots is shown in ***Figure 2-24***. Transmission loss and ray trace plots for shallow water are also used to show how predicted profiles are practically implemented in this study.

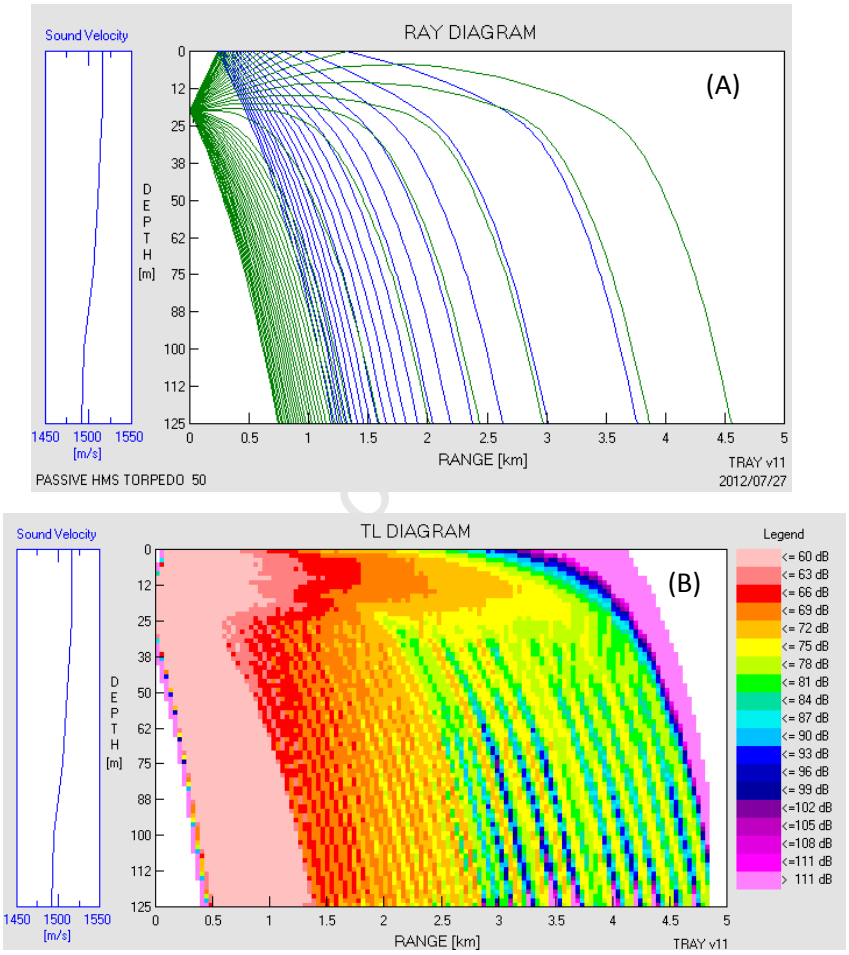

Figure 2-24*: An example of a Ray Trace (A) and Transmission loss (B) plot as output from the IMT SMOD model, setup for deep water, showing 0 – 125 m depth range and 5 km horizontal range. The left hand side panel of each plot shows the sound velocity profile used as input. The legend of (B) shows transmission loss in units of decibels or dB.*

3. METHODOLOGY

The analysis methodology of this study consists of a combined parametric-probabilistic based approach as described by Nhu and Zidek (2006): (a) The parametric approach is a model based curve fitting procedure to produce standard profiles as part of the data preparation, and (b) The probabilistic approach is a classification of profiles according to a number of representative profile groups defined by a Self Organising Map (SOM). These two approaches are shown as the steps C (in the Pre-processing of the data-designated as *) and D (in the later Analysis and Testing-designated as **) respectively in ***Figure 3-1***.

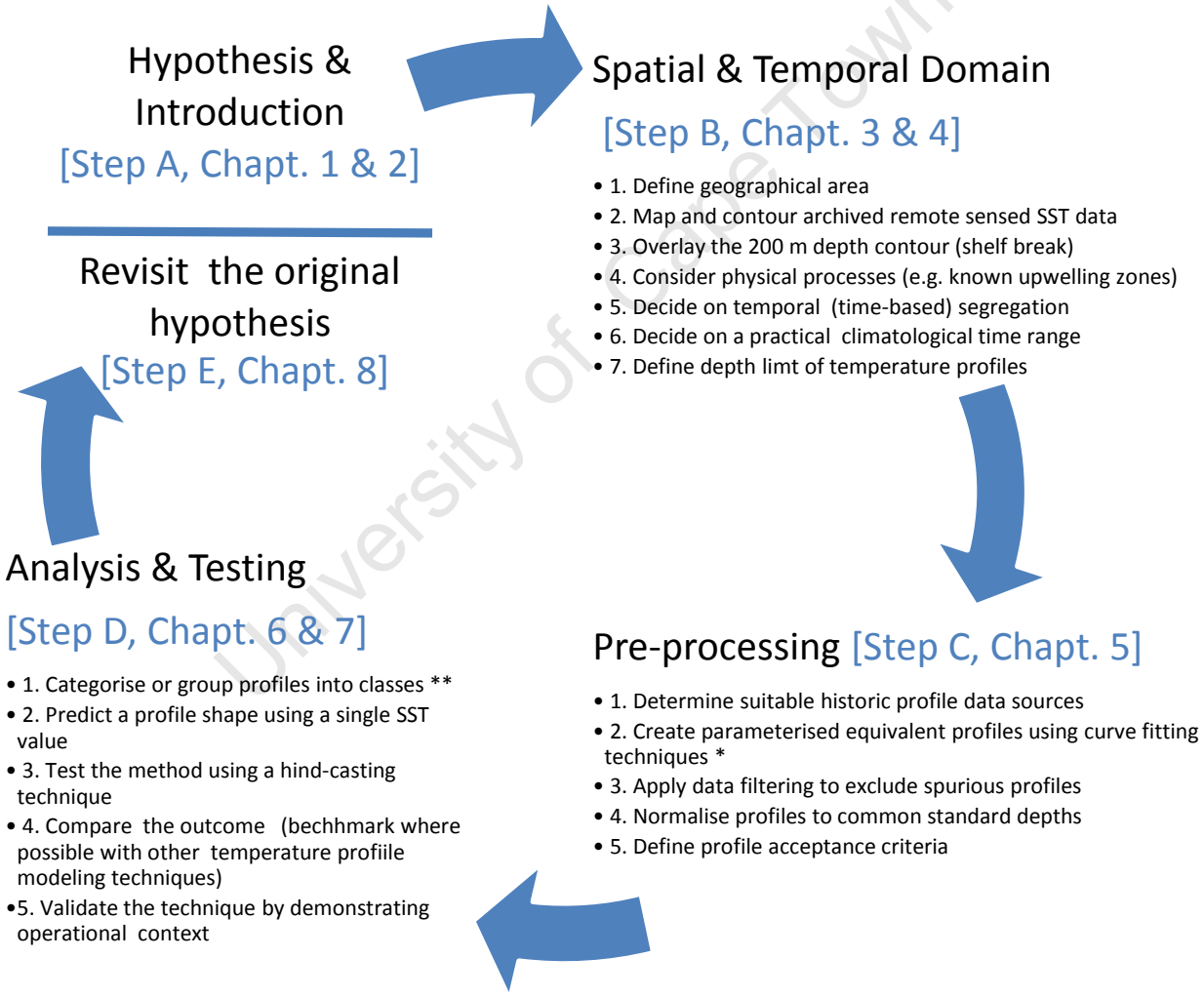

Figure 3-1: *Research process flow as addressed in the chapters that follow. The single asterisk * in Step C refers to a parametric approach whereas double asterisk ** in Step D refers to a probabilistic approach. Note: This figure is a replica of Figure 1-2.*

In this study, the static climatology is supplied by neural network Self Organising Map (SOM) output, whilst the dynamic SST climatology (entered by the computer operator) is supplied as if originating from near-real time satellite overpass. A SOM in this context is a form of characterising or grouping profiles into a continuum of synthetic profiles that represents the full range of the observational dataset. This method is defined as a static-dynamic climatology method as described by Fox et al (2002).

The hypothesis assumes that if a SST value is known (or provided); a synthetic temperature profile can be inferred, with some acceptable level of statistical confidence. This implies that some relationship between the SST value and temperature profile information exists, as addressed in the introduction. Numerical modeling is generally used to define these relationships. The main disadvantage of these methods however is that they often require extensive measured water-column and atmospheric data, collected simultaneously to populate numeric formulae. Such datasets are very difficult and expensive to acquire, since they require extensive met-ocean sensors and supporting hardware (ocean buoys), providing suitable vertical measurements for a long period of time over extensive areas. Such measurements are not common in the southern hemisphere, especially in waters of South Africa, where oceanographic research funding is severely constrained.

A practical option adopted here is to define offshore SST regions, bounded according to their geographical location, climatology and physical oceanographic properties. These areas or 'provinces' are used to group all similar sub-surface temperature profiles that occur within their bounds. Once grouped, these profiles can be further processed to characterise their structure. Once profiles have been type-casted, their surface temperature values can be used to define their profile shapes. If supplied with an independent SST value, such as from a remote sensed satellite source (also referred to as dynamic data) the type-casted profiles can be scanned for a similar surface temperature value and hence used as a predictive profile.

Finally, for naval context the predicted temperature profile is then converted to a sound velocity profile and incorporated into an existing sound propagation model (SMOD – A model developed by The Institute for Maritime Technology for use by the South African Navy). A wide range of SMOD setup options (source frequency, beam width, water depth and sea floor composition, amongst others) were kept constant and used repeatedly to show the final outcome in terms of ray trace and probability of detection plots.

4. OCEANOGRAPHIC SETTTING [Steps B.1 and B.4 in Figure 3-1]

In this section, the Benguela system is described in the context of this study, providing some explanation for the vertical temperature structures and other physical oceanographic characteristics in the modeled data. It is especially evident from the text that the choice of locality, with its geo-spatial complexity and variability poses a challenge to describing it via a parametric method such as this.

An advanced understanding and predictive capability of the natural environment within this region is of obvious benefit to South African naval operations and planning. The South East Atlantic Ocean is an important region to South Africa, especially for the protection of sovereign rights. It should be noted that all maps shown in this study are depicted with north towards the top of the page.

The study area was determined mostly according to sea surface temperature regimes, bathymetry, physical oceanographic features and naval operational context, as described in section 5.a. The selected area is shown in this section in ***Figure 4-1*** as an enclosed red polygon with each contributing measured profile for all months. Of note is the generally ubiquitous coverage of the data, with some increase in sampling density in the bottom right (south eastern) region, closer to the major sea ports of South Africa. The red polygon outline in this figure is used throughout this section, as an illustration of the spatial coverage relevant to other published maps used hereafter. The eastern boundary of the polygon was chosen based on the location of the 200 m depth contour or shelf break.

Processes discussed in this chapter are summarised from a recent comprehensive literature review on the topic provided by Veitch (2009) in her introduction to a numerical modeling study of the Benguela system.

The south eastern limb of the South Atlantic subtropical gyre is generally referred to as the Benguela Current. This is also the eastern boundary current of the South Atlantic Ocean (e.g. Peterson and Stramma (1991)). The cooler near shore region however is referred to as the Benguela upwelling regime (Veitch (2009)). In the context of this study, the Benguela Current nomenclature will be used to refer to the region offshore of the shelf break, roughly located at the 200 m isobath. Since the inshore upwelling regime is highly dynamic, it represents a separate neighbouring eastern boundary mesoscale upwelling system (shown by the mean SST values in ***Figure 5-1***, depicted as Identification No. 4 in ***Table 5***), and is not part of the present study.

Reid (1989) described the Benguela current as being set northward at about 34°S and becoming increasingly north-westwards towards the north whilst separating from the African coast near 30 °S. The current was defined as being shallow and depth limited, with a transport of 21 Sv (Peterson and Stramma (1991)), based on observationally derived geostrophic flow which showed south ward flow at 1500 m water depth.

To the north (10 °S) is the 2000 km diameter Angola Gyre, with its centre roughly at 10 °S and 5 °E extending to a depth of 300 m, with a thin 10 – 20 m surface wind driven layer. To the east, the coastal Angola current advects equatorial water pole ward to approximately 15 - 18 °S (Gordon and Bosley (1991)), coinciding with the northward extent of the Benguela upwelling regime

The study area is situated within the Benguela system (see ***Figure 4-2***), traversed by the Benguela current (referred to as BOC in ***Figure 4-2***). A shelf edge jet occurs on the eastern side near the eastern boundary of the demarcated polygon.

In the south, the Benguela current (in the upper 1500 m) is fed by waters from the south at a rate of 15 Sv, of which 10 Sv is periodically fed by waters from the Agulhas current (originating from the South Indian Ocean), while the remaining 5 Sv originates from the South Atlantic current. This flow is also influenced by perturbations in the subtropical front (Gordon et al (1992)). Approximately 7 Sv of flow can be attributed to Agulhas current eddies. In another estimate, Garzoli and Gordon (1996) found that at 30 °S in the upper 1000 m, 50 % of the water entering the Benguela originated from the Central Atlantic, 25 % from the Indian Ocean and remaining 25 % from a tropical/Indian ocean blend. This accounts for a significant component of Indian Ocean water into the Benguela current.

This was validated by Garzoli et al (1996) who found that the variations in the Benguela current transport were related to variations of the Agulhas input. Garzoli and Gordon (1996) also defined an Agulhas eddy corridor in the Benguela current through which Agulhas rings and eddies migrate into the Atlantic Ocean (See ***Figure 4-3***) at a rate of 4 - 9 per year (van Ballegooyen et al (1994)) and has a significant impact on the characteristics of the Benguela current.

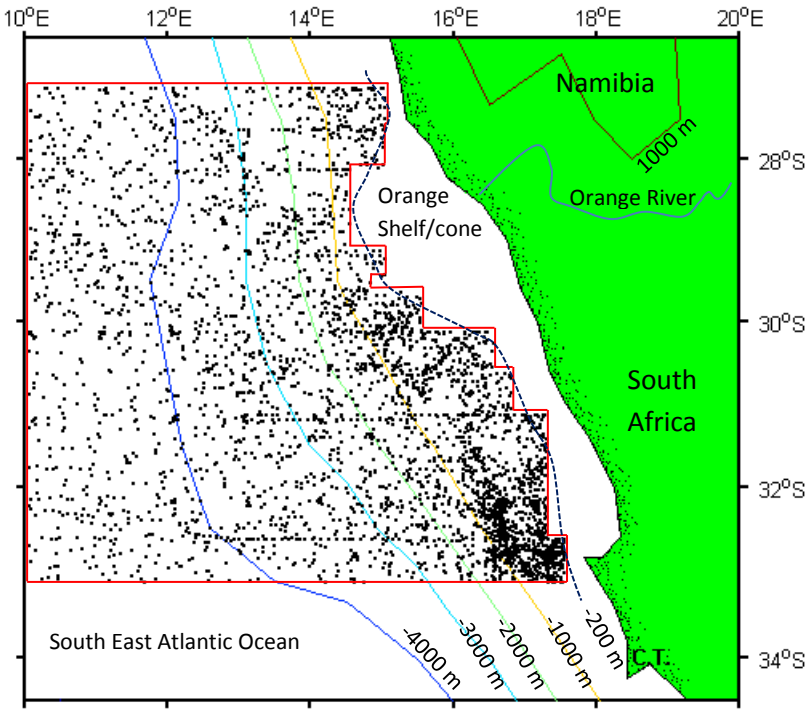

Figure 4-1: *Map showing the geographic setting within the Benguela Current of the South East Atlantic ocean, with locations of profiles used in this study depicted as black dots bounded by a red polygon (used in the maps that follow). Height above sea level and depth below sea level in meters are shown as coloured contours lines. The 200 m depth isobath (continental shelf limit) is shown as a broken black line.*

Boebel et al (2003) termed the 'Benguela system' region the 'Cape Cauldron' based on the turbulent mixing that takes place in the Cape Basin, the dynamic coastal upwelling regime and interaction with Agulhas current rings and eddies.

Shillington (1998) showed, using Acoustic Doppler Current Profiler (ADCP) measurements that NNE-set currents of 25 - 50 cm.s^{-1} occurred between the 200 m and 1000 m isobaths south of the Orange River shelf/cone. Somewhat higher values (50 – 75 cm.sec^{-1}) occurred further south off Cape Columbine, the southern-most extend of this study (see ***Figure 4-4***).

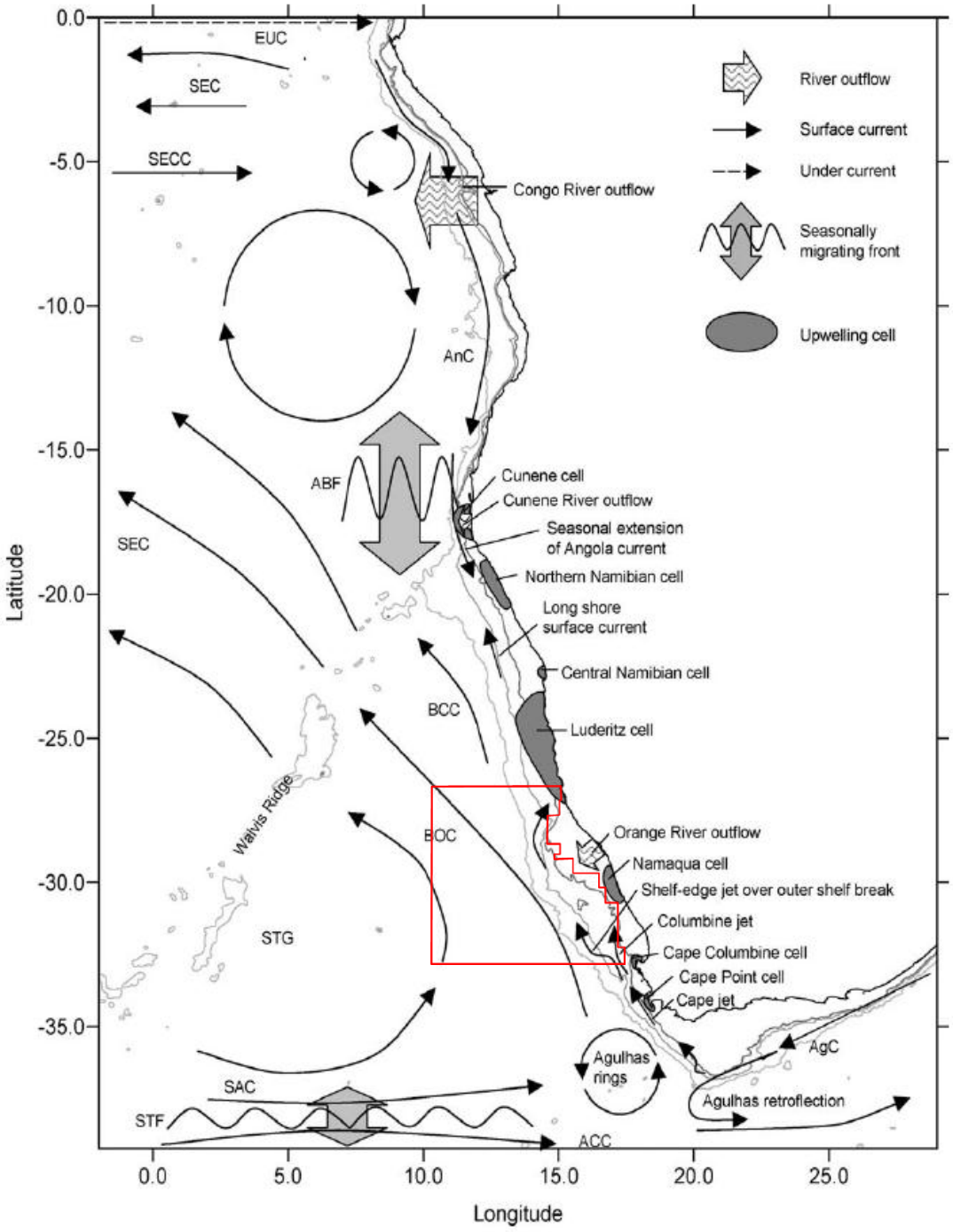

Figure 4-2: *Schematic map of large and small scale Benguela system features, after Hardman-Mountford et al (2003). The enclosed red polygon represents the spatial extent of the data used in this study. Legend: EUC – Equatorial Under Current, SEC – South Equatorial Current, SECC – South Equatorial Counter, Current, AnC – Angola Current, BOC – Benguela Oceanic Current (referred to as the Benguela current in this study), BCC – Benguela Counter Current, SAC – South Atlantic Current, AgC – Agulhas Current, ABF – Angola Benguela Front, STF – Subtropical front, STG – Subtropical Gyre, ACC – Antarctic Circumpolar Current, Cape Jet – Goodhope Jet.*

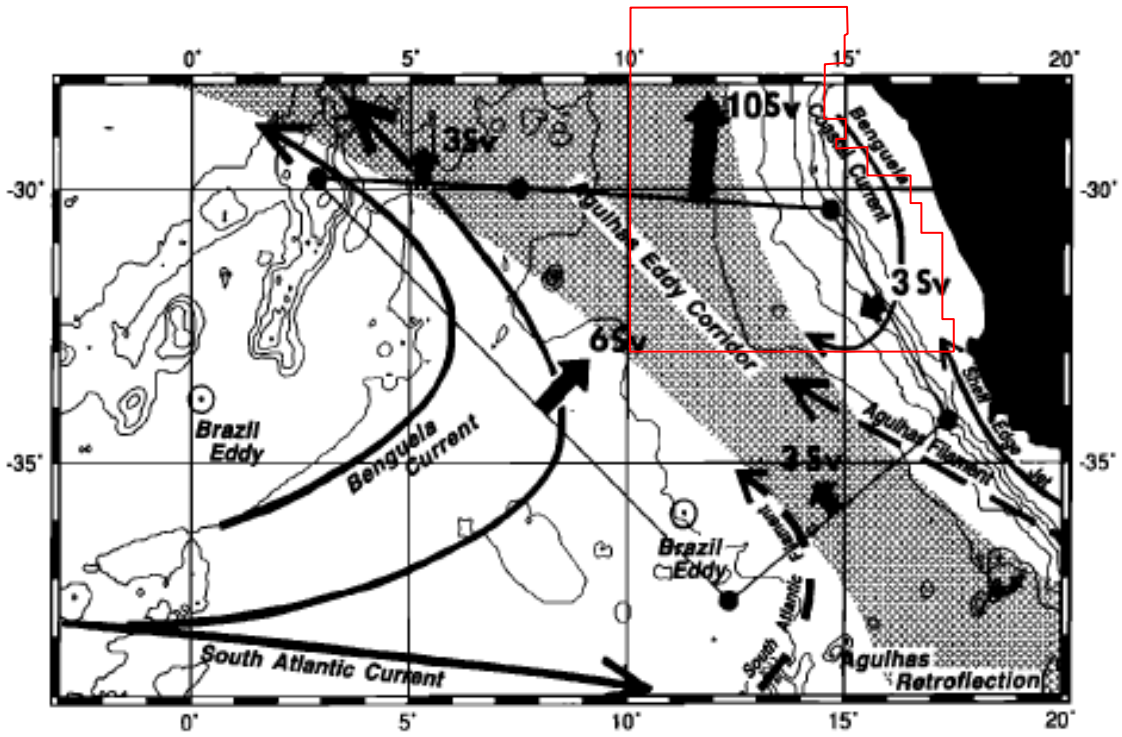

Figure 4-3*: Schematic map showing Agulhas Eddy Corridor and other transport elements as defined by* Garzoli and Gordon (1996). *The enclosed red polygon represents the spatial extent of the data used in this study.*

Shillington et al (2006), described surface, central and intermediate waters of the Benguela system as being more saline and warmer if originating from the tropics or less saline and cooler if influenced by Antarctic or sub-Antarctic waters.

To the east at the shelf break, the Benguela current is bordered by a convoluted long-shore thermal front that follows the shelf edge (Shannon and Nelson (1996)). Coupled with these thermal fronts are upwelling induced filaments that are easily observed via satellite data and thoroughly documented by a number of authors (Lutjeharms and Stockton (1987)-see ***Figure 4-5***, Shillington et al (1990), Duncombe-Rae et al (1992), Shillington et al (1992) and Nelson et al (1998)). These filaments were reported by van Foreest et al (1984) to have an offshore extent of 100 – 500 km beyond the upwelling front, often extending into the area demarcated in this study. These filaments meander offshore as they interact with the passage of Agulhas rings (Lutjeharms et al (1991)). Variability such as these Agulhas ring instabilities and filament occurrences are not easily predicted and likely contributed to the wide range of temperature extending to 125 m (and deeper) as seen in this study (see hind cast plots in ***Figure 7-3***). The existence of these features probably reduced the accuracy of the SOMs clustering technique used in this study.

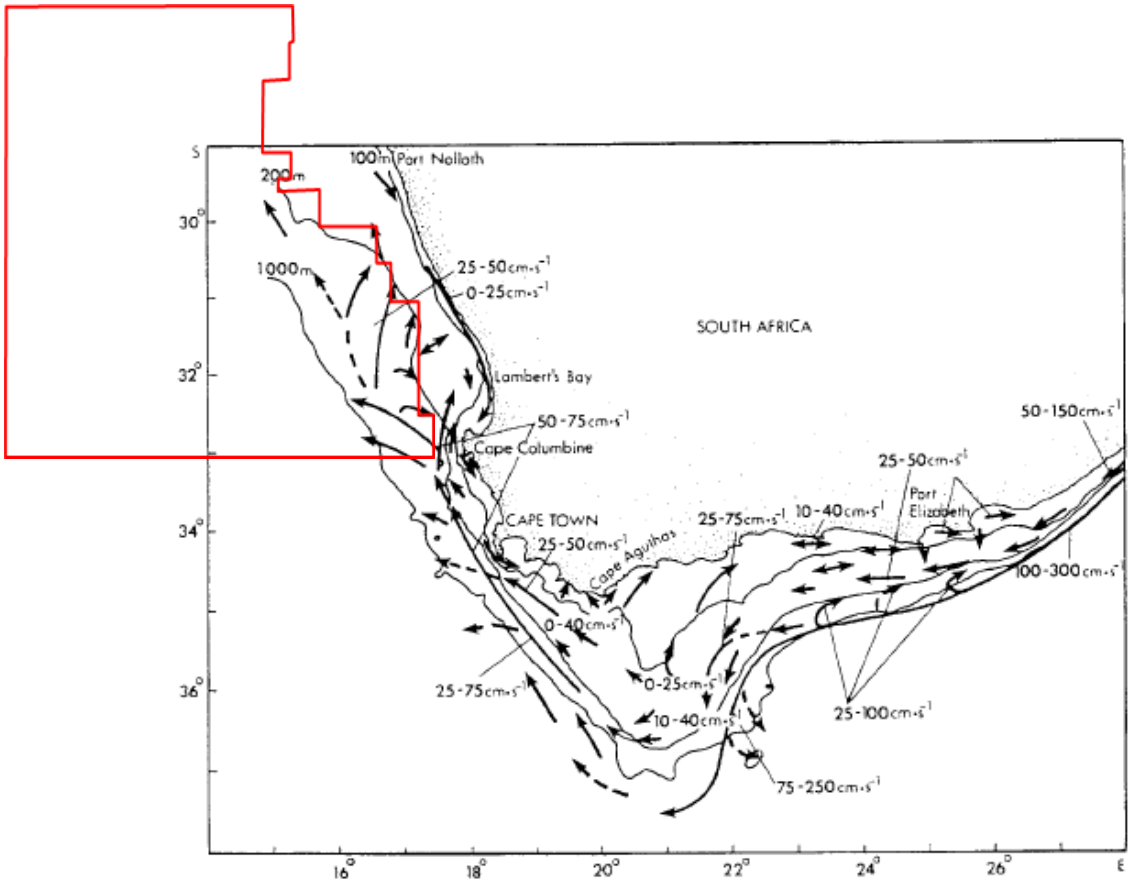

Figure 4-4: *Schematic map of currents over the shelf, based on ADCP measurements obtained between November 1989 and January 1992, after Shillington (1998), The enclosed red polygon represents the spatial extent of the data used in this study.*

Duncombe-Rae et al (1992) found that a single filament extending 450 km could have resulted in offshore volume flux of ~1.5×10^6 $m^3.s^{-1}$.

Largier and Boyd (2001), see ***Figure 4-6*** , reported on drifter tracks released at the interface of the Benguela Current / Benguela upwelling regime, which showed NNE contour-steered flow in the south, with offshore diversion north of the Orange River shelf/cone.

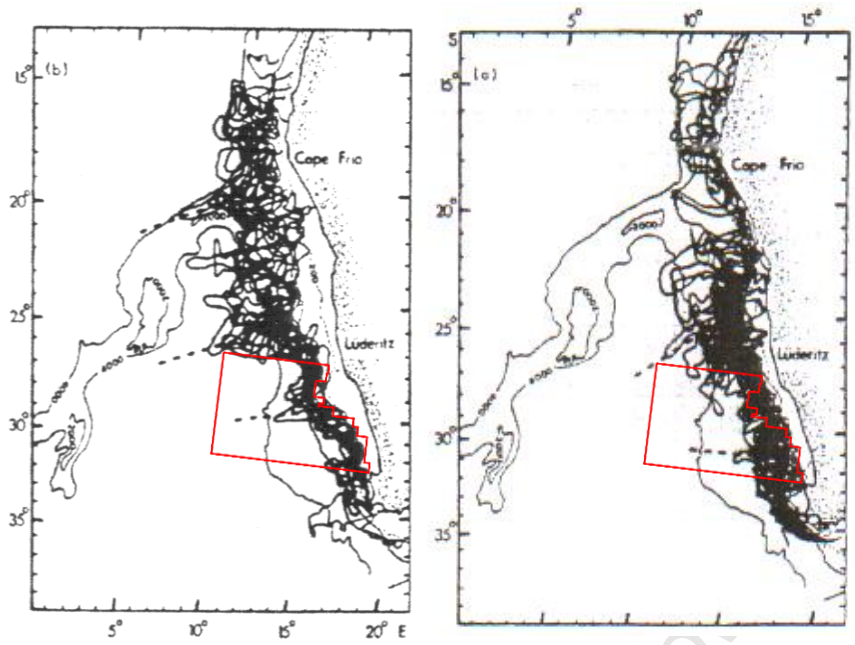

Figure 4-5: *Summer (left) and winter (right) maps showing a montage of frontal boundaries extracted from MEOTEOSAT II SSTs of the Benguela system, after Lutjeharms and Stockton (1987). The enclosed red polygon roughly represents the spatial extent of the data used in this study.*

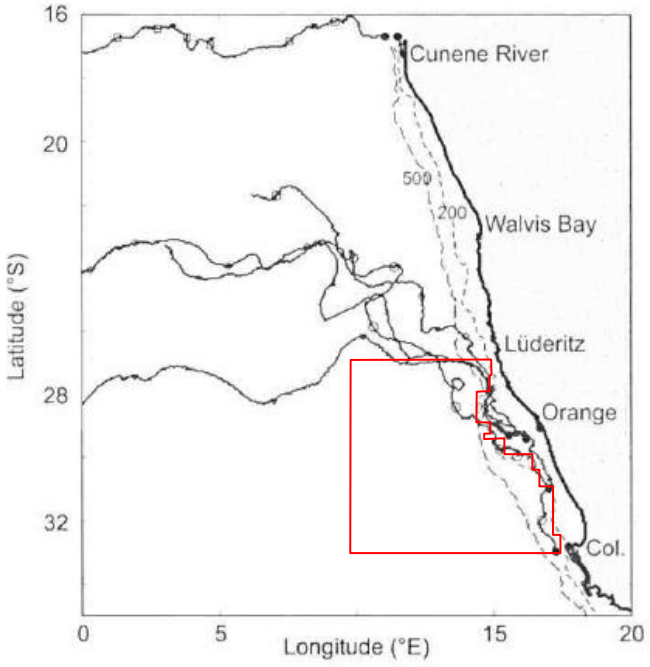

Figure 4-6: *Drift tracks from 11 drifters released between mid-1999 to February 2000, with solid dots marking the locations of the releases, after Largier-Boyd (2001). The enclosed red polygon represents the spatial extent of the data used in this study.*

Veitch (2009) in a numerical modeling approach that defined the equilibrium dynamics of the Benguela system, concluded that the northern and southern regions exhibit distinctly different characteristics and that the influx of Agulhas rings contribute significantly to the meandering path of the offshore stream of the Benguela current. This Agulhas influx was also found to contribute to modifying the seasonal signal of the Goodhope Jet (see ***Figure 4-2***) by extending it over a broader region.

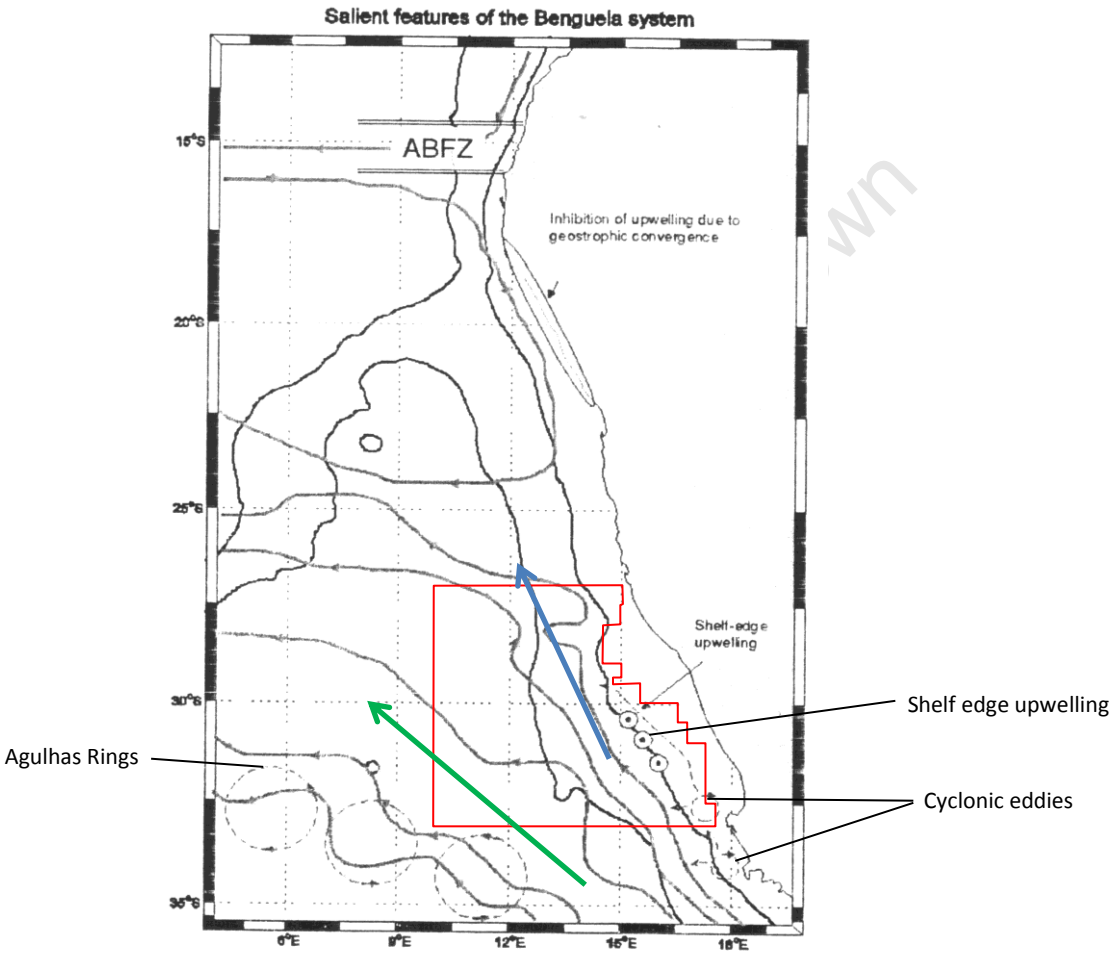

Figure 4-7: *Schematic map of the salient features of the Benguela system, after Veitch (2009). The enclosed red polygon roughly represents the spatial extent of the data used in this study. Two streams of the Benguela current are shown as an offshore stream (green arrow) and a preferential path or shelf edge stream (blue arrow).*

In the schematic map in ***Figure 4-7***, 2 distinct Benguela streams were defined: an offshore stream that intersects this area of interest and a shelf edge stream, within the spatial context of this study. The trajectory of the shelf edge cyclonic eddies also appear within the dynamics of the Benguela current, as well as specific upwelling associated with current divergence. Each feature, in

combination with atmospheric influences, has an impact in a 3-dimensional way on the temperature profiles of the region

At its eastern boundary, the broader Orange Shelf (Shannon 1985) extends the shelf break further offshore as a north/south discontinuity, whilst being closer to the coast in the north and south.

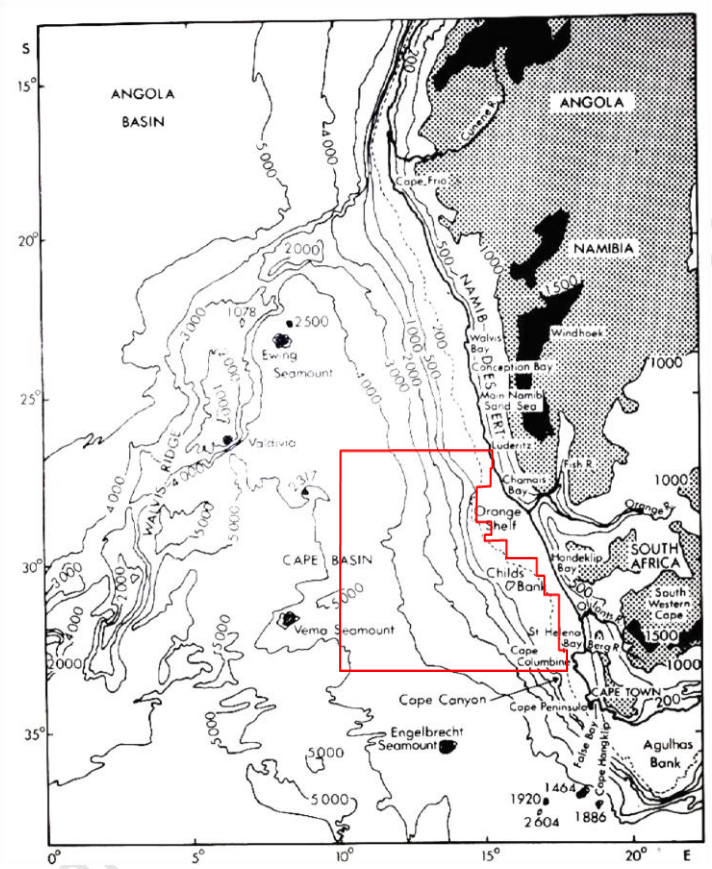

Figure 4-8: *Map showing the bathymetry of the south-east Atlantic Ocean, after Shannon (1985). The enclosed red polygon roughly represents the spatial extent of the data used in this study.*

The geomorphology of the region used in this study can be described as the rather flat eastern flank of Cape Basin. These are not shown in the coarse depth contours of **Figure 4-1**, but are depicted in the more detailed contours of ***Figure 4-8***. The Cape Canyon seafloor feature (Shannon (1985)) is known to steer advected mid and bottom water into the system. The only major prominent seafloor feature in this area of interest is Childs Bank (Shannon 1985 – see ***Figure 4-8***) at about 31 °S between 500 and 100 m water depth. Shannon and Nelson (1996), in their T-S plot (see Appendix H) as shown in ***Figure 4-9*** identified Benguela water masses based on specific T-S characteristics for

surface, thermocline and mean conditions across certain Benguela latitude ranges. The T-S characteristics shown by them are consistent with the temperature profiles used in this study.

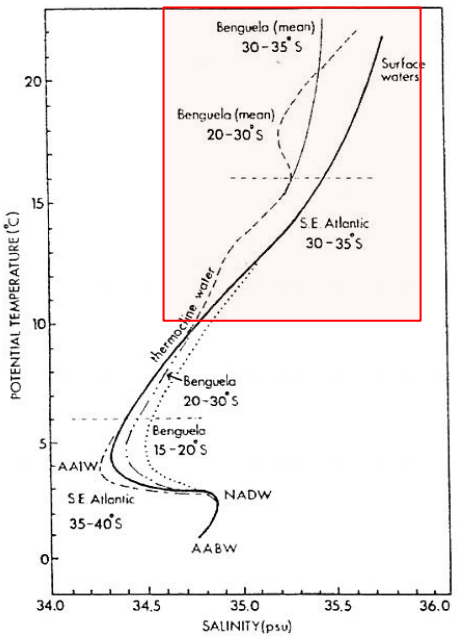

Figure 4-9: *Water masses and their characteristic potential temperature-salinity properties, after Shannon and Nelson (1996). The shaded red block represents the approximate range of temperature profiles used in this study.*

Atmospheric conditions are dominated by the existence of the pulsing and seasonally shifting South Atlantic Anticyclone that gives rise to alongshore equator-ward winds (Preston-Whyte and Tyson (1993)), with upwelling conditions at the coast. This pulsing or modulation occurs every 3-10 days according to changes of amplitude and configuration of Rossby waves in the Subtropical Jet Stream Nelson and Hutchings (1983). In winter the larger waves in the Jet stream increase the modulation frequency to about 1 month (Jury et al (1990)).

Wind stress curl is a fundamental forcing component of the ocean (Veitch (2009)), extending 200-300 km offshore (Kamstra (1985)), broadening as a wedge-shape to the north. This feature is within the Benguela current flow region and certainly influences the extent of vertical mixing observed in the temperature profile data seen later. The region covered by this study can be described as being largely influenced by anti-cyclonic wind stress curl, more consistently in the west (see ***Figure 4-10***). Together with the water column mixing dynamics seen in ***Figure 2-2***, ***Figure 2-3*** and ***Figure 2-4***

which may explain some of the variability in the depth of the wind mixed layer noticed in the hind cast profiles in ***Figure 7-3***.

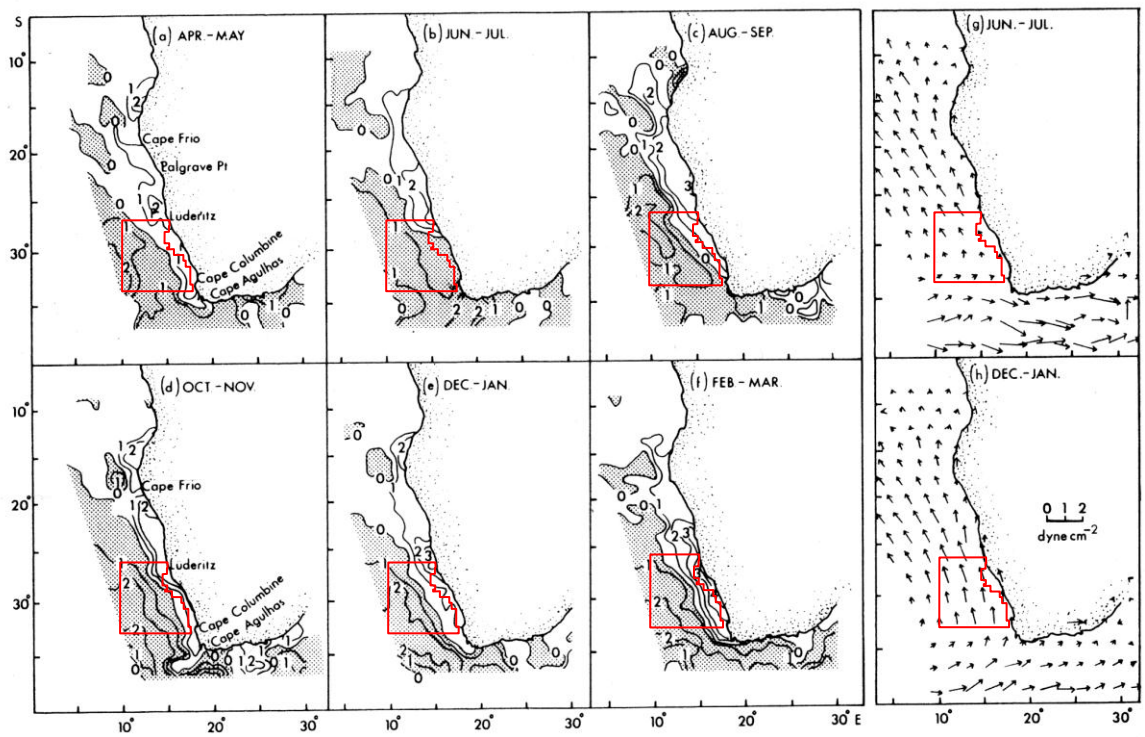

Figure 4-10*: Wind stress curl (10^{-4} dyn.cm $^{-3}$) in the Benguela system, with anti-cyclonic wind stress curl shaded and surface wind vectors, after Shannon (1985). The enclosed red polygon roughly represents the spatial extent of the data used in this study.*

5. DATA PRE- PROCESSING

In this chapter the extensive processing required prior to neural network analysis is described, whereby the scope of the datasets is defined, before input of profile data. Many of the challenges required to establish standardised or normalised profiles are addressed. The stringent qualifying criteria and the pre-processing that resulted in a sequential reduction of usable profiles are shown.

Pre- processing only describes the steps necessary to prepare historic profiles for the neural network SOM training process. A number of further processing and analysis steps are required thereafter before applying synthetic profiles to underwater sound propagation and transmission loss modeling.

a. Study area [Steps B.1 to B.4 in Figure 3-1]

Firstly it was necessary to examine the sea surface temperature (SST) climatology, to assist in defining the extent of the study area. The area of interest was defined as 5 – 50 °S and 10 °W – 50 °E covering 45 x 60 degrees of latitude and longitude respectively, the approximate maritime region of Southern Africa. Contoured SST values from 24 years of remote sensed Pathfinder data (APPENDIX A – MONTHLY PATHFINDER DATASETS) were used in conjunction with a SST monthly composite image using MODIS SST satellite data sourced from The University of Cape Town, Oceanography Department to produce a so-called 'SST provinces' as shown in ***Figure 5-1***.

Fourteen spatial provinces are proposed, based on the following criteria:-

I. Bathymetry (e.g. proximity to the 200 m depth isobath, defining the continental shelf edge).
II. Zonal (latitude) bands with known weather and/or solar heating.
III. Sea Surface Temperature ranges, conforming to the approximate geographical locations of defined sea surface temperature contours or isotherms (see ***Figure 5-1*** and APPENDIX A – MONTHLY PATHFINDER DATASETS).
IV. Geographic/oceanographic features (e.g. Demarcated by known physical properties of the ocean, such as currents and water properties).

Initially 16 provinces were defined, later reduced to 14 as the SST values offshore of Tanzania, Mozambique and Madagascar were merged as substantiated by the inability to create a smooth sea surface temperature contour for that region, where horizontally homogenous water properties were seen to occur (See APPENDIX A – MONTHLY PATHFINDER DATASETS).

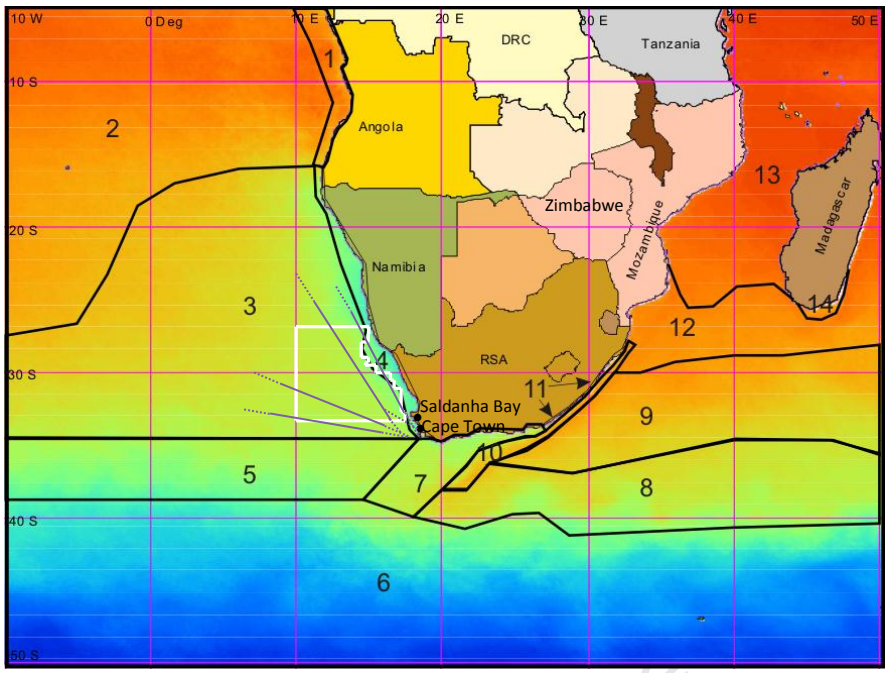

Figure 5-1: *A spatial grouping of 14 SST 'Provinces' (listed in the table below'. The colour backdrop is a 3 monthly composite image from infra-red channel of the MODIS satellite for April, May and June of 2009 (Source University of Cape Town, Oceanography Department) and contoured monthly pathfinder datasets. The enclosed white polygon represents the boundary extents (study area) of the profiles used in this study. The four lines shown roughly converging at the sea ports of Cape Town and Saldanha Bay are the approximate locations of inbound, outbound and transiting shipping vessel traffic that intersect the area of interest.*

The choice of a suitable profile sampled region was primarily based on the geomorphologic, oceanographic and atmospheric factors considered within the spatial extent of the Benguela system. Other factors such as the need to maximize the number of profiles, yet limit the inter-profile variability were also considered.

Identification	Name	Description
1	Angola coastal current	Warm on-shelf Angolan current water
2	Angola offshore	Offshore South Atlantic
3	Benguela offshore	South Eastern Atlantic Gyre
4	Benguela upwelling	Cold coastal Benguela Upwelling Zone
5	Western STCZ	Sub-Tropical Convergence Zone
6	Southern Ocean	Polar Front Water
7	Agulhas Bank	Inshore & offshore of the Agulhas Bank as an East/West coast interface
8	Agulhas retroflection and return current	Last phase of the Agulhas current as it bends back on itself and mixes with the surrounding cooler water
9	Southern arc of the Agulhas gyre region	Agulhas and South West Indian Ocean (SWIO) mixed water
10	Agulhas current	Warm very strong flowing Agulhas current water
11	East coastal current	Agulhas counter current flow on the narrow continental shelf < 200 m deep
12	Agulhas source	Source region of Agulhas current water
13	Mozambique current, Island States, Equatorial current	Mixed eddies and gyres in the Mozambique channel. Flow passing through the West Indian Islands. West Indian Ocean Equatorial Current
14	Southern Madagascar	Cooler localised flow at the south eastern tip of Madagascar

Table 5: *Showing 14 iso-thermal SST oceanic provinces defined according to their geographic and climatic properties.*

These provinces were used to quantitatively separate regions. In the context of this study, it provided a means to define the spatial boundaries, especially the eastern boundary of the selected study area (which coincided with the shelf break) as an interface between SST province 3 and 4, as well as a convenient western boundary on the 10 ^{o} E meridian.

These provinces play no further role in the quantitative aspects of this study.

The enclosed white polygon seen in **Figure 5-1** represents the boundary extent of the profiles used in this study. This polygon is the same one shown in the figures of section 4, and referred to as the 'study area' throughout this thesis. The area is a subset of region 3, which represents the approximate area coverage of Zimbabwe. The region can be oceanographically described as cross-cutting the subtropical south east Atlantic Gyre, as a segment of the oceanic Benguela current. This current flows over the homogenous deep Cape Basin, bordering the continental shelf-based Benguela upwelling regime in the east. The area is approximately the southern half of the Benguela current which is the source of the water travelling through the region and supplying the northern Benguela current. Surface and thermocline water masses (as used in this study) largely originate from a mixture of South Atlantic, Indian Ocean (especially Agulhas current eddies fronts and filaments) and Benguela coastal currents.

Atmospherically, the chosen area experiences largely SSE winds with increased wind stress curl during summer months, dictated by the nearby centre of the semi-permanent high-pressure South Atlantic anti-cyclone, with some influence from sub-tropical frontal systems in the south, especially in winter.

The mix of these natural features contributes to water column temperature ranges and variability that have consequences for underwater sound propagation and prediction.

As shown in ***Figure 5-1***, the chosen area is also intersected by 4 prominent international shipping lanes. This is a significant maritime region in terms of shipping safety, security and naval responsibilities where many large international bulk carriers, cargo carriers and tankers constantly transit this southern-most African passageway. Not shown here are the currently exploited offshore activities (and related natural resources) such as offshore fishing and mining. The sovereign significance of the region and related naval protection responsibilities also contributed to the choice of study area.

b. Defining the time and depth domains [Steps B.5 - B.7 in Figure 3-1]

Since date is one of the essential metadata fields recorded when collecting profile observations, two options existed for segregating data, either by month or season. This is in keeping with standards of climatological oceanographic and meteorological data that are often grouped or reported on the basis of the calendar month or season of the year. As sufficient number of profiles existed for the area of interest, it was possible to separate the data by calendar month in this case.

A profile depth maximum of 125 m was chosen, based on examination of the available data, while also attempting to achieve maximum reliability in the depth range, where sound refraction due to the strength of the thermocline is at a maximum.

c. Input profiles [Step C.1 in Figure 3-1]

All profile data were obtained from the Southern African Data Centre for Oceanography (SADCO). Files were provided in ASCII text format and imported into Matlab ® for further processing. The formats of these source profiles are described in Appendix B.

6858 Profiles were initially provided by SADCO. This was immediately reduced due to a 1st level data quality filtering based on the requirements of this study. The filter restricted qualifying profiles to only those with valid source categories (CTD, MBT, XBT, OSD, PFL and DPF – see descriptions later) and within the outer spatial boundaries (latitude and longitude) of the study area. This reduced the total number of profiles to 5359. This will be the total number of profiles referred to as 'source profiles' in this study.

The number of source profiles per month used later for SOM training is shown in ***Table 7***.

After examining the source profile data, it became evident that two distinctly different profile types (Discrete and Contiguous) existed, with implications for the pre-processing of the data.

a) Discrete Profiles: These were generally pioneering-type observations collected at discrete depths, sometimes standardised at specific depths, but usually limited to about 10 - 20 values per profile. The measurements resulted mainly from sampling methods available at the time and the purpose for collecting the data. The recorded temperatures at a specific depth were termed 'bottle-depth' data and were read from three specialised reversing thermometers mounted on a so-called reversing bottle, attached as part of an array of bottles to a wire rope suspended below a ship. The reversing mechanism of the bottle was 'tripped' using a brass weight that fell downwards along the wire rope, trapping the water at that depth as a sample as the bottle closed. Once winched back on-board, temperatures were read off 3 thermometers. These temperatures were later corrected for their depth 'distortion' using a lookup table of the measured temperatures from the trio of protected and unprotected glass thermometers per bottle. When plotted as a line on a temperature-depth X-Y plot, the data appeared as a poly-line joining temperature points collected at consecutive depths (see section 2. C and **Figure 5-2** (Discrete)).

In some cases the source of some discrete profiles was from more modern CTD profiles, where bottles were tripped close to specific depths and the resultant profile reported only at those so called 'bottle depths'.

Discrete profiles are coded as "OSD" in both the World Data Centre (WDC) and the Southern African Data Centre for Oceanography (SADCO) datasets. All other profiles (CTD, MBT, XBT, PFL and DPF) can be grouped under the definition of contiguous profiles.

b) Contiguous Profiles: Differing from discrete profiles (collected at specific depths) contiguous profile measurements emanated from instruments designed to collect temperature and depth continuously, as the sensor is lowered through the water column. The term contiguous was used here since the data was not strictly continuous, as it was recorded at a digitally predefined sampling and descent rate in the water column (albeit at a high sampling frequency). This approach either recorded the information in-situ within a self-contained instrument package or transmitted the data via an umbilical to a computer or data storage unit on board a vessel. With high sampling rates used, the data appears as a continuous line on a temperature vs. depth X-Y plot; where many thousands of temperature-depth data pair values typically contribute to a single profile (see **Figure 5-2** (Contiguous)).

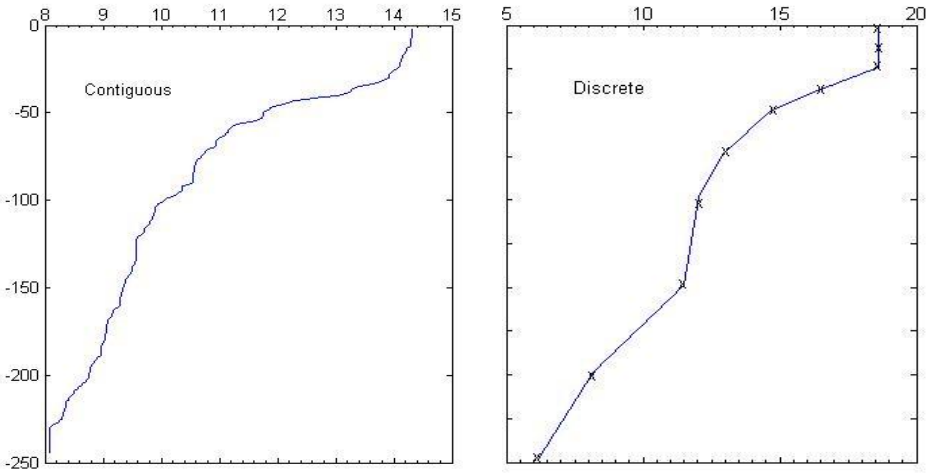

Figure 5-2: *Showing examples of a contiguous and discrete profile. The contiguous profile on the left consists of many thousands of temperature-depth value pairs. The discrete profile on the right consists of only 10 temperature-depth pair values (marked as 'x' on the line plot), joined as a polyline.*

Profile data received from SADCO were already grouped into categories suitable for separation as discrete and contiguous types:

CTD – Conductivity Temperature Depth profilers [contiguous]

MBT – Mechanical BathyThermographs [contiguous]

XBT – eXpendable BathyThermographs [contiguous]

OSD – Oxygen Standard Depth (so called bottle-depths or 'bott smpls'), [discrete]

PFL – Profile Floats (Argo floats or 'Prof flts'), [contiguous]

DPF – Delayed mode Profile Floats (Argo floats), [contiguous]

A significant majority (approximately 3 times more than other profile types) of bottle-depth or discrete profiles existed in the source dataset (**Figure 5-3**(A)). The lack of uniformity in the depths at which the samples were collected, and the stringent criteria for hind casting resulted in no discrete profiles being used for hind cast purposes. However, the high proportion of these discrete profiles in the dataset contributed significantly to the profiles sample size, necessary for the Neural Network training process, an essential step in this study. The procedures and analysis required to fit curves to these profiles were therefore considered necessary.

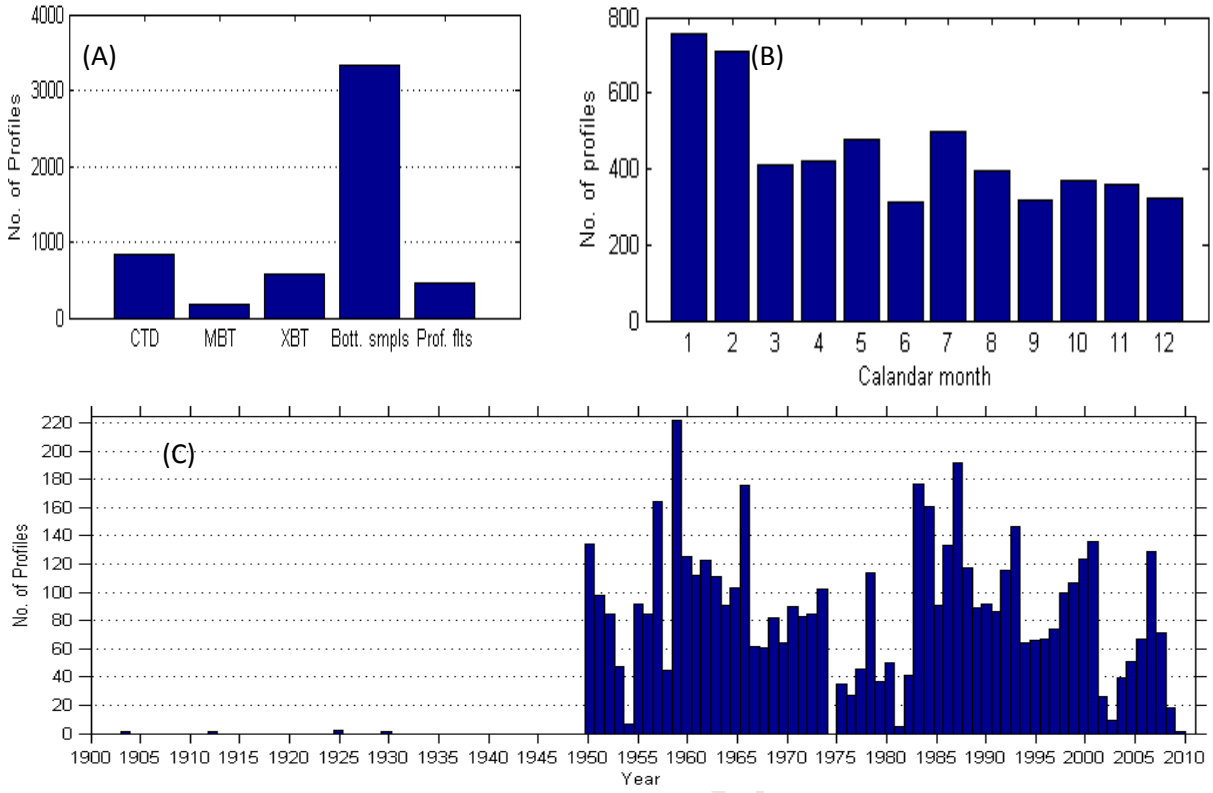

Figure 5-3: *Histogram plots of source profiles showing (A) distribution per sampler type [CTD=Conductivity, Temperature, Depth Profilers: MBT=Mechanical BathyThermograph: XBT=eXpendable BathyThermograph, Bott. Smpls=Bottle Samples: Prof. flts=Profiling floats], (B) profile distribution per calendar month and (C) profile distribution per observation year.*

After grouping profiles into calendar months, it became apparent that considerably more (approximately 25 %) profiles were collected during the months of January and February than the other months. The least number of profiles collected was during the mid-winter month of June; probably due to the higher sea state conditions during that time of the year (see **Figure 5-3**(B)). For the remainder of the months, profiles were generally evenly distributed. The quantities of profiles and their temporal spread were sufficient for a valid sensitivity analysis (see section 7. c)

Monthly spatial coverage of profiles was more densely distributed in the south eastern corner of the study area, closest to the major South African sea ports of Table Bay and Saldanha Bay (see **Figure 5-4**). The biased concentration of profiles on the eastern side of the study area implies that the upwelling processes as described by Garzoli and Gordon (1996), shown in **Figure 4-3** as the Benguela coastal current and by Veitch (2009) in ***Figure 4-7*** as shelf edge upwelling, probably also biased the dataset somewhat.

This also reflects the monitoring and research priority areas of interest, historically funded mostly for the benefit of South African fisheries resource management and research. It is interesting to note that the fortuitous concentration of profiles occurring in this study area are greater than many other regions globally (see **Figure 2-21**) and amongst the highest in the southern hemisphere. Profiles were generally spread over the past 60 years (1950-2010) with high variability in the number of profiles per year, ranging from 0 to 220 (see **Figure 5-3**).

Before conducting the SOM analysis, all profiles were converted into a new dataset with each profile having the same number of data points, **and vertical depth intervals**.

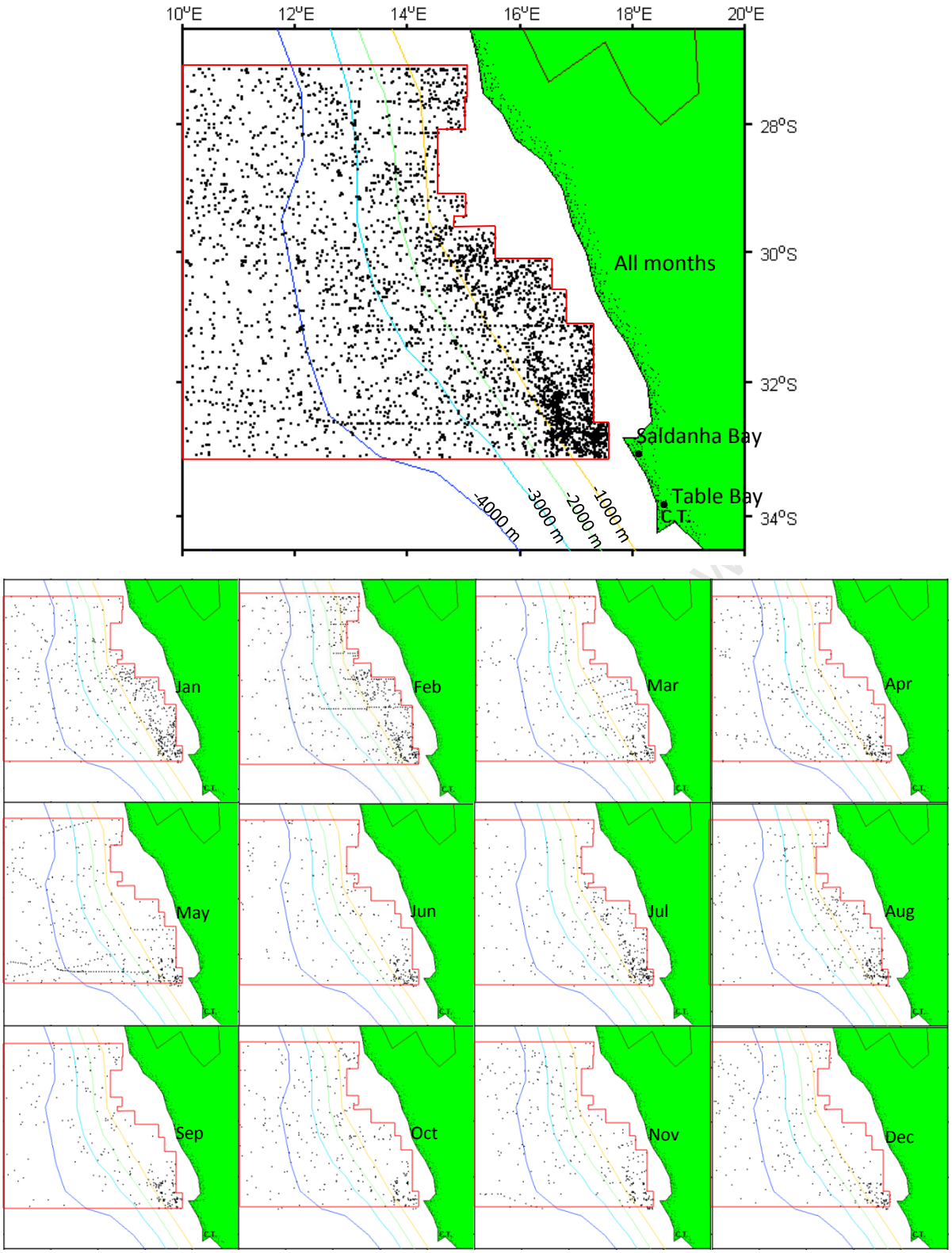

Figure 5-4: *Maps showing the spatial distribution of 5359 filtered source profiles used in this study as solid black dots. The larger uppermost plot is for all months combined, whilst the smaller maps are subsets per calendar month. Coloured lines represent contoured seafloor depths from 1000 m (brown line – near-shore) to 4000 m (dark blue line – offshore) in intervals of 1000m. Subsequent pre-processing statistics for these profiles refer to those provided in* ***Table 6****.*

d. Profile curve fitting [Step C.2 in Figure 3-1]

The variability in measurement methods (discrete and contiguous) described in the previous section, created profiles that were not suitable in their original format for characterisation purposes. Before conducting the SOM analysis, all the temperature profiles were required to be converted into a new dataset with all profiles having the same number of temperature-depth data points or depth intervals.

1. Curve fitting techniques for discrete profiles

One method of parameterising profiles is to apply a curve fitting algorithm. After exploring options for curve fitting of discrete profilers, such as logarithmic, linear, exponential power and moving averages, a polynomial fit method appeared to adequately represent most of the discrete temperature profiles.

Although not obvious in ***Figure 5-5***, an important consideration was how well the polynomial fitted the uppermost part of the profile, especially those profiles with a well-defined surface wind mixed layer. In most of cases tested (approximately 80 %), the 6th order appeared to best represent input profiles in the upper regions (0 – 50 m) of the thermocline, which was an important consideration for potentially inferring profiles from their SST values to follow, since this is where many of the standardised depth values occur. Generally, the lower order polynomials (orders 2 - 5) tended to 'over-smooth' the profile, whilst higher order polynomials (orders 8 and upwards) tended to 'over-describe' the thermal structure.

However once polynomial curves were fitted to the discrete profiles, it became evident that although the polynomial was able to suitably describe the 125 m – upper thermocline depth, some anomalous results occurred in the upper wind mixed layer, especially when small temperature changes with depth occurred. This was as a result of overshoots when fitting the polynomial to areas of sudden gradient changes. In this study, a simple post-curve fitting maximum or minimum value above the 'heel' of the thermocline was used to test and correct the surface wind mixed layer (see section to follow : Correcting curve fitting anomalies). A similar curve fitting correction technique was implemented by Carnes (2010) as a piece-wise cubic interpolating polynomial interpolator in Matlab® and GNU OCTAVE'S (pchip interpolating method). Although this was not explored, it is likely that the result using that method instead would not have substantially improved the goodness-of-fit see later). This aspect was also not core to the study and an improvement in the goodness-of-fit

better than that already achieved would not have resulted in a significant change in the 15 synthetic type casted SOMS (this aspect was not however tested).

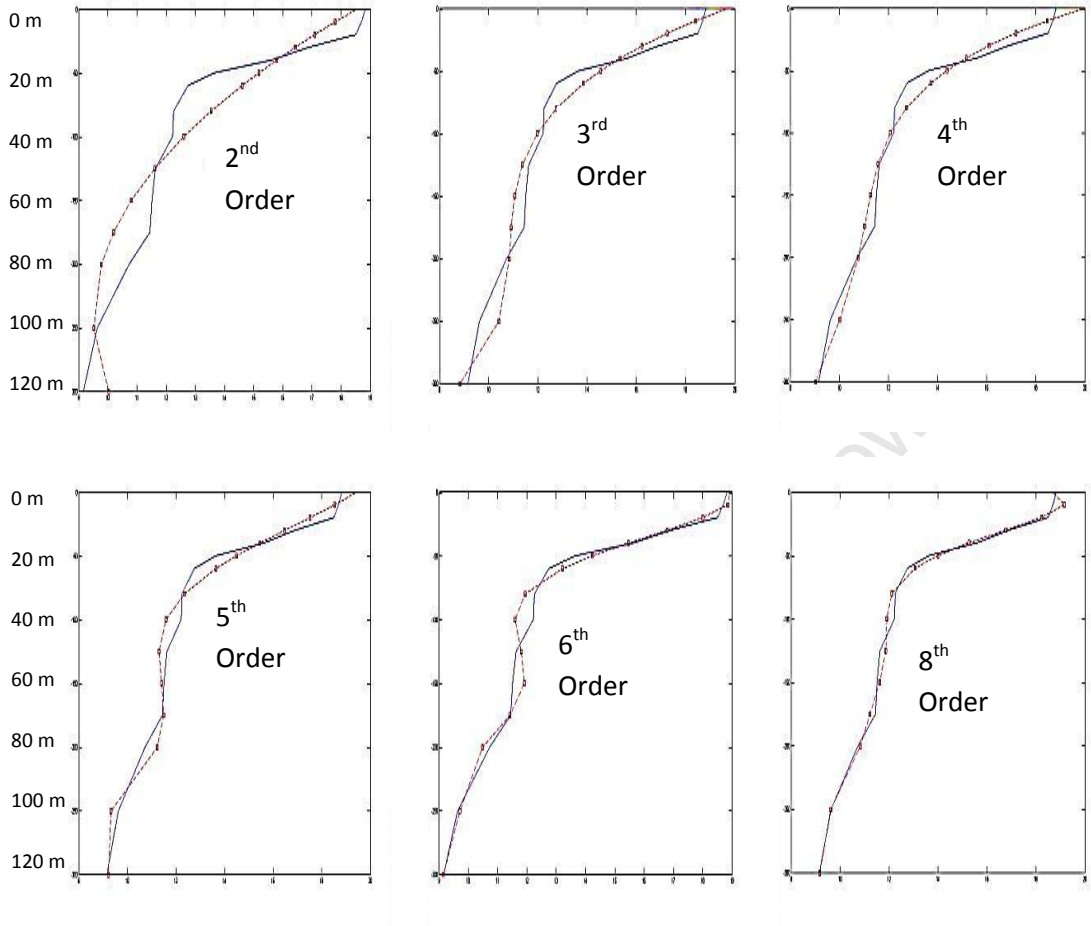

Figure 5-5: *An example of various polynomial fitting options (shown as a red line) applied to an arbitrary chosen single discrete historic profile (shown as a blue line) to determine the most appropriate polynomial fitting technique.*

The sixth order polynomial regression, $y = b+c_1x_1+c_2x^2+c_3x^3+\ldots c_6x^6$ is used to fit a profile versus depth x. Here, b and c_1, c_2, …, c_6 are regression coefficients , which are determined by the least square method. Note that the 'x' used here was only to describe the polynomial formula and does not relate in any way to the x used in ***Figure 6-1*** and section 6. a), to indicate a chosen data point or vector.

2. Correcting curve fitting anomalies

The wind mixed layer (or mixed layer depth) in the ocean, is the maximum depth to which surface atmospheric heating has penetrated, through the process of heat diffusion, assisted by winds, waves and ambient conditions to induce vertical mixing. Thermal mixing in this context is defined as a constant water temperature with increased change in depth (or a vertical line within the uppermost region of the profile plot). Wind mixed layer depths are known to vary zonally (north-south) and seasonally in all oceans. Winter cooling can also result in deep, isothermal upper mixed layers (down to 400 m – Shillington pers. Comm.).

Polynomial curve fitting algorithms proved moderately successful for many of the profiles processed, especially in the lower parts below the wind mixed layer. However in cases where a well-defined wind mixed layer occurred at the surface, the polynomial curve fitting sometimes failed. See examples in APPENDIX C – EXAMPLES OF CURVE FITTING FOR DISCRETE PROFILES. Two simple methods of limiting the maximum and minimum curve fitted temperature in the wind mixed layer were used to correct this, effectively re-creating the wind mixed layer.

Firstly, if any synthetic temperature value, as defined by the polynomial fit, was warmer than the 0 m temperature then that value was instead overwritten by the original recorded 0 m value (i.e. the value recorded at or near the sea surface). This was termed a 'top-down' correction, since the process started at the most shallow value and parsed the profile downwards.

The second phase was to parse the entire polynomial fitted profile from the deepest to the shallowest temperature value and check for any temperature cooler than the one occurring below it. If this was encountered then that temperature was instead replaced by the warmer one below it, effectively creating a wind mixed layer from the 'bottom-up'. This was termed a 'bottom-up' correction and is shown as a solid green line in examples depicted in ***Figure 5-7*** (D–G). These 'top-down' and 'bottom-up' corrections were deemed valid, since they represented dynamically unstable situations that only exist momentarily in nature and are regarded as spurious here.

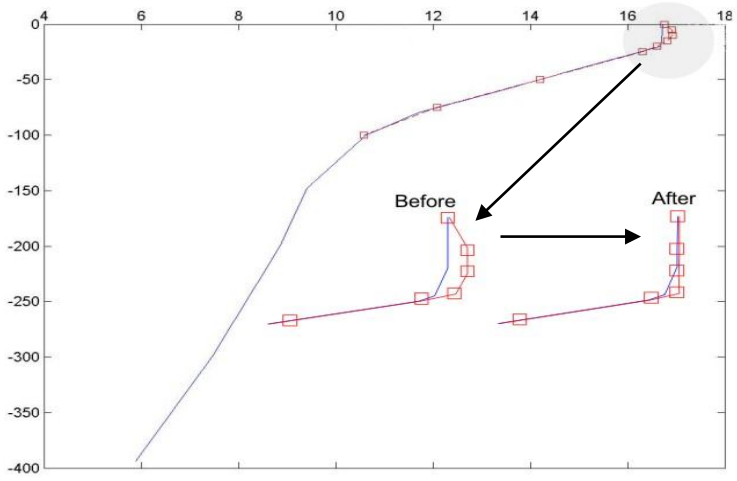

Figure 5-6: *An example of a 'top-down' correction applied to a polynomial fitted curve shown as a red line, with polynomial nodes as open red boxes. The original discrete profile is shown as a blue line. The insert shows the fitted curve 'before' and 'after' the correction was applied. A similar example of a 'bottom-up' curve fitted correction is shown as part of* ***Figure 5-7****.*

When applying these corrections, the polynomial fit was seen to modify the upper layers in close alignment with the observed wind mixed layer, as shown in the example in ***Figure 5-6*** and ***Figure 5-7****.* It could be argued that where corrections to the surface mixed layer were undertaken, that the curve fitted polynomial only described the water column below the mixed layer. More examples of these corrections can be seen in ***Figure 5-7***.

In ***Figure 5-7***, a 6th order polynomial curve was fitted to 9 examples of discrete profiles, each to a depth of 125 m. A so called goodness-of-fit representing the absolute difference between the observed and the fitted curve (at standard depths) was used as a measure of the effectiveness of this process. The value was pre-set in the software and used hereafter as one of the profile acceptance criteria (seen as red stars in ***Figure 5-7***)). In most cases the polynomial curve was found to adequately present (complied with the goodness-of-fit) the profile, as can be seen in profiles A, B, C, H and I. For these profiles the curve fitting could be used without correction and are shown as uncorrected fits. Using a curve fitting technique also means that some of the finer temperature structures may become smoothed and thereby lost, as can be seen to a varying extent in all the profiles shown in ***Figure 5-7***. As already described above, in some cases, the shape of temperature-depth profiles do not naturally represent that of a polynomial curve, as they tend towards a straight line in the shallower regions (upper wind mixed layer). The remnant bottom-up correction of the polynomial fit is shown as a solid green line overlaid on the original observed values in blue as seen by profiles D, E, F and G in ***Figure 5-7*** labelled 'corrected curve fits'.

Of the 5359 original observational profiles for all months in the area of interest, approximately 62 % consisted of discrete profiles of which 66 % could be fitted with a suitable 'goodness-of-fit' polynomial. Within these profiles, approximately 49 % required 'top-to-bottom' corrections, whilst 38 % required 'bottom-to-top' corrections.

A post-polynomial curve fitting test (including 'top-down' and 'bottom-up' corrections (see **Figure 5-6**)), using 54 profiles was undertaken as a measure of the effectiveness of the technique (see **Figure 5-8**). An absolute delta value for each discrete point of the profile was determined (in units of ^{0} C). From that the mean absolute delta value for the whole profile was calculated by using the following formula:

$$\text{Mean absolute delta value} = \frac{1}{n}\sum_{i=1}^{n} |\Delta t_i|$$

where $|\Delta t_i|$ is the absolute value of the difference between the original profile and the curve fitted profile at depth i. This value represented the so-called mean 'goodness-of-fit' of each profile. A mean absolute delta value of (0 - 0.4 ^{0} C) was arbitrarily termed a good fit, 0.4 – 0.7 ^{0} C a medium fit and > 0.7 ^{0} C a poor fit. Results showed that 51 of the 54 (or 94 %) curve fitted (and corrected) profiles were categorized as good curve fits, 2 of the 54 (or 4 %) as medium curve fits and 1 of the 54 (or 2 %) as poor curve fits (see ***Figure 5-8***).

The purpose of this test, on a subset of profiles was to determine the goodness-of-fit criteria to be used on the subsequent software executions. Based on this outcome, with such a strong bias towards the lower temperature difference values and the low ratios of medium and poor fits, it was decided to nevertheless include all medium and poor fit profiles by implementing a 1.0 °C goodness-of-fit criterion in the software. The reason for this was to maximise the profile numbers required for the SOM. It should be noted that the terms 'medium' and 'poor' fits were used arbitrarily here to describe deltas and not as an absolute criteria for curve fitting. The final implementation of a 1.0 °C delta for the discrete curve fitting that followed was therefore considered sufficiently stringent.

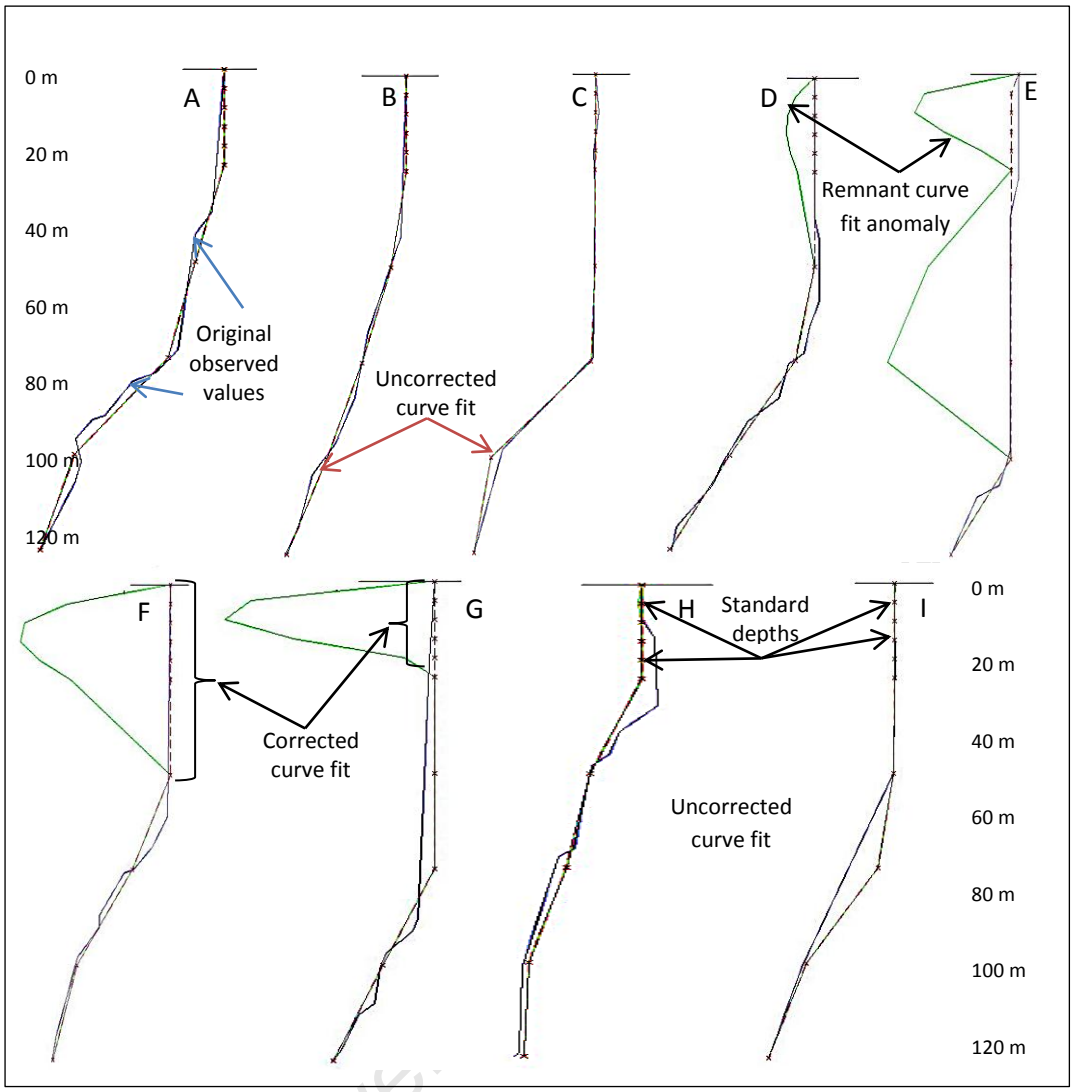

Figure 5-7: *Showing some examples of the curve fitting technique applied to discrete profiles. The solid blue line represents the original source profile, whilst the broken red line represents the final fitted polynomial. The solid green line shows the parts of original polynomial that were removed when correcting for the wind mixed layer as result of the 'bottom-up' curve correction.. 'Star' objects overlaid on the red plot are the filtered temperature values at standardised depths (0 m, 5 m, 10 m, 15 m, 20 m, 25 m, 50 m, 75 m, 100 m and 125 m) used in the normalisation process to follow.*

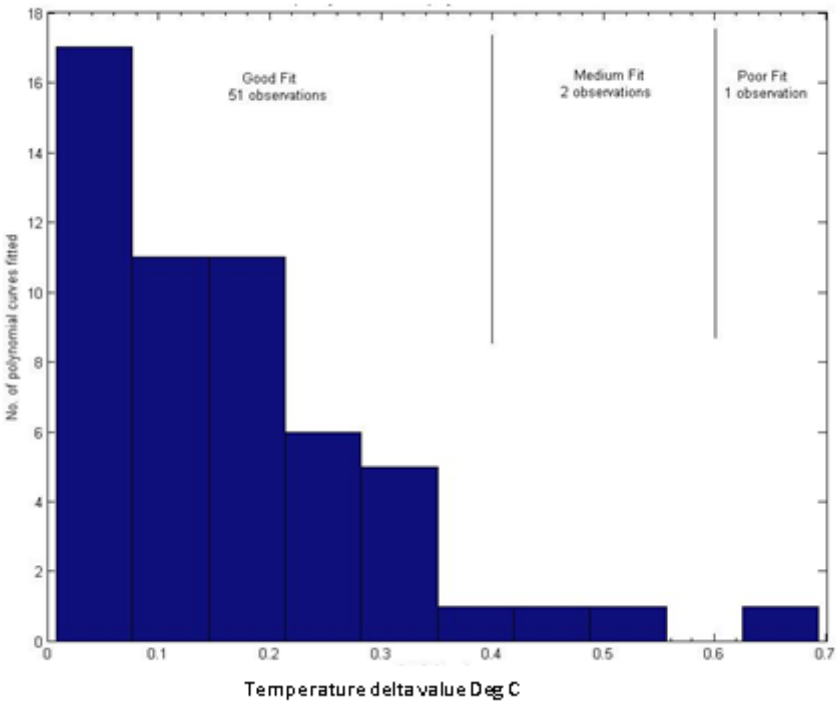

Figure 5-8*: A frequency distribution plot for the mean 'goodness-of-fit' for each profile using a 6th order polynomial curve fitting routine from 54 profile as an example, showing absolute delta values. Data distribution is shown as good fit (0 - 0.4 ^{0} C), medium fit (0.4 – 0.7 ^{0} C), and poor fit (=> 0.7 ^{0} C) values for each polynomial curve.*

3. Curve fitting techniques for contiguous profiles

Polynomial fitting of contiguous, as opposed to discrete profiles as shown above also had varying degrees of success, sometimes 'over-describing' the wind mixed layer in upper regions of the thermocline (0 – 25 m in this case), see **Figure 5-9**. Due to these limitations of the polynomial fit, other curve fitting techniques were explored for contiguous profile datasets.

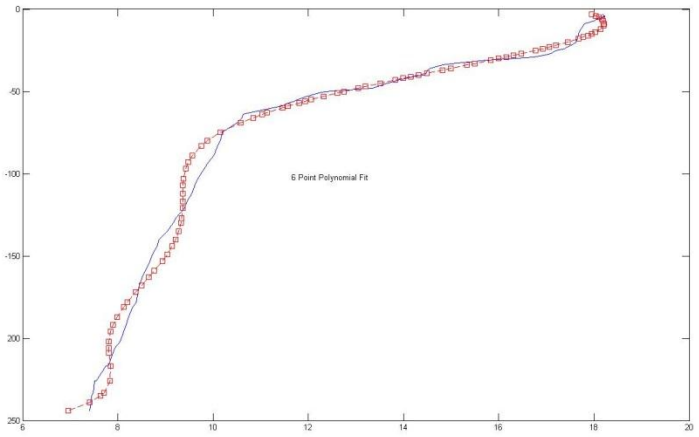

Figure 5-9: *An example of a 6th order polynomial fit (shown as a red line) applied to a single contiguous historic observed profile (shown as a blue line). Due to the poor curve fitting ability of this technique for contiguous profiles as shown here, an alternative curve fitting method was explored.*

For these kinds of profiles, often consisting of hundreds to thousands of temperature-depth data pairs per profile, a different curve technique was required, mostly to smooth (filter) erroneous temperature data spikes. Median filters are generally used to remove such data spikes. In this study, a 5 point mean appeared to adequately represent the original data sets and was applied to all contiguous profiles.

Of the 5359 original observational profiles for all months in the area of interest, approximately 30 % consisted of contiguous profiles of which all were fitted with curves for extraction of standard depth values. A summary of the statistics from pre-processing is provided in ***Table 6***.

Some examples of the median curve fitting technique and smoothing capability applied to temperature-depth profiles are provided in ***Figure 5-10***. The reader is reminded that the purpose for implementing this technique was to smooth or reduce some of the detailed real stratification that existed in the data whilst preserving the dominant stratification such as the wind mixed layer depth

and thermocline gradient. These are some of the significant factors in underwater sound propagation and are preserved in this context by representing the profile at standard depths that are more concentrated in the shallow region where stratification is often more prominent. The inclusion of this level of detail would have required orders of magnitude more standard depth temperature values that were not deemed beneficial for this study.

This curve smoothing principle can be seen to apply in ***Figure 5-10*** in most profile plots presented, but especially seen in the top right profile plot. In that plot real stratification seen in the blue line is seemingly removed by the red line smoothing process. However this is not strictly correct since the black stars seen on the red line plot are the actual only smoothed data value points used in the processing later, not the entire red line plot (see section 5. F and [Steps C.4 & C.5] in ***Figure 3-1***).

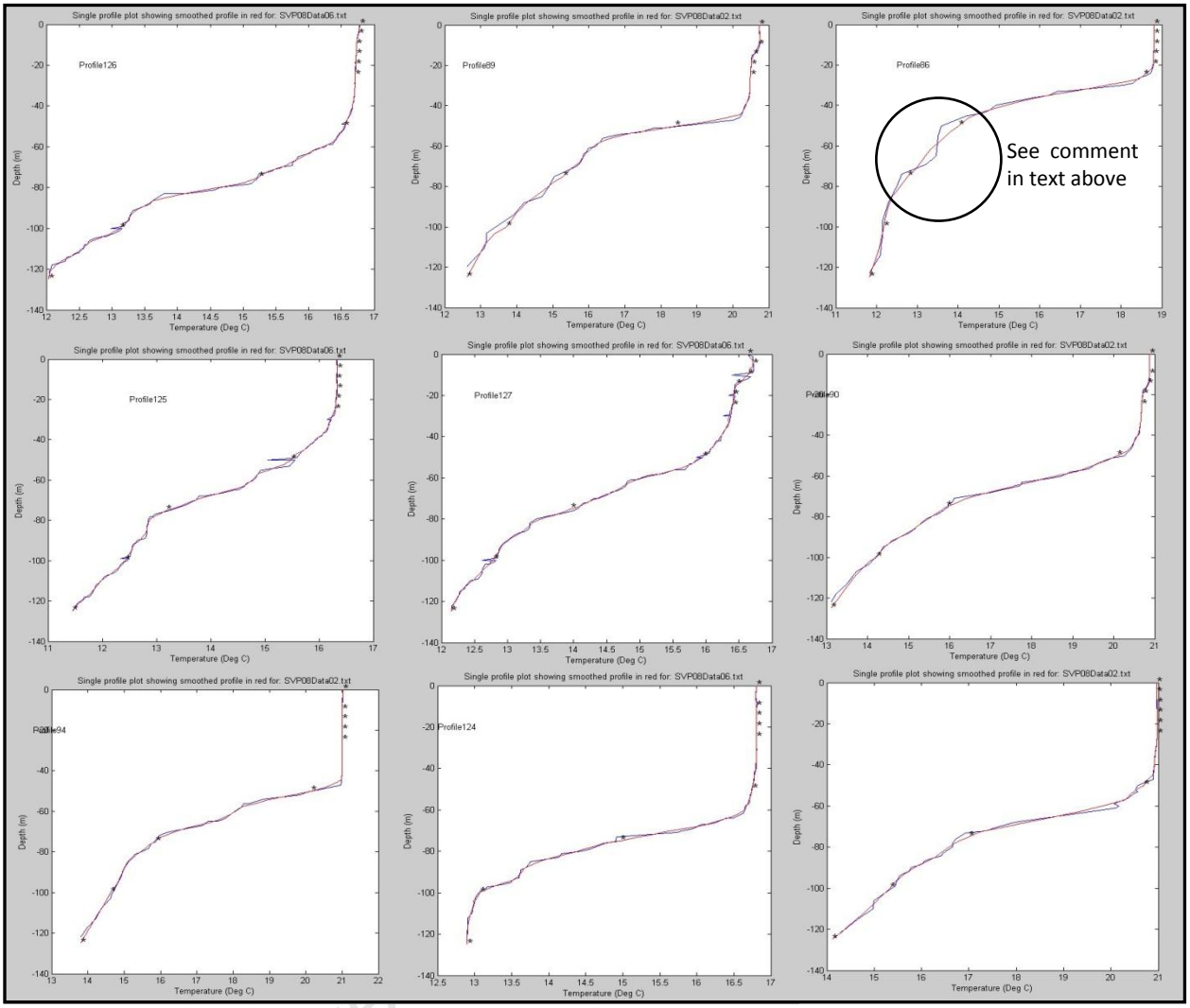

Figure 5-10: *Showing some examples of the curve fitting technique applied to contiguous profile datasets. The solid blue line represents the original source profile whilst the solid red line represents the applied 5-point running mean filter. 'Star' objects overlaid on the red plot are the filtered temperature values at standardised depths (0 m, 5 m, 10 m, 15 m, 20 m, 25 m, 50 m, 75 m, 100 m and 125 m) used in the normalisation process to follow.*

e. Filtering source profiles [Step C.3 in Figure 3-1]

Not all original sourced profiles represent ideal (without errors) temperature-depth datasets, since only limited data editing and cleaning can be undertaken at a data centre. In most cases, data stored and available to users of the database are as originally supplied to the centre. This meant that cases of inferior profile quality needed to be identified and specifically excluded from further processing. These 'spurious' profiles were flagged and disqualified from further neural network processing according to the following criteria:

1. Insufficient discrete data points to be deemed a profile [In this case a minimum of 6 temperature-depth pairs were required]. This accounted 5 % of profiles.
2. The maximum water depth sampled being less than 125 m. This accounted for approximately 5 % of profiles.
3. Identified spikes in the data. In this case, profiles were excluded if the absolute temperature range of any profile exceeded 12 ^{0}C. This accounted for approximately 28 % of profiles that were flagged as spurious. The 12 °C cut-off was used since it represented the full range of temperatures for the region and depth used in this study, as provided in the T-S curve after Shannon and Nelson (1996) as depicted ***Figure 4-9***.
4. A reserved (flagged) profile, kept aside especially for hind casting purposes. Although the number of profiles reserved for this purpose varies according to the SST value chosen, this accounted for roughly 2 % of profiles [These reserved profiles are shown later as red crosses on monthly hind cast maps in ***Figure 7-3***].

f. Extracting temperature values at standard depths [Steps C.4 & C.5 in Figure 3-1]

If sufficient number of contiguous profiles existed, then it would not be necessary to use the lower-resolution discrete profile data. However this was not the case and a large proportion of the dataset consisted of discrete profiles that were valid and required for further processing. This presented a processing challenge, since not all discrete profiles were recorded at the same depths and many more data points existed for each contiguous profile than for its discrete counterpart.

Once the 7 parameters (from the 6th order polynomial least squares fit between points) were calculated for discrete profiles and corrected for the wind mixed layer where necessary, each profile

was reconstructed (normalised) for temperature-depth on the basis of ten standardised depths (0 m, 5 m, 10 m, 15 m, 20 m, 25 m, 50 m, 75 m, 100 m and 125 m) below the sea surface.

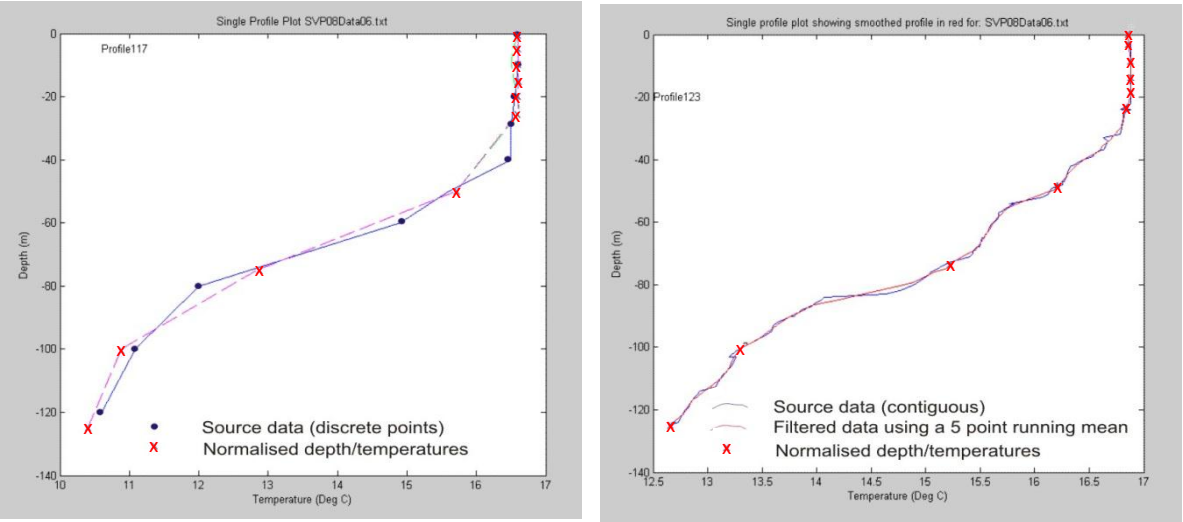

Figure 5-11: *Two examples of normalising, showing a discrete profile on the left and contiguous on the right hand side. Discrete and contiguous source data are shown as black points joined by blue lines and unedited solid blue lines respectively. The broken red line on the left hand side is the polynomial curve fitted to a discrete dataset, whilst the solid red line on the right hand side is a running mean curve fitted to a contiguous dataset. The normalised results are shown as red crosses in both cases, which mark the temperatures at ten standardised depths of 0 m, 5 m, 10 m, 15 m, 20 m, 25 m, 50 m, 75 m, 100 m and 125 m below the sea surface.*

Similarly, for contiguous profiles, temperature values of each smoothed profile at standardised depths were used if recorded at those depths. If not then a simple linear interpolation method was applied to determine the temperature between the upper and lower recorded value at any specific standard depth. The result was temperatures extracted at all standard depths for discrete and contiguous profiles, thereby normalising all qualifying profiles in preparation for the next step. An example of normalised profiles is shown in ***Figure 5-11***.

Not all valid pre-processed profiles could however be used for further processing, since some were required instead as hind cast profiles, used later for comparative purposes. To accomplish this, hind cast-potential profiles were flagged so that they did not contribute to the SOM processing. The principle followed was that every second profile with a surface value that was within the temperature range specified in the software was flagged, thereby halving the number of flagged

profiles. All flagged profiles were then reserved for dedicated use as hind cast profiles only. This resulted in a different number of pre-processed profiles for each SOM preparation, since the surface temperature value criteria changed for each execution of the software. The number of profiles used for SOM training during the hind cast test is shown in ***Table 7*** (row 4 and 5).

Flagging criteria applied to source profiles			
Name	**Description**	**Value**	
SADCO provided profiles (unfiltered)	Number of unfiltered profiles received from SADCO	6858	
Source profiles	Number of filtered profiles (filtered for profile category CTD, MBT, XBT etc. and spatial extent)	5359	
		2038 Contiguous	3321 Discrete
Maximum depth criteria	Number of source profiles that achieved the 125 m or deeper criteria (were flagged).	5109 (95.3 % of source profiles)	
Spurious profiles criteria	Number of source profiles that were flagged as spurious due to a temperature range per profile of more than 12 °C.	1508 (28 % of source profiles)	
Sufficient number of profile data points criteria	Number of source profiles that were flagged as containing sufficient depth/temperature pairs [set to a minimum of 6 in this case] per profile.	4815 (95 % of source profiles)	
Reserved for hind casting	Number of profiles exclusively reserved (flagged) for hind casting purposes	45 (0.8 % of source profiles)	

Table 6:*Flagging criteria applied to source profiles, with listed proportions. These flagged profiles were used to filter the source profiles for subsequent SOM analysis.*

In summary, the pre-processing described above was required to prepare historic observational profiles for the analysis and processing to follow. During this data pre-processing step a number of criteria were established to validate the input data. Separation of discrete and contiguous profiles was required to deal with these varying datasets independently of each other. This was accomplished by using differing curve fitting techniques to establish uniformity in the profiles as normalised output for the neural network process to follow. A sequential flow diagram for this process is shown in ***Figure 5-12***, with the profile flagging criteria filtering the datasets as shown in ***Table 6***.

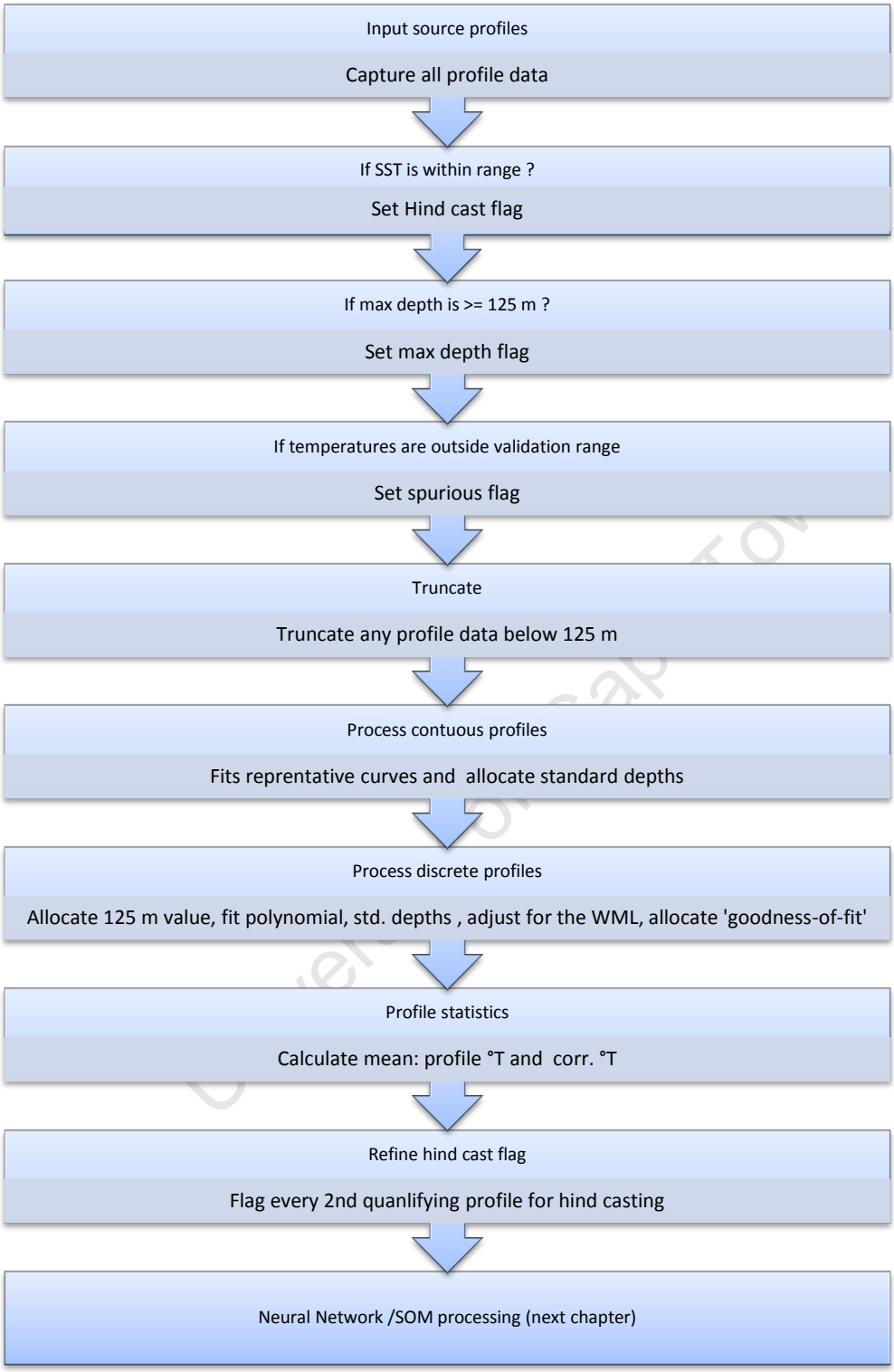

Figure 5-12: *Process flow diagram showing data pre-processing steps undertaken in preparation for the Neural Network processing to follow.*

6. NEURAL NETWORK AND SELF ORGANISING MAPS (SOM) ANALYSIS

The data pre-processing covered in section 5 used curve fitting methods to convert temperature profiles into a new dataset, with each profile having the same number of data points. In this chapter, the new datasets (described as standardised or normalised profiles) are provided as input to the SOM. The SOM in turn characterises or groups these into a continuum of synthetic profiles that represents the full range of the observational dataset. This network design is a form of predictive distribution, termed a Self Organising Map analysis (Vesanto et al (2000)), whereby predefined nodes become distributed within the output space of a dataset and thereby provides a representative grouping (prediction). Note that SOM used in this study comprised only the core processing tools required for processing, supplied as Matlab®- coded software routines. The routines or functions used are listed in APPENDIX D – SELF ORGANISING MAP TOOLBOX. These were incorporated into the extensive software routine suite custom developed for this study. No pre-compiled software applications were used.

Two SOM error variables (qe and te) as described by Vesanto et al (2000), are used to test the validity of the process. They are important Euclidean scalar SOM terms that define the resolution and topology errors respectively of the SOM process. Once completed, the SOM profiles are available as synthetic hind cast profiles for use in the next chapter.

a. Neural Network/SOM training [Step D.1 in Figure 3-1]

1. Introduction to SOM

"Self-Organising Map (SOM) is an unsupervised neural network method which has properties of both vector quantisation and vector projection algorithms" Vesanto et al (2000). The technique is a form of weighted least squares predictive classification described by Nhu and Zidek (2006) as one of many Environmental Network Designs.

This 2 layered process defines nodes, represented as vectors firstly in an input layer (or input space). Vector nodes (m) in this input space, are first initialised by a SOM setup that defines the original bounds of the data for training (using Euclidean distance) to synthetically represent datasets as a *d*-dimensional weight vector $m=[m_1,\ldots,m_d]$. The nodes are connected to adjacent nodes by a neighbourhood relation, which dictates the topology or structure of the map, after Vesanto et al

(2000) see ***Figure* 6-1** *(A).*Structure or topology in this instance refers to the arrangement or pattern of input nodes in Euclidean space, such as hexagonal or rectangular amongst (see Figure 1 in APPENDIX D – SELF ORGANISING MAP TOOLBOX).

Once the input layer is defined, the second step is to define the output layer (or output space) of the observational dataset, which then incorporates (or moves) the input nodes setup above into this new space. This is termed the output space since it defines the final output bounds or neural topological space; see ***Figure 6-1*** *(B).*

Once the nodes have been repositioned into the output space of the provided data, the nodes are ready for the training process to follow. One vector (*x*) is chosen randomly from the sample observational dataset (sample vector) and the distance between it and each of the vector nodes is determined (see the formula below). The vector node that is closest to the sample vector is then termed the Best Matching Unit (BMU), denoted here by *c*.

$$\|x - m_c\| = min_i\{\|x - m_i\|\}$$

Where || . || is some distance measure, typically Euclidian distance. The vector node is then weighted according to its distance from the sample vector as follows:

$$\|x - m\|^2 = \sum_{k \in K} \omega_k (x_k - m_k)^2$$

Where *K* is a set of known (not missing) variables of the sample vector x, x_k. m_k are the *K*th components of the sample and weight vectors. ω_k is the *K*th mask or weight value. After Vesanto et al (2000).

During the iterative weighted least-squares, step-wise training process, individual vector nodes 'jostle' or 'compete' for those that are topologically close (in Euclidean radius distance) to the underlying observational sample dataset by adjusting their weight values each time. During each step vector nodes appear to 'learn' from the sample data as topological neighbours of the BMU are treated similarly, appearing to 'stretch' the network node links while repositioning each affected neighbourhood node. See ***Figure 6-1***(C) where a single training step is shown as an example using a 4x4 network topology.

Note that the description above and the associated figure (***Figure 6-1***) are used here to illustrate SOM process in general terms only and used in the processing section of this study. For more detail concerning this section, see Appendix D.

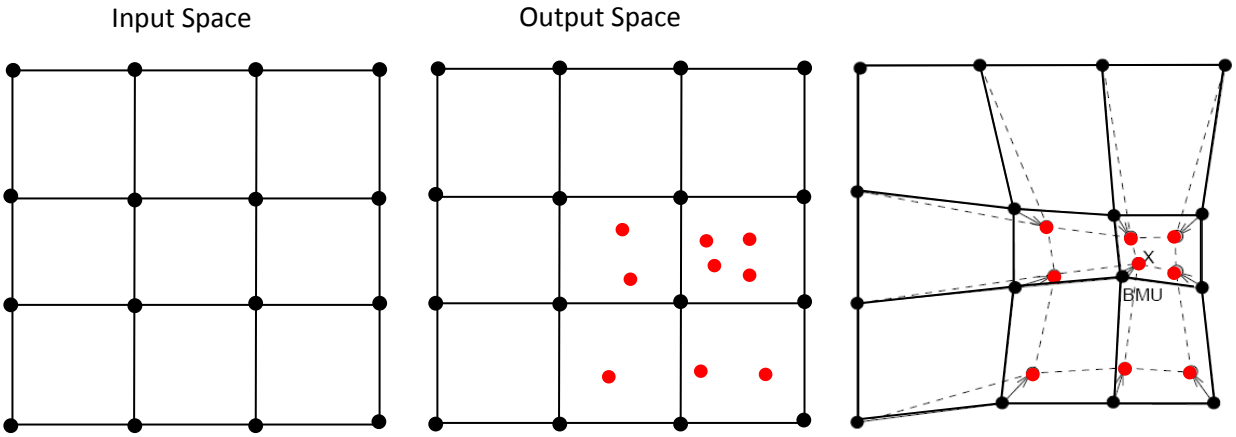

(A) A 2-dimensional 4 x 4 network of vector nodes in input space

(B) Same vector nodes in (A), moved into the output space of 9 observational sample data points shown as red dots

(C) Input vector nodes after a single step of training, after defining the Best Matching Unit (BMU), marked as 'x' and adjusting each vector node

Figure 6-1: *A schematic example of the setup, normalisation and a single training step of a 2-dimensional (4 X 4) rectangular SOM. The vector nodes were first initialized in input space (A), then imported into the output space of the provided observational sample dataset in (B), shown as 9 solid red dots. In (C) a single training step is shown whereby firstly the vector node closest to a randomly chosen observational sample data point (x) is defined as the Best Matching Unit (BMU). Thereafter each vector node within a pre-defined neighbourhood distance is weighted according to its closest observational sample point. The solid and broken lines correspond to the situation before and after updating respectively. After Vesanto et al (2000).* ***Note that the description above and the figure are used here only to illustrate SOM process*** *in general terms and are not part of the processing undertaken in this study. For more detail concerning this part see Appendix D.*

2. SOM applied to this study

As follow-on to the SOM introduction above, the application of the SOM technique to this study adopts the same terminology as above for the purposes of uniformity. This is intended to make the description of the process easier to follow. The vector nodes in the SOM introduction, shown as black dots in ***Figure 6-1*** and described in section 6.a. instead become the synthetic SOMS profiles. The observational sample data points shown as red dots in ***Figure 6-1*** and also described in section 6.a instead become the pre-processed curve-fitted profiles, all with the same number of temperature-depth paired values. These are shown as a single red cross representing 1 profile (***Figure 6-2***), creating their own new output space, based on their individual temperature values.

See ***Figure 6-1*** for the generic display of the concept and ***Figure 6-2*** for the same concept as applied to this study, using the same labelling theme to assist with connecting the theory to the application.

In place of the 2-dimenstional, 4x4 input rectangular grid (topology) used in the example above, a 1-dimensional, 1x15 hexagonal grid was used as the input space instead. In place of the 9 fictitious observational data points represented by red dots in ***Figure 6-1*** (B)), many hundreds of pre-prepared profiles are used here, represented as red crosses (1 cross per profile). The red profile crosses are plotted as a scatter plot of their surface value (SST) on one axis, against an integrated representation of each profile's temperature structure below it's surface value on the other axis. Although the scatter plot scale appears to represent temperature in this case, this is only because a simple 1 demensional structure was used within a unit-less eigenvalue 'temperature-like' grid.

It is these profiles that dictate the output space extent in which the vector nodes are incorporated, as evident in ***Figure 6-2***(B). Note that the vector nodes are ready for training at this stage, <u>not the profiles in observational profile dataset</u>.

Whereas the previous vector node schematic (***Figure 6-1***(C)) only showed a single training step, the application of SOM here shows examples of additional training steps for visualisation purposes only. Output after training the vector nodes for 1, 10, 50, 1000 and 10 000 steps are shown in ***Figure 6-2***(C)-(G)). This represents the 'self-organising' part of the SOM process.

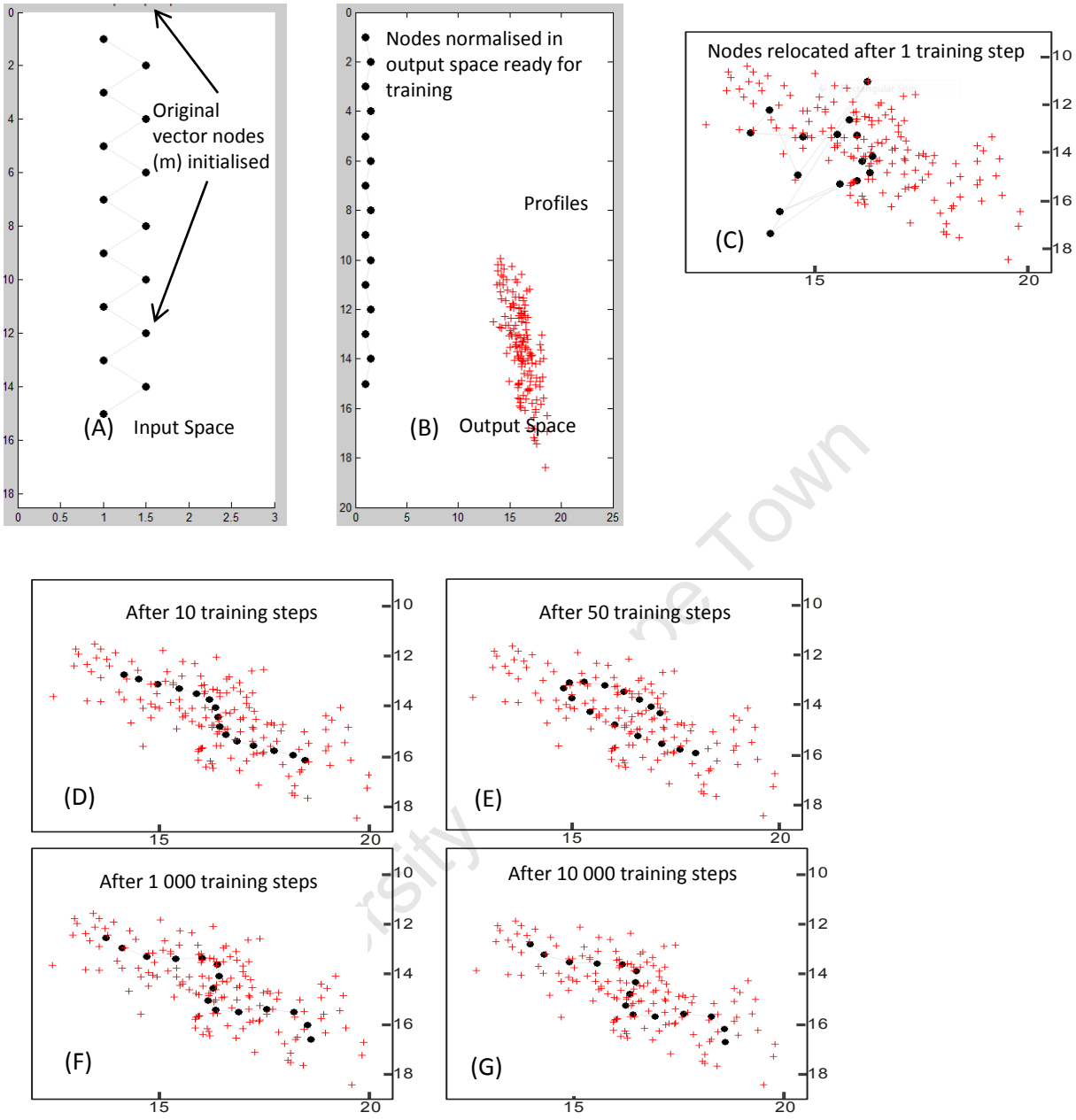

Figure 6-2: *Consecutive developmental stages of a SOM showing vector nodes, as initialised in (A) as input space and moved or incorporated to output space as defined by the pre-processed profile dataset, shown as a single red cross per profile in (B), with consecutive training stages in (C) to (G) after 1, 10, 50, 1000 and 10 000 steps. Note that Euclidean location of each red- cross (profile) does not change during the training process. Both axes scales are in unit-less Euclidean distance.*

In ***Figure 6-2***, the node setup and training process is shown in detail (A) and (B) to illustrate the SOM training concept only, since profiles displayed in this way cannot be interpreted as they are plotted in Euclidean space. The figure does however assist in illustrating convergence of the trained nodes towards a continuum shape that is visually clear as a plotted computer generated animation after a few thousand training steps and is quantified in the SOM software as two error variables, quantisation error (qe) and topology error (te).

SOM setup parameters.

1. Grid format. (e.g. 1x15 rather than for example 3x5 or similar). Refer to the description and schematic shown in ***Figure 6-1***. A linear 1-dimensional initialisation of the vector nodes was chosen since it closely represented the distribution of observational profiles when plotted for visual means in the output space (see ***Figure 6-2***(B)). This simple topology format was chosen since only one parameter (temperature) with 'implied' standardised depths was required to be categorized. This meant that depth as a factor did not contribute directly in the SOM process, since the sequence of 10 temperatures per profile prepared for SOM analysis was represented by the 0 m, 5 m, 10 m, 15 m, 20 m, 25 m, 50 m, 75 m, 100 m and 125 m depth values in each case. This is considered a rather simple SOM format and probably contributed to the low number of vector node training steps required (see ***Figure 6-6***).
2. Topology. The linear shape created by the observational dataset (profiles in this case) when viewed in the output space (see ***Figure 6-2****(B)*) meant that the choice of topology (rectangular or hexagonal) was irrelevant and did not influence the outcome or the vector node training process. Since a choice was necessary to execute the software, a 'hexagonal' grid was arbitrarily chosen. Kohonen and Honkela (2007) advised that a hexagonal grid of nodes is preferred for visual inspection.
3. Number of vector nodes.

   The following is an extract from Kohonen and Honkela (2007) where the choice of number of nodes is described:

   "Scaling of the vector components *is a very subtle problem. One may easily realize that the orientation, or ordered "regression" of the model vectors in the input space depends on the scaling of the components (or dimensions) of the input data vectors. Especially if the data elements represent variables of different kinds and are therefore given in different scale there does not exist any simple rule to determine what kind of rescaling is best before*

entering the training data to the learning algorithm. One may try heuristically justifiable re-scalings and check the quality of the resulting maps, e.g. By means of Sammon's mapping (Sammon (1969)) or the average quantization error. Often the normalization of all input variables such that, e.g., their variances become equal, is a useful strategy." Average quantisation error (qe) was used as the test variable of choice in this study, although no formal testing was undertaken to confirm the variances with respect to the number of nodes used.

An important consideration (and benefit) in this study was that only 1 data variable (temperature) was used. Most SOMS use many variables (example: Sepal length, Sepal width, Petal length and Petal width to describe Iris flower types) which complicates the choice of setup parameters such as number of nodes.

Too few nodes would result in a poor 'description' of the true detail contained in the observational dataset. In terms of temperature profiles, this meant that too few stratification stages were described in the outcome (e.g. 3 nodes resulted in well-mixed water (no stratification), partially mixed water (medium stratification) and well developed thermoclines (highly stratified). That outcome did not serve the requirements of this study, since too few vector node 'predicted' profiles only described extreme and median profile conditions. On the other hand, too many vector nodes meant that many nodes would not receive 'hits' (not allocated to Best Matching Units (BMUs)), resulting in a disjuncture of representative profile groupings. In an extreme case the number of vector nodes should not be similar than the number of observations (profiles) since categorising or grouping becomes impossible. Hence the preferred number of vector nodes was achieved when each vector node received approximately the same number of hits and a continuum of representative profiles resulted.

The SOM toolbox documentation (2005) advised that: *"If possible, the shape of the map grid should correspond to the shape of the data manifold."* Also, *"The default number of neurons is 5 * sqrt(n) where n is the number of training samples. Note that the computational load increases quadratively with the number of map units. Therefore, don't take literally the "as big as possible" thing above. In our own research, the number of map units is usually between 100-600".* In this instance (n) was 15, using 2580 samples or source profiles, see

Table 7. Using the default values above, would mean that 5*sqrt(2580) or 254 nodes would be required. Although 15 nodes may at first appear too modest, the use of more nodes would result in an impractable number of groups, making it too difficult to select a single representative node profile to as a solution. Using only 15 nodes meant that the SOM was able to summarise the data and still capture sufficient detail of in-situ temperature profiles. Hence a decision to use 15 nodes, motivated simply on the basis of achieving a representative yet continuum of profiles was justified (see ***Figure 6-3***, ***Figure 6-4*** and **Figure 6-5**)

4. Training Steps. Although (Vesanto et al (2000)) noted that training should be executed at least 10 000 times for most SOMS, it was decided to start with this number of steps and explore a maximum and minimum 'extreme' about this value to determine the effect on the outcome of the SOM. The result was that although 10 000 steps was seen to be adequate, the SOM could have accomplished the same result using say 3000 training steps. This was confirmed by the sensitivity test where "qe" (or 'topology error' was seen to converge at about 2000 training steps) – see ***Figure 6-6*** *(A*). The only consequence here was that the computer processing took somewhat longer. Based on that, it was decided that 10 000 training steps, although somewhat generous, did not detract from the outcome and was wholly adequate. The reader is also encouraged to inspect the sample training step test results as depicted in APPENDIX D – SELF ORGANISING MAP TOOLBOX. Note that the shape of the vector nodes (seen as black dots) shows no appreciable change between 1000 and 10 000 training steps.
5. Radius distance This is the neighbourhood distance radius used to start the training process, recommended by the software manual to be kept small at 1: 2 or 0.5. Refer to Appendix D. There was no reason to adjust this since the consequence of using another setting would not have made any appreciable difference to the outcome.
6. Initialisation A random initialisation (also set as default by the software) was used. This meant that the initial placement of the 15 nodes, although hexagonal in structure (see ***Figure 6-2*** (A), was placed in the output space in a random way just prior to the training process between (***Figure 6-2*** (B) and (C)). In other words in output space before the first training step occurred. This random initialisation step is therefore not depicted in ***Figure 6-2***.

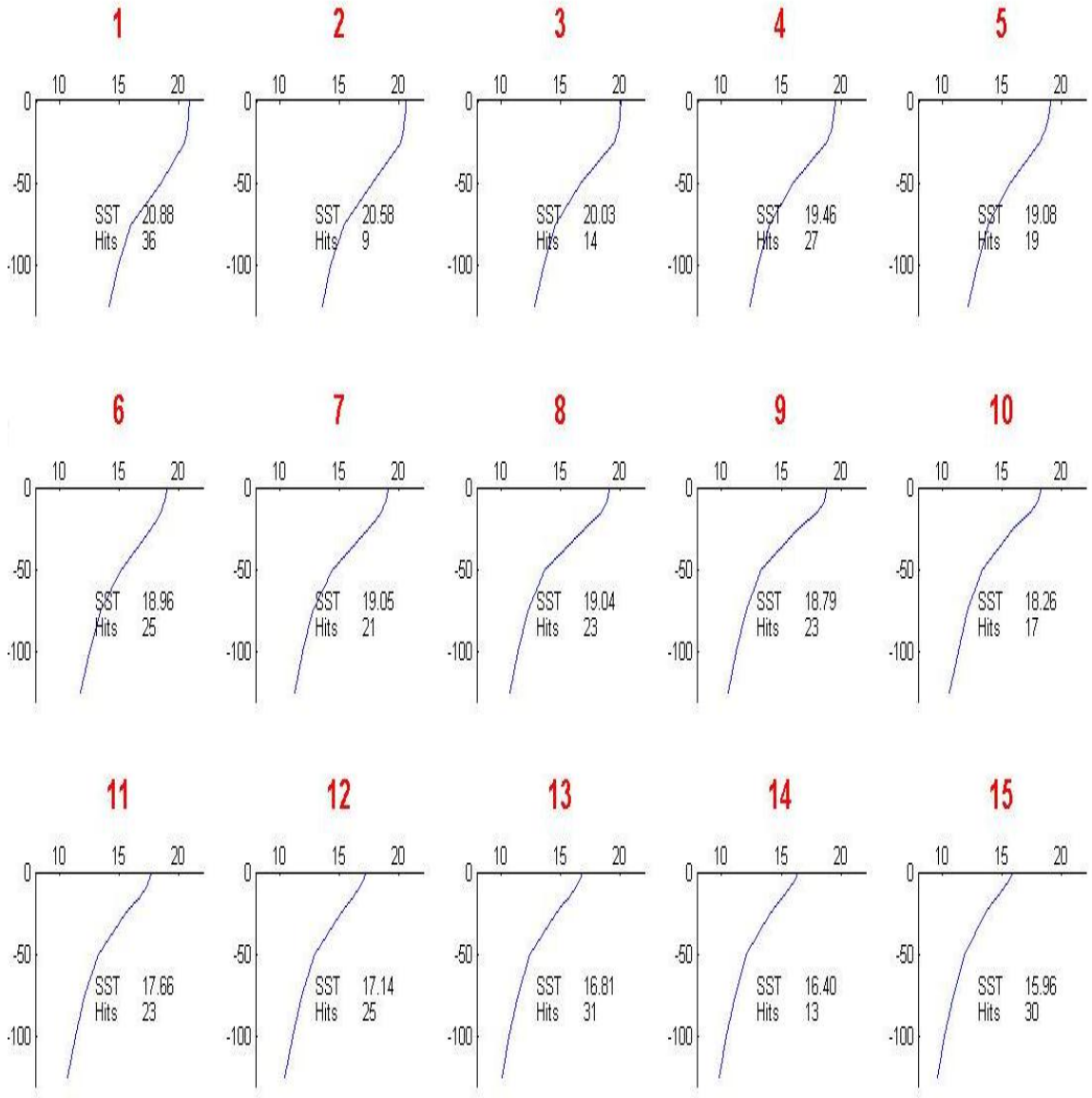

Figure 6-3: *Example of one of the SOM classification tests executed as part of this study. The SST is the uppermost temperature value of each output profile class as shown on the x-axis. 'Hits' refer to the number of input profiles that were allocated by the SOM to each identified output profile class (1-15). The x-axis is sea temperature whilst the y-axis is depth below the sea surface represented as increasing negative numbers. The result can be seen to capture the surface temperature change as well as the wind mixed layer depth, a critical feature in underwater acoustic validation step later.*

Once the nodes are trained, they represent the synthetic or categorised range of profiles. In this case synthetic profiles (trained nodes) ideally represented the full range of profiles provided in the output space. Of note in the SOM procedure, was the ability of the technique to adequately separate classes of profiles based on the natural developmental and decay status of the thermocline, described by 15 classes, creating a suitable continuum of groupings (see ***Figure 6-4***).

When plotted alongside each other, the continuum shape of the 15 output classes were clearly evident as can be seen in ***Figure 6-4*** , where node 15 (or class 15) had the coldest temperatures, with the least vertical mixing and weakest thermocline. From node 15 to 9 a steady increase in temperature was observed in the upper 20 m. Increasing temperatures were also observed to coincide with increased vertical mixing (see the progression from profile node 15 to node 1). This result corresponds with the known hydrographical properties of the region for that time of year (January) and resulted in some confidence in the technique. Further interpretation of the output is provided in the results chapter to follow. The continuum of the nodes could also be observed by the consistency of the number of hits per node as can be seen in **Figure 6-5**. Hits in this context refer to the number of sample profiles that were allocated to each of the 15 nodes, after the training occurred. A consistent hit number across all nodes is preferable, meaning that the nodes adequately resemble the underlying sample profiles. Since the SOM process starts its training in a random order, the number of hits per node generally varied somewhat with each training session.

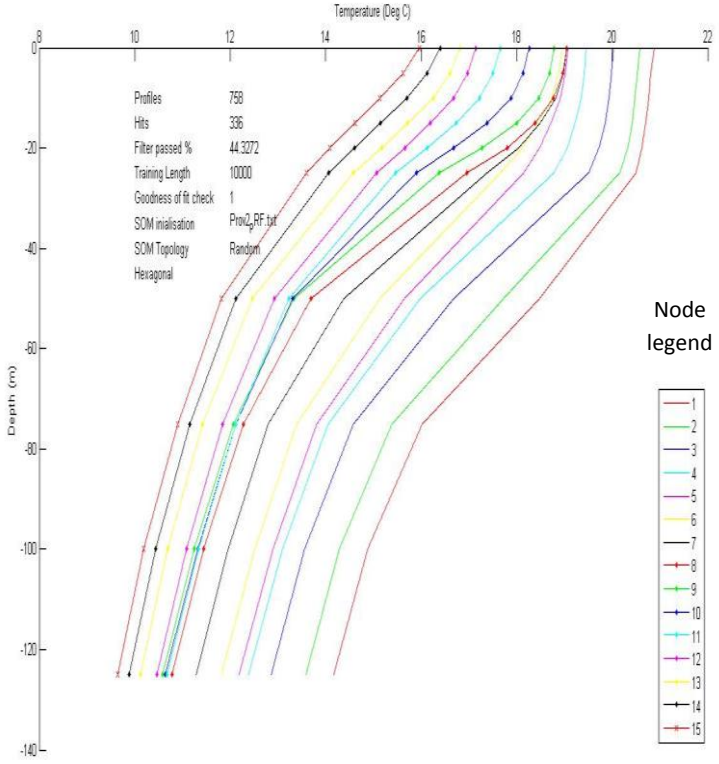

Figure 6-4: *Example of a temperature-depth plot of 15 SOM output nodes as shown in* ***Figure 6-3****, represented as synthetic profile categories for the month of January. The line-style legend in the box on the bottom right lists the 15 nodes displayed in the plot.*

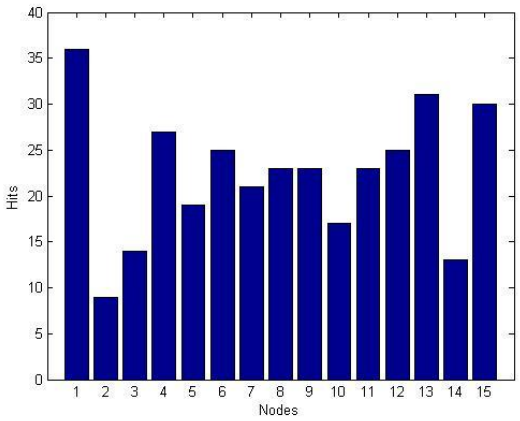

Figure 6-5: An example bar graph of 758 input profiles and 336 hits from the SOM analysis above for the 15 synthetic profile (trained nodes) classes.

b. SOM error tracking (qe and te)

SOM output quality is evaluated according two scalar criteria, resolution (qe) and topology preservation (te).

Qe or 'quantisation error' is defined as the average distance between each data vector and its BMU. For the trained nodes to adequately represent the underlying observation dataset, it is preferable for the scalar resolution (qe) to converge during the training process. In this instance, this was seen to occur after about 2000 training steps (see ***Figure 6-6*** and Appendix E).

Te or 'topographic error' is a measure of how well the original topology shape (e.g. 4 x 4 hexagonal) was preserved during the training process. In this simple 1 x 15 hexagonal shape, this was of no consequence, since te is only intended to maximise visual quality of the outcome. Te is therefore shown in ***Figure 6-6*** only for completeness of the SOM reporting.

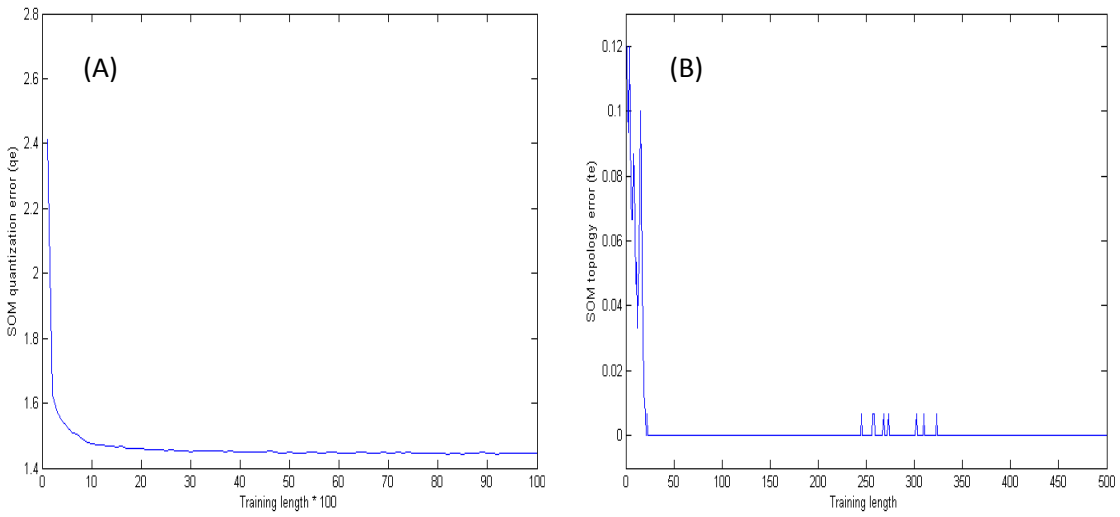

Figure 6-6: *(A)The effect of SOM training length (x-axis) on the quantisation error (qe on the y-axis) where convergence occurred after 1000-2000 training steps at a qe value of about 1.47. Note the training length scaling of 0-10000 steps. In (B), the topology error (te on the y-axis) converged abruptly to zero after 23 training steps, with minor peaks of 0.0067 between 240 and 325 training steps. Although not shown here, no further deviation of te from its zero value occurred between 500-10 000 training steps. Note, only the first 500 training steps are shown here (plot B).*

For suitable SOM analysis, the dimension of the data set or nodes to be trained (15 in this case) should be less than the dimension of the map grid profiles onto which the nodes are mapped or

trained (300-400 in this case). Although more nodes may have increased the ability to classify or describe the variability such as intrusion of Agulhas rings and filaments into the region, this would have reduced the discrete nature of the synthetic profiled surface temperatures (see ***Figure 6-4***, ***Figure 7-1*** and APPENDIX F – HIND CASTS). This would mean that the software would not be able to discriminate amongst the many neighbouring 0 m profile surface temperature values to identify a single winning profile, resulting in many too profiles being proposed as a 'solution' and the potential for ambiguity. Since the purpose of this study is to predict a single representative profile, using more than 15 In this case would likely not have improved the outcome, but instead added to the complexity of deciding on a suitable winning profile. This logic is consistent with the guidelines provided by Kohonen and Honkela (2007). Further testing for the effective number of was not undertaken, since it was felt that an adequate result was achieved with 15 nodes. Although other mapping initialisation settings may have produced a different quantisation error, the purpose of this part of the study was to test for that the number of training steps was adequate, by using qe as the measure ***Figure 6-6*** (A). Random tests using varying initialisation options would likely not have improved substantially on the simple 1-dimensional SOM input.

Results from these tests show that no significant improvement to the error values could be achieved beyond 3000 training steps (see ***Figure 6-6*** *(A*)), although a more robust number of 10 000 steps was used throughout in this study. This confirmed that the setup of the nodes and input data of the SOM parameters were suitable to achieve an acceptable characterisation result.

The topology error used in this study was less useful as measure of SOM mapping success than quantisation error. Hexagonal topology preservation in a 1 dimensional array such as used in this study becomes somewhat meaningless. This is apparent where the minimum value occurred after less than 50 training steps (see ***Figure 6-6*** (B)) and is shown here for completeness only.

7. RESULTS

This chapter starts 'closing the loop for testing the hypothesis' in Step D of ***Figure 3-1***. , by using a group of 15 profiles that were proposed above as a neural network SOM output, to represent the physical world for a selected month of the year, in a specifically defined region. However, if one is provided with only a sea surface temperature value (as may be the case from remote sensed satellite sources), then by selecting just one of the 15 SOM synthetic profiles, based on its surface temperature similarity to the remote sensed value, one could infer or assimilate the profile structure at that point.

The same concept is used here specifically to test the validity of the SOM process. By using the synthetic SOM profiles prepared above and examining only their surface temperature values, a single profile (any 1 of 15) is chosen by the software as the predicted profile. To test the success of this predictive capability, a hind casting process is used, whereby a subset of the original qualifying sample profiles is reserved for validation purposes. These hind cast profiles are then tested quantitatively for their predictive capability by using accepted norms to validate the results.

a. Representative SOM profile predictions [Step D.2 in Figure 3-1]

The SOM output produced 15 profiles that were "proposed" to represent the physical world for a selected month of the year, in a specifically defined region. However, since the hypothesis for this thesis proposes using the surface temperature value of the profile, it is important to now establish the criteria for defining that value, which was used to identify a single synthetic profile (1 of 15).

An option was set up in the software for execution at run-time, whereby the operator was able to enter a desired SST value (as if chosen from a satellite remote sensed source). A simple absolute minimum value was applied or, the minimum difference between the 0 m values of each of the 15 proposed synthetic profiles and the provided remote sensed SST value. Once the winning profile was identified, it became the predicted synthetic profile of choice by the software and was flagged as such to denote its status. In this instance 15.5 °C was used as a criterion, since it approximated to the modal 0 m temperature value in that region during that month (see ***Figure 7-1***(C)). This histogram plot was used here for information purposes, as a guide to the how well the remote sensed SST value was 'represented ' in the 0 m temperature values of each observed profile used in the SOM analysis. This was useful since it provided some indication of whether the SST value was

within the bounds of the surface temperature values of the historic profile datasets. These histograms are also used extensively later (section c) and ***Figure 7-4*** (A) to select 3 SST values (low, median and high) for each month during the sensitivity analysis. Although 15.5 °C was used here to illustrate the concept, a range of modal 0 m profile surface temperatures from 15.5 °C for the month of August to 19 °C for April was used in the hind cast testing process later (See ***Table 7*** (Row 2)).

An example of this winning synthetic profile can be seen as a solid red line plot in ***Figure 7-1***(A), due to its closest 0 m temperature value marked by an arrow at 15.5 °C. The black stars overlaid on the red line are the 10 temperature point values (at standard depths) used to generate the line plot or points of inflection on the polyline. The other 14 non-winning SOM profiles are shown as solid green lines in the same plot.

In ***Figure 7-1***(B) 15.5 °C was also used by the software to flag profiles suitable for hind cast purposes. In order to constrain the number of profiles 'lost' to this cause however a stringent user-selecatbale 'SST delta' of ± 0.25 °C was preset for all SOM executions. See the next section where this is described. Using this criteria, 8 profiles qualified for hind cast purposes for the month of August (See ***Table 7*** also).

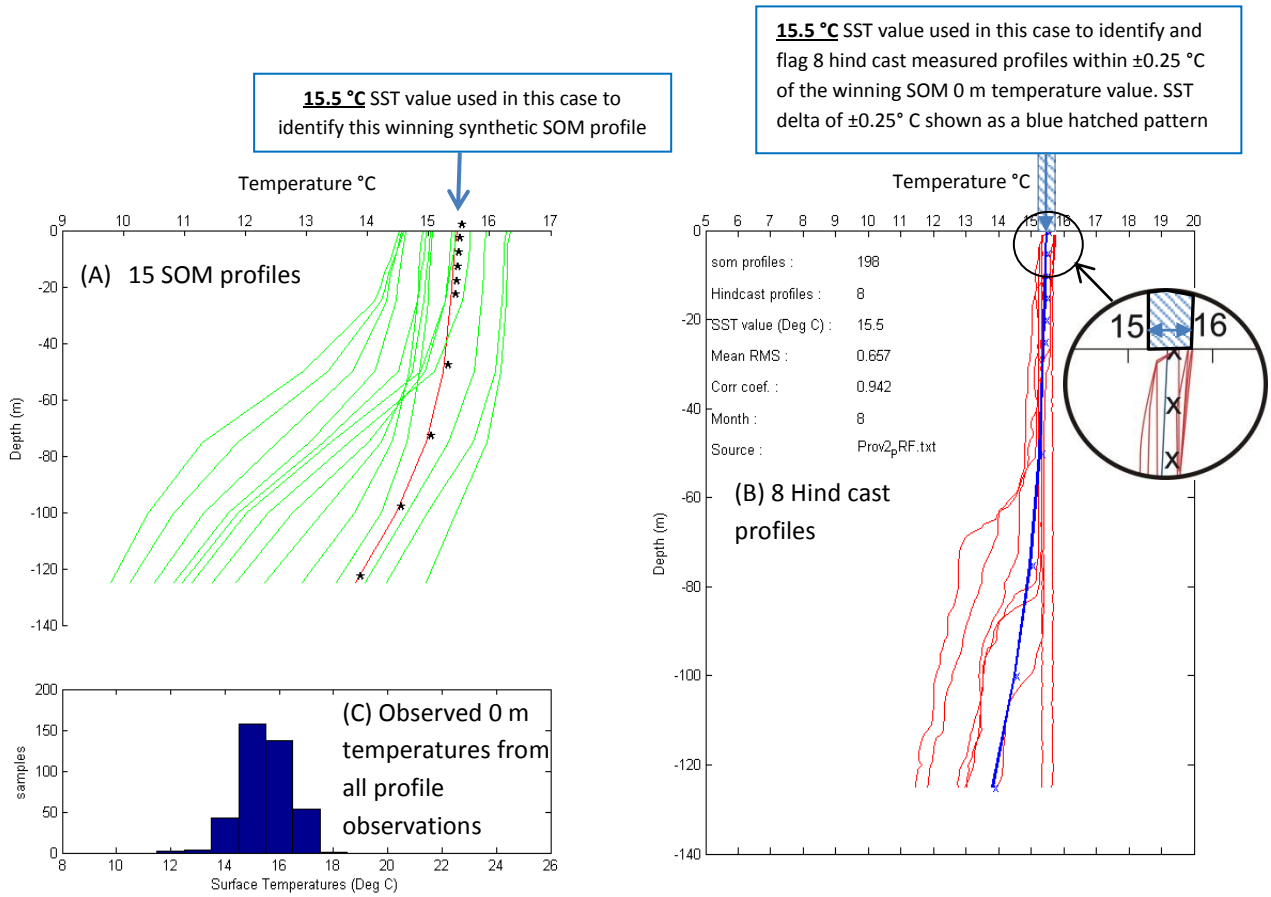

Figure 7-1: *An example output of 15 SOM output profiles and single predictive result for the month of August shown as solid green lines in (A), with the chosen (by the software) synthetic SOM profile shown as a solid red line in (A) and a solid blue line in (B), using a chosen surface temperature criteria value of 15.5 °C in this case to identify the winning synthetic SOM profile. In (B), 8 qualifying hind cast profiles as identified by the software are plotted in their original form as solid red lines. The same predictive profile is shown in (A) and (B) with standard depths depicted as black stars (*) and blue crosses (x) respectively. The inset text and graphic describes the* ± 0.25 °C *SST delta used to flag profiles for hind cast purposes. In (C), a bar graph is used to display the statistical features of the sea surface temperature values (0 m) of the observational profiles for the region during that month.*

Output plots for the remaining calendar months are provided in APPENDIX F – HIND CASTS.

b. Hind cast testing [Step D.3 in Figure 3-1]

Once a single synthetic profile was proposed/predicted, it was necessary quantify the success of the outcome. An option was setup in the software for execution at run-time, whereby the operator was able to enter a desired SST value (as if chosen from a satellite remote sensed source). This was by default, logically the same value (15.5 °C) as used in the SOM analysis for identifying the winning synthetic SOM profile.

The principle applied was to limit or minimise the number of potential profiles being flagged, to maximise the number of profiles available for SOM training. This limiting criteria was defined as the maximum allowable SST temperature error range, hereby referred to as a 'SST delta'. The SST delta value was pre-set to ± 0.25 °C for all hind casts undertaken in this study (e.g. 15.25 °C to 15.75 °C or 15.5 °C, ± 0.25 °C). See ***Figure 7-1***(B) with circle insert showing the chosen SST value and SST-delta range graphically for the 8 hind casts flagged in this instance as red line plots. The reason for constraining the SST delta value was to maximise the accuracy by minimizing the Root Mean Square (RMS) 'error' of the hind cast result since a larger SST delta would contribute to a larger RMS value. The Root Mean Square technique is explained below. This assumed then that the 0 m surface temperature value measured at a location at sea was within ± 0.25 °C of that measured from a sensor mounted on a satellite, including day/night sensor correction factors. This fact was however not tested in this study. A further method to 'sub-sample' or reduce the number of flagged profiles was employed. This consisted of only retaining the flag status of every second flagged profile, thereby further reducing the number of flagged profiles by half. The above describes how the number of hind cast profiles was determined as presented in ***Table 7*** (row 6).

Hind cast qualifying criteria for discrete and contiguous profiles were treated separately since their formats are distinctly different (see section 5.c). The principle for contiguous profiles was that recorded temperatures were used for all standard depths *(0 m, 5 m, 10 m, 15 m, 20 m, 25 m, 50 m, 75 m, 100 m and 125 m).* If a temperature value was not measured at any specific standard depth, such as only recorded at either side of that discrete standard depth (e.g. 4.75 m and 5.65 m for the 5 m standard depth) then a linear interpolation of the temperature was undertaken by the software so that a valid interpolated temperature was instead associated with the temperature-depth paired record. This principle could not be applied to discrete profiles since too few temperature-depth pair values were recorded for a valid interpolation method.

It was decided that for any discrete profile to qualify for hind cast purposes, where data integrity was paramount (hence no interpolation) a measured temperature value was required for every standard value (10 in total). With those criteria instituted, the hind cast test undertaken resulted in **no** discrete profiles having qualified as hind cast candidates. These discrete profiles were nevertheless used for training purposes. The decision to adopt such a stringent acceptance criteria for discrete profiles was deemed necessary since poorly represented discrete profiles (in the depth context) may have incorrectly skewed or degraded the RMS value, to the detriment of this study. The lack of discrete profiles contributions as hind casts can be seen in ***Table 7*** (row 6 as figures in blue colour) all as zeros.

Once these hind cast profiles were flagged within the original source dataset, they were then excluded from playing any further role in the in the subsequent SOM analysis process.

The number of profiles used for hind cast purposes (45 profiles or 0.8 % of all source profiles) was similar to the number used by Chu et al (2000): 40 profiles from 10113 training profiles or 0.4 % of all source profiles. Although only 1 hind cast was possible for the months of March, May and June, the numbers were intentionally constrained by the use of only the monthly modal SST value in each case (***Table 7*** (row 2)) to identify winning hind cast profiles, to ensure objectivity in the result. In these cases (single profiles) the calculation of mean standard deviation values was not possible (***Table 7*** (row 9)). In the context of 45 profiles for all months of the year though, this is considered valid.

It is possible that another software execution with more relaxed hind cast selection constraints may have resulted in a more representative sample size for months with lower hind casts (e.g. June). This would however likely also have increased the RMS value. That test was not however undertaken since it was deemed more objective to instead conduct a more thorough hind cast test where the sensitivity of other variables could be tested against the RMS output. In that instance, to ensure that the sensitivity test could be used together with quoted hind cast test meant that the hind cast selection criteria needed to be the same as those of the sensitivity test.

Calendar month		Jan	Feb	Mar	Apr	May	Jun	Jul	Aug	Sep	Oct	Nov	Dec	Total/ mean
Modal SST value (°C)		18	18	16	19	17	18	16	15.5	15.8	16	16	17	
Original source profiles		758	711	410	423	479	313	499	396	317	371	359	323	5359
SOM source profiles		330	387	205	192	216	161	233	198	164	176	183	135	2580
Profiles accepted for SOM (Contig. Discrete)		154 176	144 243	74 131	23 169	32 184	47 114	98 135	63 135	18 146	24 152	37 146	19 116	733 1847
Profiles reserved for hind cast purposes Contig. vs. Discrete		9 9:0	2 2:0	1 1:0	5 5:0	1 1:0	1 1:0	5 5:0	8 8:0	5 5:0	3 3:0	3 3:0	2 2:0	45 45:0
Mean for all profiles	Mean RMS	1.29	1.28	0.63	1.00	0.59	0.51	0.83	0.66	0.73	0.40	1.38	1.29	
	Mean RMS	0.883												
	Mean RMS Std.Dev.	0.56	0.38	-	0.51	-	-	0.49	0.34	0.35	0.14	0.90	0.40	0.45
	Mean Profile Corr. Coeff.	0.935	0.996	0.981	0.937	0.995	0.966	0.805	0.942	0.752	0.994	0.8664	0.988	0.93
	Mean Corr.Coeff.	0.930												
	SOM qe (Para. 7.b)	2.02	2.10	1.99	1.88	1.71	1.43	1.32	1.26	1.10	1.39	1.54	1.72	1.62
	SOM te (Para. 7.b)	0.024	0.005	0.010	0.00	0.089	0.019	0.013	0.056	0.006	0.040	0.033	0.000	0.03
Reference in ***Figure 7-3*** * also in ***Figure 7-1***		(A)	(B)	(C)	(D)	(E)	(F)	(G)	(H)*	(I)	(J)	(K)	(L)	

Table 7: *Showing the monthly number of source profiles including those suitable for SOM analysis, entered surface temperature values, the contiguous/discrete profile proportions, prediction results and the SOM quality output. Note that a single SST value was used in each case. SOM qe and te are SOM error variables described in section 7.b. All RMS and Corr. Coeff. units are °C. Cells with '-'indicate too few samples for a statistical outcome.*

A simple RMS test (as adopted by other similar research initiatives) was used to quantify the effectiveness of the process. See description of RMS in Appendix H. To accomplish this, the software was repeatedly executed for each calendar month, using an approximate mean sea surface temperature as input for identifying hind cast profiles. The settings, selected hind cast numbers and SOM results for each month are shown in ***Table 7***. During the repeated execution of the SOM analysis and prediction as shown in ***Table 7***, the following parameters were set as constants (see section 6.a.2 for detailed descriptions):

Training steps:	10 000
Goodness of the polynomial fit (applicable to discrete profiles):	*1 °C*
Maximum SOM surface temperature validation delta:	*0.25 °C*
SOM radius distance:	*2*
SOM initialisation:	*random*
SOM topology:	*Hexagonal*

Plots of the results for each month as shown in ***Table 7*** are provided in ***Figure 7-3***.

An RMS difference value as described on page 27, section 2.b is the accepted norm for this type of prediction and is used here to quantify the effectiveness of the process as a comparative benchmark. Although this result was somewhat advantaged when compared to other techniques, since a surface temperature value is provided as prior knowledge for each hind cast.

The following observations were made:

The stringent qualifying criteria, as pre-set in the software, meant that approximately half of the original source profiles were accepted for the neural network training, as SOM source profiles (see ***Table 7***). Of these, a large proportion (ratio of 2.5 to 1) consisted of discrete-type profiles. These are shown as blue (discrete) and red (contiguous) font colours in rows 5 of the text in ***Table 7***. The stringent criteria resulted in only contiguous-type profiles qualifying as hind casts, as seen in row 6 of ***Table 7***. Note that all identified and flagged hind cast profiles were excluded from the SOM training process.

There appeared to be lower variability in the more vertically mixed profiles than in the stratified ones, resulting in increased RMS differences for the warmer months of November to February, also

observed in the sensitivity analysis in ***Figure 7-2***. This result is also evident in the plot of each profile's mean RMS as shown in ***Figure 7-4***. Somewhat lower RMS values in late winter and increased values in summer were noticed.

A mean RMS difference value of 0.88 °C for all months, from 45 hind cast profiles was measured, with a minimum of 0.40 °C and a maximum of 1.38 °C. SST values used for this determination were chosen based largely on the modal SST value for each month, since this maximised the opportunities for available hind cast profiles. The monthly-mean standard deviation as listed in ***Table 7*** was 0.45 °C. The lowest mean profile RMS values occurred in the months of May, June and October (see ***Figure 7-3*** (E), (F) and (J)).

Low RMS values of less than or equal to 0.5 °C were achieved for most (43 of 45 hind cast profiles) in the upper 20 m, with exceptions for the months of January and November. This is attributed to the more variable vertical wind mixed layer conditions observed in the hind cast profiles for those months (see ***Figure 7-3*** (A) and (K)).

High correlation coefficient values were recorded for all months, with a minimum of 0.752 and a maximum of 0.988 for the months of September and December respectively (see ***Figure 7-3*** (I) and (L)).

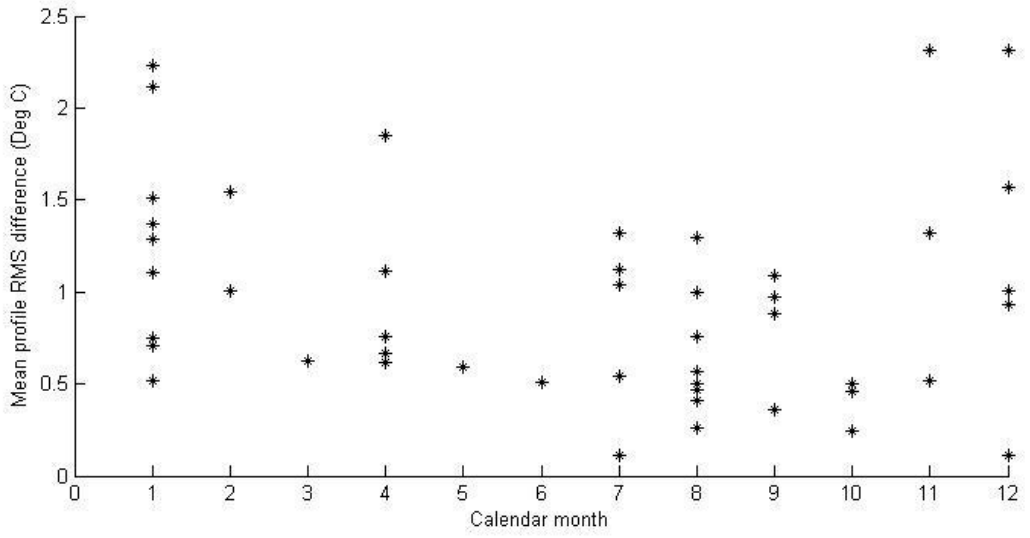

Figure 7-2: Showing mean profile 45 RMS values for a single SST value per calendar month, using the same output as shown in ***Table 7*** and ***Figure 7-3***.

In summary, the above hind cast results show the effectiveness of the analysis and prediction process in terms of RMS and correlation coefficient indicator values. In each case a single SST value was chosen for each calendar month and the software determined, based on a pre-set 0.5 °C temperature delta criteria (+ 0.25 °C and - 0.25 °C), which profiles were allocated for hind cast purposes. While this method is effective as examples of the process, it did not describe the full range of SST values and the performance of the other output parameters per month, locality and SOM error amongst others. To accomplish this, it was necessary to undertake a sensitivity analysis of the process. The results from this more rigorous test than that described above are covered in the next section.

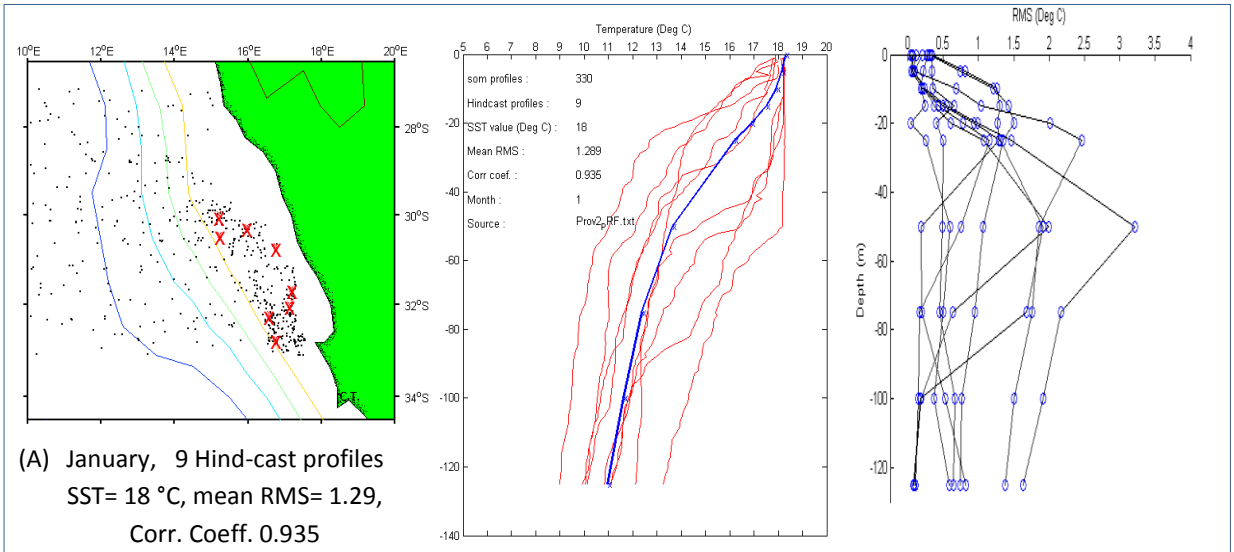

(A) January, 9 Hind-cast profiles
SST= 18 °C, mean RMS= 1.29,
Corr. Coeff. 0.935

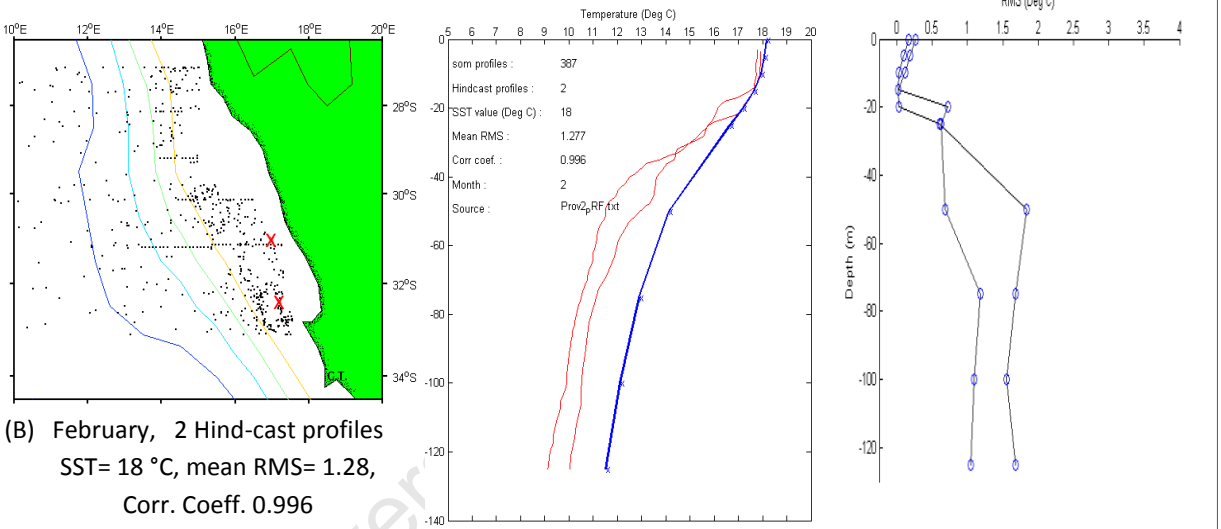

(B) February, 2 Hind-cast profiles
SST= 18 °C, mean RMS= 1.28,
Corr. Coeff. 0.996

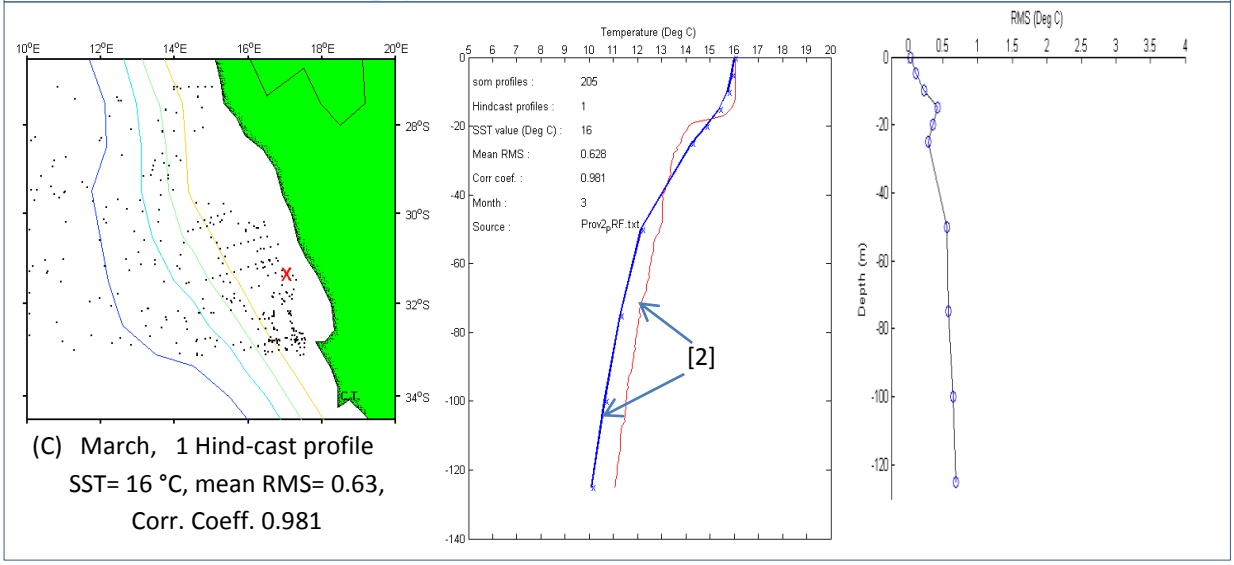

(C) March, 1 Hind-cast profile
SST= 16 °C, mean RMS= 0.63,
Corr. Coeff. 0.981

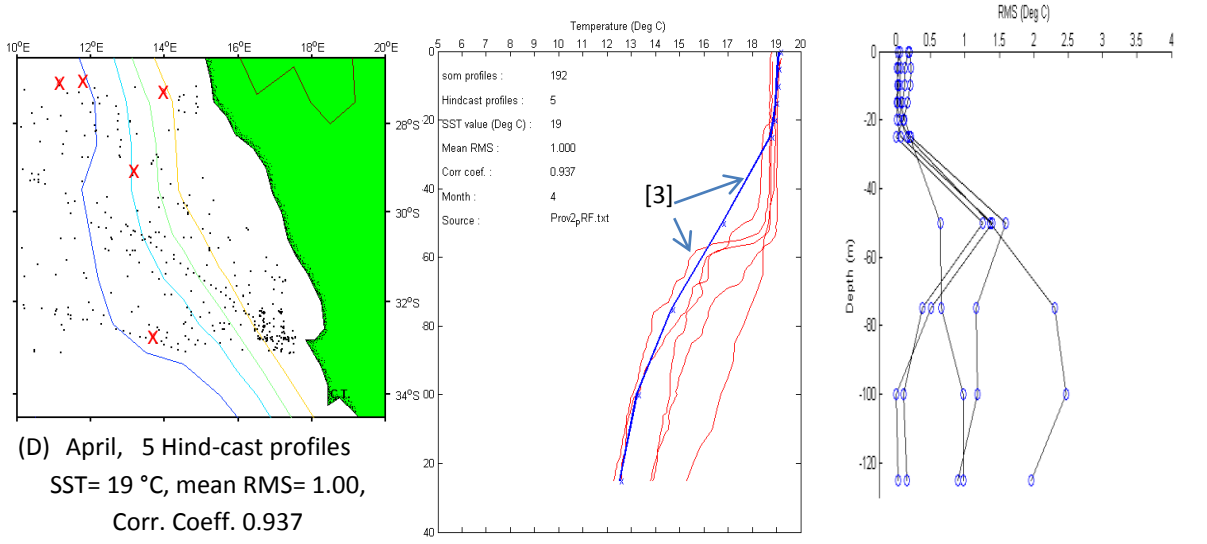

(D) April, 5 Hind-cast profiles
SST= 19 °C, mean RMS= 1.00,
Corr. Coeff. 0.937

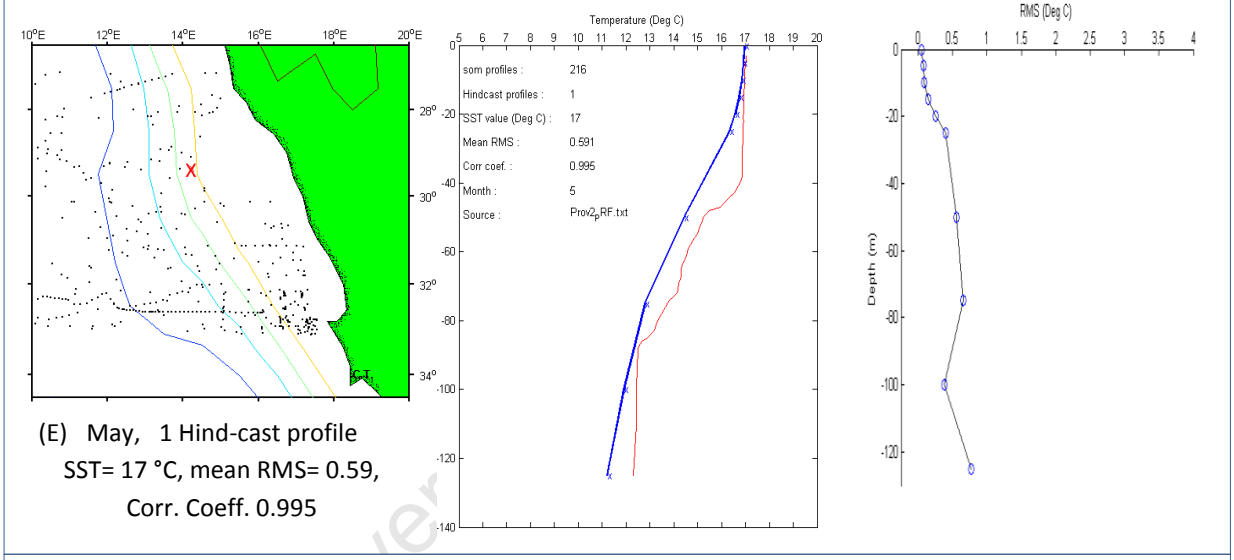

(E) May, 1 Hind-cast profile
SST= 17 °C, mean RMS= 0.59,
Corr. Coeff. 0.995

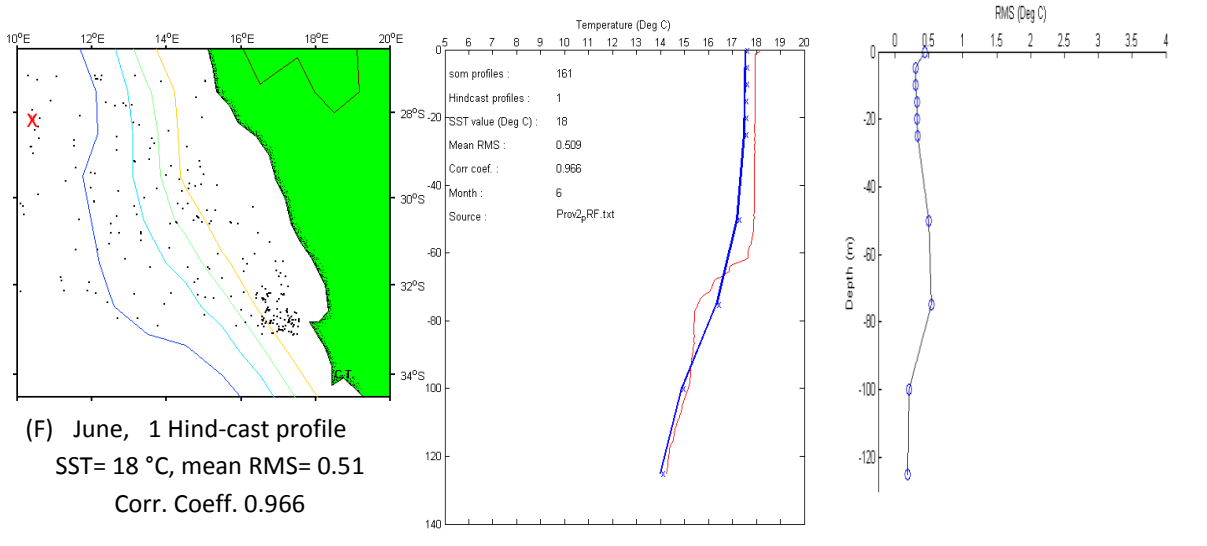

(F) June, 1 Hind-cast profile
SST= 18 °C, mean RMS= 0.51
Corr. Coeff. 0.966

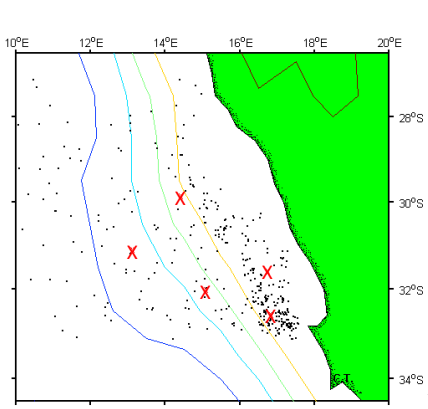

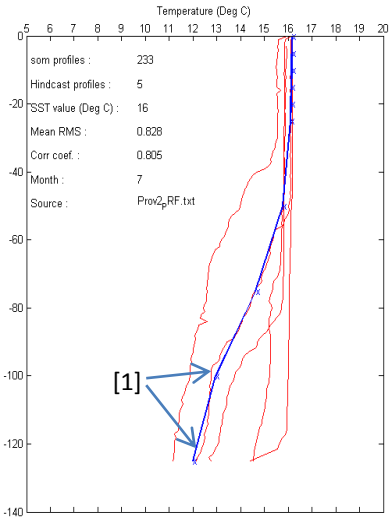

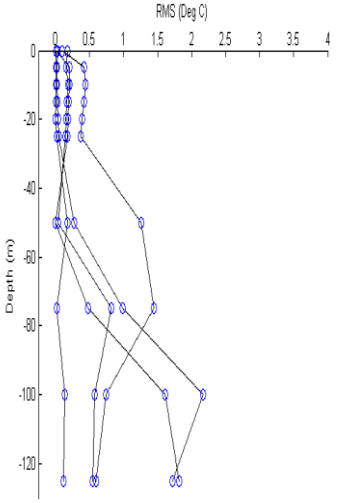

(G) July, 5 Hind-cast profiles SST= 16 °C, mean RMS= 0.83 Corr. Coeff. 0.805

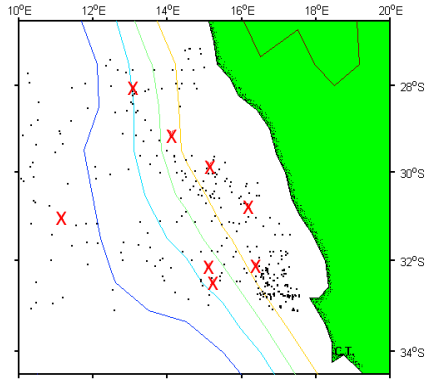

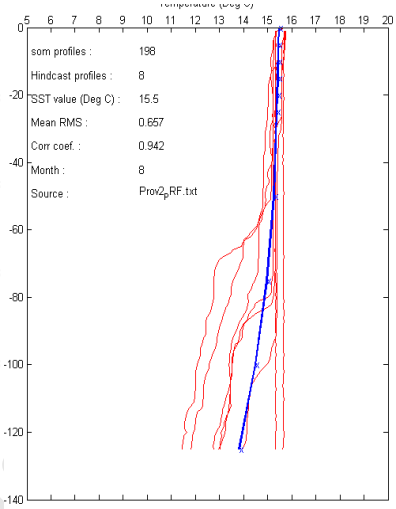

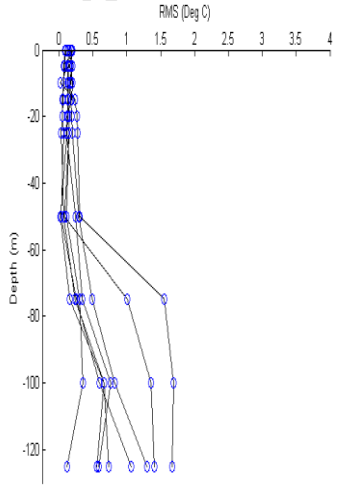

(H) August, 8 Hind-cast profiles SST= 15.5 °C, mean RMS= 0.66 Corr. Coeff. 0.942

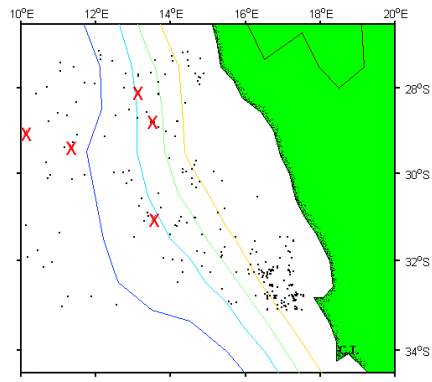

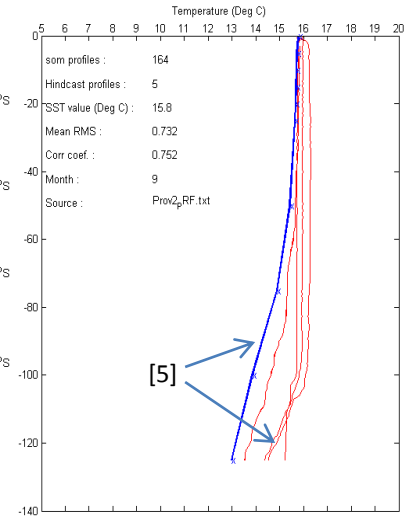

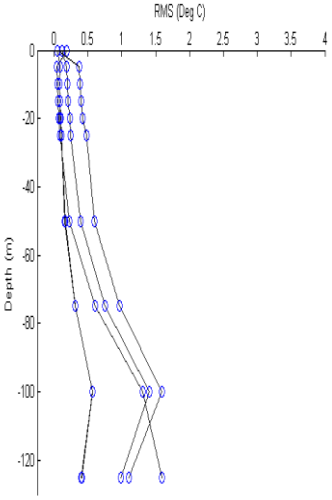

(I) September, 5 Hind-cast profiles SST= 15.8 °C, mean RMS= 0.73 Corr. Coeff. 0.752

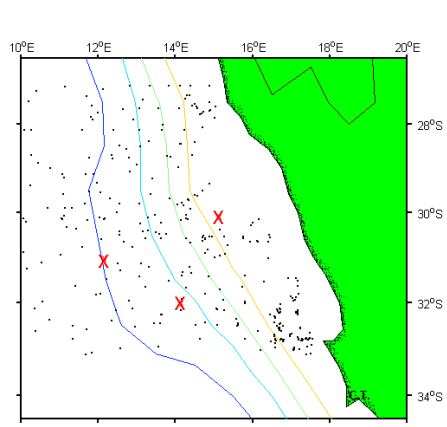

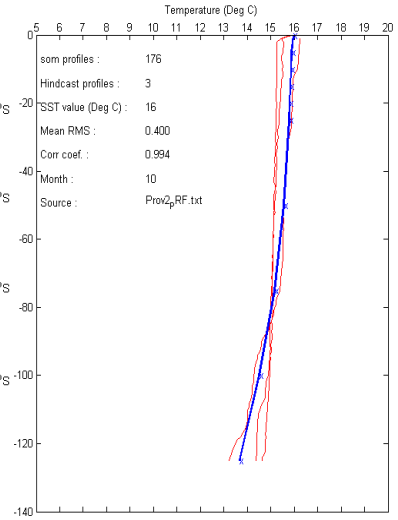

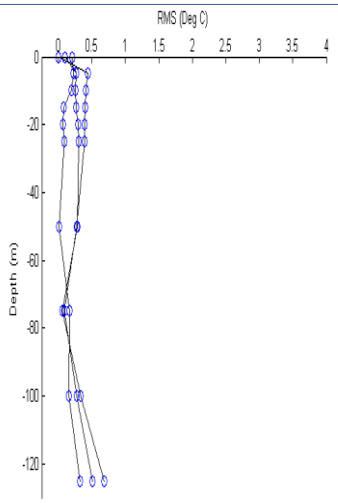

(J) October, 3 Hind-cast profiles
SST= 16 °C, mean RMS= 0.40
Corr. Coeff. 0.994

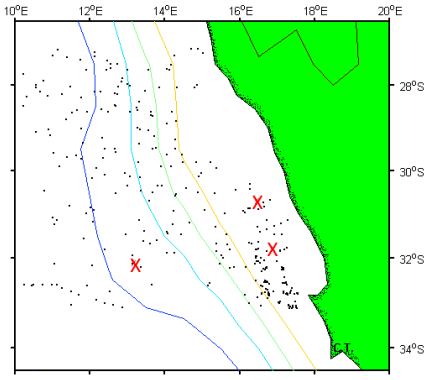

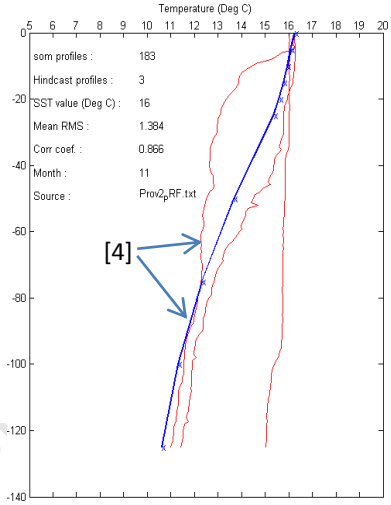

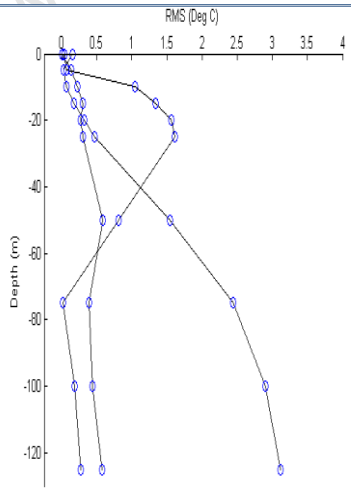

(K) November, 3 Hind-cast profiles
SST= 16 °C, mean RMS= 1.38,
Corr. Coeff. 0.866

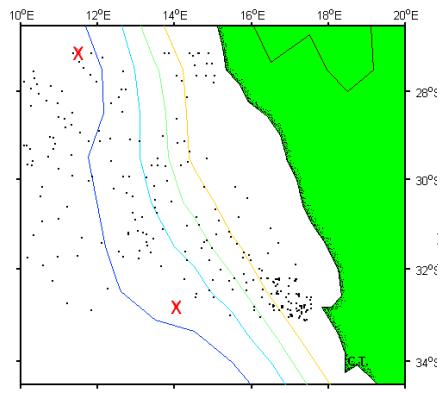

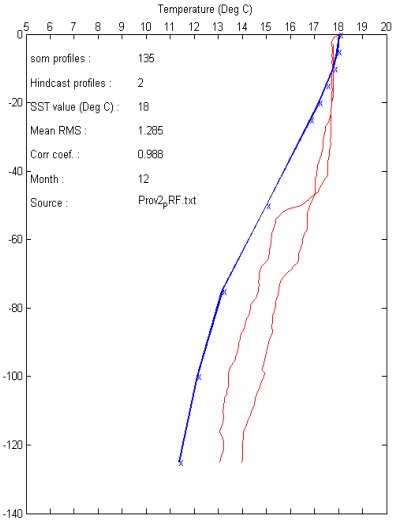

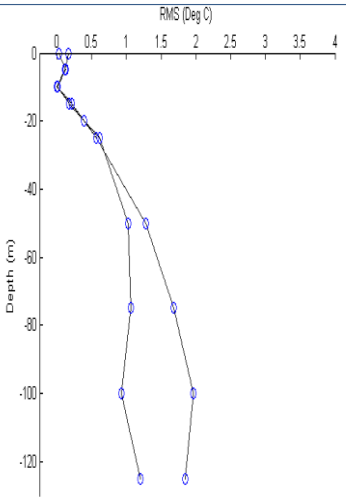

(L) December, 2 Hind-cast profiles
SST= 18 °C, mean RMS= 1.29,
Corr. Coeff. 0.988

Figure 7-3**:The above 4 pages, showing hind cast profile predictions for all calendar months, listed as (A to L) per calendar month, also referenced in**Table 7**. The map on the LHS shows the localities of all source profiles for that month as black dots and hind cast profiles as red crosses. The middle panel shows the predictive SOM-generated synthetic profile as a solid blue line with standard depths marked as stars and hind cast profiles shown as solid red lines. The RHS panel shows the RMS result of the prediction, with the respective SST and mean RMS and Correlation Coefficient values listed below the map. Profiles marked as [1] to [5] in plots (C), (D), (G), (I) and (K) were used as input to the validation step in section 7.d and **Figure 7-8.

c. Sensitivity analysis [Step D.3 in Figure 3-1]

Although the above result shows examples of a hind cast process, for a single SST value for each calendar month, it does not provide insight into the contributing factors or the sensitivity of the hind casting process to various changing parameters such as SST, calendar month, SOM error or year. For such analysis, a sensitivity test was used.

For a sensitivity analysis, it is necessary to undertake iterative tests of the process by comparing output with that of a changing variable. In this case the RMS value was used as the independent variable and was compared against changing SST, calendar month, year, depth, technologies, SOM errors (qe and te) and Correlation Coefficient. While some authors have used Correlation Coefficient or r^2 as a predictive indicator, most used RMS for that purpose, especially for similar numerical modeling practices, where modeled profiles were developed to represent the natural environment (Fox et al (2002), Rhodes et al (2002), Ali et al (2004), Chu et al (2000), Doan et al (2008) and Carnes and Mitchell (1990)). Based on this apparent *de facto* standard, RMS was used as the primary indicator of predictive success in here, while Correlation Coefficient is reported for completeness.

As a sensitivity test, the software was executed repetitively in batch mode, using a range of SST values (or temperatures at 0 m from observational profile values) from 15 °C to 22 °C, incremented every 0.5 °C for each calendar month. This represented the full range of surface temperature values as shown in ***Figure 7-6*** (B). The test used varying numbers of training profiles (usually between 300 and 400) each time from a total 5359 source profiles (the same dataset as that used earlier in Data Pre-processing –see section 5 and ***Table 7***), originating from various instruments, spanning the years 1954 – 2009, in which 2580 suitable profiles were extracted using the best available datasets. See section 5. for a description of the profile qualifying criteria. These stringent qualifying criteria resulted in only contiguous profiles being selected by the software for hind cast purposes. The

number of profiles that were accepted for SOM training in this sensitivity analysis (total=634) was different from that used to for hind cast testing (See ***Table 7*** , row 5 = 733). This was due to the hind cast tests being restricted to 1 temperature (the modal surface temperature – i.e. the temperature category with the most number of observations) for each month. In contrast, the sensitivity analysis made use a range of 0 m surface temperatures from 15 °C to 22 °C, incremented every 0.5 °C for each calendar month. This resulted in 113 executions of the SOM process in batch mode for sensitivity analysis purposes, producing 634 hind cast profiles (compared to 45 hind cast profiles identified in the hind cast testes earlier). Such larger numbers were required for the more inclusive sensitivity test to produce a meaningful result. The output of this sensitivity test is shown in ***Figure 7-4***, ***Figure 7-5***, ***Figure 7-6*** and ***Table 8***.

Results for the SST comparison showed that fewer hind casts were possible at the outer ranges of the SST values (21 °C to 23 °C and 15 °C), although this did not result in any appreciable RMS trend (See ***Figure 7-4*** (A) and ***Figure 7-6*** (B)). A wider range of RMS values occurred when using SST values of 18.5 °C to 21 °C.

Although a weak trend was observed in the RMS result plotted against calendar month in ***Figure 7-2***, when examined in the sensitivity test in ***Figure 7-4*** (B), a minimum at months 9 and 10 was apparent. The RMS values were noted to be lower (mean and range) for the southern hemisphere spring season months of September and October, with higher values observed in the summer months from December to February. The differences in the RMS plots can likely be attributed to the lesser number of hind cast datasets used in the first run as shown in ***Figure 7-2***. Another explanation could be the increased vertical mixing caused by the anti-cyclonic wind stress curl for those months.

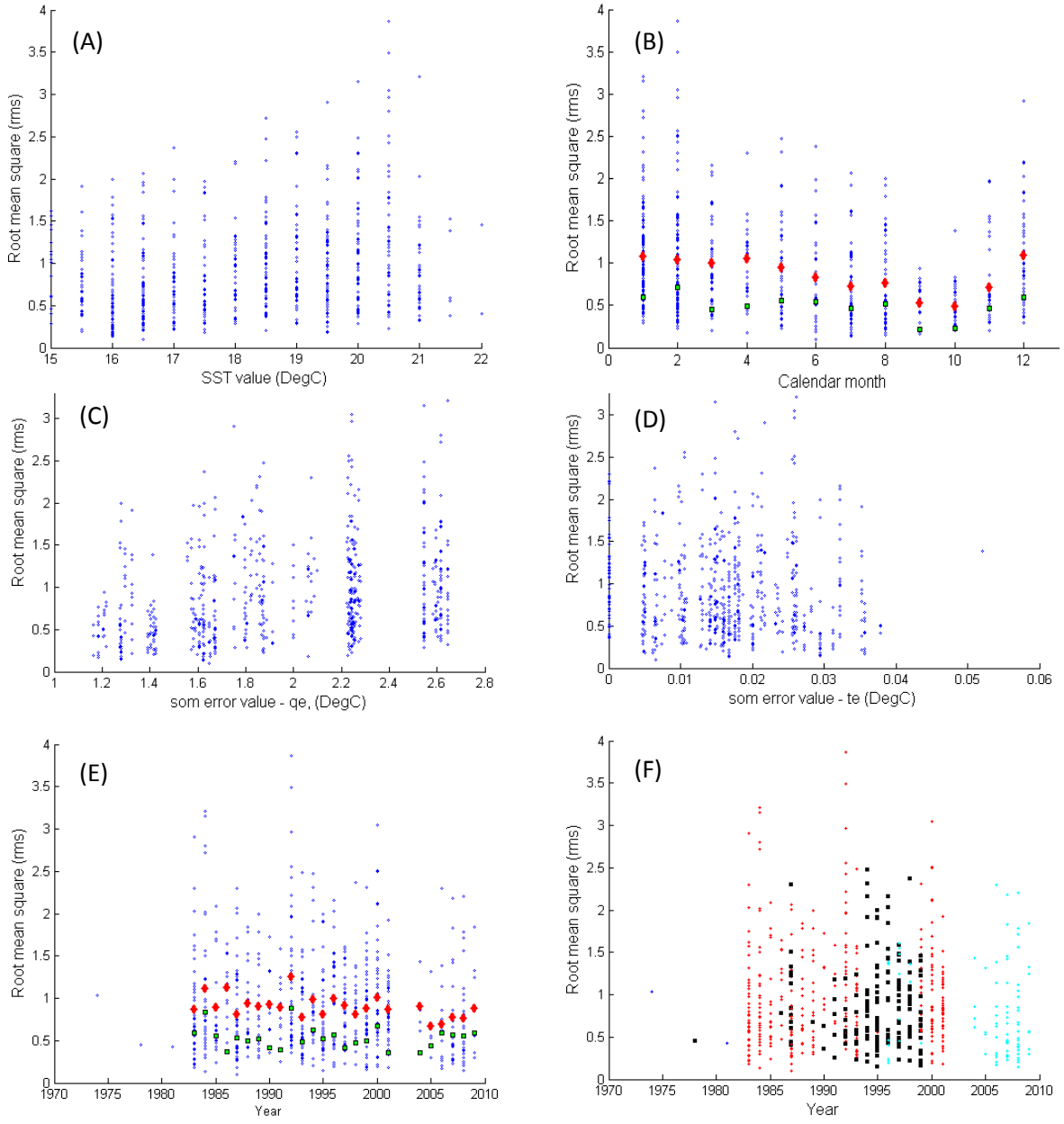

Figure 7-4: *Showing sensitivity test results using 634 Input profiles in terms of 113 SOM executions tested against 285 hind cast profiles with RMS values plotted against (A) SST, (B) calendar month, (C&D) SOM errors(qe and te) ,(E) year of observation and (F)sensor devices. In panels (B) and (E), mean RMS values are shown as solid red diamond shapes and standard deviations as solid greed squares. Panel (F) represents 3 differing sensors (CTDs shown in red and XBTs in black and profiling floats in cyan) for all years under review. Statistics for these plots are listed in* ***Table 8****.*

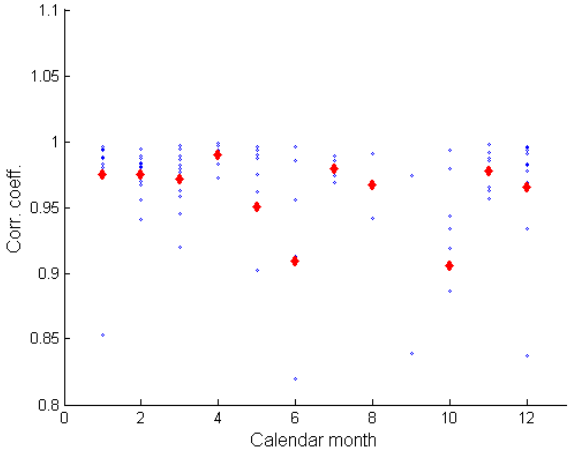

Figure 7-5: *Showing mean Correlation Coefficients, per calendar month for the same 634 profiles used in* ***Figure 7-4****. Monthly mean Correlation Coefficient values are shown as solid red diamond shapes.*

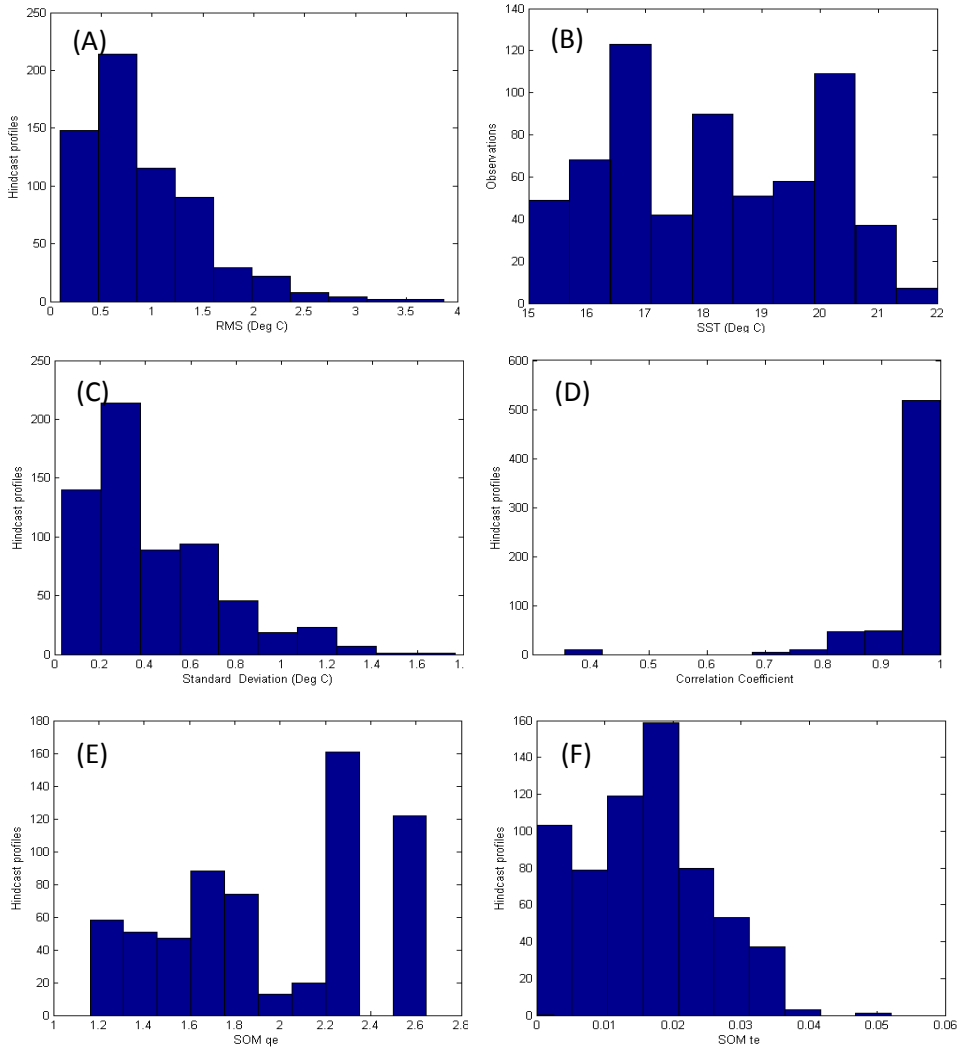

Figure 7-6: *Histogram plots of (A) RMS, (B), SST, (C) Standard Deviation, (D) Correlation Coefficient, (E) SOM quantification error and (F) SOM topology error.*

Statistics from 634 hind cast profiles used in the sensitivity analysis					
	RMS	***Corr. Coeff.***	***SST***	***qe***	***te***
Min	0.0999	0.355	15	1.162	0
Max	3.866	0.999	22	2.646	0.052
Mean	0.9141	0.945	18.15	1.963	0.016
Std. Dev.	0.577	0.104	1.78	0.443	0.010
Range	3.766	0.643	7	1.485	0.052
Reference in (***Figure 7-4***) and [***Figure 7-6***]	(A) to (E) and [A]	[D]	(A) and [B]	(C) and [E]	(D) and [F]

Table 8: *Data statistics for the hind cast sensitivity analysis using 634 hind cast profiles as shown in* ***Figure 7-4****, for RMS, SST, SOM quantisation and topology errors (qe and te).*

The SOM quantisation error parameter (qe) that defines the resultant Euclidean distances after the neural network training process was completed is shown in ***Table 8*** and plotted against the hind cast RMS values in ***Figure 7-4*** (C). A lower qe value describes a better fit. No clear trend or pattern relative to RMS output was observed in this result, meaning that the qe values were independent of the RMS result. Most qe values were between 1.2 and 2.6. A similar result was observed for the topology error (te), which described how well the hexagonal topology was preserved, is shown in ***Figure 7-4*** (D) and summarised statistics listed in ***Table 7*** and **Table 8**. As with the qe result, no clear trend or pattern relative to RMS output was observed, meaning that the te values were independent of the RMS result. Given that this was a simple 1-dimensional topology example, the te result is of little value (see section 6.b) and only provided here for completeness.

Accuracies of various sensors (Boyer et al (2006)) that were inherent in the source profile data used in this study are listed below as:

1. Reversing thermometers 0.02 °C
2. CTDs from 0.01 °C to 0.001 °C
3. MBTs either 0.5 °C or 0.5 °F
4. XBTs: ± 0.15 °C to ±0.1 °C (with a depth accuracy of ± 2% and ±0.1 °C and depth accuracy of ± 2% or 5 m, whichever is larger. Including XBT depth-time equation error of about 2.5 % at 800 m.
5. Argo floats from 0.01 °C to 0.002 °C

In addition to the above, other circumstances also contribute to data uncertainty. These are calibration frequency and levels of quality control applied to the data, amongst others. The result is that the combined error or confidence limit of the profile data cannot unfortunately be accurately determined. However, RMS values reported in this study are in most cases greater than the published accuracies of the sensors, resulting in some statistical reliability of the result.

A weak trend of reducing mean RMS values from 1983 to 2009 can be inferred. Standard Deviation values were consistently lower than the mean as shown in ***Figure 7-4*** (E), adding credibility to the result. There would be serious concerns about the validity of the process if this were not the case. This marginal reduction in RMS values is likely attributed amongst others to changing trends in preferred measurement instrumentation as shown in ***Figure 7-4*** (F) and described in section 2. c. Here CTD measurements dominated from 1983 to 1994 and 2000 to 2001, XBTs from 1994 to 1999 and profiling floats from 2004 to 2009.

In contrast to the RMS result per month, the correlation coefficient values (see ***Figure 7-5***) were more variable, with a distinctly worsening correlation trend for the months of April to June and July to October. A mean of 0.945 and a Standard Deviation of 0.104 were recorded, although it should be noted that these are averages per mean for each of the 94 hind cast runs. The trend observed here is co-incident with the reduced stratified conditions (increased mixing) observed for the same months as seen in ***Figure 7-3***.

Although a mean RMS value of 0.9141 (see ***Table 8***) was achieved, the median of 0.7704 was somewhat less due to the skewed histogram plot result as shown in ***Figure 7-6*** (A). The similar skewed RMS Standard Deviation seen in ***Figure 7-6*** (C) shows that the success rate of the prediction process is likely somewhat better than that described by the mean value.

Although the mean correlation coefficient measured was 0.945, a wide range of 0.643 existed with a Standard Deviation of 0.104, which is evident in the histogram plot in ***Figure 7-6*** (D), where the minimum value 0.355 can be seen as an outlier.

d. Comparative testing [Step D.4 in Figure 3-1]

Numerical modeling of temperature with depth in the oceans has a long history, as outlined in section 1. Fundamentally differing methods were used: 1. Parameterisation - by understanding the natural processes and developing methods and models, and 2. Statistical methods – using static information to describe or derive a representative outcome. This study is a type 2 method. The range of spatial, temporal and depth-wise published techniques, data sources and approaches within such a specialised topic was clearly evident in the literature, although few in number. The absolute validation (with another identical method, locality and dataset) of this analysis technique is therefore not possible, making it unique.

The purpose of using specific references in this section was to establish comparative statistical variables such as Root Mean Square (RMS) and correlation coefficient. This appears to be a popular published measure of temperature-depth profile synthesis. In some published cases, temperature 'deltas' or 'errors' or 'error differences' are instead referred to as the absolute difference between the measured and modeled temperature value at any specified depth. These cases are: Ali et al (2004) and Gildenhuÿs and Wainman (2007) as marked with a * in column 4 of ***Table 10***. They are therefore mentioned here as background only. It should be noted that absolute temperature difference as a measure of success in these cases is less stringent than RMS used here. This meant that a RMS value of say 0.7 °C will have an equivalent lesser error difference value of about 0.5 °C. The difference in approach of the two methods meant that those that did not use RMS, were excluded from the comparative test. (Refer ***Table 9*** and ***Table 10***).

By using the synthetic SOM profiles and examining only their surface temperature values, a single synthetic profile (any 1 of 15 characterised groupings) was selected by the software as a predictive profile. This synthetic profile was then compared against a sample set of previously observed (software selected) hind cast profiles and the temperature differences at specific depths in the water column were compared this common root mean squared (RMS) validation method.

The mean hind cast profile RMS results achieved in this study ranged from 0.4 °C to 1.38 °C, with a mean of 0.883 °C for the hind cast test as shown in ***Table 7*** (row 7 & 8). Standard Deviation (SD) ranged from 0.14 °C to 0.9 °C with a mean profile RMS SD of 0.452 °C for the same hind cast test ***Table 1*** (row 9). Standard Deviation values were less than the mean RMS values in each case, ***Table 7*** (row 7 & 9).

In the hind cast sensitivity analysis of section 7. c, many more (634 versus 45) hind cast profiles were tested, where profile RMS results achieved ranged from 0.0999 °C to 3.87 °C, with a mean of 0.91 °C for the hind cast test as shown in ***Table 7*** (row 7 & 8). Although this was the valid number of tested hind casts for the complete SOM sensitivity test, in real terms, some profiles were used more than once. This occurred when hind cast candidates' surface temperatures closely matched more than one winning SOM profile in separate software executions of the sensitivity test. It must be borne in mind that in such a test, all profiles are also repeatedly used for each SOM execution. In absolute terms it is estimated that 2% of profiles were used as hind cast candidates during each separate sensitivity test run. Standard Deviation (SD) ranged from 0.14 °C to 0.9 °C with a mean profile RMS SD of 0.58 °C for the same hind cast sensitivity test (***Table 8***). The hind cast test mean Standard Deviation for the sensitivity analysis was also less than the mean RMS value (see ***Table 8***), providing confidence in the validity of the process.

In summary, comparability in the context of this study is the relative comparison, using RMS as the popular statistical variable of choice, with all other parametric and statistical methods for determining the changes of temperature with depth in oceanographic terms.

It was necessary to separate usable and comparative references from non-comparable ones. The selection is shown in ***Table 9*** and ***Table 10*** where author references that are comparable to this study appear in shaded cells of column 1 in both tables. In some cases, RMS values were inferred from published plots, as indicated in column 2 of ***Table 10***. For each comparable reference, 0.883 (the mean RMS value obtained in this study) was subtracted from the published RMS values and the percentage improvement of the full mean RMS error range calculated. These validation results are shown in ***Table 10*** (right hand column) and plotted as a bar graph in ***Figure 7-7***.

Author/s	Technique/methodology	Comparison with this study (spatial, temporal and depth-wise)
Khedouri-Szczechowki (1983)	Inferred subsurface thermal structure from by using dynamic height as a function of thermocline. From XBT datasets of repeated Gulf Stream crossings.	Not comparable, different application and technique used here as background only
Carnes and Mitchell (1990)	EOF comparison of derived synthetic temperature profiles from Geosat altimeter data with air-dropped XBT profiles across the Gulf Stream	Minimally comparable, undertaken in lower variability region within a dominant ocean current to greater depths (with reduced variability) that favoured a reduced RMS value.
Chu et al (2000)	Compared 2 methods, regression and climatological of 40 profiles, for the month of May in the South China Sea.	Not comparable, undertaken for 1 month, with a single validation per location
Rhodes et al (2002)	Parameterisation technique using NLOM Sea Surface height. Using 4900 unassimilated global XBTs and a global XBT subset of ~800 records.	Global spatial scale for month of February and March
Fox et al (2002)	Various data assimilation methods of temperature profiles compared with observations from SeaSoar in Japan/East Sea, May-June 1999. Using Levitus, GDEM, Modas, Dynamic. Modas and Modas_Syn.	A single location for 2 months
Fox et al (2002)	Dynamic MODAS data assimilation of temperature profiles compared with static climatology for Western North Atlantic, Pacific – Kuroshio and Global Ocean.	Compared with static climatology
Ali et al (2004)	Neural Network, Arabian Sea, October 1994 – October 1995. Estimated from SST, SSH, wind stress, net radiation and net heat flux.	Not comparable, used a single point, within a closed sea from an extensive range of additional parametric variables. Not RMS
Gildenhuÿs - Wainman (2007)	Single profile, subjective 'best-guess' predictions from SST and historic data for the SE Atlantic Ocean. Early proof of concept, IMT internal report (unpublished).	Not comparable, subjective - proof of concept only. Not RMS
Doan et al (2008)	A GP technique to predict temperature profiles in the South China Sea using a trained AsiaEx dataset for 5 and 2 day time periods in May 2001.	Not comparable, Static climatology comparison for daily periods in May for a single year
This study (2012)	Estimating the upper ocean vertical temperature structure from a single surface temperature using a neural network technique for a defined area of the SE Atlantic Ocean (Benguela). Using [a] specific SST values per month from 45 hind cast profiles and a range of SST values from 15 °C to 22 °C, every 0.5 °C from 634 hind casts.	 This study, when compared to those above is novel in terms of its locality, depth range, spatial & temporal coverage and link to a supplied SST value for predictive purposes.

Table 9: *A Comparative listing showing examples of RMS used as a quantitative measure of numerically modeled temperature profiles. These are former research initiatives somewhat allied to this study, depicting their relevance and differences. Shaded cells are those used in this study.*

Author/s	Technique/methodology	Depth Range (m)	RMS Diff (^{0}C) / Corr. Coeff.	Ref. in this text	Difference between published RMS and this study using lowest RMS attained of 0.883 °C
Khedouri-Szczechowki (1983)	Inferred subsurface thermal structure from by using dynamic height as a function of thermocline. From XBT datasets of repeated Gulf Stream crossings.	0-700 at 5 discrete depths	0.84 / 0.94	Pg. 31	Not comparable, since it predicts using dynamic height, depth range and few depths
Carnes and Mitchell (1990)	EOF comparison of derived synthetic temperature profiles from Geosat altimeter data with air-dropped XBT profiles across the Gulf Stream	0-200	1.0 to 2.5	***Figure 2-7***	0.117 °C or 12 % to 1.617°C or 65 %
Chu et al (2000)	Compared 2 methods (regression [a] and climatological [b]) of 40 profiles, for the month of May in the South China Sea.	0-600	0.72[a] 1.06[b] / 0.79	***Figure 2-9***	Not comparable due to depth range and applied to climatology
Rhodes et al (2002)	Parameterisation technique using NLOM Sea Surface height. Using 4900 unassimilated global XBTs [a] and a global XBT subset of ~800 records[b]. Note: Values interpreted from the graphic.	0-125	1.3[a] 1.6[b]	***Figure 2-10*** (A) and (B)	0.417 °C or 32 % To 0.717 °C or 45 %
Fox et al (2002)	Various data assimilation methods of temperature profiles compared with observations from SeaSoar in Japan/East Sea, May-June 1999. [a]-Levitus, [b]-GDEM, [c]-Modas, [d]-Dy. MODAS, [e]-MODAS_Syn. Note: Values interpreted from the published graphic.	0-350, (0-120)	1.9[a] 2.2[b] 1.7[c] 2.3[d] 1.3[e]	***Figure 2-12***, **Table 1**	1.017 ° C or 54 % 1.317 ° C or 60 % 0.817 °C or 48 % 1.417 °C or 62 % 0.417 °C or 32 %
Fox, et al (2002)	Dynamic MODAS data assimilation of temperature profiles compared with static climatology for [a] Western North Atlantic, [b] Pacific – Kuroshio and [c] Global Ocean. Note: Values interpreted from the published graphic.	0-1000, (0,50,100 m)	1.7[a] 1.8[b] 1.2[c]	***Figure 2-13*** ***Table 2***	0.817 °C or 48 % 0.917 °C or 51 % 0.317 or 26 %
Ali et al (2004)	Neural Network, Arabian Sea, October 1994 – October 1995. Estimated from SST, SSH, wind stress, net radiation and net heat flux. Note *: Abs. Error mean, not RMS was quoted.	0-300	0.584* / Approx 0.75-0.99	***Figure 2-15***	Not comparable due to locality, reported format and point data source
Gildenhuÿs - Wainman (2007)	Single profile, subjective 'best-guess' predictions from SST and historic data for the SE Atlantic Ocean. Early proof of concept, IMT internal report (unpublished). Note*: Abs. Error mean, not RMS was quoted.	0-100	0.9 *	***Figure 2-18***	Not comparable due to reported format and subjectivity
Doan et al (2008)	A GP technique to predict temperature profiles in the South China Sea using a trained AsiaEx dataset for 5 [a] and 2 [b] day time periods in May 2001.	0-350	0.49[a] 0.60[b] / 0.99[a] 0.99[b]	***Table 3*** (B) ***Figure 2-19***	Not comparable as it is applied to few days and climatology only
This study (2012)	Estimating the upper ocean vertical temperature structure from a single surface temperature using a neural network technique for a defined area of the SE Atlantic Ocean (Benguela). Using [a] specific SST values per month from 45 hind cast profiles and [b] using a range of SST values from 15 °C to 22 °C, every 0.5 °C from 634 hind casts.	0-125	0.883[a] 0.914[b] / 0.930[a] and 0.945[b]	***Table 7***,8 ***Figure 7-2***, ***Figure 7-3***, ***Figure 7-4*** ***Figure 7-6***	Mean comparison of above / 0.83 °C or 45 %

Table 10: *Showing a comparative* summary of other numerically modeled tests using *similar test criteria RMS and Correlation Coefficient (shown in the shaded cells) techniques. Note that in some cases RMS values were inferred from published graphic plots. Shaded cells are those used in this study.*

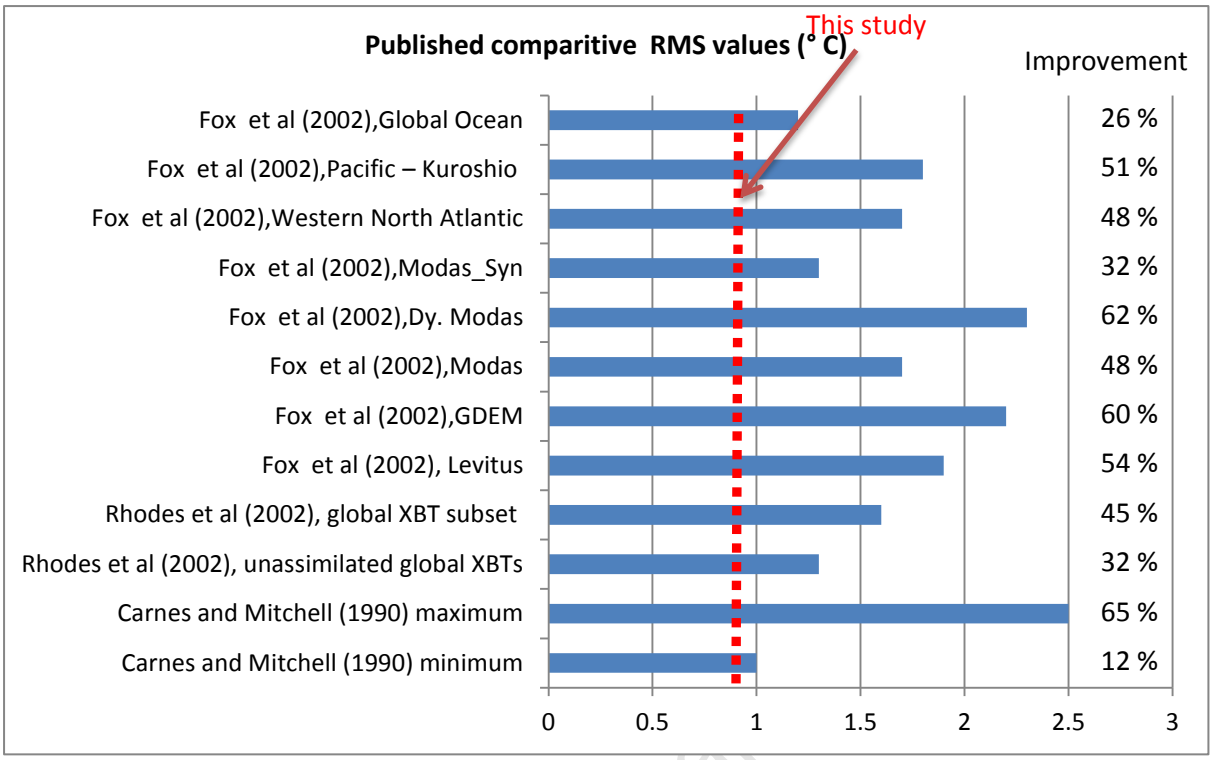

Figure 7-7: *Graph of published, somewhat- comparative RMS values in ° C shown as blue bar plots. These are overlaid with the RMS results achieved in this study shown as a broken red line representing 0.883 ° C to 0.914 ° C. Improvements to the values published are listed in the column on the right. References refer to those listed in the shaded cells of column 1 in* ***Table 9*** *and* ***Table 10****.*

In this study, with it's the relatively shallow depth range (0- 125 m), in a region where the variable wind mixed layer dominates, temporal expanse (1 month for 12 months), large spatial coverage (roughly 36 000 NM^2) and variability known to exist in this open ocean tested area (southern Benguela), all impacted negatively on achieving a lower RMS value. With such constraints, the mean RMS values attained: 0.883 °C and 0.914 °C (See ***Table 7***, ***Table 8*** and ***Table 10***), are therefore an improvement and expansion on other related techniques. Even with the limited comparability between this study and published results, these RMS values are shown to be an improvement of between 12 % and 65 % (see ***Figure 7-7***).

e. Validation [Step D.5 in Figure 3-1]

Whilst RMS is a useful comparative technique for checking the statistical validity of predicted temperature profiles, it does not address the practical outcome in terms of naval application as described in section 2. d. To accomplish this, the temperature profiles are required to be 'converted' into sound velocity profiles, with eventual input to a sound propagation model (See later).

Although a sufficiently low predictive RMS value is a pre-requisite for underwater sound propagation prediction, other factors are also important. Such as change in media or interface that occurs in the water column. An example of media change in this context is a change in water density such as occurs at a thermocline. The more intense a thermocline (greater change of temperature with depth), the more a sound wave will be refracted, as described in the section 2. d, The nature of the thermocline, both in shape, intensity, depth range and extent are additional factors that need to be considered when predicting sound propagation. Since sound propagation modeling and prediction was not however the core topic in this study, this part is less quantitative since it was undertaken only to demonstrate and validate the outcome.

Before input to the sound propagation model could be undertaken, it was useful to characterise (type-cast) 'predicted-vs.-measured' profiles shapes visually, using the criteria other than the absolute temperature profiles, based on their potential success to produce a viable operational outcome. Five such types were defined as referred to in the text below and schematically in **Figure 7-8.** The black arrows shown in the figure illustrate the poignant characteristic differences (described below) in the profile shapes, with relevance to the sound propagation plot characteristics covered next.

Type [1]: A 'close' match with low RMS values for the measured versus predicted profile. An example is shown in ***Figure 7-3*** (G) – July. This type accounted for approximately 20 % (by visual inspection) of the 45 hind cast profiles.

Type [2]: A measured profile with a more enhanced thermocline than the predicted profile, usually also with 'significantly' **colder** or **warmer** conditions below the thermocline. See ***Figure 7-3*** (C) – March. This type accounted for approximately 13 % (by visual inspection) of the 45 hind cast profiles.

Type [3]: A 'significantly' **deeper measured** thermocline (or increased wind mixed layer above the main thermocline) than the predicted profile. An example is shown in ***Figure 7-3*** (D) – April. This type accounted for approximately 27 % (by visual inspection) of the 45 hind cast profiles.

Type [4]: A measured profile with a weak thermocline that 'strays' from the predicted profile shape. However the surface and bottom values compare well. An example is shown in ***Figure 7-3*** (K) – November. This type accounted for approximately 20 % (by visual inspection) of the 45 hind cast profiles.

Type [5]: A measured profile with a very weak or non-existent thermocline (inferred as representing well mixed conditions). These conditions usually extend deeper than the other types and exhibit significantly warmer water at depth. An example is shown in ***Figure 7-3*** (I) – September. This type accounted for approximately 20 % (by visual inspection) of the 45 hind cast profiles.

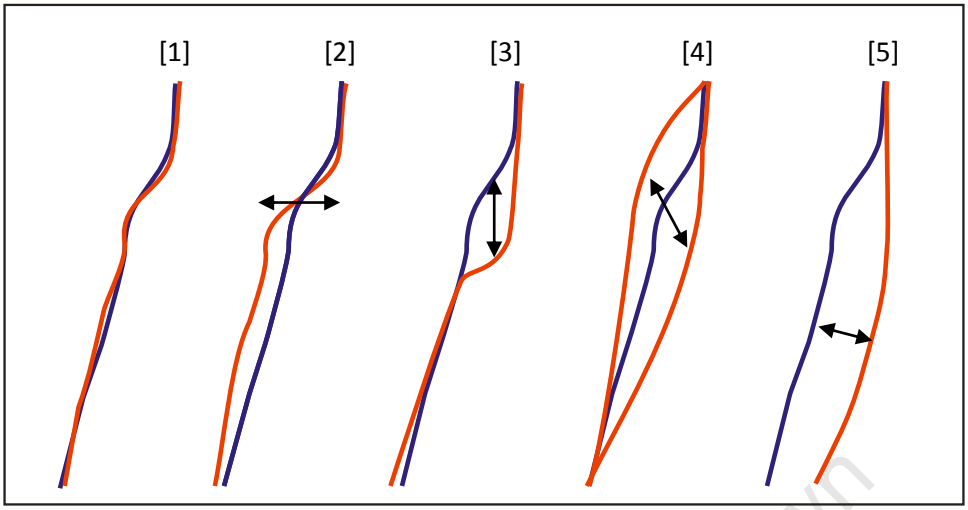

Figure 7-8: *A schematic showing 5 characteristic (type-casted) profiles shapes* ***differences*** *as observed in the hind cast analysis and described in the text. The blue profile represents a fictitious predicted SOM profile, whilst the red profile represents a measured comparative profile. The arrows illustrate dominant differences that are tested later in terms of sound propagation. Similar examples are labelled in* ***Figure 7-3****, together with their respective identification numbers [1 to 5].*

To demonstrate naval operational value, the 2 x 5 paired profiles were converted from temperature to sound velocity profiles (see section 2. d) in preparation for the final analysis step - sound propagation modeling. An existing empirical software model (SMOD), developed by the Institute for Maritime Technology, A Division of Armscor Defence Institutes (Pty) Ltd. was used for this part of the study. Sound MODeling and ranging software (SMOD Ver. 12) uses a suite of empirical sonar equations (not addressed in the scope of this study) to determine sound propagation, transmission loss and probability of detection emanating from a predefined underwater sound source. An introduction to this topic is provided in section 2.d.

For convenience and continuity, the same measured and predicted profile dataset as produced by the hind cast analysis process earlier (section 7.b) was used in this section. A single paired characteristic example was selected from ***Figure 7-14*** as representative of the 5 types. These are labelled as [1] to [5] in ***Figure 7-14*** for the months of July, March, April and September.

Figure 7-9: *SMOD pre-set variables (shown as a black font), used at run-time to produce sound propagation plot results. The bathy plot shown on the right hand side is the sound velocity profile provided as input for each run.*

SMOD was then provided with a sound velocity profile as input for 10 (2x5) executed runs. By way of example, a realistic scenario was setup, of a submarine operating in an acoustic passive mode at a depth of 50 m, 'listening' for an active transmitting noise source such as a corvette travelling at a speed of 10 knots. All settings such as sonar, target and environmental properties of the transmitted sound source were left unchanged during the repeated model predictions. This allowed for a comparable output whilst only varying the input sound velocity profile. These pre-set values such as sonar frequency, bandwidth, vessel speed, depth of sound source etc. can be seen in **Figure 7-9**. The SMOD output of the comparative 5 measured versus predicted sound velocity profile pairs is shown in ***Figure 7-10*** to ***Figure 7-14*** .

As a guide to interpreting these plots, two comparative ray trace diagrams, as originating from the measured profile (left hand side) and predicted (right hand side) are shown in the top row. The probability of detection plot, as a 'product' of sound transmission loss for the same input profiles as in the top row are shown in the lower row of each figure. The depth range is 0 – 125 m and the horizontal range is 10 km. The sound velocity profile, calculated from temperature profile is shown on the left hand side of each plot. Colours of the ray trace are represented as green=non refracted,

blue=sea surface refracted and brown=sea floor refracted. Colours of the probability-of-detection plot are represented on a linear scale of 0 (dark blue) to 1 (bright red).

When examining the output, a number of common 'features' become apparent: Sound waves are refracted due to their incident angle with the changed medium (intensity of the thermocline and increased water pressure). This refraction will either steer the sound waves upwards or along the surface, or downwards towards the sea floor. Where isothermal conditions occur in shallower water depths (less than 500 m) sound is known to propagate horizontally resulting in a so-called sound duct or sound channel formed due to the increasing depth. Sound waves directed at the seafloor as a refracted wave in this case are often reflected back into the water column according to the reflective nature of the seafloor. These may then be further reflected off the surface layer, resulting in sinusoidal shape propagating from the source until the sound wave is completely attenuated. To visualise this, it would be necessary to display the output in spatial terms of tens to hundreds of kilometres horizontally and thousands of meters vertically. Given the shallow (0 – 125 m) vertical range adopted for this study, such small-scale spatial plots would not serve to illustrate the concept. It is for this reason that a range of 0 – 125 m and 10 km was used. This adequately demonstrated the Ray-Trace (RT) and Probability of Detection (PoD) sensitivity to error differences in the prediction process. RT and PoD are explained in section 2. d. Prediction success is therefore rated in these terms of its ability to identify or describe salient sound propagation features. One feature is the width of a high PoD band in the vertical below the sound source, generally insensitive to SVP changes. Another is the occurrence (or not) and extent of ducted horizontal sound range propagation conditions, seen as increased PoD at some vertically restricted depth band.

For type [1] predictions, as shown in ***Figure 7-10*** where little difference (low RMS values) between the measured and predicted profile was observed, a similar ray trace (RT) and probability of detection (PoD) resulted, as could be expected. An important consequence of this result was not only that the low RMS values were reduced, but also that the upper mixed layer and thermoclines closely matched the measured and predicted profile shapes. It is these combined features that created the refractive conditions as seen in the RT and PoD plots. Approximately 20 % of the first set of 45 profiles used in the hind cast analysis earlier could be grouped into this category.

Type [1] prediction

Source - **measured** temperature hind cast profile

Source - **predicted** synthetic temperature profile

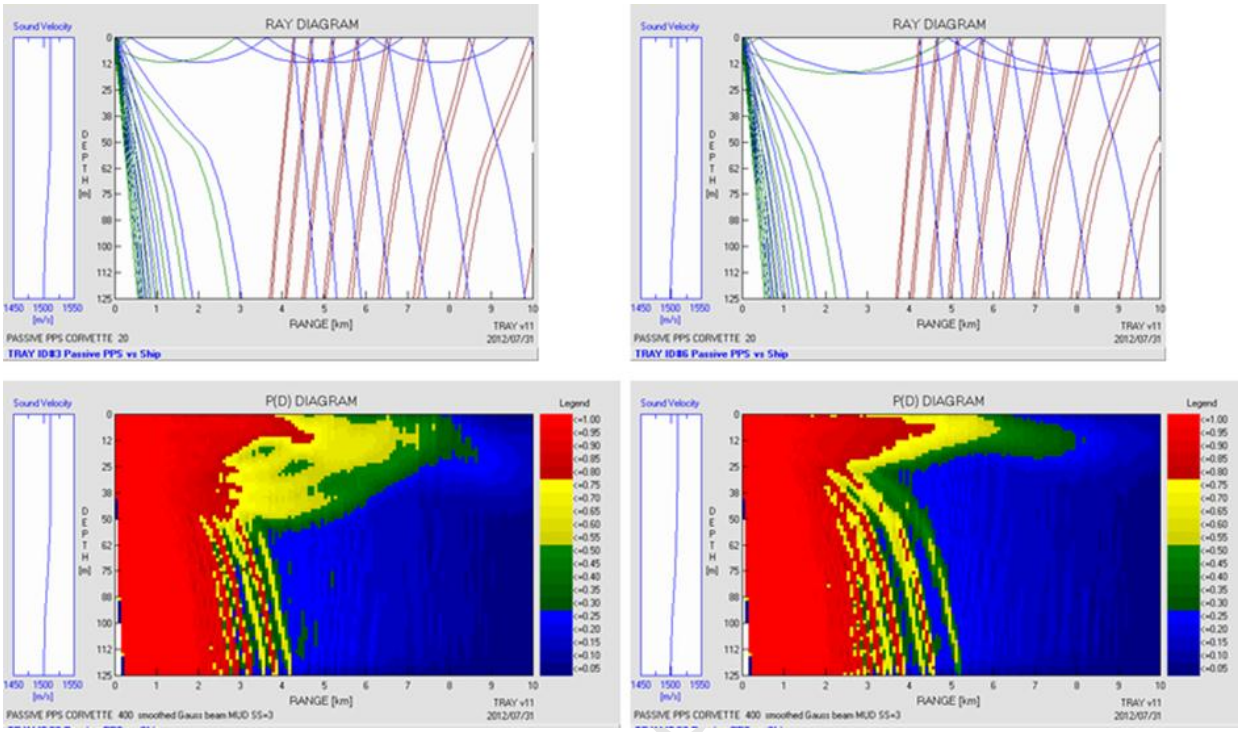

Figure 7-10: *A Comparative plot of type [1] predictions as output from SMOD's sound ray-trace (top) and probability-of-detection (bottom, originating from hind cast (left hand side) and predicted (right hand side) temperature profiles. See text for a detailed description of the setup parameters and analysis undertaken. Refer to Figure 7-3 July (G) where these profiles are labelled as type [1] - see text for explanation.*

For type [2] predictions, as shown in ***Figure 7-11***, the measured profile exhibited a more defined thermocline than the predicted profile, this translated in RT and PoD terms into surface ducting conditions, not predicted by the SOM profile. Since the remaining parts (below the thermocline) of the 2 profiles shapes compared well, the RT and PoD in the vertical and horizontal match closely. Approximately 13 % of the 45 profiles used in the hind cast analysis earlier could be grouped into this category.

Type [2] prediction

Source - **measured** temperature hind cast profile

Source - **predicted** synthetic temperature profile

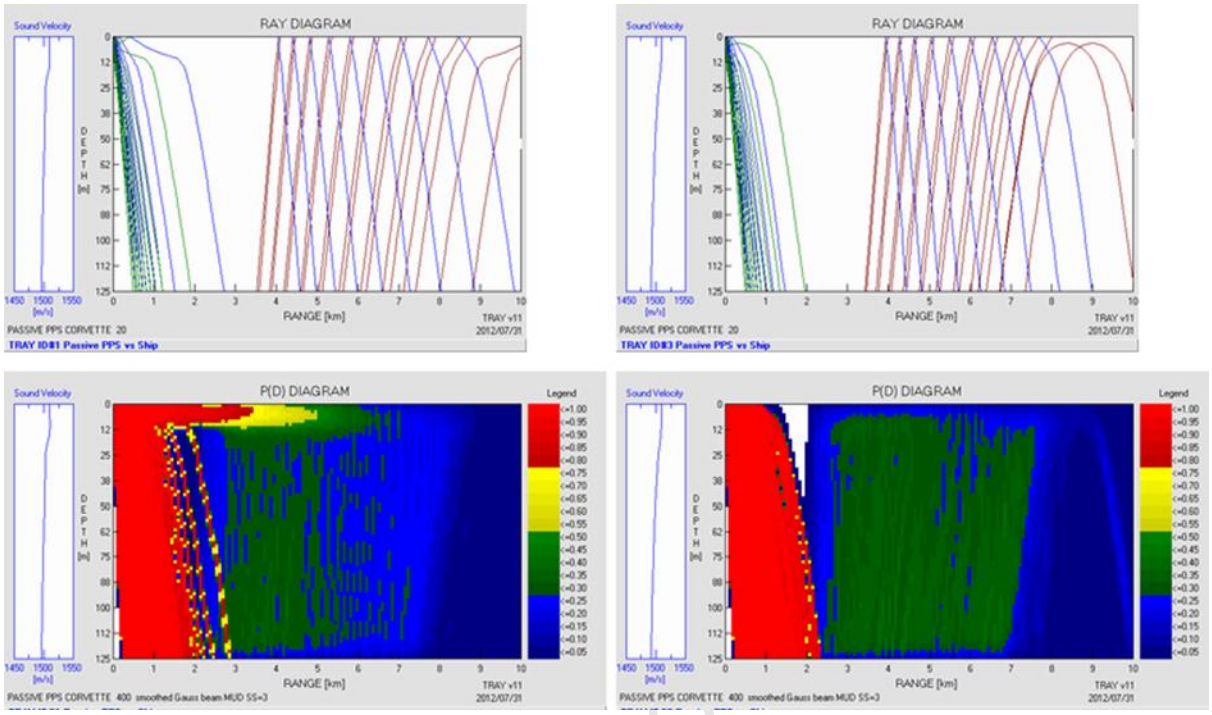

Figure 7-11: *A Comparative plot of type* ***[2]*** *profiles as output from SMOD's sound ray-trace (top) and probability-of-detection (bottom, originating from hind cast (left hand side) and predicted (right hand side) temperature profiles. See text for a detailed description of the setup parameters and analysis undertaken. Refer to* ***Figure 7-3*** *March (C) where these profiles are labelled as type [2] - see text for explanation.*

For type [3] predictions, as shown in ***Figure 7-12*** the measured profile exhibited a more extensive wind mixed layer range than the predicted profile, seen as a deeper thermocline. Measured and predicted temperatures (in absolute terms), above and below the thermocline compared well. This produced a similar result to that seen in type [3] predictions, where a sound duct is formed due to the presence of an extensive wind mixed layer. A difference in the vertical extent of the wind mixed layer therefore resulted in predicted profile not exhibiting such a feature. Approximately 27 % of the 45 profiles used in the hind cast analysis earlier could be grouped into this category.

Type [3] prediction

Source - **measured** temperature hind cast profile

Source - **predicted** synthetic temperature profile

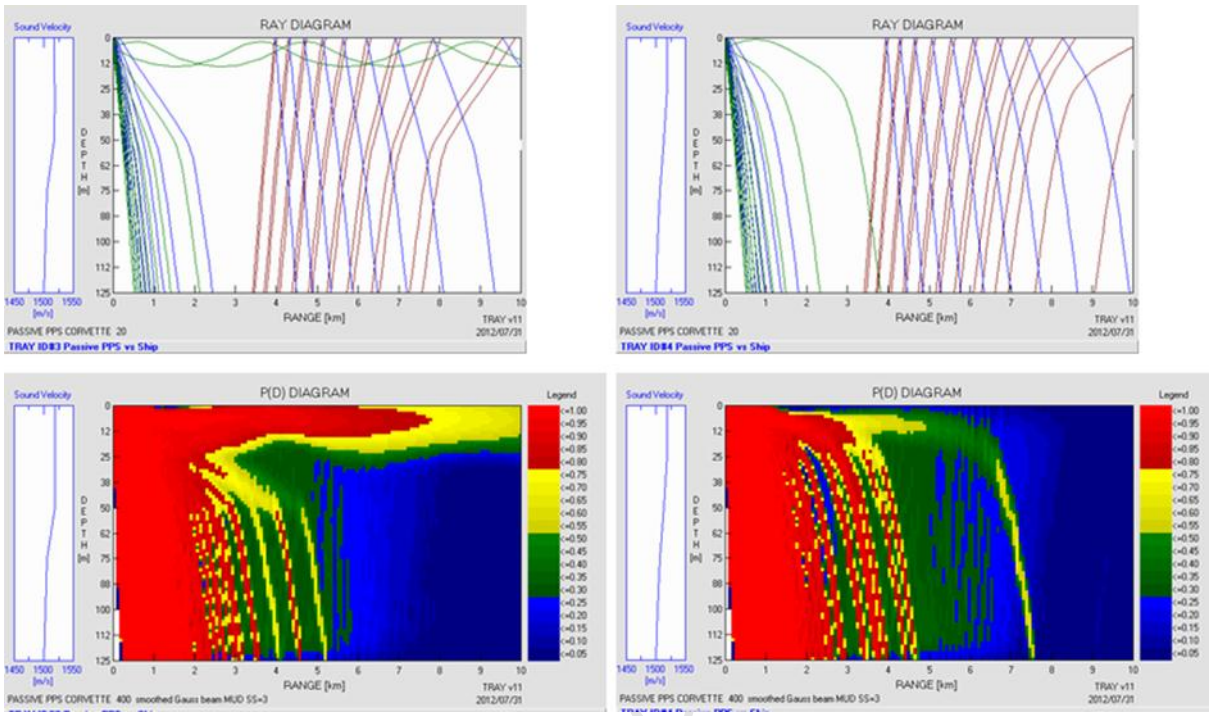

***Figure 7-12**: A Comparative plot of type [3] profiles as output from SMOD's sound ray-trace (top) and probability-of-detection (bottom, originating from hind cast (left hand side) and predicted (right hand side) temperature profiles. See text for a detailed description of the setup parameters and analysis undertaken. Refer to **Figure 7-3** April (D) where these profiles are labelled as type [3] - see text for explanation*

For type [4] predictions, as shown in ***Figure 7-13*** where although the absolute measured versus predicted temperatures may have differed, the thermocline was not significantly more enhanced (temperature or depth-wise) in the measured profile. Even a subdued wind mixed layer with a weakened thermocline of the measured profile did not produce a significantly different RT and PoD plot. Approximately 20 % of the 45 profiles used in the hind cast analysis earlier could be grouped into this category.

Type [4] prediction

Source - **measured** temperature hind cast profile

Source - **predicted** synthetic temperature profile

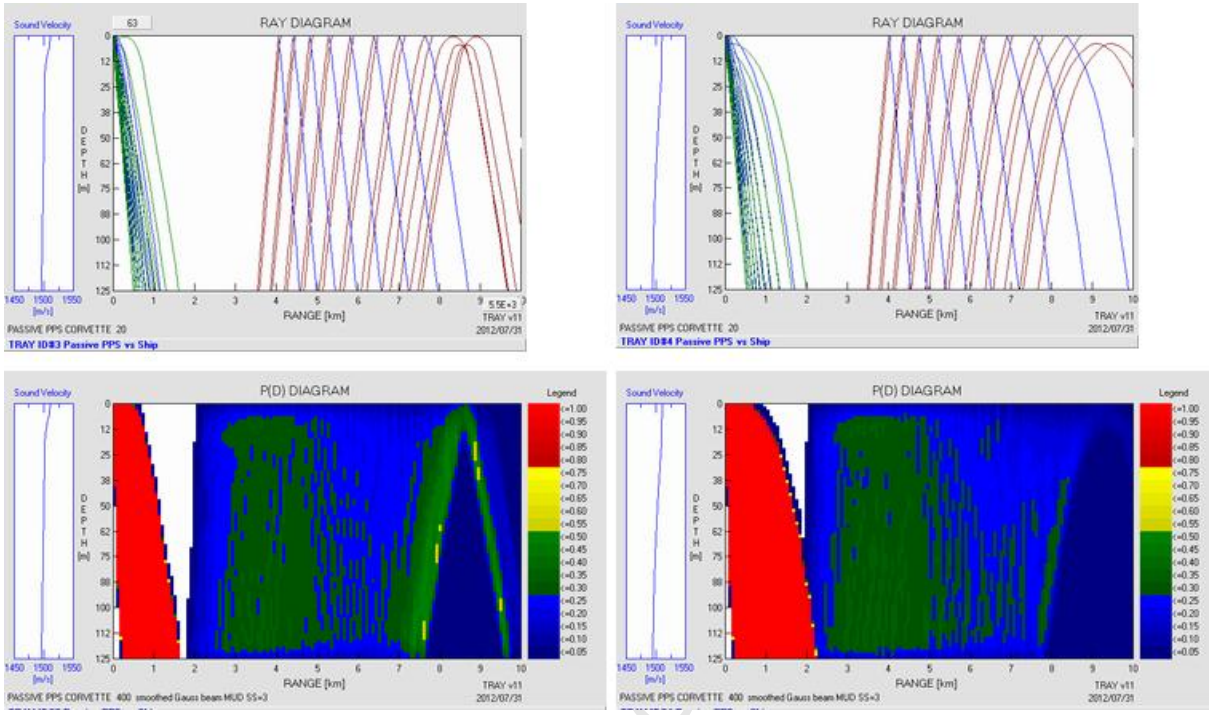

Figure 7-13: *A Comparative plot of type [4] profiles as output from SMOD's sound ray-trace (top) and probability-of-detection (bottom, originating from hind cast (left hand side) and predicted (right hand side) temperature profiles. See text for a detailed description of the setup parameters and analysis undertaken. Refer to* ***Figure 7-3*** *November (K) where these profiles are labelled as type [4] - see text for explanation.*

For type [5] predictions, as shown in ***Figure 7-14*** the measured profile appeared to 'deviate' from the predicted shape below the weak surface wind mixed layer, exhibiting generally cooler water conditions than the measured profile. However since a distinct thermocline was not apparent in both the measured and predictive case the RT and PoD plots are a close resemblance of each other, with a slight enhancement of ducting due to the somewhat more intense thermocline of the predicted profile. Approximately 20 % of the 45 profiles used in the hind cast analysis earlier could be grouped into this category.

Type [5] prediction

Source - **measured** temperature hind cast profile

Source - **predicted** synthetic temperature profile

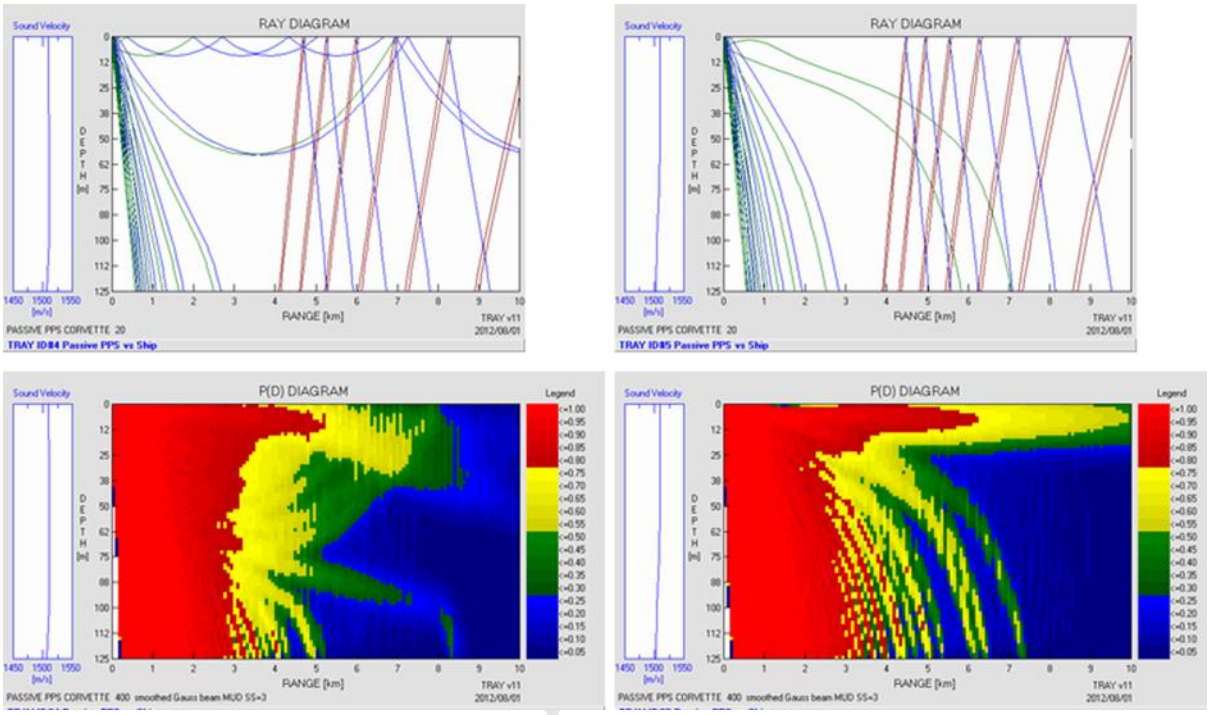

Figure 7-14: *A Comparative plot of type [5] profiles as output from SMOD's sound ray-trace (top) and probability-of-detection (bottom, originating from hind cast (left hand side) and predicted (right hand side) temperature profiles. See text for a detailed description of the setup parameters and analysis undertaken. Refer to* ***Figure 7-3*** *September (I) where these profiles are labelled as type [5] - see text for explanation.*

In summary, based on a visual inspection of the profiles in ***Figure 7-3***, approximately 60 % of the 45 profiles used in the hind cast analysis earlier could be described as valid for practical application. These included predicted types [1], [4] and [5] (see ***Figure 7-10***, ***Figure 7-13*** and ***Figure 7-14***). Twenty seven percent of the predicted profiles were considered generally valid, but did not completely describe the surface duct conditions that existed (see type [3] in ***Figure 7-12***). The remaining 13 % of the predicted profiles correctly described the vertical refraction and horizontal width of the propagated sound beams but failed to describe surface duct conditions that were evident in the measured profiles (see type [2] in ***Figure 7-11***).

Generally, the vertically refracted (downward refracted) sound wave was correctly predicted in all cases. These can be seen as a 'waterfall-type' display on the left hand side of each RT and in red (high probability of detection) of the PoD in ***Figure 7-10*** to ***Figure 7-13***. While this validation exercise addressed the ability of the winning SOM synthetic profile to predict operational significant output, it did not demonstrate the ability of the 15 SOM synthetic profiles to capture the salient features in the water column. That is covered in the next section.

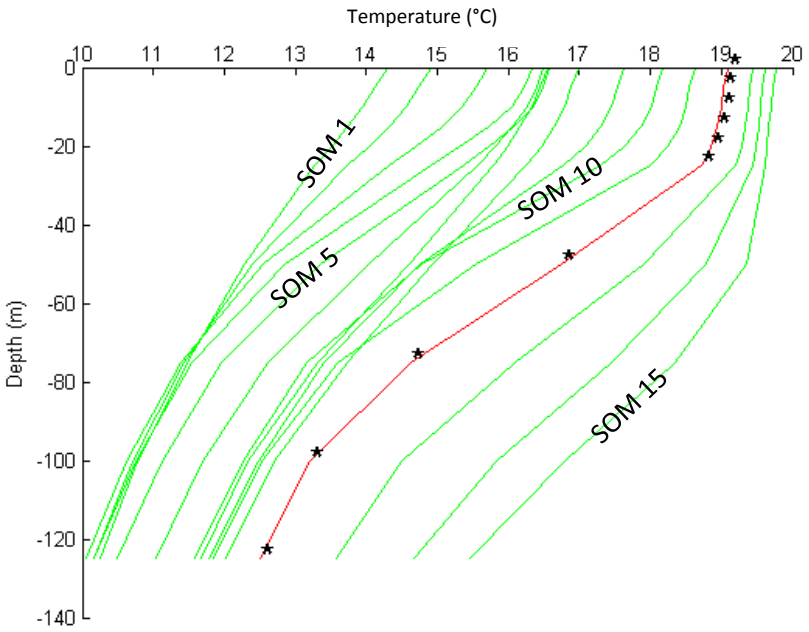

Figure 7-15: *Plot of 15 SOMS synthetic temperature profiles for the month of April. The red line is the predicted SOM profile used for hind cast analysis as shown in* ***Figure 7-3****(D) as a blue line. The green coloured profiles labelled 'SOM 1, 5, 10 and 15' are those used in****Figure 7-16****. The sequential numbering order of the SOM profiles is for convenience purposes to demonstrate the influence of the varying profile shapes as input to the sound velocity analysis below.*

When considering the above result, it may at first appear as if the SOM temperature profile predictions tended to over-smooth the profile detail due to its SOM type-casting technique , since grouping of profile types is unlikely to describe detail in such highly variable conditions. This may be the case for certain individual hind cast profiles as already shown. However where surface temperature-depth structure such as well-developed thermoclines and more extensive wind mixed layers dominate, these are captured by the technique, as shown in **Figure 7-15**. To illustrate this in terms of practical operational value, the 15 synthetic SOM profiles generated by the neural network software for the hind cast analysis undertaken earlier were examined. The month of April was

selected in this case since it represented the full range or sequence of profile conditions. These are: from a colder, very weak thermocline (SOM 1) to an intermediate thermocline with the start of a wind mixed layer (SOM 5), to a well-defined thermocline and increased wind mixed layer depth (SOM 10) and finally a deeper thermocline with an accompanying deep wind mixed layer (SOM 15).

The 4 selected SOMs synthetic output profiles were then provided as input to SMOD. Identical pre-processing and SMOD setup steps and parameters, as those used in the previous measured and predicted tests above were repeated for this test.

The result as seen in ***Figure 7-16*** shows that the temperature structure captured by the SOMs is completely represented in the RT and PoD plots. The weak or non-existent thermocline of SOM 1 provides an unvarying temperature interface to the approaching sound waves that are uniformly directed downwards, with a narrow downward directed wedge of high probability of detection. The partly developed wind mixed layer and slightly formed thermocline of SOM 5 did not alter the SMOD output considerably. Sound propagation conditions were similar to SOM 1 with somewhat more spreading (refraction). In the RT plot of SOM 10, spreading or refraction of the sound can be noticed with an increase of about 30 % more coverage of high probability of detection (red) zone. This can be attributed to the increased thermocline intensity when compared to SOM 1 and SOM 5. With the slightly deeper thermocline noticed in SOM 15, the sound wave ray traces are only spread somewhat more than those of SOM 10. The more important feature here is the development of a duct layer not seen in the previous SOM plots.

It is clear from these plots that the SOM variability in terms of temperature, depth, thermocline intensity and surface wind mixing are well described. These features were translated to differing sound refraction outcomes that provides a useful practical application in terms of the probability of a sea going vessel to be acoustically detected by a passive sonar of another vessel.

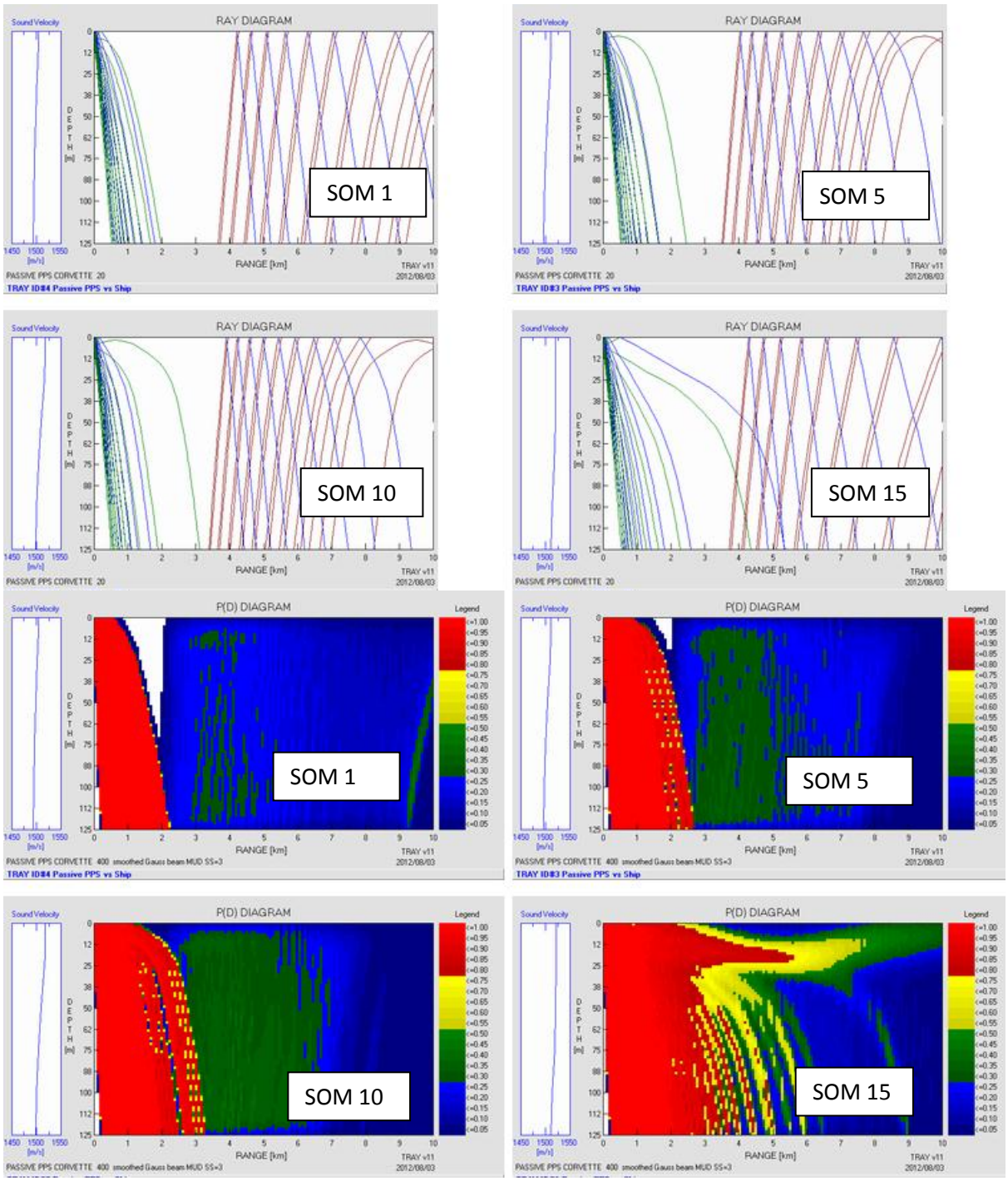

Figure 7-16: *A Comparative plot of 4 SOM synthetic profiles (SOM 1, SOM 5, SOM 10 and SOM 15) as referred to in the text and* ***Figure 7-15,*** *as output from SMOD's sound ray-trace (top 4 plots) and probability-of-detection (lower 4 plots).*

8. DISCUSSION

Oceanographic and meteorological information are important to all users of the ocean. This is especially true for naval users, where tactics and strategy based on an advanced understanding of the surrounding natural environment provides significant advantage. The ability to predict these parameters with some level of confidence and accuracy creates increased situational awareness to naval operators' and fleet planners, with significant advantage as a so-called 'force-multiplier'.

The study area can be oceanographically described as bordering the subtropical south east Atlantic Gyre (***Figure 4-2***) as a segment of the oceanic Benguela current. This flows over the homogenous deep Cape Basin (***Figure 4-8***), bordering the continental shelf-based Benguela upwelling regime in the east (***Figure 4-7***). The area is approximately the southern half of the Benguela current (***Figure 4-2***) which is the one of the sources of the water travelling through the region and supplying the northern Benguela current. Surface and thermocline water masses (as used in this study) largely originate from a mixture of South Atlantic, Indian Ocean (especially Agulhas current eddies fronts and filaments) and Benguela coastal currents after, Garzoli et al (1996) and Garzoli and Gordon (1996). Atmospherically, the area chosen experiences largely South-South-East winds with increased wind stress curl during summer months (***Figure 4-10***), dictated by the nearby centre of the semi-permanent high-pressure South Atlantic anti-cyclone, with some influence from sub-tropical frontal systems in the south, especially during winter (Jury et al (1990)).

Ocean processes, such as diurnal heating and cooling, heat transfer, insolation, solar radiation, return radiation, evaporation, precipitation, heat flux, convection, advection, water masses at continental shelves, fronts, eddies, turbulence and internal waves all contribute to a complex natural environment that is challenging to forecast. The study was conducted over a relatively shallow depth range (0 - 125 m), where a variable wind mixed layer prevails. A monthly temporal period from January to December was chosen, within an extensive spatial coverage of high variability known to exist in the southern Benguela. These factors negatively impacted on attaining low comparative error values.

Historically, vertical ocean thermal structure forecasting techniques used mostly empirically derived graphs and equations for air-sea interaction relationships, with data provided from on-scene data collections (Bishop (1984)), these are termed a parameterisation methods. In contrast, the statistical methodology implemented in this study made use of suitably pre-processed historic measurements in a Self Organising Map to identify a representative temperature profile, based on the profile's

surface temperature value. The method combines static (climatological) temperature profiles and dynamic (near real time) surface temperatures to form a 'quasi-dynamic' solution.

Although early attempts at such predictions were undertaken leading up to the year 2000, it appears that operational application of the process was only implemented after 2000, when modeled profiles were simulated as part of the NLOM output, primarily for use by the United States Navy. It appears that these developments have set the standard for such predictions and created the momentum for continued improvement of the prediction process as shown in the Dynamic MODAS Syn results (Carnes (2010)) in ***Figure 2-10***, **Figure 2-12**, ***Table 1***, and more recently in ***Figure 2-19***, ***Figure 2-20*** and ***Table 3***). Of note is the global extent of those predictions, with the regional extractions (***Figure 2-13***) that produced varying RMS results. Extensive on-going research, numerical processing and operational effort invested, over more than a decade as resulted in various output products originating from the MODAS_Syn (Carnes (2010)). It would appear that the originators of the technique, The Naval Research Laboratory of the United States Navy at The Stennis Space Centre and the Naval Postgraduate School at Monterey are leaders in this field (Carnes et al (1990), Chu et al (1999), Fox et al (2001), Rhodes et al (2002), Carnes (2009) and Carnes (2010)).

Prior work as shown in section 7.d was useful only in terms of calibrating the methodology of this study, since they provided commonly published error standards (RMS and Correlation Coefficient). They are all however significantly different when compared to this study, as summarised in ***Table 9***, with more detail in ***Table 10***. No repeated use of a single technique and locality was identified in popular literature. These comparisons are however greatly influenced by differences in terms of their method, locality and practical application. An example of this was especially evident, where one reference used a wide area, with a single modeled profile representing the climatology of a region, for a few days (Doan et al (2008)), while another reference used data from a single-point deep-water mooring in parametric way to predict temperature profiles (Ali et al (2004)). In most cases the only comparable aspect (with that addressed in this study) was that temperature-depth profiles were generated mathematically or statistically and reported in terms of RMS. It was for this reason that Root Mean Square (RMS) and Correlation Coefficient (Corr. Coeff.) were used in this study. This provided a method to calibrate the combined predictability of the pre-processing (parametric curve fitting) technique with that of the SOM (probabilistic) method.

Mean RMS values attained for the 2 hind casts tests: 0.883 °C and 0.914 °C (See ***Table 7***, ***Table 8*** and ***Table 10***), are an improvement and expansion on other related techniques. Even with the limited

comparability between this study and published results, these RMS values were shown to be lower in all cases (see ***Figure 7-7***).

Although the technique was tested firstly using only 45 hind cast profiles, this was expanded by also undertaking a more rigorous sensitivity analysis that used 634 hind cast profiles from 113 SOM executions, which resulted in a somewhat increased RMS value (from 0.883 °C to 0.914 °C) .

Whilst RMS was used primarily for comparative purposes, it also assisted in developing a quantifiable level of confidence in the technique necessary for the next step (validation). This was necessary since mean RMS as a statistical value did not address the requirement for a practical outcome in terms of naval application as described in section 2.d. For this, temperature profiles are generally 'converted' into sound velocity profiles, for subsequent input to a sound propagation model. This was undertaken in the validation step of section 7.e.

The merits of the combined curve fitting and SOM techniques are:

a. ***Table 7*** Mean RMS values attained for the 2 hind casts tests: 0.883 °C and 0.914 °C See (***Table 7***, ***Table 8*** and ***Table 10***), are a marked improvement and expansion on other related techniques. Even with the limited comparability between this study and published results, these RMS values were shown to be lower in all cases (see ***Figure 7-7***).The values were surprisingly low for such as turbulent, variable region that is fed by waters from 4 major differing water bodies (Central Atlantic, Indian Ocean, Indian/tropical blend and Benguela coastal. These become mixed into a 'cauldron' and further impacted upon by wind events forced by perturbations in the subtropical front. However, the input data produced a sufficiently diverse output in the time domain (by month) to explain the variety. It is believed that the attainment of low RMS prediction values was attributed to the integrating capability of the technique. In addition, the combination of appropriate observational data and processing methods used, demonstrated the ability of the technique to capture the complexity of the region.
b. This process provides an easier method to estimate underwater thermal structures than common regression of SST to parameters in which it is usually hard to achieve a unique profile from a single SST value.
c. With a sufficiently large dataset of profiles, it is possible to produce improved spatial and temporal representative synthetic profiles. (E.g. in a smaller or other region or over a shorter time span) than presently used.

d. The uppermost layer (0 - 125 m) layers of the ocean, where most of the variability occurs is described in more detail (every 5 m in the upper 25 m, every 25 m thereafter to 125 m) than the lower layers. This is commonly where the most profile variability (stratification) occurs. Despite this, considerable variability mostly occurring during the month of January was noticed below this depth as well (see ***Figure 7-3*** (A)). This may be attributed to the advection of distinctly differing oceanic and shelf water properties. It is possible that re-processing using an on-shelf/off-shore region would resolve this and improve the RMS result. However this benefit will likely be nullified by the sparse profile data coverage at depth, with reduced confidence in the result.

e. The two types of curve fitting methods combined with standardising or normalising techniques is able to make effective use of a both discrete and contiguous profile datasets. The ability to combine these, especially in areas of data scarcity benefitted the outcome and provided a new method for analysis of these datasets. The differences in format of these datasets, normally makes analysis difficult.

f. A continuum of synthetic profiles is produced that allows potential users of a developed system the choice of an appropriate profile and exploring the consequence of these on RT and PoD plots. This would however be dependent on the user having a thorough understanding of the impact of local weather conditions on the temperature profiles, such as recent wind events and localised diurnal heating or cooling amongst others.

g. The range of representative profiles produced by the SOM can assist in describing climatological signals such as mixed layer depths, thermocline intensity, vertical and horizontal mixing amongst others. This can be used to assimilate or examine 'what-if' type scenarios entered separately into SMOD (Sonar prediction and MODeling) to examine differing conditions. This was not however explored in this study.

h. Where a continuum of synthetic profiles can be achieved, this could be used to identify places or times where/when water masses interact, such as when 2 synthetic profiles have the same or similar surface temperature features but exhibit differing sub surface profile shapes (e.g. weak or well developed thermoclines). In the context of this region, it is possible that these may relate to the differing water masses that impact on the study area such as Agulhas Rings, Benguela Current, Benguela Coastal Current, Upwelling water and Tropical/Indian Ocean water. In such circumstances, the sound propagation model output would benefit from a number of alternative predictive profiles being considered as input, further lowering risk and increasing naval advantage. (This was not explored in this study)

i. The option to implement the profile selection criteria, goodness-of-fit, SOM setups and allowable SST range amongst others makes the process well suited for repeated software runs that can be trialled and tested as an operational facility.

The shortfalls of the combined curve fitting and SOM techniques are:

a. Approximately one half of the area chosen is within the Agulhas Eddy Corridor (See ***Figure 4-3***), whilst the eastern half is within the Benguela coastal current and self- edge upwelling zone (See ***Figure 4-3*** and ***Figure 4-7****)*. This water is then further mixed by the north ward and northwest ward moving Benguela system streams (***Figure 4-7****)*. While this has merit for the SOM, since it is able to capture this detail, it could also be interpreted as a shortfall, since the complexity could be better described if a smaller area was chosen. This was not examined in this study since the data tended to appear too sparse in the extreme offshore regions of the study area (***Figure 4-1***).
b. Although a certain amount of detail or variability can be seen in the continuum of 15 synthetic profiles produced by the SOM, the curve fitting and grouping (categorising) of the process does smooth or attenuate some of the profile detail. It should be noted however that a SVP profile is generally smoothed when imported into models such as SMOD, since SMOD processing is limited by the number of vertical depth points it is able to model.
c. Extensive pre-processing and screening of the observational profiles is required.
d. A large historical profile dataset is required to train the SOM.
e. The training of the SOMS profile nodes uses a full suite of historic data, without data quality considerations (apart from those implemented by the data custodian). This has implications for levels of confidence in the result. Such 'nested' data confidence levels were not addressed or quantified.
f. While the chosen depth range (0 – 125 m) was sighted as providing merit, this was also a shortfall since it was noticed that the profile shapes seen in the plots of the deeper layers did not converge at 125 m (see Appendix F). This meant that the bottom of the seasonal thermocline was not as well represented as the upper parts. This was probably also due to the complexity of the region and may be attributed to 3 contributing water bodies (see ***Figure 4-2*** and ***Figure 4-3***). Convergence of the temperature-depth profile plot lines occurred in the cited literature at approximate water depths of :
    i. 400 m in higher latitudes of the South China Sea (Chu et al (2000)).
    ii. 800 m for the global dataset examined by Rhodes et al (2002).

iii. 300 m for the South China Sea for May-June 1999 (Fox et al (2002)).

iv. 200 m (roughly) for a 5 and 2 day period during May 2001 in the South China Sea (Doan et al (2008).

v. 400 m for a sub region of the Black Sea during January, February and March (Carnes (2009)).

vi. The thermocline cut-off in a T-S diagram. Defined by a temperature boundary of warmer than 6 ^{o}C (Shannon and Nelson (1996)). The 15 SOM profiles in this study portrayed a minimum temperature at the deepest portion of the profiles of approximately 10 ^{o}C.

a. Hypothesis revisited [Step E in Figure 3-1]

The original hypothesis question was stated as:

"Can thermal characteristics of the water column be modeled from a single sea surface temperature value, if provided with historic temperature-depth profiles for that region?"

The hypothesis in this thesis is that thermal characteristics of the water column in the southern Benguela can be numerically modeled and deduced from a single Sea Surface Temperature (SST) value, if provided with sufficient historic temperature-depth profiles for that region. For operational use, the SST would ideally be provided from near real time remotely sensed satellite derived data.

This study has shown that historic modeling of thermal water column conditions can be traced back to heat diffusion research of 1855, based on first principles in fluid dynamics, to the later development of equations to describe eddy viscosity, diffusivity, heat flux and wind stress vertical mixing. These were early modeling developments that relied on the input of many measured parameters to achieve a suitable outcome. This is termed parametric processes.

A parametric approach was used here fit a polynomial curve to a large number of discrete profiles and a curve smoothing routine for contiguous profiles. A large number of profiles were provided for a specific region, separated by month and provided as input to a probabilistic SOM model. During the process a single surface temperature value was entered 'externally' to identify 1 of 15 matching synthetic profiles. The combined method was compared with 'similar' methods, using commonly accepted norms, which were shown to be an improvement in all instances tested.

To validate the technique, the synthetic temperature profiles were first converted to sound velocity profiles. The detail in the sound velocity profiles adequately described variability in terms of temperature-depth, thermocline intensity and mixed layer depth to be practically used in a an underwater sound propagation model. Products such as acoustic Ray-Trace and Probability-of-Detection plots were used to show that 60 % of the profiles correctly described 'valid' acoustic conditions, 27 % were valid or usable but did not completely describe ducting conditions (an important feature for probability of detection) while 13 % failed to describe known ducting conditions.

It is the opinion of the author that the scheme proposed in this thesis could be used operationally in a successful way and this is one option that will be tested in future.

9. CONCLUSION

Underwater Sound Velocity Profiles (SVP) are used throughout the world by their respective navies for submarine and surface vessel strategic operations and exercises. Together with the sonar equations, the sound velocity profiles are of paramount importance to solve underwater sound detectability problems as they provide insight into the highly variable sound transmission loss. Oceanographic records of sea temperature-depth profiles are ordinarily incorporated into a sonar propagation model to determine the sound level at any point (range and depth). The ability to predict these environmental conditions with a defined level of confidence and accuracy significantly increases the situational awareness of in-theatre naval operators and fleet planners.

The hypothesis in this thesis is that thermal characteristics of the water column in the southern Benguela can be numerically modeled and deduced from a single Sea Surface Temperature (SST) value, if provided with sufficient historic temperature-depth profiles for that region. For operational use, the SST would ideally be provided from near real time remotely sensed satellite derived data.

This study uses an approach that largely ignores the natural processes and focuses instead on defining the statistical or mathematical properties of the water column in a demarcated region defined by its mean sea surface temperature properties. A large number of previously measured temperature-depth profiles (also called static information) are then 'normalised' in terms of their depth values (standard depths) by using curve-fitting and line-smoothing techniques. They are then clustered into a representative synthetic continuum of profiles available for predictive purposes. Based only on the profile's surface temperature similarity to a sea surface temperature provided 'externally', a winning synthetic profile is assigned by the software. An association between profiles and their single surface temperature value is necessarily implicit in this process. The method combined static (climatological) temperature profiles and dynamic (near real time) surface temperatures to form a 'quasi-dynamic' solution.

As an effectiveness test, a small number of qualifying source profiles were flagged for hind cast purposes and were excluded from contributing to the dataset in any other way.

When comparing the 'winning' or synthetic SOM profile with hind cast profiles, a statistically significant result was achieved; mean RMS values of 0.883 °C (with a mean correlation coefficient of 0.930) and 0.914 °C (with a mean correlation coefficient of 0.945) for 45 and 634 hind cast profiles

respectively. Although no identical comparative method existed, the results were an improvement on those identified as 'somewhat' similar, by between 12 % and 65 % (see ***Figure 7-7***).

Although the curve-fitting method was proposed (e.g. Teague et al. (1990); Chu el al (2000)) and used by the United States Navy in ocean hind cast systems (Fox et al. (2002)) more than a decade ago, the estimation of underwater thermal structure from a SST continues to use common regression methods of SST to parameters.

The naval operational concept of this research is to use available Sea Surface Temperature (SST) information from a remote sensed infra-red, earth-orbiting satellite sensor to match with vertical temperature values of a suitably representative (in time and space) 'synthetic' profile. This temperature profile is then converted into a sound velocity profile for incorporation into an existing sound propagation and transmission loss model, with practical applicability to a Navy. Benefit of this enhanced technique can be derived from most instances where underwater acoustics is used in a passive or active mode. Some examples include:

1. Improved submarine underwater surveillance through having a remote capability in a sense 'detached' from any current location whilst at sea. Knowing the sound propagation conditions of a distant sound source will greatly assist tracking and location of the vessel.
2. Reduced own probability of detection (counter detection) by more accurate information on shadow zones and detection probability regions.
3. Improved operational effectiveness by not necessarily having to rely on a measured in-situ temperature profile.
4. The entire procedure from SST to sound propagation is relatively simple since it does not require extensive real time data sources to populate deterministic equations. This implies that it could be easily incorporated into existing propagation models for use at sea or on land. A robust operational system would however require sufficient historic data for all areas.
5. Allows smaller navies access to a solution of a complex problem normally requiring more extensive databases, infrastructure and specialist expertise.
6. As a post mission analysis tool where in-situ SVP measurements were not collected during the exercise.

Although only some examples are listed above, in general, this identification of thermal vertical structure from SST observation has the potential to greatly improve the safety and planning, strategy and tactics as so called force multiplier. As a consequence, this technique may contibutue

to maritime security and protection of sovereign rights in a state's Exclusive Economic Zone. These include amongst others, protection of offshore maritime assets, resources and shipping lanes.

In summary, the results of this study provide an improvement to ocean scientific research and naval oceanography and are considered unique mainly in terms of its advancement in methodology and naval application.

10. ACKOWLEDGEMENTS

The author gratefully thanks the following persons that assisted in their own way to the success of this study:

Professor Emeritus Geoff Brundrit for his time spent in providing his most valued advice and direction, Professor Frank Shillington for his supervisory role, Professor John Field for comments and constructive criticism.

Members of the South African Navy's Combat Development Team, and especially Mr Neels Fourie (programme manager, STSS funding source) and senior management (Mr Mackenzie Johnson) at The Institute for Maritime Technology, a Division of Armscor Defence Institutes, for having confidence in the concept, by providing funding and on-going support to undertake this research.

Mr Christo Whittle, UCT Oceanography MARE centre for providing the MODIS and pathfinder remote sensed SST data, Me Ursula Ansorge for developing the SADCO profile extraction routines, Me S Gildenhuÿs for assistance provided with the original proof-of-concept project and proof reading, Dr Hannes van Wyk for reviewing the statistical components, Mr Phillip le Grange for his assistance with the sound propagation and SMOD parts and finally Me Benita Maritz for her part in the proof reading as well. Mr & Mrs Gerhard and Lisa Scholtz are also thanked for their part in resolving some of the editorial aspects.

The technical correctness and exceptional thoroughness, especially from one of the external examiners was an essentiall part of this thesis that assisted in steering it towards a more inclusive and comprehensive result, I thank you for that.

A special thanks to my dear wife Cheryl for her unselfish and unfailing personal support to the outcome of this project over the past 4 years.

11. REFERENCES

Ali, M., M. D. Swain, and R. A. Weller (2004), Estimation of ocean subsurface thermal structure from surface parameters: A neural network approach. *Geophys. Res. Lett*., *31, L20308*, *doi:10.1029/2004GL021192.*

Bishop, J. M. (1984), Military uses of the ocean. *APPLIED OCEANOGRAPHY, Chap. 14, 223-231, Elsevier.*

Boebel, O., J. Lutjeharms, C. Schmid, W. Zenk, T. Rossby, and C. Barron (2003), The Cape Cauldron: a regime of turbulent inter-ocean exchange. *Deep-Sea Res. 11, Vol. 50, 57-86.*

Boyer, T. P., J. I. Antonov, H. E. Garcia, D. R. Johnson, R. A. Locarnini, A. V. Mishonov, M. T. Pitcher, O. K. Baranova, and I. V. Smolyar (2006). *World Ocean Database 2005*. S Levitus, Ed., NOAA Atlas NESDIS 60, U. S. Government Printing Office.

Brown, J., A. Colling, D. Park, J Phillips, D Rothery, and J Wright (1989). *SEAWATER: IT'S COMPOSITION, PROPERTIES AND BEHAVIOR: Light and Sound in Seawater. The Open University, Pergamon Press.*

Bryan, K. (1969), A numerical method for the study of the circulation of the world ocean. *J. Comput. Phys., Vol. 4, 347-376.*

Carnes, M. R., and J. L. Mitchell (1990), Synthetic Temperature Profiles Derived from Geosat Altimetry: Comparison with Air-Dropped Expendable Bathythermograph Profiles. *J. Geophys. Res., Vol. 95, No. C10, 17979-17992.*

Carnes, M. R. (2009), Description and Evaluation of GDEM-V 3.0, (unpublished*). Internal report of Naval Research Laboratory, NRL/MR/7330—09-9165.*

Carnes, M. R. (2010), Validation Test Report for GDEM4, (unpublished*). Internal report of Naval Research Laboratory, NRL/MR/7330—10-9271.*

Chu, P.C., C. Fan, and W. T. Liu (2000), Determination of Vertical Thermal Structure from Sea Surface Temperature. *J. Atmos. Oceanic Technology., 17, 971-979.*

Derber, J., and A. Rosati (1989), A Global Oceanic Data Assimilation System. *J. Phys. Oceanogr., Vol. 19, 1333-1347.*

Doan, C.D. , S. Y. Liong, and E. S.Chan. R.J. Abrahart et al. (eds.) (2008), Data Driven Models for Projecting Ocean Temperature Profile from Sea Surface Temperature. *Practical Hydroinformatics., 421-433.*

Duncombe-Rae, C., F. Shillington, J. Agenbag, J. Taunton-Clark, and M. Grundlingh (1992), An agulhas ring in the South Atlantic ocean and its interaction with the Benguela upwelling frontal system. *Deep-Sea Res.11/12, Vol. 39, 2009-2027.*

Etter, P. C. (1991), *UNDERWATER ACOUSTICS MODELLING, Elsevier.*

Narasimhan, T., N. (2004), *Eos, Vol.85, No. 47, 499-501.*

Feidler, P. C. (1988), Surface Manifestations of Subsurface Thermal Structure in the California Current. *J. Geophys. Res., Vol. 93, No. C5, 4975-4983.*

Fox, D. N., W. J. Teague, and C. N. Barron (2002), The Modular Ocean Data Assimilation System (MODAS). *J. Atmos. Oceanic Technology., 19, 240-252.*

Galperin, B., L. H. Kantha, S. Hassid, and A Rosati (1987), A Quasi-equilibrium Turbulent Energy Model for Geophysical Flows. *J. Atm. Sci., Vol 45, 55-62*.

Garzoli, S., and A. Gordon (1996), Origins and variability of the Benguela current. *J. Geophys. Res., Vol. 101, No. C1, 897-906.*

Garzoli, S., A. Gordon, V. Kamenkovich, D. Pillsbury, and C. Duncombe-Rae (1996), Variability and sources of the southeastern Atlantic circulation. *J. Mar. Res., Vol. 54, 1029-1071.*

Gildenhuÿs, S., and C. K. Wainman (2007), Military Oceanography: Investigation into forecasting of bathy profiles. *IMT internal document TV0010-207022-730. Restricted.*

Gordan, A., R. Weiss, W. Smethie, and M. Warner (1992), Thermocline and intermediate water communication between the south Atlantic and Indian oceans. *J. Geophys. Res., Vol. 97, No. C5, 7223-7240.*

Gordon, A., and K. Bosley (1991), Cyclonic Gyre in the South Atlantic. *Deep-Sea Res., Vol. 38 [Supp.1], 323-343.*

Haney, R. L. (1971), Surface Thermal Boundary Condition for Ocean Circulation Models. *J. Phys. Oceanogr.,Vol. 1, 241-248.*

Hardman-Mountford, A., A. Richardson, J. Agenbag, E. Hagan, L. Nykjaer, F. Shillington, and C. Villacastin (2003), Ocean climate of the south east Atlantic observed from satellite data and wind models. *Progr. Oceanogr., Vol. 59, 181-221.*

Hodges, R. P. (2010). *Underwater Acoustics: Analysis, Design and Performance of Sonar, John Wiley.*

http://www.argo.net/ , (6 August 2012).

http://www.oc.nps.edu/nom/day1/parta.html , (12 August 2012).

http://www.wikipedia.org/ (12 August 2012)

Jury, M., C. MacArthur, and G. Brundrit (1990), Pulsing of the Benguela upwelling region. Large-scale atmospheric controls. *S. Afr. J. mar. Sci., 9, 27-41.*

Kamstra, F. (1985), Environmental features of the southern Benguela with special reference to wind stress*, South African Ocean Colour Experiment. L. V. Shannon, Ed., 213-217, Sea Fisheries Research Institute.*

Khedouri , E., and C. Szczechowki (1983), Potential Oceanographic Applications of Satellite Altimetry for Inferring Subsurface Thermal Structure. *Oceans'83, Proc. Mar. Techol. Soc., 274-280.*

Kohonen, T., and T. Honkela (2007), Scholarpedia, 2(1):1568. *http://www.scholarpedia.org/article/Kohonen_network.*

Kraus, E. B., and J. S. Turner (1967), A One-dimensional Model of the Seasonal Thermocline. *Tellus, Vol. 19, 98-106.*

la Grange, P. L. (1993), *Sonar Handbook. IMT internal document KT076-060000-731001. Confidential.*

Largier, J., and A. Boyd (2001), Drifter observations of the surface water transport in the Benguela Current during the winter of 1999. *S. Afr. J. mar. Sci. 97.*

Lutjeharms, J., F. Shillington, and C. M. Duncombe-Rae (1991), Observations of extreme upwelling filaments in the Southeast Atlantic Ocean. *Science, Vol. 774, No. 3.*

Lutjeharms, J., and P. Stockton (1987), Kinematics of the upwelling front off southern Africa. *S. Afr. J. mar. Sci. 5: 35-49.*

Mellor, G. L., and P. A. Durbin (1975), The Structure and Dynamics of the Ocean Surface Mixed Layer. *J. Phys. Oceanogr., Vol. 5, 718-728.*

Munk, H. W., and E. R. Anderson (1948), Notes on a Theory of the Thermocline. *J. Marine Res., 276-295.*

Narasimhan, T. N. (2004), Fick's Insights on Liquid Diffusion. *Eos, Vol. 85, No. 47, 499-501.*

Nelson, G., A. Boyd, J. Agenbag, and C. M. Duncombe-Rae (1998), An upwelling filament north-west of Cape Town, South Africa. *S. Afr. J. mar. Sci. 19: 75-78.*

Nelson, G., and, L. Hutchings (1983), The Benguela upwelling area. *Progr. Oceanogr., Vol. 12 No. 3.*

Nhu, D. Le., and J. V. Zidek (2006), *Statistical Analysis of Environmental Space-Time Processes*, *Springer.*

Pacanowski, R., and S. G. H. Philander (1981), Parameterization of Vertical Mixing in Numerical Models of Tropical Oceans. *J. Phys. Oceanogr., Vol. 11, 1443-1451.*

Peterson, R., and L. Stramma (1991), Upper-level circulation in the South Atlantic. *Progr. Oceanogr., Vol. 26, 1-73.*

Posmentier, E. C. (1980), A Numerical Study of the Effects of Heat Diffusion Through the Base of the Mixed Layer. *J. Geophys. Res., Vol. 85, No. C9, 4883-4887.*

Preston-Whyte, R., and P. Tyson (1993), *The atmosphere and weather of southern Africa, chap. 11, 207-249, Oxford University Press.*

Rahmstorf, S (1992), Modelling Ocean Temperatures and Mixed-layer Depths in the Tasman Sea off the South Island, New Zealand. *New Zealand Journal of Marine and Freshwater Research, Vol. 26, 37-51.*

Reid, J. (1989), Geostrophic circulation of the south Atlantic Ocean. *Progr. Oceanogr., Vol. 149-244.*

Rhodes, R. C., H. E. Hurlburt, A. J. Wallcraft, C. N. Barron, P. J. Martin, E. J. Metzger, J. F. Shriver, D. S. Ko, O. M. Smedstad, S. L. Cross, and A. B. Kara (2002), Navy Real Time-time Global Modeling Systems. Navy Operational Models: Ten Years Later. *Oceanography, Vol. 15, No.1/2002, John Wiley.*

Richardson, A. J. (2002), Identifying characteristic chlorophyll *a* profiles in the coastal domain using an artificial neural network. *Journal of Plankton Research, Vol. 24, No. 12, 1289-1303.*

Rosati, A., and K. Miyakoda (1988), A General Circulation Model for Upper Ocean Simulation. *J. Phys. Oceanogr., Vol. 18, 1601-1626.*

Rossby, C. G., and R.B. Montgomery (1935), The layers of frictional influence in wind and ocean currents. *Pap. Phys. Oceanogr. Meteorol., Vol. 3, No. 3, 101.*

Sammon, J. (1969), A nonlinear mapping for data structure analysis. *IEEE Trans. Comp., Vol. 18 No. 5, 401-409.*

Shannon, L. (1985), The Benguela ecosystem part 1: physical features and processes. *Oceanographic and Marine Biology Annual Review, Vol. 23, 105-182.*

Shannon, L., and G. Nelson (1996), The South Atlantic: Present and past circulation, *chap. The Benguela: Large-scale features and processes and system variability, 163-210. Springer.*

Shillington, F. (1998), The Global Coastal Ocean, Regional Studies and Syntheses, *The Sea, Vol. II, chap. The Benguela upwelling system off southwestern Africa., 583-604, Wiley.*

Shillington, F., L. Hutchings, T. Probyn, H. Waldron, and W. Peterson (1992), Filaments in the Benguela frontal zone: offshore advection or reticulation loops? *S. Afr. J. mar. Sci.12: 207-218.*

Shillington, F., W. Peterson, L. Hutchings, T. Probyn, H. Waldron, and J. Agenbag (1990), A cool upwelling filament off Namibia, southwest Africa: preliminary measurements of physical and biological features. *Deep-Sea Res. 11, Vol. 37, 1753-1772.*

Shillington, F., C. Reason, C. Duncombe-Rae, P. Florenchie, and P. Penven (2006), Benguela: Predicting a Large Marine Ecosystem. *Large Marine Ecosystems, Vol. 14, chap. 4: Large scale variability of the Benguela current large marine ecosystem (BCLME), 49-70, Elsevier.*

Shonting, D.H. (1964), Some observations of short term heat transfer through the surface layers of the ocean. *Limnol. Oceangr. 4, Vol. 9, 576-588.*

Silulwane, N. F, A. J. Richardson, F. A. Shillington, and B. A. Mitchell-Innes (2001), Identification and classification of vertical chlorophyll patterns in the Benguela upwelling system and Angola front using an artificial neural network, A Decade of Namibian Fisheries Science. Payne, A. I. L., Pillar. S. C. and R. J. M. Crawford (Eds), *S. Afr. J. mar. Sci. 23: 37-51.*

Smith, W. L., P. K. Rao, R. Koffler, and W. R. Curtis (1970), The Determination of Sea-Surface Temperature from Satellite High Resolution Infrared Window Radiation Measurements. *Monthly Weather Review, Vol. 98, No. 8, 604-611.*

SOM Toolbox 2.0 documentation (18 March 2005).
http://www.cis.hut.fi/somtoolbox/documentation/index.shtml.

Teague, W. J., M. J. Carron, and P. J. Hogan (1990), A comparison between the generalized digital environmental model and Levitus climatologies. *J. Geophys. Res., Vol. 95, 7167-7183.*

Tennekes, H., and J. L. Lumley (1983). *A First Course in Turbulence, The MIT Press.*

Urick, R. J. (1967). *Principles of Underwater Sound for Engineers, McGraw-Hill.*

van Ballegooyen, R., M. Grundlingh, and J. Lutjeharms (1994), Eddy fluxes of heat and salt from the south west Indian ocean into the south east Atlantic Ocean: a case study. *J. Geophys. Res., Vol. 99, No. C7, 14053-14070.*

Van Foreest, D., F. Shillington, and R. Legeckis (1984), Large scale, stationary, frontal features in the Benguela current system. *Continental Shelf Research, Vol. 3, No. 4, 465-474.*

Veitch, J (2009), Equilibrium dynamics of the Benguela system: a numerical modeling approach. *Ph.D. thesis, University of Cape Town, South Africa.*

Vesanto, J., J. Himberg, E. Alhoniemi, and J. Parhankangas (2000), SOM Toolbox for Matlab 5. *Helsinki University of Technology Report A57 April 2000. http://cis.hut.fi/projects/somtoolbox/, 15 May 2009.*

APPENDIX A – MONTHLY PATHFINDER DATASETS

4 km resolution RSMAS/NODC AVHRR data was sourced from the extensive Pathfinder on-line archive at http://www.nodc.noaa.gov/sog/pathfinder4km/available.html. The data covers a 24 year span from 1981 to 2005 and is represented as mean values per month. Software routines were developed in Matlab® to import, orientate contour and graphically display the output.

Isotherms that apply for all months are labelled the month of April. The enclosed polygon used to demarcate the study area is shown for each month as a feint red line, also labelled for the month of Aril.

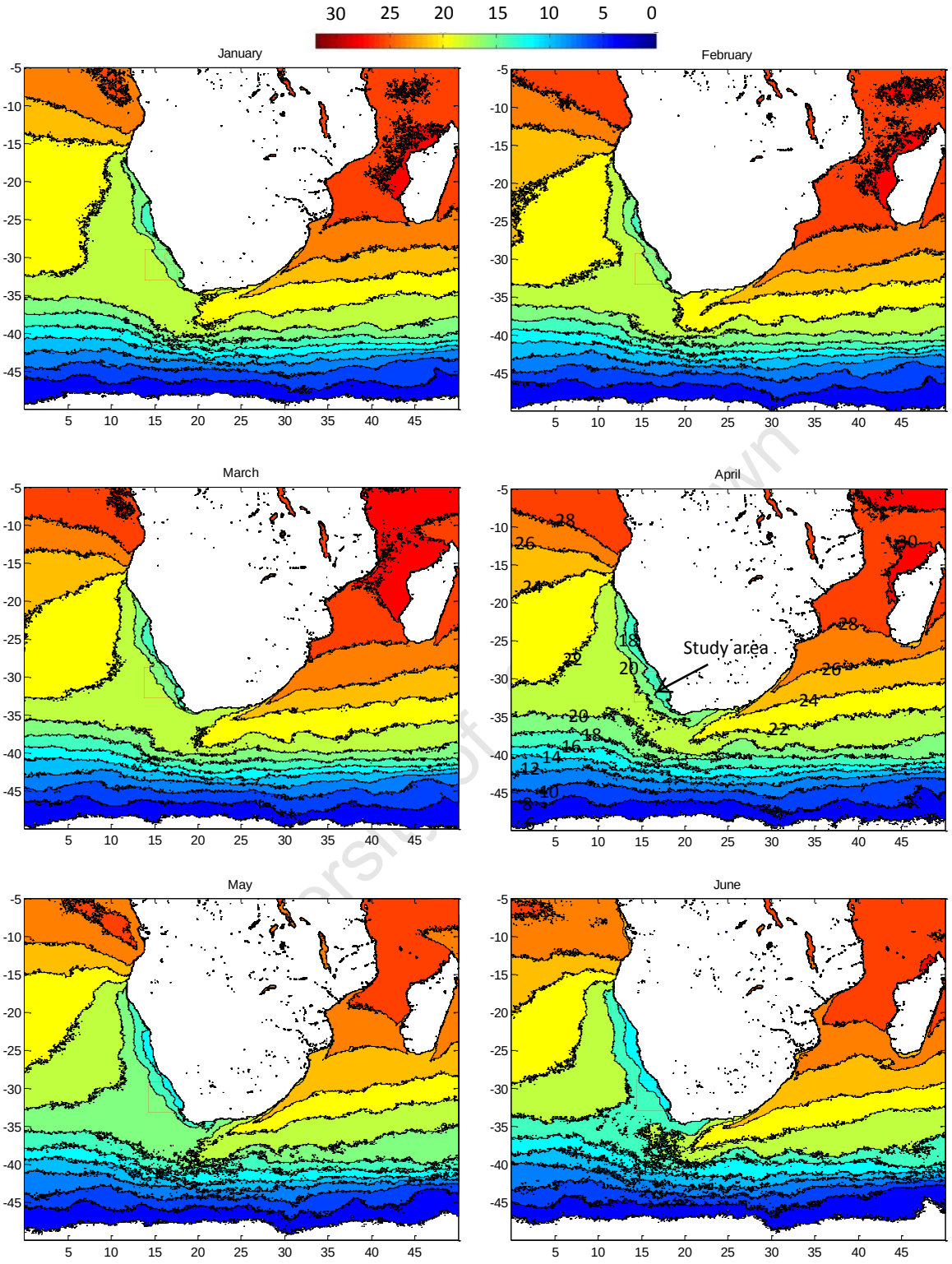
30 25 20 15 10 5 0
January
February
March
April
May
June
Study area

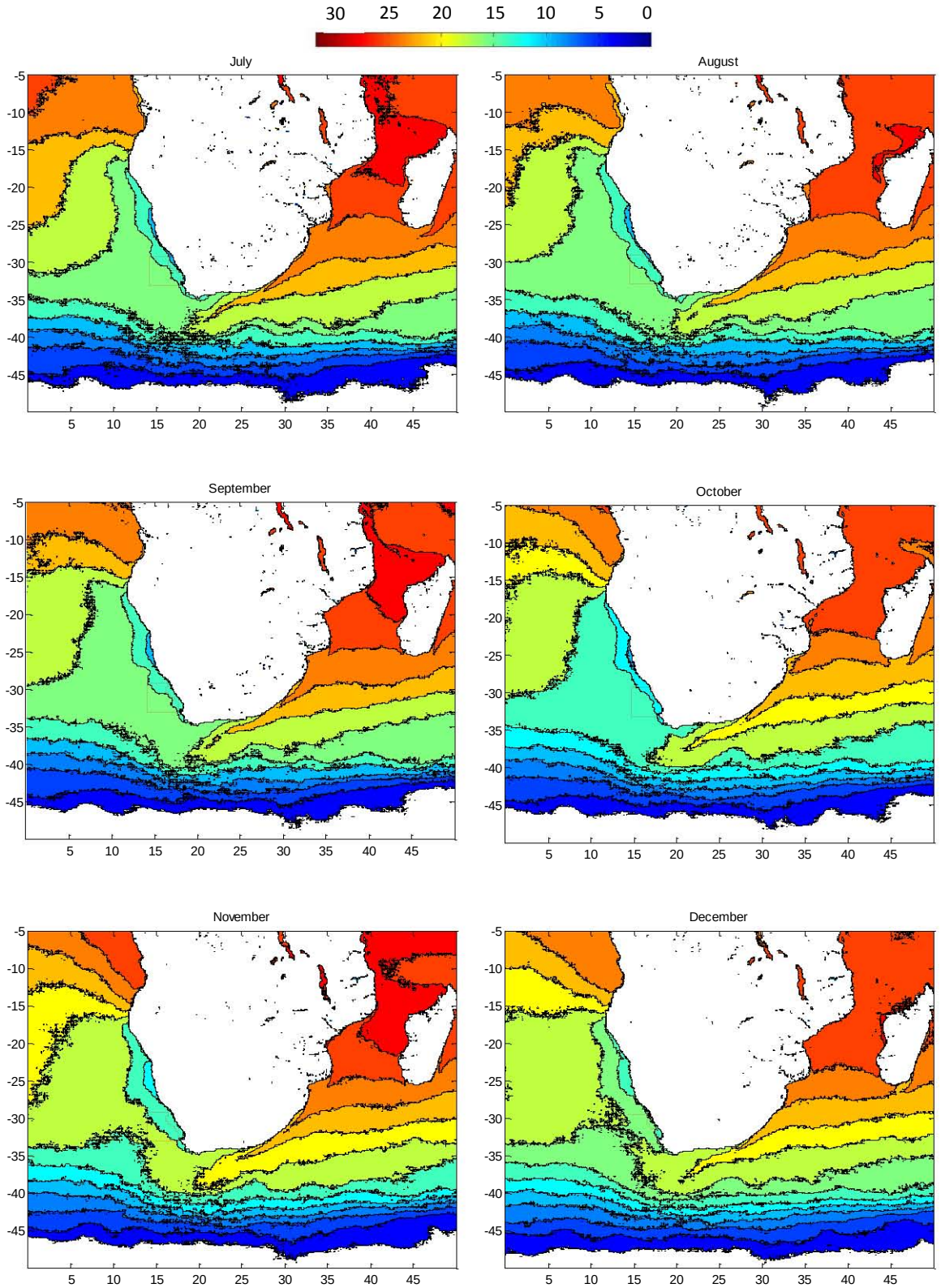
30 25 20 15 10 5 0
July
August
September
October
November
December
-5 -10 -15 -20 -25 -30 -35 -40 -45
5 10 15 20 25 30 35 40 45

APPENDIX B – SOURCED PROFILE DATA

All profile data were obtained as an off-line batch request from the Southern African Data Centre for Oceanography (SADCO), the national custodian for this data. These were in ASCII text format and imported into Matlab ® for further processing. The Dataset consisted of two distinctly varying profile types (Discrete and Contiguous) grouped into the following categories.

CTD – Conductivity Temperature Depth profilers [contiguous]

MBT – Mechanical BathyThermographs [contiguous]

XBT – eXpendable BathyThermographs [contiguous]

OSD – Oxygen Standard Depth (so called bottle-depths or 'bott smpls' in ***Figure 5-3*** (A)), [discrete]

PFL – Profile Floats (Argo floats or 'Prof flts' in ***Figure 5-3***), [contiguous]

DPF – Delayed Profile Floats (Argo floats), [contiguous]

Each profile contained a header record (see example below as reference):

"Prov1"- A unique identifier referring to a geographical polygon used in this study (see red demarcated area in ***Figure 5-4***). Only province 1 was used for this study.

"Profile562"- Unique sequential profile identifier

"USD001316" – So called station number, a convenient customised identifier allocated at the time of collecting the data.

"1975-01-15" – Profile collection date as yyyy-mm-dd

"OSD" – Code for the type of sensor used to collect the data (See list above)

"110" – an additional field not used in this study

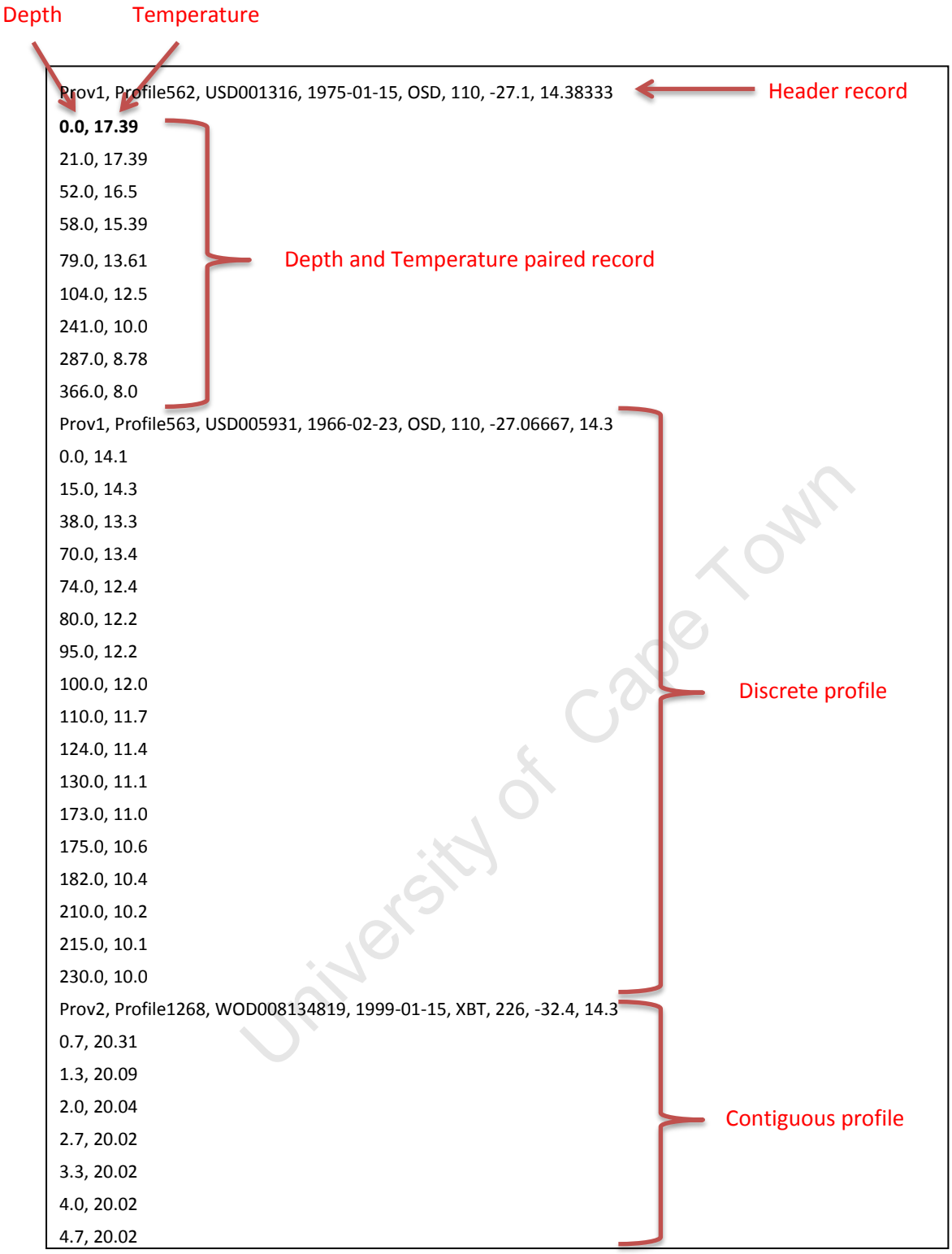

"-27.1" – Latitude in degrees decimal of the geographical location of the profile (-ve=south of the equator, +ve=north of the equator)

"14.3833" – Longitude in degrees decimal of the geographical location of the profile (-ve=west the Greenwich meridian, +ve=east of the Greenwich meridian)

Every header record was followed by sequential depth (in meters below the surface), temperature (^{0}C) pair.

The first 2 examples below are discrete type profiles, whilst the third profile is contiguous. Only the 7 depth temperature pairs are shown in the third profile.

APPENDIX C – EXAMPLES OF CURVE FITTING FOR DISCRETE PROFILES

Some examples of 6th order polynomial curves (broken red line) fitted to discrete profiles (solid blue line) in the upper 125 m (only 100 m polynomial fits shown here). Depth is shown as increasing negative numbers on the y-axis and temperature in ^{0}C on the x-axis. In the final analysis, a depth range of 0-125 m was used. Profiles shown here to demonstrate the varying shapes of the polynomial curves based on varying amounts of vertical mixing. The 9 values shown alongside each line plot are the differences between the original discrete profile and the fitted polynomial at each standard depth to a maximum of 100 m (not the complete range, down to 125 m as used in the analysis in the text). They are shown hare for illustrative purposes of the polynomial fitting process only. A mean delta or absolute difference value is also shown above each profile.

Note* these plots were extracted during the first stage of curve fitting, a step prior to any correction (overshoot) applied to the wind mixed layer. Red squares with accompanying values are the temperature delta values (differences between the curve fitted temperature and the measured values). The mean delta for each curve is shown separately.

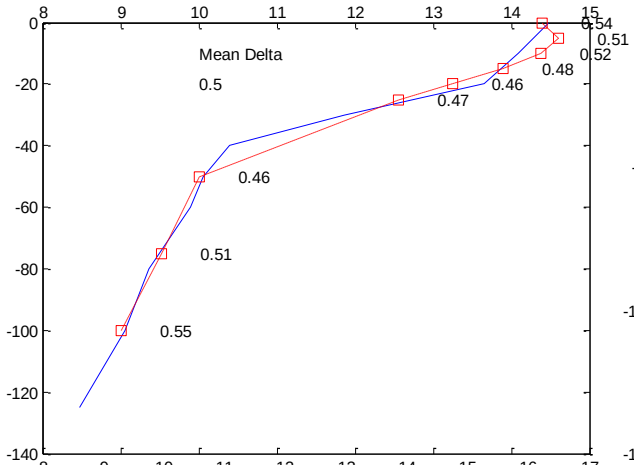
Mean Delta
0.5
0.46
0.51
0.55
0.47
0.46
0.48
0.52
0.54
0.51

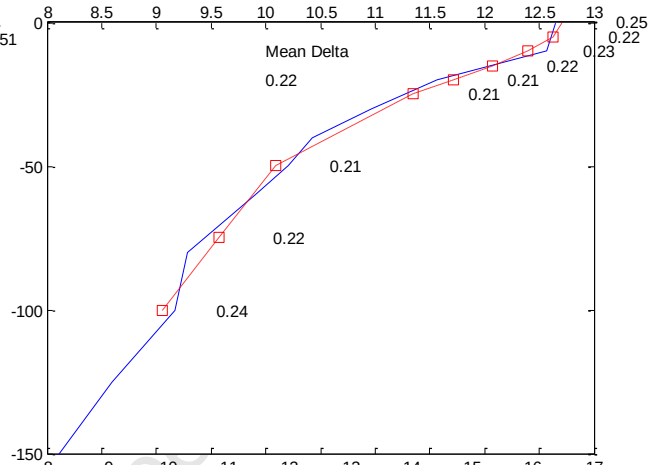
Mean Delta
0.22
0.21
0.22
0.24
0.21
0.22
0.21
0.23
0.22
0.25

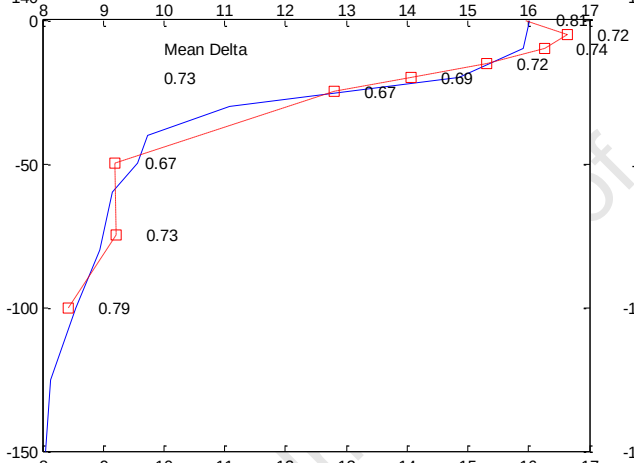
Mean Delta
0.73
0.67
0.73
0.79
0.67
0.69
0.72
0.74
0.81
0.72

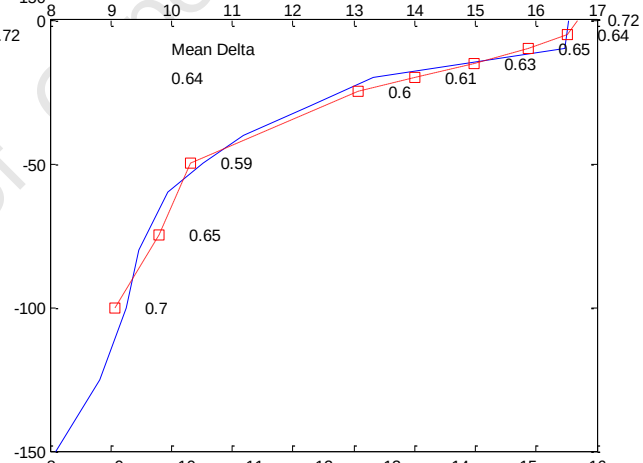
Mean Delta
0.64
0.59
0.65
0.7
0.6
0.61
0.63
0.65
0.64
0.72

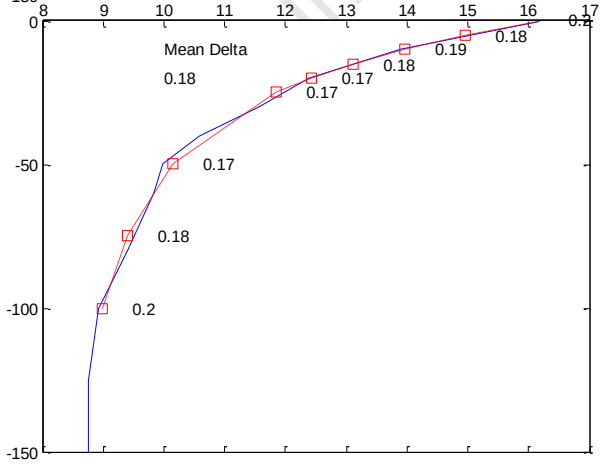
Mean Delta
0.18
0.17
0.18
0.2
0.17
0.17
0.18
0.19
0.18
0.2

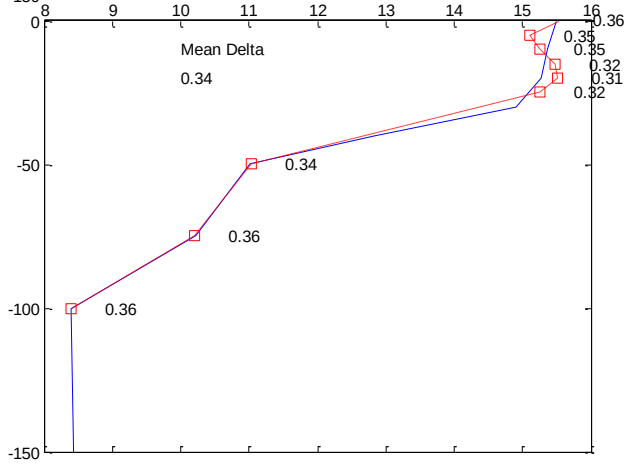
Mean Delta
0.34
0.34
0.36
0.36
0.32
0.31
0.32
0.35
0.35
0.36

APPENDIX D – SELF ORGANISING MAP TOOLBOX

This public domain suite of scripts and functions are provided as freeware for scientific software development that requires the Matlab® 'engine' for execution. A few of the available suite of functions were used in this study (see list below).

Function	Description
som_data_struct	create & initialize a data structure
som_autolabel	automatically labels the SOM based on given data
som_seqtrain	sequential training algorithm
som_grid	visualization of SOM grid
som_stats	statistics of a data set
som_quality	quantization and topographic error of SOM
som_hits	calculates the response of data on the map
som_bmus	calculates BMUs for given data vectors

The following is an extract of pertinent parts of a paper compiled by the software developers of the SOM toolbox describing the theory of the SOM (Vesanto et al (2000)).

The toolbox was sourced from http:/www.cis.hut.fi/projects/somtoolbox/

SOM implementation in SOM Toolbox

On this page, the structure of SOM and the SOM algorithm are described.

In SOM Toolbox, all information regarding a SOM is gathered in a map struct. This struct has a number of fields, including the map codebook, map topology, component names and training history. There are also other structs, for example topology and training structs.

Structure of SOM

Map grid

A SOM is formed of neurons located on a regular, usually 1- or 2-dimensional grid. Also higher dimensional grids are possible, but they are not generally used since their visualization is much more problematic.

The neurons are connected to adjacent neurons by a neighbourhood relation dictating the structure of the map. In the 2-dimensional case the neurons of the map can be arranged either on a rectangular or a hexagonal lattice, see Figure 1. If the sides of the map are connected to each other, the global shape of the map becomes a cylinder or a toroid, see figure Figure 2.

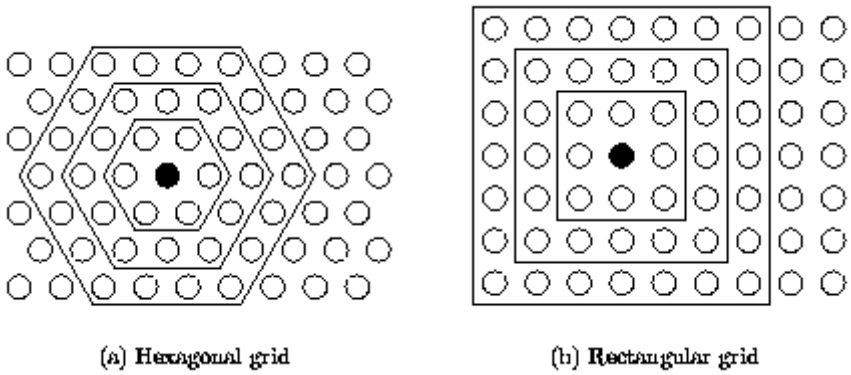

Figure 1: Neighbourhoods (size 1, 2 and 3) of the unit marked with black dot: (a) hexagonal lattice, (b) rectangular lattice.

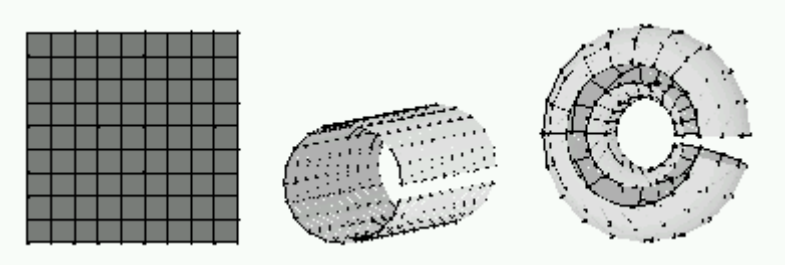

Figure 2: Different map shapes: sheet on the left, cylinder in the centre and toroid on the right. In the two latter, the connections across the gaps exist. They just have not been drawn.

SOM Toolbox supports both hexagonal and rectangular lattices and cylinder and toroid shapes. They are specified in the lattice and shape fields of the topology struct.

Prototypes

Each neuron *i* of the SOM has an associated *d*-dimensional prototype (aka weight, reference, codebook or model) vector $\mathbf{m}_i = [m_{i1}\ m_{i2}...\ m_{id}]$, where *d* is equal to the dimension of the input vectors.

The prototype vectors of the map are in the codebook matrix of the map struct. The rows of the matrix's Map.codebook(i,:) are the prototype vectors and the column's Map.codebook(:,i) are the variables (aka components). The map struct also has fields for names of the variable's Map.comp_names, normalization operations associated with each of the variables sMap.comp_norm as well as labels associated with each of the neuron's Map.labels.

Each neuron has actually two positions: one in the input space -- the prototype vector -- and another in the output space -- on the map grid. Thus, SOM is a vector projection method defining a nonlinear projection from the input space to a lower-dimensional output space. On the other hand, during the training the prototype vectors move so that they follow the probability density of the input data. Thus, SOM is also a vector quantization algorithm. Simplified, SOM is nothing more than an algorithm that combines these two tasks: vector quantization and projection.

Neighbourhood function

Immediate neighbours, the neurons that are adjacent, belong to the 1-neighborhood N_{i1} of the neuron *i*. Neighbourhoods of different sizes in rectangular and hexagonal lattices are illustrated in Figure 1. The innermost polygon corresponds to 1-neighborhood, the second to the 2-neighborhood and the biggest to the 3-neighborhood.

The neighbourhood function determines how strongly the neurons are connected to each other. The simplest neighbourhood function is the bubble: it is constant over the whole neighbourhood of the winner unit and zero elsewhere. Another is the Gaussian neighbourhood function

$$exp\left(-\frac{||\mathbf{r}_c-\mathbf{r}_i||^2}{2\sigma^2(t)}\right)$$

, where r_c is the location of unit *c* on the map grid and the *sigma (t)* is the neighbourhood radius at time *t*.

Notice that this is a function of distance between map units on the map grid $||r_c - r_i||$, rather than of the neighbourhood sets in Figure 1. Function som_neighborhood.m can be used to find the neighbourhood sets, but the training functions use the distance on map grid, calculated with som_unit_dists.m.

Neighbourhood function and the number of neurons determine the granularity of the resulting mapping. The larger the area where neighbourhood function has high values, the more rigid is the map. The larger the map, the more flexible it can become. This interplay determines the accuracy and generalization capability of the SOM.

SOM Toolbox has four different kinds of neighbourhood functions, shown in Figure 3. The used neighbourhood function is defined in neigh field of map and training structs.

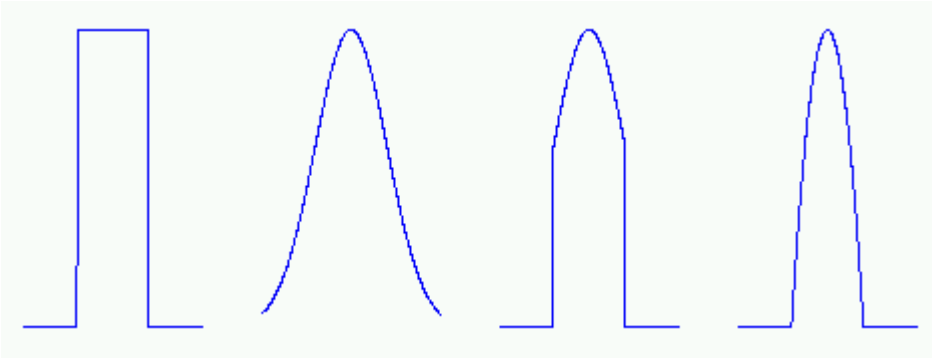

Figure 3: The four neighbourhood functions in SOM Toolbox: bubble, gaussian, cut gaussian and epanechicov (which is essentially max (0,1-x^2)).

SOM algorithm

Size and shape

In the classical SOM, the number of neurons and their topological relations are fixed from the beginning. There are four issues which need to be decided: the number of neurons, dimensions of the map grid, map lattice and shape.

The number of neurons should usually be selected as big as possible, with the neighbourhood size controlling the smoothness and generalization of the mapping. The mapping does not considerably suffer even when the number of neurons exceeds the number of input vectors, if only the neighbourhood size is selected appropriately. However, as the size of the map increases e.g. to tens of thousands of neurons the training phase becomes computationally impractically heavy for most applications.

In SOM Toolbox, the default number of neurons is *5 * sqrt(n)* where *n* is the number of training samples. Note that the computational load increases quadratively with the number of map units. Therefore, don't take literally the "as big as possible" thing above. In our own research, the number of map units is usually between 100-600.

If possible, the shape of the map grid should correspond to the shape of the data manifold. Therefore, the use of toroid and cylinder shapes is only recommended if the data is known to be circular. For the default sheet shaped map, it is recommended that side length along one dimension is longer than the others, e.g. msize = [15 10], so that the map can orientate itself properly. One could possibly use the eigenvalues of the training data set as a guideline in setting the map grid side lengths.

The use of hexagonal lattice is usually recommended, because then all 6 neighbours of a neuron are at the same distance (as opposed to the 8 neighbours in a rectangular lattice). This way the maps become smoother and more pleasing to the eye. However, this is mostly a matter of taste.

In SOM Toolbox, the map grid side lengths are determined by the ratio between eigenvalues of the training data. Also the compression of map units in case of hexagonal lattice (in vertical direction by a factor of *sqrt(0.75)*) is taken into account.

Initialization

Before the training, initial values are given to the prototype vectors. The SOM is very robust with respect to the initialization, but properly accomplished it allows the algorithm to converge faster to a good solution. Typically one of the three following initialization procedures is used:

- random initialization, where the weight vectors are initialized with small random values
- sample initialization, where the weight vectors are initialized with random samples drawn from the input data set
- linear initialization, where the weight vectors are initialized in an orderly fashion along the linear subspace spanned by the two principal eigenvectors of the input data set. The eigenvectors can be calculated using Gram-Schmidt procedure.

  In SOM Toolbox, random and linear initializations have been implemented. Random initialization is done by taking randomly values from the *d*-dimensional cube defined by the minimum and maximum values of the variables. Linear initialization is done by selecting a mesh of points from the *d*-dimensional min-max cube of the training data. The axis of the mesh are the eigenvectors corresponding to the *m* greatest eigenvalues of the training data (*m* is the map grid dimension). Notice that the shape (e.g. cylinder) of the map is not taken into account in initialization: it is always assumed to be a sheet.

Training

In each training step, one sample vector **x** from the input data set is chosen randomly and a similarity measure is calculated between it and all the weight vectors of the map. The Best-Matching Unit (BMU), denoted as *c*, is the unit whose weight vector has the greatest similarity with the input sample **x**. The similarity is usually defined by means of a distance measure, typically Euclidian distance. Formally the BMU is defined as the neuron for which

$$||\mathbf{x} - \mathbf{m}_c|| = \min_i\{||\mathbf{x} - \mathbf{m}_i||\},$$

where $||.||$ is the distance measure.

After finding the BMU, the prototype vectors of the SOM are updated. The prototype vectors of the BMU and its topological neighbours are moved closer to the input vector in the input space. This adaptation procedure stretches the prototypes of the BMU and its topological neighbours towards the sample vector. This is illustrated in Figure 4. The SOM update rule for the weight vector of the unit *i* is:

$$\mathbf{m}_i(t+1) = \mathbf{m}_i + a(t)\, h_{ci}(r(t))\, [\mathbf{x}(t) - \mathbf{m}_i(t)],$$

where *t* denotes time, *a(t)* is learning rate and $h_{ci}(r(t))$ the neighbourhood kernel around the winner unit *c*, with neighbourhood radius *r(t)*.

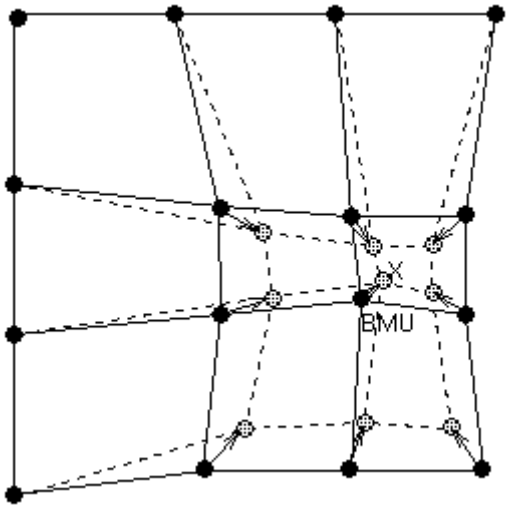

Figure 4: Updating the best matching unit (BMU) and its neighbours towards the input sample marked with x. The solid and dashed lines correspond to situation before and after updating, respectively.

In SOM Toolbox, finding of BMU is slightly more complex, because the data samples may have missing components (NaNs), and each variable has an associated weighting factor, defined in field mask of map and training structs.

Missing components are handled by simply excluding them from the distance calculation (i.e. it is assumed that their contribution to the distance $||\mathbf{x} - \mathbf{m}_i||$ is zero). Because the same variable(s) is ignored in each distance calculation (over which the minimum is taken), this is a valid solution. The weighting factor mask is primarily used in binary form for excluding certain variables from the BMU-finding process (1 for include, 0 for exclude). However, the mask can get any values, so it can be used for weighting variables according to their importance. With these changes, the distance measure becomes:

$$||\mathbf{x} - \mathbf{m}||^2 = \sum_{k \in K} w_k |x_k - m_k|^2$$

where K is the set of known (not missing) variables of sample vector $\mathbf{x}$, x_k and m_k are kth components of the sample and prototype vectors and w_k is the kth mask value (mask(k)). Note though that the update rule does not change, so the weighting only affects finding of BMU.

Training parameters

The learning rate *a(t)* is a decreasing function of time between [0,1]. Two commonly used forms are a linear function and a function inversely proportional to time: *a(t) = A / (t+B)*, where*A* and *B* are some suitably selected constants. Use of the latter function type ensures that all input samples have approximately equal influence on the training result.

In SOM Toolbox, there are three learning rate functions: linear, inverse-of-time, and a power series. These are illustrated in Figure 5. The power series is defined as

$$\alpha_0 \left(\frac{\alpha_T}{\alpha_0}\right)^{t/T}$$

where α_0 is the initial learning rate, α_T the final learning rate, t is time and T the training length.

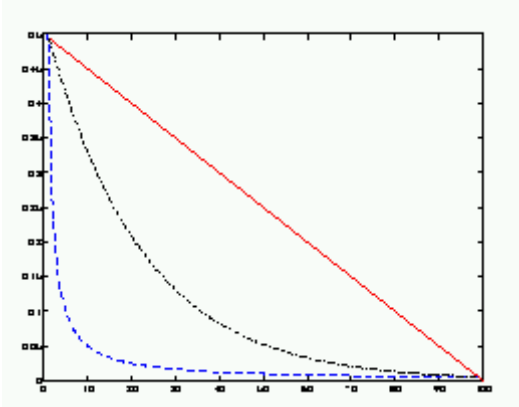

Figure 5: The three learning rate functions in SOM Toolbox: linear (red), power series (black) and inverse-of-time (blue).

Also neighbourhood radius typically decreases with time. Since large neighbourhood radius makes the SOM more rigid, it is usually used in the beginning of training, and then it is gradually decreased to a suitable final radius. A suitable final radius is, for example, one. Notice that if neighbourhood radius is set to zero *r=0*, the SOM algorithm reduces to *k*-means algorithm.

The total training time -- or, the number of samples presented to the SOM --- is an important consideration. The number of training steps should be at least 10 times the number of map units.

The training is usually performed in two phases. In the first phase, relatively large initial learning rate and neighbourhood radius are used. In the second phase both learning rate and neighbourhood radius are small right from the beginning. This procedure corresponds to first tuning the SOM approximately to the same space as the input data and then fine-tuning the map. If the linear initialization procedure is used the first training phase can be skipped.

In SOM Toolbox, the default is to train the map in two phases. The function som_train_struct.m defines the default training parameters. This is quite complex, but in principle, learning rate begins from 0.5 in the first phase, and from 0.05 in the second phase. Neighbourhood radius starts from

max(msize)/4 and goes down to one fourth of that (unless this would be less than 1). On second phase, neighbourhood radius starts from where it stopped in first phase, and goes down to 1. The length of second phase is 4 times that of the first phase.

The training parameters are saved to a training struct, which can be found from the trainhist field of the map struct.

Batch training algorithm

An important variant of the basic SOM is the batch algorithm. In it, the whole training set is gone through at once and only after this the map is updated with the net effect of all the samples. Actually, the updating is done by simply replacing the prototype vector with a weighted average over the samples, where the weighting factors are the neighbourhood function values.

$$\mathbf{m}_i(t+1) = \frac{\sum_{j=1}^{n} h_{ic(j)}(t)\mathbf{x}_j}{\sum_{j=1}^{n} h_{ic(j)}(t)},$$

where *c(j)* is the BMU of sample vector $\mathbf{x}_j$, $h_{i,c(j)}$ the neighbourhood function (the weighting factor), and *n* is the number of sample vectors.

The default training algorithm in SOM Toolbox is this batch algorithm. This is because it is much faster to calculate in Matlab than the normal sequential algorithm, and the results are typically just as good or even better.

Variants

There are many variants to the basic SOM. One variation theme is to use neuron-specific learning rates and neighbourhood sizes. Another is to use adaptive or flexible neighbourhood definitions or even growing map structures. The goal of these variations is to enable the SOM to follow better the topology of the underlying data set or to achieve better quantization results. A usual defect of these methods is that the visualization properties suffer or that the algorithm becomes computationally heavier. Another family of variations aims at making the SOM a better classifier.

Of the variants, SOM Toolbox has (at least) implementation of neural gas (neural_gas.m) and supervised SOM (som_supervised.m). There are also implementations of *k*-means (kmeans.m), kNN (knn.m) and LVQ (lvq1.m, lvq3.m).

APPENDIX E – NEURAL NETWORK/SELF ORGANISING MAPS OUTPUT

An example of repeated SOM execution showing nodes as linked black circles in the output space of the profiles, shown as red crosses. Each image is the result of a sequential training process, with the number of training steps shown as a number above.

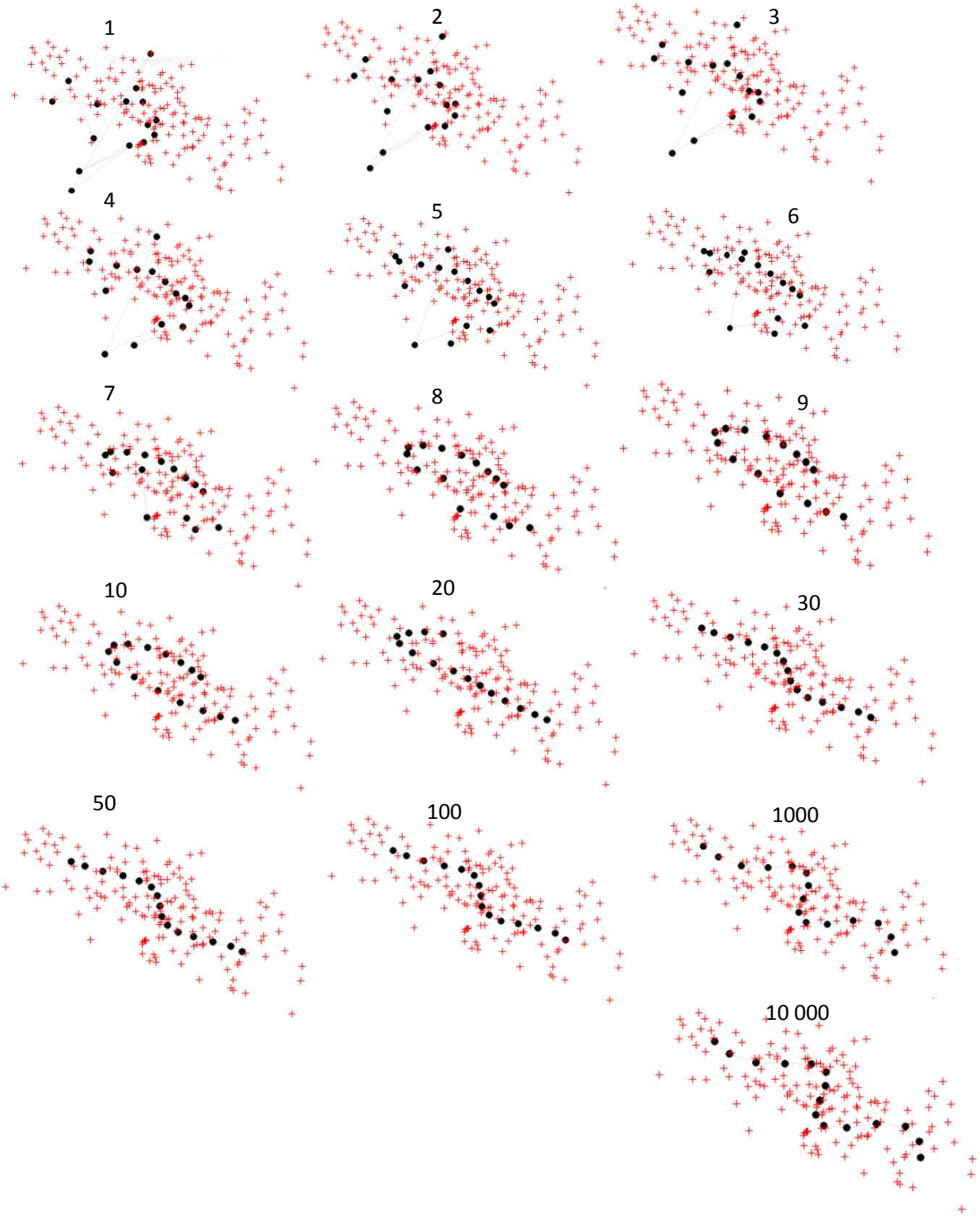

APPENDIX F – HIND CASTS

The same output for the remaining calendar months as presented in ***Figure 7-1***. All 12 months are shown as labelled in the right hand panel (B) of each plot.

Hind cast plots of 15 SOM output profiles and single predictive result for all months shown as solid green lines in with the chosen (by the software) synthetic SOM profile shown as a solid red line in upper left hand panel (A) and a solid blue line in the upper right hand panel (B), using a varying surface temperature as described in the text (see section7 a.), to identify the winning synthetic SOM profile. In the upper right hand side panel (B), a number of qualifying hind cast profiles as identified by the software are plotted in their original form as solid red lines. The same predictive profile is shown in (A) and (B) with standard depths depicted as black stars (*) and blue crosses (x) respectively. In (C), a bar graph is used to display the statistical features of the sea surface temperature values (0 m) of the observational profiles for the region during that month. It is this approximate modal value of this bar graph that was used to choose the SST temperature values used for the hind cast. Various headings for each hind cast are provided in the right hand panel (B).

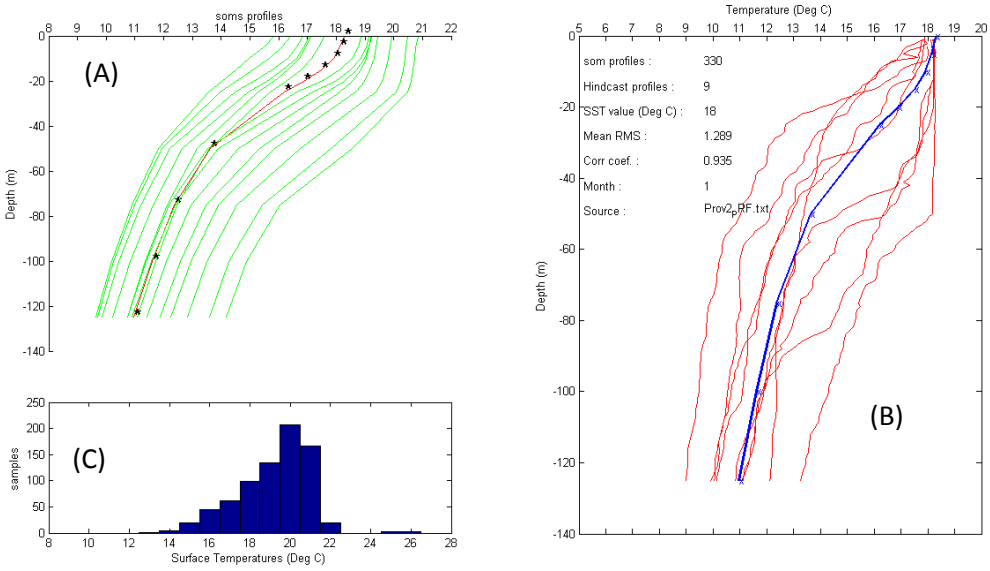

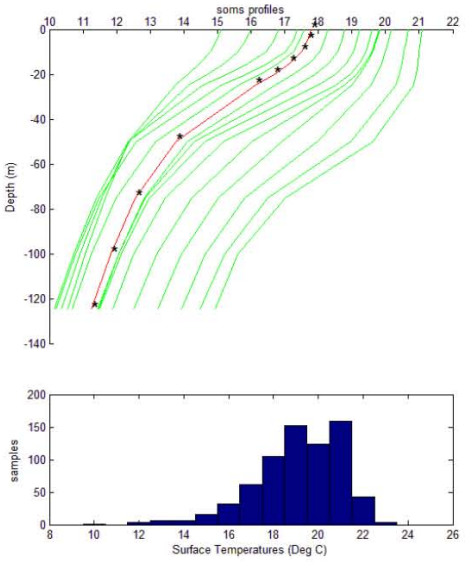
soms profiles
Depth (m)
samples
Surface Temperatures (Deg C)

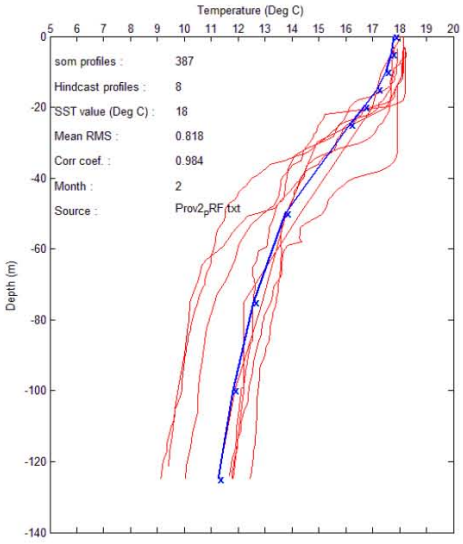
Temperature (Deg C)
som profiles : 387
Hindcast profiles : 8
SST value (Deg C) : 18
Mean RMS : 0.818
Corr coef. : 0.984
Month : 2
Source : Prov2_pRF.txt
Depth (m)

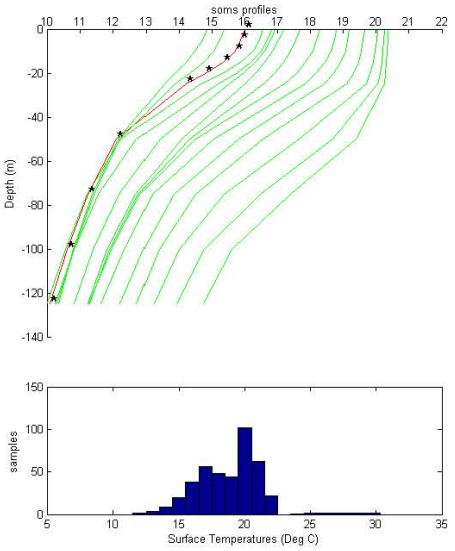
soms profiles
Depth (m)
samples
Surface Temperatures (Deg C)

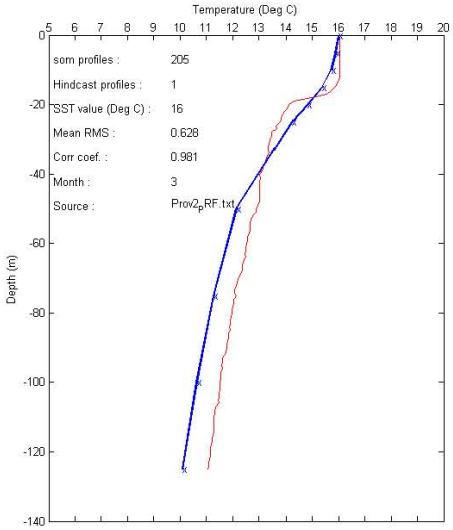
Temperature (Deg C)
som profiles : 205
Hindcast profiles : 1
SST value (Deg C) : 16
Mean RMS : 0.628
Corr coef. : 0.981
Month : 3
Source : Prov2_pRF.txt
Depth (m)

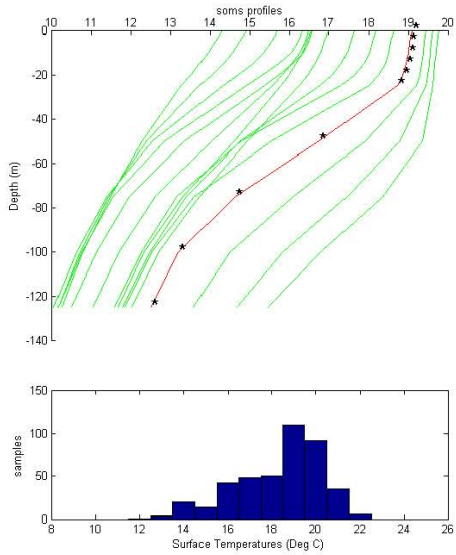
soms profiles
Depth (m)
samples
Surface Temperatures (Deg C)

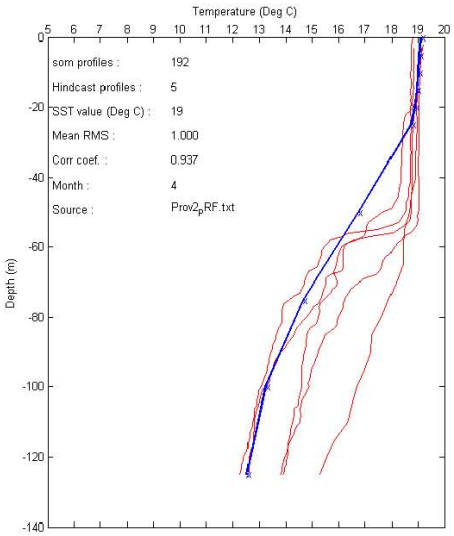
Temperature (Deg C)
som profiles : 192
Hindcast profiles : 5
SST value (Deg C) : 19
Mean RMS : 1.000
Corr coef. : 0.937
Month : 4
Source : Prov2_pRF.txt
Depth (m)

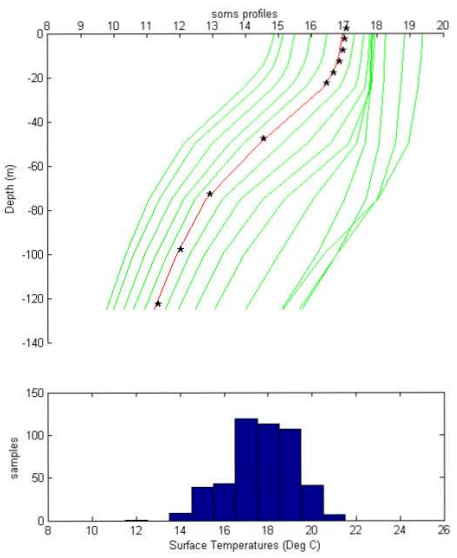
soms profiles
Depth (m)
samples
Surface Temperatures (Deg C)

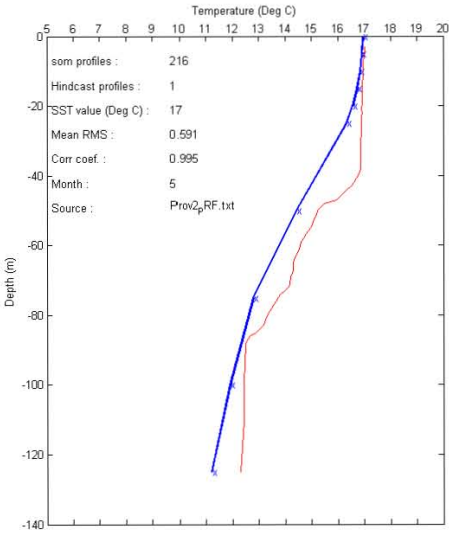
Temperature (Deg C)
som profiles : 216
Hindcast profiles : 1
SST value (Deg C) : 17
Mean RMS : 0.591
Corr coef. : 0.995
Month : 5
Source : Prov2_pRF.txt
Depth (m)

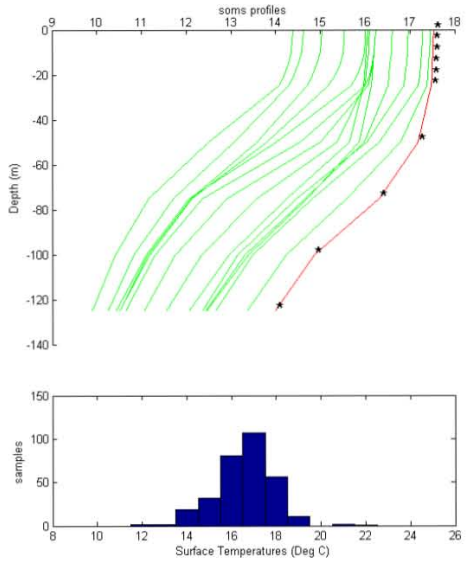
soms profiles
Depth (m)
samples
Surface Temperatures (Deg C)

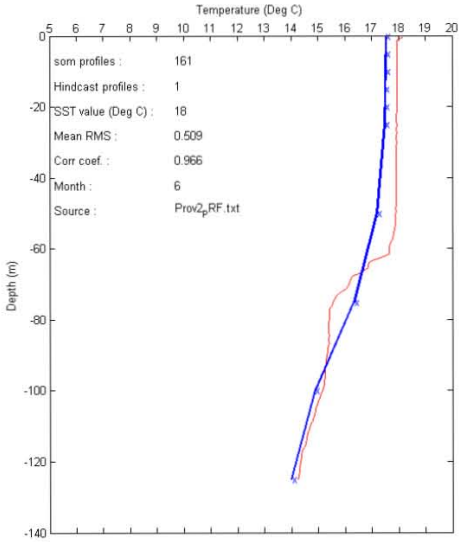
Temperature (Deg C)
som profiles : 161
Hindcast profiles : 1
SST value (Deg C) : 18
Mean RMS : 0.509
Corr coef. : 0.966
Month : 6
Source : Prov2_pRF.txt
Depth (m)

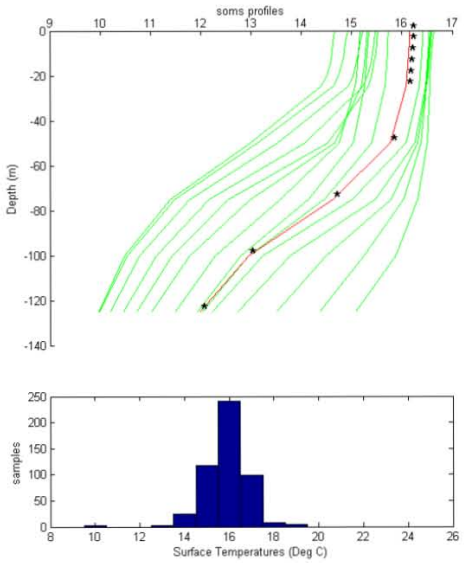
soms profiles
Depth (m)
samples
Surface Temperatures (Deg C)

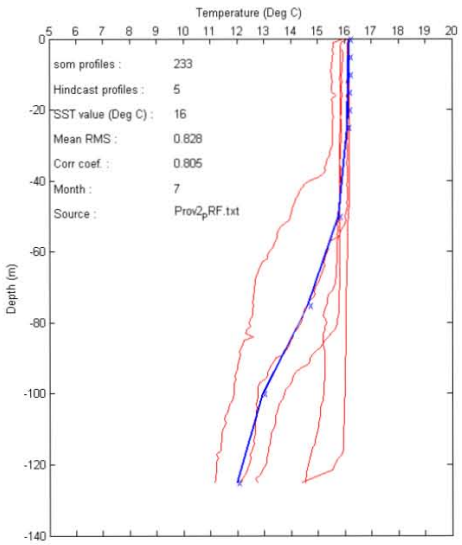
Temperature (Deg C)
som profiles : 233
Hindcast profiles : 5
SST value (Deg C) : 16
Mean RMS : 0.828
Corr coef. : 0.805
Month : 7
Source : Prov2_pRF.txt
Depth (m)

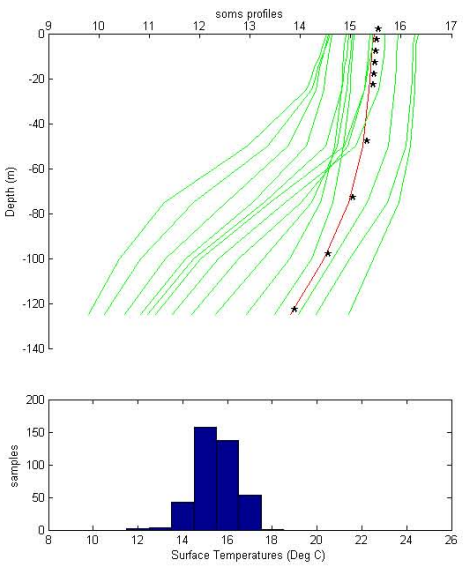
soms profiles
Depth (m)
samples
Surface Temperatures (Deg C)

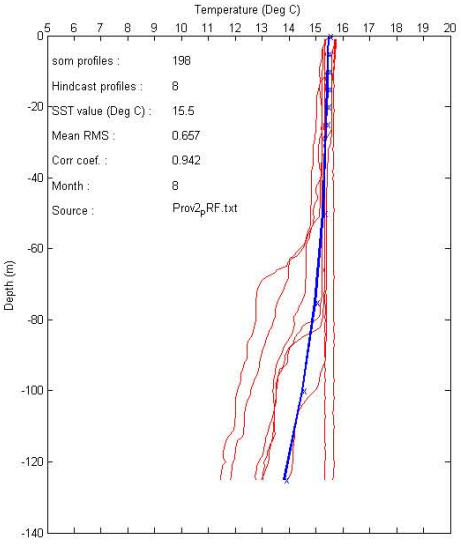
Temperature (Deg C)
som profiles : 198
Hindcast profiles : 8
SST value (Deg C) : 15.5
Mean RMS : 0.657
Corr coef. : 0.942
Month : 8
Source : Prov2_pRF.txt
Depth (m)

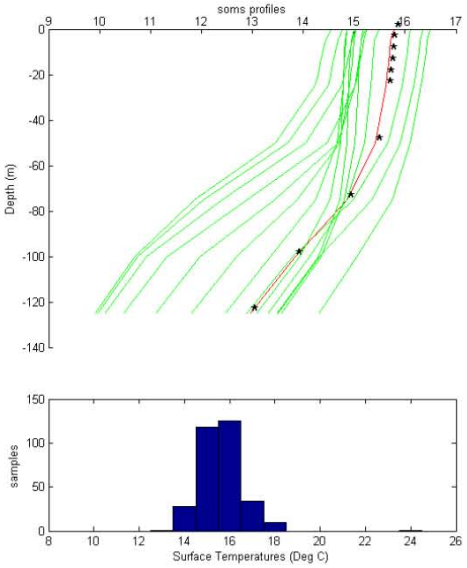
soms profiles
Depth (m)
samples
Surface Temperatures (Deg C)

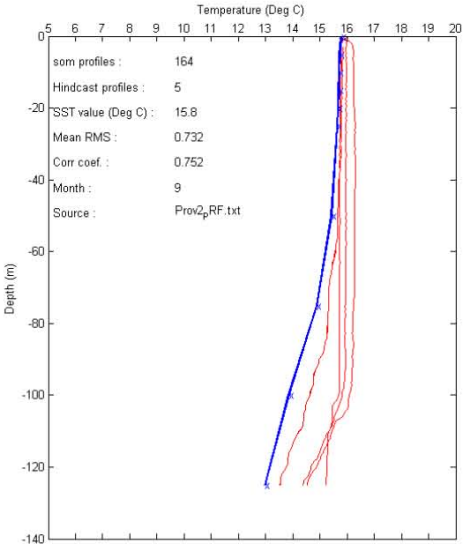
Temperature (Deg C)
som profiles : 164
Hindcast profiles : 5
SST value (Deg C) : 15.8
Mean RMS : 0.732
Corr coef. : 0.752
Month : 9
Source : Prov2_pRF.txt
Depth (m)

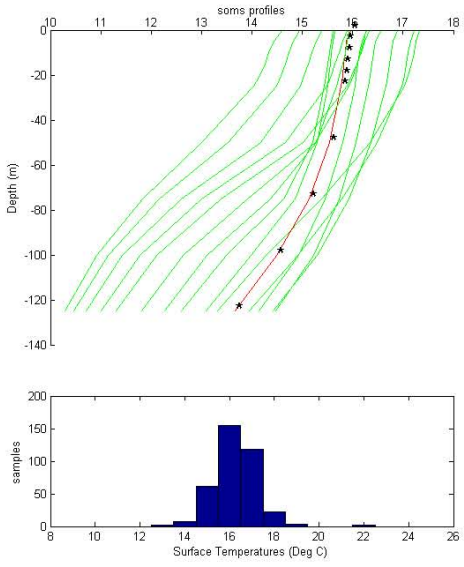
soms profiles
Depth (m)
samples
Surface Temperatures (Deg C)

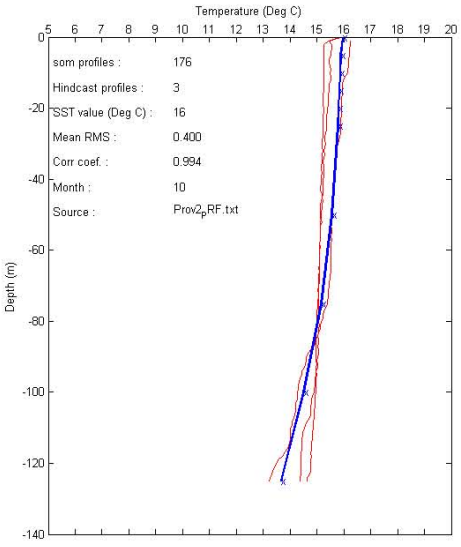
Temperature (Deg C)
som profiles : 176
Hindcast profiles : 3
SST value (Deg C) : 16
Mean RMS : 0.400
Corr coef. : 0.994
Month : 10
Source : Prov2_pRF.txt
Depth (m)

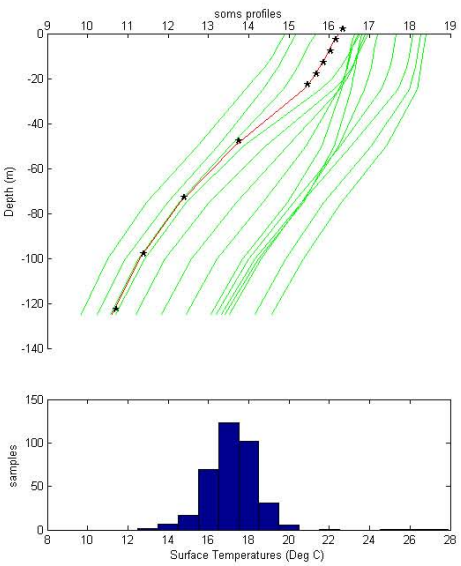
soms profiles
Depth (m)
samples
Surface Temperatures (Deg C)

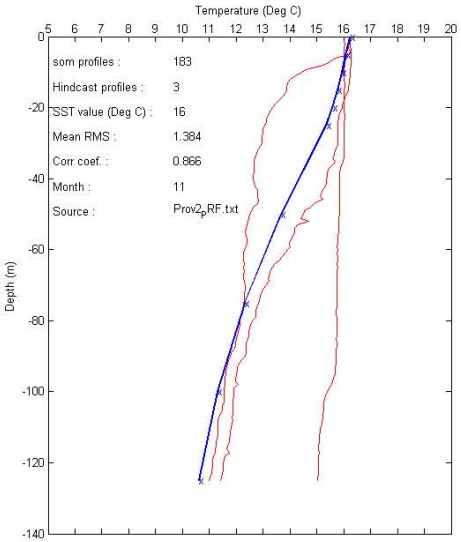
Temperature (Deg C)
som profiles : 183
Hindcast profiles : 3
SST value (Deg C) : 16
Mean RMS : 1.384
Corr coef. : 0.866
Month : 11
Source : Prov2_pRF.txt
Depth (m)

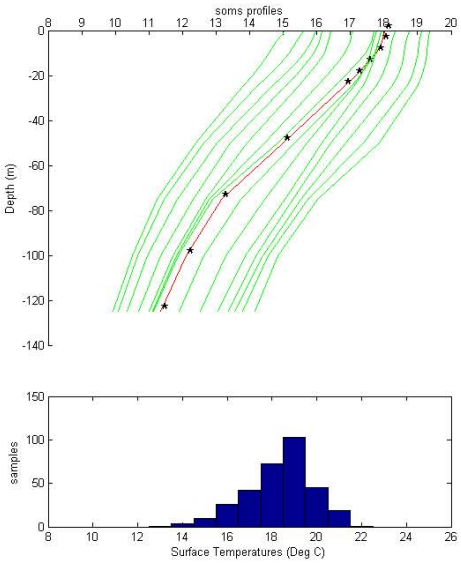
soms profiles
Depth (m)
samples
Surface Temperatures (Deg C)

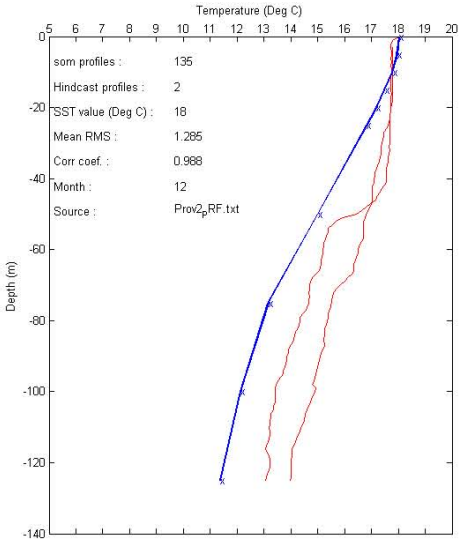
Temperature (Deg C)
som profiles : 135
Hindcast profiles : 2
SST value (Deg C) : 18
Mean RMS : 1.285
Corr coef. : 0.988
Month : 12
Source : Prov2_pRF.txt
Depth (m)

APPENDIX G – ACRONYMS

ADCP – Acoustic Doppler Current Profiler

ASCII – American Standard Code for Information Interchange

AVHRR – Advanced Very High Resolution Radiometer

BMU – Best Matching Unit

Bott. Smpls – Bottle Samples

BT – BathyThermograph

Chl a - Chlorophyll a

CTD – Conductivity, Temperature & Depth

Corr. Coeff. – Correlation Coefficient

CPML – Cape Point Monitoring Line (commonly referred to as the 'SARP' line)

ENSO - El Niño-Southern Oscillation

EOF – Empirical Orthogonal Function

EEZ – Exclusive Economic Zone

GDEM-Generalized Digital Environmental Model

GEOSS-Global Earth Observing System of Systems

GP - Genetic Programming

DPF – Delayed mode Profiling Float

IMT- Institute for Maritime Technology. A Division of Armscor Defence Institutes (PTY) Ltd.

JES – Japan/East Sea

MBT – Mechanical Bathy Thermograph

MLD – Mixed Layer Depth

MODAS-Modular Ocean Data Assimilation System

MOODS – United States Navy Master Oceanographic Observations Data Set

NASA – National Aeronautics Space Agency

NLOM- Naval Research Laboratory Layered Ocean Model

NM – Nautical Miles

NN – Neural Network

NNE -North North East

NNW - North North West

NODC – National Oceanographic Data Centre

OSD – Oxygen Standard Depth

PFL or Prof. flts – Profiling Float

Phd – Doctor of Philosophy

PSU - Practical Salinity Units

qe – quantisation error

R – Correlation coefficient

RMS – Root Mean Square

RSMAS – Rosenstiel School of Marine and Atmospheric Science

SADCO – Southern African Data Centre for Oceanography

SARP – Alternative acronym used for the Cape Point Monitoring Line (CPML)

SD or SDV or Std. Dev – Standard Deviation

SE-South East

SSE - South South East

SSP – Sound velocity Profile

SHBML – St Helena Bay Monitoring Line

SMOD – Sonar prediction and MODeling , Version 12

SOFM – Self Organising Feature Map

SOM – Self Organising Map

SOFAR – SOnar Frequency And Ranging

SONAR- SOund Navigation And Ranging

SSH – Sea Surface Height (explain the meaning here)

SST – Sea Surface Temperature

STSS – Scientific and Technology Support Service

STCZ – Sub Tropical Convergence Zone

Sv – Sverdrup, 1 Sv=10^6 $m^3.s^{-1}$

SVP – Sound Velocity Profile

SWIO – South West Indian Ocean

TBD – Thermocline Bottom Depth

te – topology error

TTG – Thermocline Temperature Gradient

T-S – Temperature Salinity

US – United States

WDC - World Data Centre

WOD - World Ocean Database

XBT – Expendable Bathy Thermograph

APPENDIX H – DEFINITIONS

Definitions of some of the terms used in this study.

Chlorophyll a

A type of chlorophyll that is most common and predominant in all oxygen-evolving photosynthetic organisms such as higher plants, red and green algae. It is best at absorbing wavelength in the 400-450 nm and 650-700 nm of the electromagnetic spectrum. Its molecular formula is $C_{55}H_{72}O_5N_4Mg$.

Ref. http://www.biology-online.org/dictionary/Chlorophyll_a 12 August 2012

Correlation Coefficient

A correlation coefficient is a number between -1 and 1 which measures the degree to which two variables are linearly related. If there is perfect linear relationship with positive slope between the two variables, we have a correlation coefficient of 1; if there is positive correlation, whenever one variable has a high (low) value, so does the other. If there is a perfect linear relationship with negative slope between the two variables, we have a correlation coefficient of -1; if there is negative correlation, whenever one variable has a high (low) value, the other has a low (high) value. A correlation coefficient of 0 means that there is no linear relationship between the variables.

There are a number of different correlation coefficients that might be appropriate depending on the kinds of variables being studied.

Ref. http://www.stats.gla.ac.uk/steps/glossary/paired_data.html#corrcoeff 12 August 2012

Dynamic height

In oceanography, this refers to the pressure associated with a column of water. Horizontal variations of this (due to horizontal variations in temperature and salinity) are mapped to determine what is called the dynamic topography and its corresponding *geostrophic flow* field in the ocean. The dynamic height is measured in *dynamic meters* and is defined by

$$D(p_1, p_2) = \int_{p_1}^{p_2} \delta(T, S, p)\, dp$$

where p_1 and p_2 are two reference pressure levels, δ the *specific volume anomaly*, T the temperate, S the salinity, and p the pressure. This is analogous to a meteorologist's use of a pressure chart, with the direction of flow aligned with the contours and the intensity of flow inversely proportional to the contour spacing. Dynamic heights are preferred over geometric heights in oceanography and meteorology because energy is generally lost or gained when a parcel of fluid moves along a surface of equal geometric height but not when it moves along

a surface of equal dynamic height. This quantity has also been called dynamic thickness, dynamic distance, geopotential height, geopotential thickness, and geopotential distance.

Ref. http://stommel.tamu.edu/~baum/paleo/paleogloss/paleogloss.html 12 August 2012

Empirical orthogonal function

EOF analysis provides a convenient method for studying the spatial and temporal variability of long time series of data over large areas. It splits the temporal variance of the data into orthogonal spatial patterns called empirical eigenvectors. A set of orthogonal spatial modes can be identified such that, when ordered, each successive eigenvector explains the maximum amount possible of the remaining variance in the data, and each eigenvector pattern is associated with a series of time coefficients that describe the time evolution of the particular spatial mode. The modes are orthogonal, which means that any two modes are uncorrelated in space and time and, as such, no one mode is related to any other. See Peixoto and Oort (1992) and Preisendorfer (1988).

Ref. http://stommel.tamu.edu/~baum/paleo/paleogloss/paleogloss.html 12 August 2012

Exclusive Economic Zones

The exclusive economic zone is an area beyond and adjacent to the territorial sea, subject to the specific legal regime established in this Part, under which the rights and jurisdiction of the coastal State and the rights and freedoms of other States are governed by the relevant provisions of this Convention.

Ref. http://www.un.org/depts/los/convention_agreements/texts/unclos/part5.htm

12 August 2012

GDEM

Abbreviation for General Digital Environmental Model, a four-dimensional (latitude, longitude, depth, and time) digital model of temperature and salinity for the North and South Atlantic, the Pacific, the Indian Ocean north of 40 ºS, the Arctic Ocean, the Mediterranean Sea, and the Black Sea. It consists of coefficients of mathematical expressions describing vertical profiles of temperature and salnity on a half degree latitude-longitude grid for seasonal and annual time frames, with the actual profiles generated by combining the coefficients with the equations. Some regions are being updated to 10 minute resolution. Data for creating the GDEM were obtained from the Master Oceanographic Observational Data Set (MOODS) as well as from the Levitus climatology. It is used by the U.S. Navy for most of its operational systems. See Teague et al. (1990).

Ref. http://stommel.tamu.edu/~baum/paleo/paleogloss/paleogloss.html 12 August 2012

Mixed layer depth

In oceanography, a nearly isothermal surface layer of around 40 to 150 m depth caused by wind stirring and convection. In the winter, low surface temperatures and large waves (with their accompanying turbulent mixing) can deepen the mixed layer all the way to the permanent thermocline. Higher temperatures and a less energetic wave climate in the summer can lead to the development of a *seasonal thermocline* at the base of the mixed layer that overlies the permanent thermocline.

Ref. http://stommel.tamu.edu/~baum/paleo/paleogloss/paleogloss.html 12 August 2012

Root Mean Square

For a set of n numbers or values of a discrete distribution x_1, ..., x_n, the root-mean-square (abbreviated "RMS" and sometimes called the quadratic mean), is the square root of mean of the values x_i^2, namely

$$x_{\mathrm{RMS}} = \sqrt{\frac{x_1^2 + x_2^2 + \ldots + x_n^2}{n}}$$

$$= \sqrt{\frac{\sum_{i=1}^{n} x_i^2}{n}}$$

$$= \sqrt{\langle x^2 \rangle},$$

where $\langle x^2 \rangle$ denotes the mean of the values x_i^2.

Ref. http://mathworld.wolfram.com/Root-Mean-Square.html 12 August 2012

Salinity

An oceanographic concept conceived to provide a measure of the mass of salt per unit mass of seawater. The first systematic attempt to define this was made by a commission appointed by the International Council for the Exploration of the Sea in 1899 and chaired by Knudsen. Attempts to measure salt content by drying samples were accompanied by losses of volatile compounds along with the water, and the hygroscopic nature of the residue also served to complicate matters. A dry residue method where the sample was evaporated and dried to a stable weight at 480 ◦C after processing with hydrochloric acid was offered as an alternative method. This led to the definition of the salinity as ``the total amount of solid material in grams contained in one kilogram of seawater when all the carbonate has been

converted to oxide, all the bromine and iodine replaced by chlorine, and all the organic material oxidized.''

When this dry residue method also provided practical difficulties aboard ship the commission defined a *chlorinity* that could be determined via a volumetric titration using silver nitrate. This measurement could be combined with the assumption of constant ionic ratios in seawater to obtain a measure of the salinity, with the relationship between the two quantities being defined as

$$S(^{\circ}/_{\circ\circ}) = 0.03 + 1.805\,\mathrm{Cl}(^{\circ}/_{\circ\circ}).$$

A small adjustment was made in the definition of chlorinity in the late 1920s, but it remained basically the same until the development of reliable and precise electronic instrumentation in the 1950s led to a qualitative redefinition of the chlorinity, and therefore the salinity, in terms of measurements of the electrical conductivity of a water sample. This led to the creation and publication of the the International Oceanographic Tables giving salinity as a function of conductivity ratio above 10 ₀. These tables were adequate for the laboratory determination of salinity, but could not be used with in-situ salinometers since most such measurements were made at temperatures below 10 ₀C. A separate set of tables were developed in the mid-1960s that covered the range 0-30 ₀C, although this led to discrepancies between in-situ and bench measurements of salinities and many separate attempts to patch together the two data sets. This in turn led to confusion in the comparison of salinity data amongst the major oceanographic institutes.

A solution was found in 1978 in the form of a new definition called the Practical Salinity Scale where the practical salinity is defined in terms of the ratio of the electrical conductivity of a seawater sample at atmospheric pressure at 15 ₀C to that of KCl solution containing 32.4356 g of KCl in a mass of 1 kg of solution at the same pressure and temperature. This ratio K_{15} defines practical salinity of a sample according to

$$S(^{\circ}/_{\circ\circ} = a_0 + a_1 K_{15}^{1/2} + a_2 K_{15} + a_3 K_{15}^{3/2} + a_4 K_{15}^{2} + a_5 K_{15}^{5/2}$$

where a_0= 0.0080, a_1= -0.1692, a_2= 25.3851, a_3= 14.0941, a_4= -7.0261, and a_5= 2.7081. This definition suffices for laboratory determination of salinity for samples at the aforementioned pressure and temperature, but corrections must be made for in-situ measurements in water of salinity *S* and temperature *T*. These are available in the form of additional tables and equations. See Lewis (1980) and Lewis and Perkin (1978).

Ref. http://stommel.tamu.edu/~baum/paleo/paleogloss/paleogloss.html 12 August 2012

Sea Surface Height

Sea-surface height (SSH) is the height (or topography or relief) of the ocean's surface. On a daily basis, SSH is most obviously affected by the tidal forces of the Moon and the Sun acting on the Earth. Over longer timescales, SSH is influenced by ocean circulation.

Ref. http://en.wikipedia.org 12 august 2012

Thermocline

Specifically the depth at which the temperature gradient is a maximum. Generally a layer of water with a more intensive vertical gradient in temperature than in the layers either above or below it. When measurements do not allow a specific depth to be pinpointed as a thermocline a depth range is specified and referred to as the thermocline zone. The depth and thickness of these layers vary with season, latitude and longitude, and local environmental conditions. In the midlatitude ocean there is a permanent thermocline residing between 150-900 meters below the surface, a seasonal thermocline that varies with the seasons (developing in spring, becoming stronger in summer, and disappearing in fall and winter), and a diurnal thermocline that forms very near the surface during the day and disappears at night. There is no permanent thermocline present in polar waters, although a seasonal thermocline can usually be identified.

The basic dynamic balance that maintains the permanent thermocline is thought to be one between the downward diffusive transport of heat and the upward convective transport of cold water from great depths. A review of the governing dynamics of the permanent thermocline can be found in Pedlosky (1987).

Ref. http://stommel.tamu.edu/~baum/paleo/paleogloss/paleogloss.html 12 12 August 2012

T-S diagram

A graph showing the relationship between temperature and salinity as observed together at, for example, various depths in a water column. A T-S diagram for a given station is typically prepared by plotting a point for the temperature/salinity combinations at a range of depths and then joining them by straight lines in order of depth. The resulting line is called the T-S curve. Isopleths of constant density are often also drawn on the same diagram as a useful additional interpretation aid. In the ocean certain T-S combinations are preferred which leads to the procedure of identification via the definition of *water types* and *water masses* and their distributions.

Ref. http://stommel.tamu.edu/~baum/paleo/paleogloss/paleogloss.html 12 August 2012